MINISTÉRIO DA CIÊNCIA, TECNOLOGIA, INOVAÇÕES E COMUNICAÇÕES
INSTITUTO NACIONAL DE PESQUISAS ESPACIAIS

sid.inpe.br/mtc-m21c/2018/08.30.12.28-TDI

# CUT-OFF LOWS IN THE SOUTHERN HEMISPHERE: CLIMATOLOGY, STRUCTURE AND ENERGETICS

Henri Rossi Pinheiro

Doctorate Thesis of the Graduate Course in Meteorology, guided by Drs. Kevin Ivan Hodges, and Manoel Alonso Gan, approved in September 18, 2018.

URL of the original document:
<http://urlib.net/8JMKD3MGP3W34R/3RNJCL8>

INPE
São José dos Campos
2018

**PUBLISHED BY:**

Instituto Nacional de Pesquisas Espaciais - INPE
Gabinete do Diretor (GBDIR)
Serviço de Informação e Documentação (SESID)
CEP 12.227-010
São José dos Campos - SP - Brasil
Tel.:(012) 3208-6923/7348
E-mail: pubtc@inpe.br

**COMMISSION OF BOARD OF PUBLISHING AND PRESERVATION OF INPE INTELLECTUAL PRODUCTION (DE/DIR-544):**

**Chairperson:**

Dr. Marley Cavalcante de Lima Moscati - Centro de Previsão de Tempo e Estudos Climáticos (CGCPT)

**Members:**

Dra. Carina Barros Mello - Coordenação de Laboratórios Associados (COCTE)
Dr. Alisson Dal Lago - Coordenação-Geral de Ciências Espaciais e Atmosféricas (CGCEA)
Dr. Evandro Albiach Branco - Centro de Ciência do Sistema Terrestre (COCST)
Dr. Evandro Marconi Rocco - Coordenação-Geral de Engenharia e Tecnologia Espacial (CGETE)
Dr. Hermann Johann Heinrich Kux - Coordenação-Geral de Observação da Terra (CGOBT)
Dra. Ieda Del Arco Sanches - Conselho de Pós-Graduação - (CPG)
Silvia Castro Marcelino - Serviço de Informação e Documentação (SESID)

**DIGITAL LIBRARY:**

Dr. Gerald Jean Francis Banon
Clayton Martins Pereira - Serviço de Informação e Documentação (SESID)

**DOCUMENT REVIEW:**

Simone Angélica Del Ducca Barbedo - Serviço de Informação e Documentação (SESID)
André Luis Dias Fernandes - Serviço de Informação e Documentação (SESID)

**ELECTRONIC EDITING:**

Ivone Martins - Serviço de Informação e Documentação (SESID)
Murilo Luiz Silva Gino - Serviço de Informação e Documentação (SESID)

MINISTÉRIO DA CIÊNCIA, TECNOLOGIA, INOVAÇÕES E COMUNICAÇÕES
INSTITUTO NACIONAL DE PESQUISAS ESPACIAIS

sid.inpe.br/mtc-m21c/2018/08.30.12.28-TDI

# CUT-OFF LOWS IN THE SOUTHERN HEMISPHERE: CLIMATOLOGY, STRUCTURE AND ENERGETICS

Henri Rossi Pinheiro

Doctorate Thesis of the Graduate Course in Meteorology, guided by Drs. Kevin Ivan Hodges, and Manoel Alonso Gan, approved in September 18, 2018.

URL of the original document:
<http://urlib.net/8JMKD3MGP3W34R/3RNJCL8>

INPE
São José dos Campos
2018

Cataloging in Publication Data

Pinheiro, Henri Rossi.

P655c Cut-off lows in the Southern Hemisphere: Climatology, structure and energetics / Henri Rossi Pinheiro. – São José dos Campos : INPE, 2018.

xxxii + 241 p. ; (sid.inpe.br/mtc-m21c/2018/08.30.12.28-TDI)

Thesis (Doctorate in Meteorology) – Instituto Nacional de Pesquisas Espaciais, São José dos Campos, 2018.

Guiding : Drs. Kevin Ivan Hodges, and Manoel Alonso Gan.

1. Cut-off low. 2. Objective identification. 3. Reanalysis. 4. Climatology. 5. Vertical Structure. I.Title.

CDU 551.589:551.511.61

Esta obra foi licenciada sob uma Licença Creative Commons Atribuição-NãoComercial 3.0 Não Adaptada.

This work is licensed under a Creative Commons Attribution-NonCommercial 3.0 Unported License.

Aluno (a): ***Henri Rossi Pinheiro***

Título: **"CUT-OFF LOWS IN THE SOUTHERN HEMISPHERE: CLIMATOLOGY, STRUCTURE AND ENERGETICS"**

**Aprovado (a) pela Banca Examinadora em cumprimento ao requisito exigido para obtenção do Título de *Doutor(a)* em *Meteorologia***

**Dr. José Antonio Aravéquia**

***Presidente / INPE / Cachoeira Paulista - SP***

***( ) Participação por Video - Conferência***

***(Y) Aprovado ( ) Reprovado***

**Dr. Kevin Ivan Hodges**

***Orientador(a) / UR / Reino Unido -***

***(X) Participação por Video - Conferência***

***(X) Aprovado ( ) Reprovado***

**Dr. Manoel Alonso Gan**

***Orientador(a) / INPE / SJCampos - SP***

***( ) Participação por Video - Conferência***

***( ) Aprovado ( ) Reprovado***

**Dr. Gustavo Carlos Juan Escobar**

***Membro da Banca / CPTEC / Cachoeira Paulista - SP***

***( ) Participação por Video - Conferência***

***( ) Aprovado ( ) Reprovado***

***Este trabalho foi aprovado por:***

***( ) maioria simples***

***( ) unanimidade***

***São José dos Campos, 18 de setembro de 2018***

Aprovado (a) pela Banca Examinadora em cumprimento ao requisito exigido para obtenção do Título de *Doutor(a)* em

*Meteorologia*

Dr. Tercio Ambrizzi

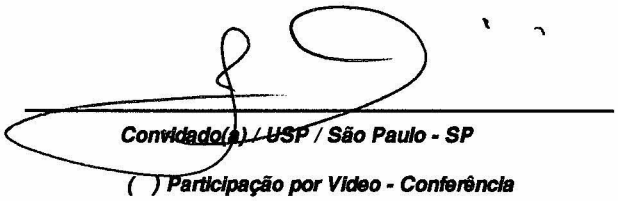

*Convidado(a) / USP / São Paulo - SP*

*( ) Participação por Video - Conferência*

*(X) Aprovado* *( ) Reprovado*

Dr. Pedro Leite da Silva Dias

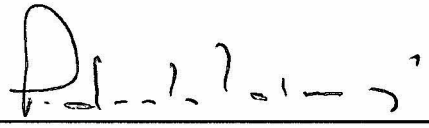

*Convidado(a) / USP / São Paulo - SP*

*( ) Participação por Video - Conferência*

*(X) Aprovado* *( ) Reprovado*

*Este trabalho foi aprovado por:*

*( ) maioria simples*

*( ) unanimidade*

*São José dos Campos, 18 de setembro de 2018*

*“The greater the difficulty, the more glory in surmounting it”*

*Epicurus*

*To my wife Kelen and my son Gabriel.*

## ACKNOWLEDGEMENTS

First of all, I would like to express my gratitude to the Creator of the universe for giving me the abilities needed to do this work, and for blessing me with this opportunity to do what I love. I would really like to thank my first supervisor Dr. Manoel Gan for his continued support and academic guidance, being always supportive and helpful in every aspect of my work. I am also deeply grateful for Dr. Kevin Hodges for his external guidance and help with explaining patiently to me how to use his software (and many other programs!) and for his encouragement and enthusiasm on this project. I always appreciate your great help for reading meticulously this thesis and helping to improve my English writing and the quality of my results, giving many constructive suggestions. I have learned so much from both of you.

I am grateful to the committee members, Drs. Nelson Ferreira and Dirceu Herdies, for the time spent in reviewing my thesis project and giving valuable suggestions. A special thanks goes to Dr. Nelson Ferreira for putting me in contact with my external supervisor, and for his constant enthusiasm and the numerous scientific discussions we had. I also want to thank the committee members who accepted to review this thesis.

There have been many people over the last four years who provided me lots of support. Thank you for Cesar Oliveira and Philipp Dias da Silva that promptly gave their time to solve the computational problems I could have. A huge thanks to my office-mates in São José dos Campos for many conversations, shared lunches, barbecues and cakes sessions. Thanks for the Library staff at the INPE in São José dos Campos and Cachoeira Paulista for their assistance in the literature search, particularly André Fernandes whose help was crucial to organise the manuscript. Thank you to my friends and colleagues from the Forecast Group (GPT) of the Center for Weather Prediction and Climate Studies (CPTEC), particularly for Gustavo Escobar for imparting his knowledge and experience of synoptic analysis and forecasting, and for the fruitful weather discussions for years. Acknowledgements also go to other important people working at CPTEC as a whole for providing support during the PhD studies.

I would also like to thank the two reviewers and the editor for the helpful suggestions on the manuscript prior to publication in the *Climate Dynamics*, included here in the

Annex A. To Michelle Reboita for the opportunity to contribute and learn in her course of Synoptic Meteorology at UNIFEI during my teaching program in Itajubá. Thanks also go to Rodolfo Ferraz for providing emotional support over the years

I would like to thank my home institution, the National Institute for Space Research (INPE) and the CPTEC for creating a scientific environment to work for the last four and a half years. I feel also thankful for the University of Reading, particularly the Department of Meteorology, for welcoming me during my one-year internship, providing infrastructure for the development of this thesis. I also would like to say thank you Heather McKeever and Dawn Turner for all efforts and help to find an accommodation to me and my family in Reading, making our time there very pleasant and smoothly. Many thanks to Flavia Rodrigues, Rachel Peterson and Fernando Ii for the deep and surprising friendship during my journey abroad.

I would also like to thank the Brazilian federal government for the financial support through the Coordination for the Improvement of Higher Education Personnel (CAPES) and the National Council for Scientific and Technological Development (CNPq) for my scholarship, and also the CNPq for the internship opportunity through the Sciences without Boarders program.

Finally, I would like to express my deep and sincere gratitude to my wife Kelen who patiently stayed with me and supported me all the moments of the PhD study. I am eternally grateful for her love, patient, understanding and support during all the time, and for giving me my greatest treasure, our lovely son Gabriel who makes me a better and happier person. Not less important, I would wish to thank my parents, José Renes and Marta, for their love and invaluable support (in every aspects!) and encouragement throughout my life.

## ABSTRACT

Annually, subtropical regions are exposed to stormy conditions caused by mid-upper level cold lows, known as Cut-off Lows (COLs), a weather system that bring heavy rainfall and flooding in different parts of the world. It is therefore very important to understand where and how COLs form, and which factors control their development. In this thesis, the objective tracking algorithm, TRACK, is used with different methodologies to study the COLs in the Southern Hemisphere (SH) with the focus on their climatology, structure and energetics. The hemispheric distribution of COLs is obtained by using both vorticity and geopotential at 300 hPa. This analysis confirms that the peak activity occurs around the main continents: Australia, South America and southern Africa. A comparison of COLs between five different reanalysis products indicates significant improvements in the agreement between the newer reanalyses ERAI, NCEP-CFSR, MERRA-2, and JRA-55 compared to the older JRA-25, particularly with respect to location and intensity. Different features of the three-dimensional structure of COLs are identified through the composites of the strongest systems, such as the symmetrical circulation at upper levels and the baroclinic zones across the edges of the cold core (400-500 hPa) and the warm core (~100 hPa). Results indicate that the upper-level fronts propagate downstream throughout the COL life cycle. As a result of the COL formation, large amounts of stratospheric air are introduced into the troposphere, modifying the vertical distribution of potential vorticity and ozone. The precipitation in COLs varies widely according to the life cycle, reaching a peak 24 hours after the maximum intensity in vorticity. There is a clear association between the medium and high cloud cover and precipitation, where maximum values are found east of the COL centre due to moist uplift at middle levels and strong divergence at upper levels. The possible link between intensity/moisture and precipitation associated with COLs suggests that moisture is important for controlling the areal coverage of precipitation, while intensity affects the magnitude of precipitation. The largest precipitation zones are found for the summer and autumn COLs, though winter and spring have the strongest COLs. Results confirm earlier findings that deeper COLs cause more precipitation than shallower COLs. A new method is proposed to estimate the COL vertical depth, indicating that COLs are relatively deep in Australia and southwestern Pacific, where more than 30% of the total number extend vertically toward the surface. A similar structure was found for the COLs occurring east of the Andes, where the mountain effect may contribute to the COL deepening, and the moisture and heat transport from the Amazon region increasing the precipitation. The ageostrophic flux convergence (AFC) together with the baroclinic (BRC) conversion are found to be the primary mechanisms for the COL development. The AFC is important for the formation and intensification of the COL, while the BRC conversion is important to maintain the system. The dissipation of the COLs occurs due to dispersive fluxes together with other processes such as friction and latent heat release. The barotropic (BRT) conversion act to transfer Eddy kinetic energy to zonal flow

kinetic energy during the growth phase, but this is not enough to prevent the COL intensification. Results show that the COLs originating in the lee side of the Andes are deeper due to local effects, which enhance the vertical motion and the system is intensified mostly due to BRC conversion.

Keywords: Cut-off low. Objective Identification. Reanalysis. Climatology. Vertical Structure. Energetics.

# VÓRTICES CICLÔNICOS DE ALTOS NÍVEIS: CLIMATOLOGIA, ESTRUTURA E ENERGÉTICA.

## RESUMO

Ao longo do ano, regiões subtropicais estão sujeitas a tempestades causadas por baixas frias na troposfera média e alta, conhecidas por Vórtice Ciclônicos de Altos Níveis (VCANs), um sistema sinótico responsável por provocar chuvas fortes e enchentes em diversas partes do mundo. Portanto, é importante entender onde e como os VCANs se formam, e quais são os fatores que controlam o desenvolvimento destes sistemas. Nesta tese, um algoritmo de identificação objetiva de trajetórias, conhecido como TRACK, é usado com diferentes metodologias para estudar os VCANs no Hemisfério Sul (HS), com ênfase em aspectos relacionados com a climatologia, estrutura e energética. A distribuição espacial dos VCANs no HS é obtida usando os campos de vorticidade e geopotencial em 300 hPa. Esta distribuição confirma que o pico de atividade ocorre ao redor das principais áreas continentais: Austrália, América do Sul e sul da África. Uma comparação dos VCANs entre cinco diferentes produtos de reanálises indica um significativo avanço em relação à concordância entre as novas reanálises ERAI, NCEP-CFSR, MERRA-2 e JRA-55 em comparação à reanálise mais antiga JRA-25, principalmente em relação à localização e intensidade dos VCANs. Diferentes características da estrutura tridimensional dos VCANs são identificadas através dos compostos dos VCANs mais intensos, mostrando uma circulação assimétrica em altos níveis e zonas baroclínicas através das bordas do núcleo frio (400-500 hPa) e do núcleo quente (~100 hPa). Resultados indicam que as frentes em ar superior se propagam corrente abaixo através do ciclo de vida dos VCANs. Como resultado da formação dos VCANs, elevadas concentrações de ar estratosférico são introduzidas para o interior da troposfera, modificando a distribuição vertical da vorticidade potencial e do ozônio. A precipitação nos VCANs varia bastante ao longo do ciclo de vida, alcançando um pico 24 horas após a máxima intensidade dos VCANs, medida na vorticidade. Há uma nítida associação entre a distribuição espacial de nuvens altas e médias e a precipitação, onde os máximos valores são encontrados a leste do centro do VCAN, devido ao ar úmido ascendente em níveis médios e à forte divergência em altos níveis. Uma possível conexão entre a intensidade/umidade e a precipitação associada aos VCANs sugere que a umidade é importante para controlar a área de abrangência da precipitação, enquanto que a intensidade afeta a magnitude da precipitação. As zonas mais extensas de precipitação estão associadas aos VCANs que ocorrem no outono e verão, enquanto que o inverno e a primavera apresentam os VCANs mais intensos. Os resultados deste estudo confirmam a forte associação entre a profundidade do VCAN e a precipitação associada, indicando que os VCANs mais profundos produzem mais precipitação em relação aos VCANs confinados na troposfera alta. Um novo método foi implementado para estimar a profundidade vertical dos VCAN. Esta análise mostra que os VCANs são mais profundos na Austrália e setor oeste do Oceano Pacífico Sul, onde mais de 30% do número total se estendem verticalmente até a superfície. Uma estrutura semelhante foi observada nos VCANs que atuam a leste da Cordilheira dos Andes, onde o efeito montanha pode contribuir para o aprofundamento do sistema, e o transporte de calor e umidade da região Amazônica para o aumento da precipitação. A convergência do fluxo ageostrófico (AFC – termo em inglês) junto com a conversão baroclínica

(BRC) constituem os mecanismos mais importantes para o desenvolvimento dos VCANs. A AFC desempenha um papel importante para a formação e intensificação dos VCANs, enquanto que a conversão BRC é fundamental para a manutenção dos VCANs. A dissipação dos VCANs ocorre devido aos fluxos dispersivos e a outros processos como o atrito e a liberação de calor latente próximo ao centro dos VCANs. A conversão barotrópica (BRT) atua transferindo energia cinética da perturbação para o estado básico durante a fase de crescimento dos VCANs, embora esse mecanismo não seja suficiente para evitar a intensificação dos VCANs. Os resultados mostram que os VCANs que se originam a sotavento dos Andes são mais profundos devido à ação de efeitos locais, que aceleram os movimentos verticais e o sistema é intensificado através da conversão BRC.

Palavras-chave: Vórtice Ciclônicos de Altos Níveis. Identificação Objetiva. Reanálises. Climatologia. Estrutura Vertical. Energética.

## LISTA DE FIGURAS

**Pag**.

## LISTA DE TABELAS

**Pag**.

## LISTA DE SIGLAS E ABREVIATURAS

| | |
|---|---|
| AFC | Ageostrophic Flux Convergence |
| AIRS | Atmospheric Infrared Sounder |
| ATOVS | Advanced TOVS |
| BRC | Baroclinic |
| BRT | Barotropic |
| CFS | Climate Forecast System |
| CFSR | Climate Forecast System Reanalysis |
| CMIP | Coupled Model Intercomparison Project |
| COL | Cut-off Low |
| DANA | Depresíon Aislada em Niveles Altos |
| DJF | December-Januray-February |
| DOE | Department of Energy |
| DSD | Downstream Development |
| ECMWF | European Centre for Medium-Range Weather Forecasting |
| EKE | Eddy Kinetic Energy |
| ENSO | El Niño Southern Oscillation |
| EAPE | Eddy Available Potential Energy |
| ERAI | ECMWF Interim Reanalysis |
| ERA-5 | Fifth generation of the ECMWF Reanalyses |
| ERA-20C | $20^{th}$ Century Reanalysis of the ECMWF |
| ERA-40 | 40-year Reanalysis of the ECMWF |
| GEOS | Goddard Earth Observing System |
| GFDL | Geophysical Fluid Dynamics Laboratory |
| GFS | Global Forecast System |
| GPM | Geopotential Meters |
| GODAS | Global Ocean Data Assimilation System |
| GSI | Gridded Statistical Interpolation |
| SOI | Southern Oscillation Index |
| IR | Infrared |
| JJA | June-July-August |
| JRA | Japonese Meteorological Agency |
| KFC | EKE Flux Convergence |

| | |
|---|---|
| LHS | Left Hand Side |
| MACC | Monitoring Atmospheric Composition and Climate |
| MAM | March-April-May |
| MERRA | Modern Era Retrospective Reanalysis for Research and Applications |
| MSLP | Mean Sea Level Pressure |
| NASA | National Aeronautics and Space Administration |
| NH | Northern Hemisphere |
| NCAR | National Center for Atmospheric Research |
| NCEP | National Center Environmental Prediction |
| PDO | Pacific Decadal Oscillation |
| PSA | Pacific South American |
| PV | Potential Vorticity |
| PVU | Potential Vorticity Unit |
| QBO | Quasi-Biennal Oscillation |
| RES | Residual |
| RHS | Right Hand Side |
| RWB | Rossby wave breaking |
| SAM | Southern Annual Mode |
| SAO | Semi-annual Oscillation |
| SH | Southern Hemisphere |
| SON | September-October-November |
| SSM/I | Special Sensor Microwave Imager |
| SST | Sea Surface Temperature |
| SSW | Sudden Stratospheric Warming |
| TFP | Thermal Frontal Parameter |
| TIROS | Television and Infrared Observation Satellite |
| TOVS | TIROS Operational Vertical Sounder |
| TPI | Trans-Polar Index |
| T42 | Triangular truncation at wave 42 on a Gaussian grid |
| T63 | Triangular truncation at wave 63 on a Gaussian grid |
| UTC | Universal Time Coordinated |
| WV | Water Vapor |
| 3D-var | Three-Dimensional Variational Data Assimilation |
| 4D-var | Four-Dimensional Variational Data Assimilation |

## LISTA DE SÍMBOLOS

| | |
|---|---|
| $\alpha$ | Specific volume |
| $\vec{V}$ | Horizontal wind |
| $\phi$ | Geopotential |
| $\omega$ | Vertical velocity |
| $p$ | Surface pressure |
| $'$ | Prime - eddies or deviation from the mean state |
| $\bar{}$ | Overbar - time mean flow |
| W | West |
| E | East |
| N | North |
| S | South |
| U, V | Horizontal wind components |
| $U_{300}$ | Zonal winds at 300 hPa |
| $Z_{300}$ | Geopotential height at 300 hPa |
| $Z'_{300}$ | Geopotential height anomaly at 300 hPa |
| $\xi_{300}$ | Relative vorticity at 300 hPa |
| $\xi_{850}$ | Relative vorticity at 850 hPa |
| $T_{300}$ | Temperature at 300 hPa |
| $T'_{500-300}$ | Temperature anomaly |
| $PV_{300}$ | Potential vorticity at 300 hPa |
| $O_3$ | Ozone concentration |
| $\bar{d}$ | Average displacement over three frames |
| $d_{max}$ | Upper-bound displacement |
| $\psi_{max}$ | Upper-bound track smoothness constraint |

**SUMÁRIO**

**Pag.**

# 1 INTRODUCTION

Cut-off Lows (COLs) are synoptic-scale low pressure systems at upper levels, identified as minima with closed contours on the geopotential charts. They develop from a pre-existing cold trough in mid-latitudes that extends equatorward, leaving an isolated cyclonic vortex from the westerly flow (PALMÉN; NEWTON, 1969). The historical interest in COLs is motivated by their importance on the weather since they are often responsible for heavy precipitation and floods in different regions of the world (LLASAT et al., 2007; MCINESS; HUBBERT, 2011; SINGLETON; REASON, 2006). COLs also play an important role in the stratosphere-troposphere exchange, and occasionally lead to episodes of high ozone concentration in the lower troposphere (ANCELLET et al., 1994).

The term "Cut-off Low" probably originated from the concept introduced by the German school (SCHERHAG, 1937) when using the expression *Kaltlufttropfen*, which means cold air pool. *Kaltlufttropfen* is defined as "a marked depression non-existent at ground level and only appreciable at the upper levels, with the coldest air at its central part". In the literature, a large number of terminologies have been used to describe a COL, such as cold lows, cold pools, cut-off cyclones, upper-level vortices, among many other forms.

In the mid-twentieth century, Erik Palmén provided the first detailed synoptic analysis of a COL in North America (PALMÉN, 1949). Since this pioneering work, there have been several other studies focusing on the characteristics of COLs in different regions, with early studies for the Northern Hemisphere (NH) (FRANK, 1966, 1970; PALMÉN; NEWTON, 1969; PALMER, 1951; RAMAGE, 1962; SIMPSON, 1952), and more recently for the Southern Hemisphere (SH) (FUENZALIDA et al., 2005; PINHEIRO et al., 2017; REBOITA et al., 2010).

Over the Mediterranean basin (southern Europe and northern Africa), COLs are often associated with heavy rainfall and severe flooding (DELGADO et al., 2007; GARCÍA et al., 1982; KNIPPERTZ; MARTIN, 2005, 2007; LLASAT et al., 2007; NIETO et al, 2007b; ROMERO et al., 1999; TRIPOLI et al., 2005) with some cases resulting in loss of life and economic losses (PORCÙ; CARASSI, 2009). In the mid-twentieth century, the terminology gota fría became mistakenly popularized in Spain as any

meteorological event causing catastrophic rains with significant social impact. The term mainly became popular after floods in the city of Valencia in Spain in 1982 when 580 mm of rain was recorded in 24 hours (MIRÓ-GRANADA GELABERT, 2003). This episode caused numerous deaths and was associated with a COL. In order to avoid confusion about the concept of COLs, the term DANA (Spanish acronym *Depresíon Aislada en Niveles Altos*, which means Isolated Depression at High Levels) was introduced as a more appropriate terminology in operational forecasting for this region (MARTÍN, 2003).

In the subtropical central and eastern Pacific Ocean, COLs are known as *Kona* Lows (SIMPSON, 1952). The term *Kona* is of Polynesian origin and has been used by the Hawaiians to describe a local rainstorm where the persistent trade winds are replaced by the southerly winds (LAWRENCE; DAINGERFIELD, 1921). These storms are historically responsible for damaging winds, flash floods, landslides, large surf and swell, and they are often associated with an upper-level COL. Simpson (1952) described how *Kona* Cyclones can occasionally change into systems with tropical cyclone characteristics. This requires the development and maintenance of convection near the COL centre, which gradually destroy the cold core with a subsequent transition into a weak warm-cored disturbance and intensification of the surface circulation. A similar development has been described by Emanuel (2005) for Mediterranean mesocyclones called Medicanes that originate from upper-level cold lows. The Hurricane Catarina, the first documented hurricane in the South Atlantic Ocean, is a spectacular example of tropical transition of a nontropical cyclone (MCTAGGART-COWAN et al., 2006; VEIGA et al., 2008). Such a development is unusual and quite difficult to forecast due to its rapid evolution and poor representation within numerical models (HART, 2003).

COLs are the major cause of elevated coastal sea level and floods in Australia (MCINESS; HUBBERT, 2011). During the cool season (April-October), COLs are found to account for about half of the total precipitation and 80% of the daily precipitation in the Mallee region, while frontal systems account for a third of the total precipitation (POOK et al., 2006). Different parts of Australia are influenced by the COLs, which produce more of the heavier rainfall events in the south eastern part

(RISBEY et al., 2009) and more than 40% of the total rainfall in autumn and spring in the south western part of this country (POOK et al., 2012).

In southern Africa, COLs are often associated with floods on the Eastern Cape coast (SINGLETON; REASON, 2006) and unusual rainfall conditions in arid regions, as occurred during the austral summer 2005-2006 in parts of the Namib Desert and the Kalahari Desert (MULLER et al., 2008). However, episodes of extreme precipitation in arid regions have a long return period.

In the South American region, because COLs are essentially upper-level disturbances, they largely impact the weather in the high Andes, causing strong winds and snowfall particularly during the autumn and winter (QUISPE; AVALOS, 2006; VUILLE; AMMANN, 1997) and sudden changes in ozone concentrations (RONDANELLI et al., 2002). COLs are responsible for unseasonal precipitation in desert regions of northern Chile and southern Peru - the Atacama Desert - corresponding to about 50-80% of the total precipitation (GODOY, 2013; VUILLE; AMMANN, 1997). In these regions, COLs are called *Bajas Segregadas* (RIVERO, 1971). Reboita and Veiga (2017) described an extreme episode of rainfall (> 65 mm – equivalent of a 13-year period) that occurred in the southern part of the Atacama Desert. This event was associated with an intense upper-level COL which resulted in floods and damage, such as energy disruption.

On the lee-side of the Andes Cordillera, COLs have potential to cause severe weather and cold air outbreaks (REINKE et al., 2006), and in some cases are responsible for cyclogenesis (MIKY FUNATSU et al., 2004). Satyamurty and Seluchi (2007) describe the main characteristics of the COLs that affect South America, also known by the Portuguese acronym VCAN: *Vórtice Ciclônico de Altos Níveis*, which means Cyclonic Vortex at Upper Levels. This term has been used to refer to two different types of COLs: one that affects the subtropical latitudes with the development following the classical definition of Palmén (1949), and is described in several studies (FEDOROVA, 1999, LOURENÇO, 1996; PINHEIRO, 2010; SATYAMURTY; SELUCHI, 2007). The second type of COL occurs in the tropical Atlantic Ocean, particularly in the summer, and frequently moves toward the continent modifying the weather in Northeast Brazil (KOUSKY; GAN, 1981; RAMIREZ, 1997).

## 1.1 Motivation and scientific questions

There are many reasons why it is important to study COLs, perhaps the most important one is related to precipitation and its impact on human activities, as described in many studies. Thus, a better knowledge of the typical COL behaviour and the processes behind this system is relevant. Over the past years, there have been great efforts to have a better understanding of the observed COLs. The advances and improvements in computer systems and observations (e.g. more modern reanalysis products and remote sensing data) have motivated a large number of studies of COLs based on analysing individual cases (SATYAMURTY; SELUCHI, 2007), numerical experimentation (GARREAUD; FUENZALIDA, 2007), climatologies (FUENZALIDA et al., 2005; NIETO et al., 2005; PINHEIRO et al., 2017) with an emphasis on their interannual variability (SINGLETON; REASON, 2007; FAVRE et al., 2012), and more recently their energetics (GAN; PIVA, 2013, 2016). The use of objective methods to identify COLs has allowed the statistics to be reproduced fairly consistently over time by using larger samples of data and larger domains than used in earlier studies based on manual methods (KENTARCHOS; DAVIES, 1998; LOURENÇO, 1996; PRICE; VAUGHAN, 1992; TALJAARD, 1985).

The location of the main areas of COL activity in the SH is generally acceptable in the literature since the maximum frequency is observed near the continents (FUENZALIDA et al., 2005; NDARANA; WAUGH, 2010; PINHEIRO et al., 2017; REBOITA et al., 2010), but the seasonality and numbers differ largely between the studies. Therefore, one research question arises as to whether the differences between studies are merely due to uncertainties in using different reanalyses (since most earlier studies use older and less reliable observations) or whether the methods used to identify COLs affects the results, as discussed in Pinheiro et al. (2017). In relation to the latter, large differences are found between the statistics produced by tracking algorithms based on vorticity or geopotential, since these fields focus on different spatial scale features. The large differences found between studies motivate this study to investigate the sensitivity of COLs to the identification criteria and how well COLs are represented in the new modern reanalyses compared to older datasets. The understanding of the structure and energetics of COLs and the regional dependence of these properties are poorly known

and limited to few studies focusing on restricted areas. Their nature is often more complicated than that represented in the simple conceptual models of COLs given the coupling of many different classes of cyclones with the upper-level disturbances (CATTO, 2016; DEVESON et al., 2002; EVANS et al., 1994; SINCLAIR; REVELL, 2000). This study addresses the hypothesis that the vertical depth (extension) is highly variable in COLs, and crucial to determine the cloud and precipitation properties, as suggested in earlier studies (PORCÙ et al., 2007; FRANK, 1970; KOUSKY; GAN, 1981). Large samples of data obtained from a homogeneous set of COLs are used with a compositing methodology that goes beyond the scope of earlier case studies, making results more statistically robust.

In addition to the question related to the vertical structure, very little attention has been given to the mechanisms and large-scale influences that affect the development of COLs, and no studies indicating which mechanisms influence the deepening of the COL circulation. The perspectives obtained from the downstream baroclinic development have been encouraged to use the local eddy kinetic energy (EKE) diagnoses of Orlanski and Katzfey (1991) for over decades, although very few attempts have been made to investigate the energetics of COLs. In the recent study of Gan and Piva (2016), the energetic terms are analysed for a set of COLs that occur particularly in the southeast Pacific Ocean, but they have not been examined for the COLs in other regions of the SH, where the main mechanisms may differ from those found by Gan and Piva (2016). Moreover, there is a void in the literature regarding the effects of the energetic terms on the deepening of COLs, since some mechanisms may be important to understand why some COLs lead to cyclogenesis and others remain confined at upper levels.

Given the poor understanding of the vertical structure and energetics of COLs, the most relevant scientific questions are:

1. How sensitive are COLs to identification criteria?
2. How can COLs be objectively identified in gridded data sets such as reanalyses, and what is the uncertainty between reanalyses?

3. What is the hemispheric distribution of COLs and what are their main properties, in particular those related to precipitation?

4. What is the structure of COLs, how does this vary regionally and how is it related to precipitation?

5. What are the main development mechanisms of COLs and which mechanisms are more important in deepening the COLs?

## 1.2 Objectives

The primary aim of this study is to provide a better understanding of the properties of COLs in the SH, in particular their vertical structure and energetics, and the mechanisms that are conducive to their development. The specific objectives are described as follows:

- Evaluate the sensitivity of identifying COLs to the field used for tracking (vorticity or geopotential) and to the different identification methods, used to separate COLs from other systems, that make use of simple schemes (using only horizontal winds) and multiple step schemes (using also temperature and potential vorticity).

- Evaluate the sensitivity of the determination of COL vertical depth to the parameters in the method used to determine the depth.

- Provide an extensive perspective on how the SH COLs compare between different reanalyses and verify the improvements and deficiencies of the newer reanalysis products, the European Centre for Medium-Range Weather Forecasting (ECMWF) Interim Reanalysis (ERAI), the National Centers for Environmental Prediction (NCEP) Couple Forecast System Reanalysis (NCEP-CFSR), the National Aeronautics and Space Administration (NASA) Modern Era Retrospective Reanalysis for Research and Applications-2 (MERRA-2) and the reanalysis produced by the Japanese Meteorological Agency (JRA), the 55 year reanalysis (JRA-55), compared to the older the 25 year reanalysis (JRA-25).

- Provide a detailed analysis of the spatial structure and life cycle of the COLs by using compositing of the 200 strongest systems in the SH. Also, evaluate the sensitivity of the compositing of COLs that are identified using multiple criteria.

- Examine the regional aspects of SH COLs in terms of their spatial and temporal distributions, and determine the sensitivity of their vertical depth for different regions.

- Investigate the potential effect of the Andes Cordillera on the vertical structure of the COLs where genesis occurs in the southeast Pacific Ocean.

- Evaluate the main mechanisms that govern the growth/decay of the EKE in the COLs regionally and for the most intense systems in the SH.

## 1.3 Thesis Outline

The thesis is organised as follows:

**Chapter 2** is a background chapter, which provides a general overview of the COLs including the modern definition, the conceptual models of development, the vertical structure, the cloud and precipitation properties, the role in the troposphere-stratosphere exchange, the temporal variability, and the energetics. A comparison between previous studies in terms of seasonality of the SH COLs is discussed.

**Chapter 3** gives a description of data and methodology used to identify and analyse COLs. In the methodology, a description of the tracking algorithm and the criteria to identify COLs are presented. Details of the techniques used for producing the composites and vertical structure diagnostics of COLs are included in this chapter. Finally, the terms of the EKE budget are described.

**Chapter 4** discusses the use of different methodologies to identify COLs by assessing three schemes to separate COLs from open troughs. The sensitivity of identifying COLs using multiple criteria is analysed in terms of number, seasonality and intensity. Lastly, a new methodology is proposed to determine the vertical depth of COLs.

**Chapter 5** examines the synoptic-scale features of the SH COLs using spatial statistics and frequency distributions for different seasons. The vertical structure of COLs is investigated in terms of spatial and temporal distributions. Lastly, a comparison of COLs using four recent reanalyses ERAI, NCEP-CFSR, MERRA-2, and JRA-55 and one older reanalysis JRA-25 is performed, indicating the similarities and differences between the data sets.

**Chapter 6** provides a detailed analysis of the spatial structure and lifecycle of the SH COLs by compositing the 200 most intense systems. The main synoptic features and lifecycle of the strongest COLs are examined such as the cold-core, high potential vorticity (PV) intrusion, baroclinic zones, vertical tilt and the cloud and precipitation patterns. This also shows the sensitivity of compositing COLs that are identified using multiple criteria.

**Chapter 7** outlines regional aspects of austral COLs for three main sectors located in the neighbourhood of subtropical Africa, Oceania and South America. Some aspects are analysed in particular detail for the COLs originating in the southeastern Pacific near South America, emphasizing the differences between intensity and vertical depth of a COL. The potential effect of the Andes Cordillera on the vertical structure of the COLs is also investigated.

**Chapter 8** examines the EKE budget of the SH COLs by using the energetic terms developed by Orlanski and Katzfey (1991). This discusses the sensitivity of residual to the volume size chosen to compute the energetics. The major dynamical mechanisms typically controlling the development of COLs, such as the downstream development, and the baroclinic and barotropic conversions are examined in the composite of the strongest systems and in individual cases. The energetics is also verified for the COLs that affect South America.

**Chapter 9** gives a summary of the main results and conclusions, and recommendations for future work.

# 2 LITERATURE REVIEW

This chapter provides a review of previous work on COLs in the literature including those that discuss conceptual models of COLs, with a particular emphasis on the SH. Section 2.1 presents an overview of the main characteristics of COLs. In section 2.2, different aspects of the COL development are described such as large-scale features and energetics. The vertical structure of COLs and its effect on precipitation is discussed in Sections 2.3. Section 2.4 gives a description of the cloud and precipitation structures. The role of COLs on the stratosphere-troposphere exchange is discussed in Section 2.5. Section 2.6 presents a review of the studies that focus on the variability of COLs in different time scales. Section 2.7 compares previous climatologies with respect to the method, dataset, vertical level and region used in each study.

## 2.1 General characteristics of Cut-off Lows

COLs are defined as cold-core lows that develop from an upper-tropospheric trough in mid-latitudes (PALMÉN; NEWTON, 1969). The formation occurs when a pre-existing trough deepens equatorward, so the trough axis tilts westward and the equatorial part moves slower (westward at times) than the polar part, leading to the vortex detachment from the westerly flow. The result of this rupture is a cold-low pressure system completely cut-off from the westeslies and located at the equatorial side of the jet stream, as shown in Figure 2.1. After the cut-off, the jet stream is no longer able to control the motion of the COLs, so that their movement becomes irregular and difficult to predict (NIETO et al., 2005).

Figure 2.1: Example of two Cut-off Lows occurring in the southeast Pacific and Andes Cordillera Region.

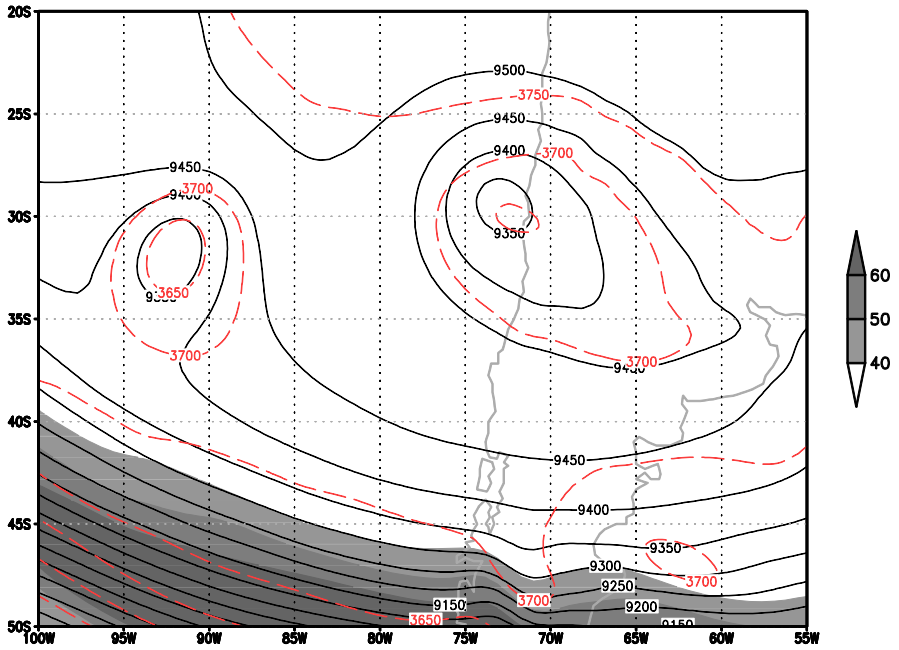


Geopotential height at 300 hPa in geopotential meters (gpm) (black solid line), thickness 500-300 hPa in gpm (red dashed line), and horizontal winds in m/s (shaded) for intervals 10 m/s. Analysis performed using the ERAI reanalysis at 06 UTC 07 March 2003.

Source: Author's production.

The trajectories of COLs can be quite variable in terms of their velocities. Most COLs in the subtropics and mid-latitudes are quasi-stationary systems during their mature stage due to the balance between the relative vorticity advection and the divergence (GODOY et al., 2011). COLs generally propagate slowly eastward, though they eventually remain stationary or move westward as observed at lower latitudes, particularly during the austral summer (KOUSKY; GAN, 1981; PINHEIRO et al., 2017). These aspects are also observed in subtropical lows such as Catarina (MCTAGGART-COWAN et al., 2006) and other similar systems in Australia (KATZFEY; MCINNES, 1996; MCINNES; HUBBERT, 2001).

The COL propagation speeds typically vary from 3 to 6 m/s (FUENZALIDA et al., 2005), but are higher at higher latitudes (PINHEIRO et al., 2017). According to Pinheiro et al. (2017), the fastest COLs are found in winter while summer has the slowest systems. COLs generally move north-eastward during the growth stage and

south-eastward during the decay stage. The mechanical effect associated with large mountain ranges usually affect the COL displacements, such as observed near the Andes Cordillera, where velocities are reduced (accelerated) when the COLs are approaching (leaving) the mountains (PINHEIRO et al., 2017). Favre et al. (2012) observed that the average distance travelled by the SH COLs is 925 km, which is much smaller than the observed distances covered by extratropical cyclones through their life cycle (MENDES et al., 2010).

Most COLs have a short lifespan generally persisting for 2 or 3 days (FAVRE et al., 2012; FUENZALIDA et al., 2005; REBOITA et al., 2010). Lifetimes are shorter in summer and longer in winter (PINHEIRO et al., 2017). The region is an important factor in determining the typical COL lifetime, since COLs located at high latitudes have longer lifetimes than those observed in the lower mid-latitudes (KENTARCHOS; DAVIES, 1998; PRICE; VAUGHAN, 1992). The COLs in the tropics are long-lived systems where a few last more than one week (COSTA, 2010; COUTINHO et al., 2010; KOSUKY; GAN, 1981), although the development mechanisms differ from those observed in non-tropical regions (MISHRA et al., 2001). The factors that determine the duration of COLs are not well understood, although recent reports have suggested that the Ageostrophic Flux Convergence (AFC) may increase the lifetime of COLs (GAN; PIVA, 2013; 2016). However, processes such as diabatic heating or friction are probably the most important contributors to COL decay (GARREAUD; FUENZALIDA, 2007; HOSKINS et al. 1985; KOUKSY; GAN, 1981; SAKAMOTO; TAKAHASHI, 2005).

The size of COLs, defined as the horizontal width, differs considerably between different regions, where larger systems are found at high latitudes and smaller systems at lower mid-latitudes (KENTARCHOS; DAVIES, 1998; PRICE; VAUGHAN, 1992). In the mature stage, COLs are generally smaller than extratropical cyclones (NIETO et al., 2005). Satyamurty and Seluchi (2007) studied the COLs that affect South America, and observed that the COLs occurring in the subtropics have a circular symmetric shape with a diameter of about 800 km, consistent with the findings of Singleton and Reason (2007) for southern African COLs. The COLs that occur in the tropical South Atlantic,

on the other hand, are more elongated in the N-S or NW-SE direction and their diameter is about 1000 km.

In the SH, COLs occur preferentially near the continents, such as southern Australia, western South America and southern Africa (FUENZALIDA et al., 2005; PINHEIRO et al., 2017; REBOITA et al., 2010). The maximum activity is found in southern Australia and the western Pacific due to the climatological split jet structure, which coincides with the high activity of blocking (MARQUES, 1996; MARQUES; RAO, 1999, 2000; TRENBERT; MO, 1985). The seasonal track density of the SH COLs obtained from a 36-year period of the ERAI is described in Pinheiro et al. (2017), shown in Figure 2.2. This agrees fairly well with the spatial distribution of COLs observed in previous studies (FUENZALIDA et al., 2010; REBOITA et al., 2010), although the seasonality is controversial since this depends critically on the vertical level, region, dataset and method used for the identification. A more detailed discussion on this topic can be found in section 2.6.

Figure 2.2: Track density of the Southern Hemisphere Cut-off Lows for austral seasons a) Autumn (MAM), b) Winter (JJA), c) Spring (SON), and Summer (DJF).

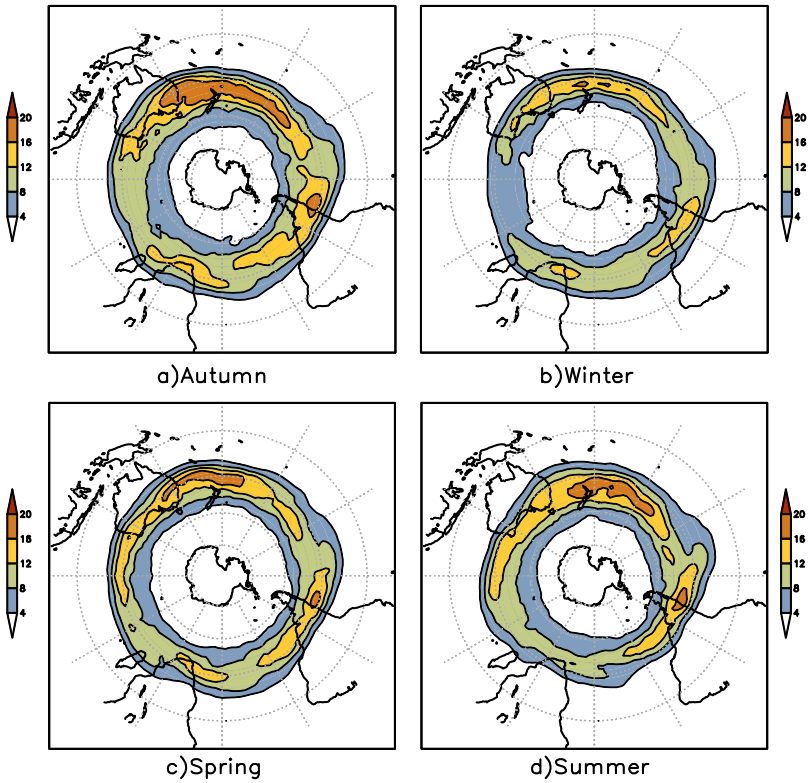


Source: Pinheiro et al. (2017).

## 2.2 Theory of Cut-off Low development

### 2.2.1 Large-scale features

There are different ways in which a COL can form. Palmén (1949) observed that the COL development begins as a wave-like deformation of the upper-level flow, which increases in amplitude until the cold air associated with a mid-latitude trough is cut-off from its polar source region. According to Hoskins et al. (1985), many COLs can develop in association with blocking highs as part of the same phenomenon, which can be distinguished by the sign of the isentropic PV anomaly. A similar development was observed by Ramírez et al. (1997), who analysed two COLs that occurred in the South Pacific Ocean. This study indicated that the COL formation occurred due to the split jet stream associated with the intensification of the upper-level ridge and subsequent rupture of the downstream cyclonic vortex from the westerly flow, which is in accordance with the statement of the PV conservation, discussed by Hoskins et al. (1985) and Bell and Bosart (1993).

Previous studies have shown that the propagation of upper-level short waves in the atmosphere associated with the jet stream transfer energy to the larger scale flow, contributing to the intensification of the upstream ridge from a pre-existing trough (BELL; BOSART, 1993). As a result of the PV conservation, the downstream upper-level trough also amplifies, leading to the formation of a cold-core vortex, which is related to the theory of Downstream Development (DSD) proposed by Orlanski and Sheldon (1995). Additionally, the stratospheric intrusion is an important mechanism for COL formation, which is facilitated because of the tropopause folding (BELL; KEYSER, 1993; HIRSCHBERG; FRITSCH, 1991; HOSKINS et al., 1985).

An acceptable conceptual model for the development of COLs was proposed by Nieto et al. (2005, 2008), divided into four stages (Figure 2.3): 1) the upper-level trough, 2) the tear-off, 3) the cut-off or maturity, and 4) the final stage. The first stage is characterized by an amplifying upper-level trough in mid-latitudes with a marked westward tilt. In the second stage, the trough deepens and the cold air is detached from its polar source. The term “polar source” does not mean that the air associated with the trough originates from a polar region, but that it forms at higher latitudes and moves equatorward. The third stage represents the mature phase of the COL, when the vortex

is completely isolated from the westerlies, and the intensity of the upper-level COL reaches its peak. The final stage represents the COL decay, which occurs when the cold-core is destroyed by diabatic effects, or moves back into high latitudes after being absorbed by a mid-latitude trough (GARREAUD; FUENZALIDA et al., 2007; HOSKINS et al., 1985; KOUSKY; GAN, 1981). The whole life cycle of a COL usually takes 2-5 days.

Figure 2.3: Conceptual model for the evolution of a Cut-off Low in the Southern Hemisphere. Contours represent the 300-hPa streamlines.

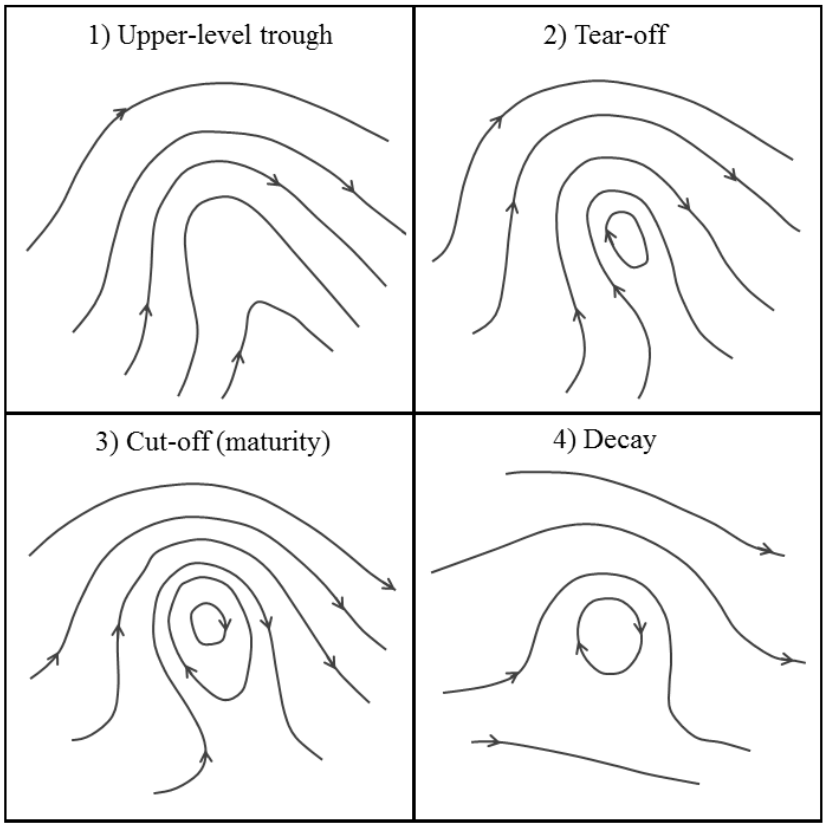


Source: Adapted from Nieto et al. (2005; 2008)

### 2.2.2 Energetics

Over the past years, a large body of literature has documented the evolution of mid-latitude disturbances since the classical studies of Charney (1947), Eady (1949), and Kuo (1949), contributing to our understanding of the baroclinic growth and barotropic decay. Later, other factors have been considered influencing the development of cyclonic disturbances in mid-latitudes, such as diabatic processes (DAVIES et al., 1993; MARTÍNEZ-ALVARADO et al., 2014), the surfaces fluxes (KUO et al., 1991;

NOGUÉS-PAEGLE; MO, 1997; PIVA et al., 2011), the topography (BUZZI et al., 1987; HAYES et al., 1987; GAN; RAO, 1994; MIKY FUNATSU et al., 2004), and the interaction between the upper-tropospheric PV with the lower-tropospheric cyclonic features (HOSKINS et al., 1985; MIKY FUNATSU et al., 2004).

Although numerous studies have unquestionably demonstrated the contribution of the baroclinic processes as the most important mechanism for the growth of mid-latitude disturbances, the concept based on the idea of the atmospheric energy dispersion (ROSSBY, 1945; YEH, 1949), known as downstream development (DSD) (ORLANSKI; KATZFEY, 1991) has been applied in some studies. According to this theory, the development of baroclinic eddies is a result of the energy dispersed from decaying systems upstream, which propagates eastward nearly with a Rossby wave group velocity (CHANG; ORLANSKI, 1994; PEDLOSKY, 1987). Orlanski and Sheldon (1995) observed that cyclone waves grow initially due to the upstream energy source and later because of the baroclinic conversion (ascent in the warm air and descent in the cold air), referred to as downstream baroclinic development. Several studies have confirmed the earlier assumption that the DSD is important for the development of particular cyclones together with the baroclinic instability (CHANG, 1993; 2000; DANIELSON et al., 2004, 2006; DECKER; MARTIN, 2005; PIVA et al., 2010; RIVIÈRE et al., 2015).

Recently, the study of Gan and Piva (2013) used the NCEP Department of Energy (DOE) reanalysis and the EKE equation developed by Orlanski and Katzfey (1991) to analyse the evolution of a COL in the South Pacific Ocean. They found that the dominant mechanisms differ from those typically observed in extratropical cyclones, since the AFC (also known as DSD) was the primary source of energy for the maintenance of the COL, whereas the baroclinic conversion had a secondary role, and it was only important for the formation of the system. The barotropic term remains negative during the whole life cycle, representing an important dissipative mechanism. These results were confirmed in a composite study using fifty cases of COLs that occurred in the South Pacific Ocean (GAN; PIVA, 2016). However, earlier investigations have shown that the downstream amplification mechanism associated with the upper cold lows off Northeast Brazil is a result of Rossby, and mixed Rossby-

gravity wave dispersion (SILVA DIAS et al., 1983) with predominant period of 3-6 days (YANAI; MARUYAMA, 1966), which have the peak activity during the summer (MAGAÑA; YANAI, 1995). This type of disturbance can act as a precursor to upper tropospheric vortices triggered by various processes such as lateral forcing (MAK, 1969), thermal forcing (LAMB, 1973), and wave-CISK (conditional instability of the second kind) (HAYASHI, 1970).

## 2.3 Vertical Structure

The understanding of the structure of COLs is one of the keys to understand the evolution of COLs. There have been several studies focusing on mid and upper COLs in both hemispheres, but the literature is very poor concerning the vertical structure of COLs and their relation to surface cyclones and impacts such as precipitation. Some definitions of COLs are strictly related to depressions at high levels with no surface cyclone (SCHERHAG, 1939). In theory, COLs are stronger in the upper troposphere and weaken toward the surface, and it is not uncommon to find an anti-cyclonic circulation at low levels (KUO, 1949). However, there are situations in which the vortex deepens downward, leading to surface cyclogenesis (MIKY FUNATSU, 2004).

The earliest study of the three-dimensional structure of a COL was made by Palmén (1949) using upper-level weather observations. This considered the vertical cross-section through a North American COL and revealed a nearly symmetric circulation in the upper troposphere (Figure 2.4a), where maximum winds occur at about 200 hPa and intersect with the tropopause region. The analysis of isentropes and isotherms (Figure 2.4b) indicate a well-defined thermal structure with a tropospheric cold-core (unstable profile) and a stratospheric warm-core aloft. This study also suggested the presence of a frontal layer in the upper troposphere, represented by stronger isotherm gradients. Another interesting feature is the anomalous tropopause that sinks in the COL centre, contributing to massive stratospheric air intrusion into the troposphere.

Figure 2.4: Vertical cross-sections in the west-east direction for a COL in North America.

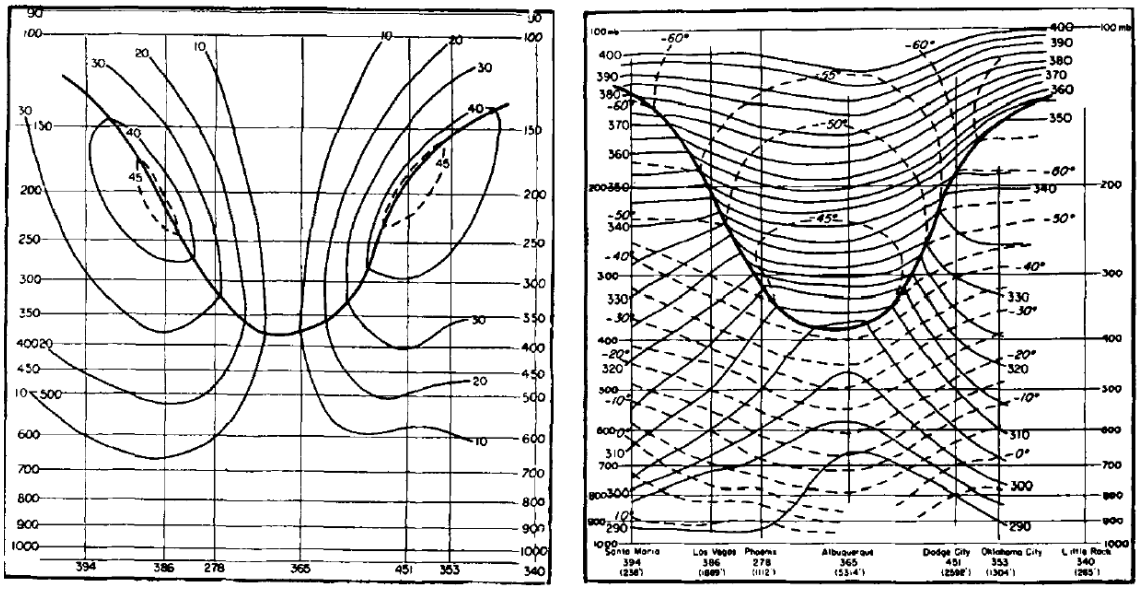

Fields are a) horizontal winds (solid line) and b) isentropes (solid line) and isotherms (dashed line). Heavy line indicates the tropopause, at 03 UTC 4 of November 1946.

Source: Palmén (1949).

Earlier findings suggest that COLs exhibit a quasi-barotropic structure in the mid and upper troposphere once the vortex is cut-off from the main flow (GARREAUD; FUENZALIDA, 2007; HOSKINS et al., 1985). The vertical circulation is typically associated with descent on the west side of the COL and ascent on the east side (MIKY FUNATSU et al., 2004; GODOY et al., 2011; KENTARCHOS et al., 1999a). The subsidence tends to inhibit the convection west of the COL centre, while the ascent enhances clouds and precipitation on the east side. The circulation pattern associated with COLs in the subtropics differs from that observed in the upper-tropospheric cyclonic vortices near the equator, where cold air sinks in the centre and warm air rises in the periphery (FRANK, 1970; RICKS, 1959; KOUSKY; GAN, 1981). These systems also present a quasi-barotropic structure (MISHRA et al., 2001), although a few can tilt toward the east at upper levels (FIGUEROA, 1997; PAIXÃO, 1999; MORAIS, 2016).

Frank (1970) was perhaps the first author to describe the association between the vertical depth of a COL and the associated weather. He studied the cold lows in the

subtropical North Atlantic and observed that the majority are confined to the upper troposphere, while only 10% of the total reach the surface. A direct relation between the vertical depth of COLs and the associated weather indicates that deeper COLs experience more cloudiness. This makes sense since deeper COLs increase the vertical coupling of the processes that maintain upward vertical motion required to transport moisture upwards. This evidence was confirmed later by Porcù et al. (2007), who demonstrated that the deeper COLs in the Mediterranean Region are associated with high rainfall rates affecting relatively large areas, while the shallow COLs (here defined as the vortices confined at high levels) do not produce precipitation. According to Porcù et al. (2007), most COLs extend through a deep layer in the troposphere, and 38% reach the surface. This result differs from that reported by Nieto et al. (2005) for the same region, where 47% of COLs have a surface cyclone.

There are some existing studies that have been concerned with the vertical depth of COLs in the SH. Campetella and Possia (2007) observed that 25% of the COLs that occur in South America and surroundings correspond to cyclones at low levels, against 35% found by Reboita et al. (2012) for the COLs in the southwest Atlantic. In contrast, the vertical depth is much smaller for the COLs in Northeast Brazil, where only 2% reach the surface (MORAIS, 2016). There are at least two reasons explaining the differences between these studies. One is the geographical region in which the COLs occur. The other factor is the method used to perform the vertical matching, where the results depend on the particular values chosen for the search. This is clear from the comparison between the studies of Nieto et al. (2005) and Porcù et al. (2007), since their results were obtained for the same region.

## 2.4 Cloud and precipitation structures

The spatial distribution of clouds and precipitation in COLs have been studied for different regions such as south-western Europe (DELGADO et al. 2007, GARCÍA-HERRERA et al., 2001; LLASAT et al., 2007; NIETO et al., 2008), South America (FEDOROVA et al., 1999; RAMÍREZ et al., 2000; SATYAMURT; SELUCHI, 2007), southern Africa (FAVRE et al., 2013) and Australia (GRIFFTHS et al., 1999). COLs have a well-defined and asymmetrical cloud structure, which is thicker on the east side of the COL and thinner on the west side. Figure 2.5 shows an example of a COL

identified in an infrared (IR) satellite image. This indicates the typical distribution of clouds for COLs, with most clouds (including convective clouds) located on the east edge of the vortex, but relatively dry on the western side.

Figure 2.5: Image of a Cut-off Low from the GOES-13 infrared (IR) channel with superimposed geopotential, isotachs and winds at 500-hPa.

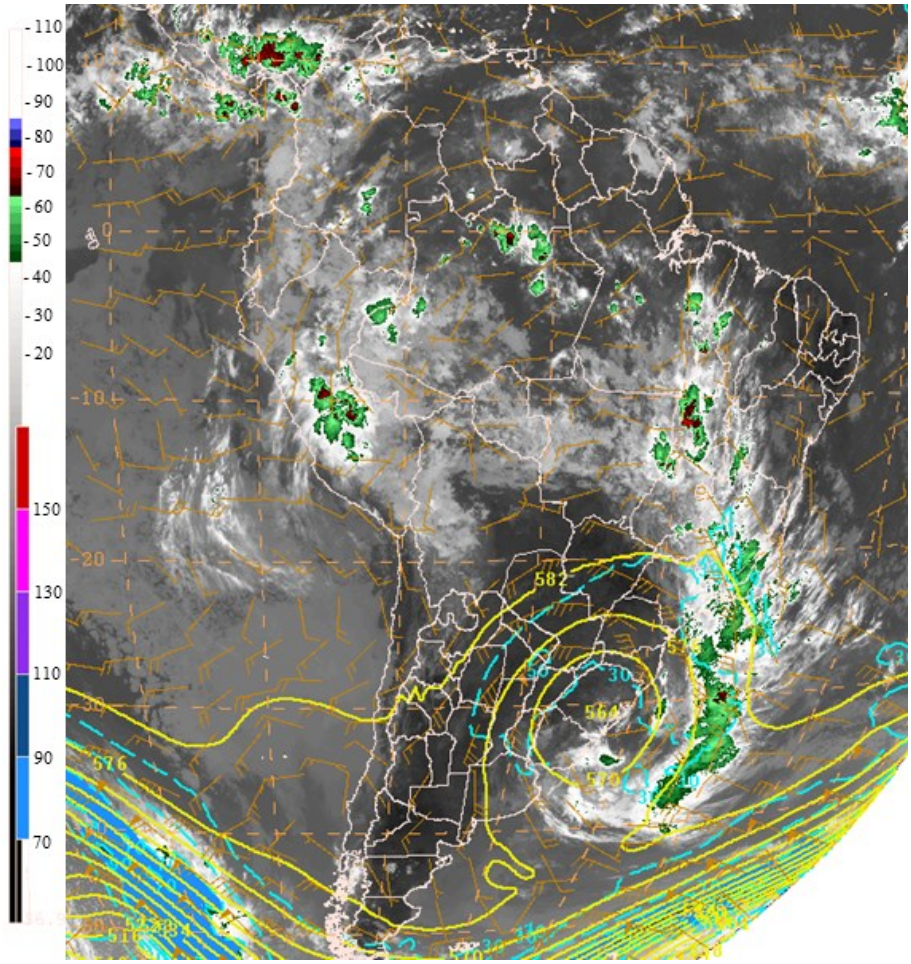


Units are brightness temperature for IR channel (blue and red shades), gpm (scaled by $10^{-1}$) for 500-hPa geopotential height with contour intervals of 60 gpm (yellow solid line), knots for 500-hPa isotachs (brown arrows), knots for 500-hPa horizontal winds with contour intervals of 20 knots (blue dashed line < 70 knots; blue shade ≥ 70 knots). Analysis performed using the Global Forecast System (GFS) analysis at 12 UTC 15 December 2011.

Source: Author's production.

Nieto et al. (2007) described a conceptual model of the typical life cycle of cloudiness for COLs, based on their experience with COLs occurring in the Iberian Peninsula and

Mediterranean Region. They suggest that the type of clouds depends on different aspects of the COLs such as the surface characteristics beneath the COL, the COL vertical depth, and the stage of the life cycle. When the COL is over a continent (Figure 2.6), lower clouds are usually found in the central part, inhibiting the development of convection. In contrast, COLs located over ocean areas (where the moisture supply is larger), convective clouds are likely to develop in the centre of the COL, increasing the possibility of moderate or heavy precipitation. This conceptual model is likely to be applicable to the relatively warm Mediterranean Sea, whereas a cold sea surface temperature may inhibit the convection. A similar behaviour has been observed when COLs move over a heated continent, enhancing deep convection due to the increase of instability (KOUSKY; GAN, 1981). In terms of the COL vertical depth, deep COLs are more likely to produce convective clouds and large rainfall compared to shallow COLs (FRANK, 1970; NIETO et al., 2007; PORCÙ et al., 2007). The stage of the COL life cycle is another factor affecting the cloud and precipitation properties, where most clouds are found in the mature stage (DELGADO et al., 2007; NIETO et al., 2008).

Figure 2.6: Cloud structure of Cut-off Lows occurring over a sea or land.

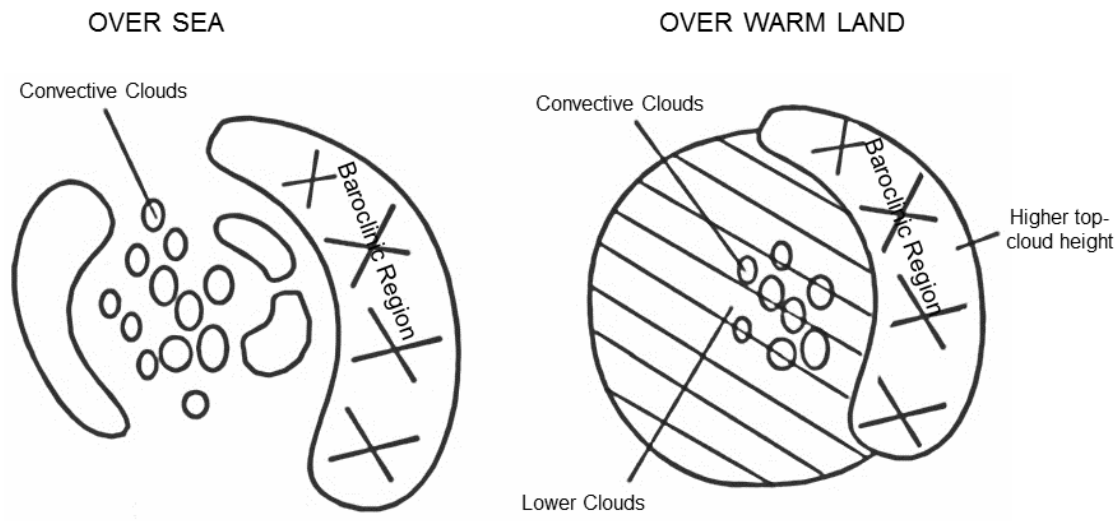


Source: Adapted from Nieto et al. (2007b).

The use of satellite imagery is an important tool for monitoring the evolution of COLs (RAMÍREZ et al., 2000). Images from the water vapor (WV) channel are very useful as a visual analysis of synoptic-scale systems in the mid to upper troposphere (VELDEN,

1997), and an alternative for the COL identification. Bengtsson (1982) proposed a procedure to identify COLs using WV images, which consists of locating the dry spiral (dark shades) that rotate cyclonically inward toward the COL centre, surrounded by relatively moist air in the periphery (light shades). This technique is useful for analysing COLs without significant clouds, which is the case for most shallow COLs (FRANK, 1970; PORCÙ et al., 2007). This advantage is demonstrated in Figure 2.7 for the identification of a COL located in the South Pacific Ocean. This system is not associated with a lot of cloud, therefore the identification and monitoring is possible only through the WV images.

Figure 2.7: a) Water vapor and b) infrared GOES-12 satellite image from 16 UTC of 4 January of 2007. Red arrows indicate the location of the centre of the COLs.

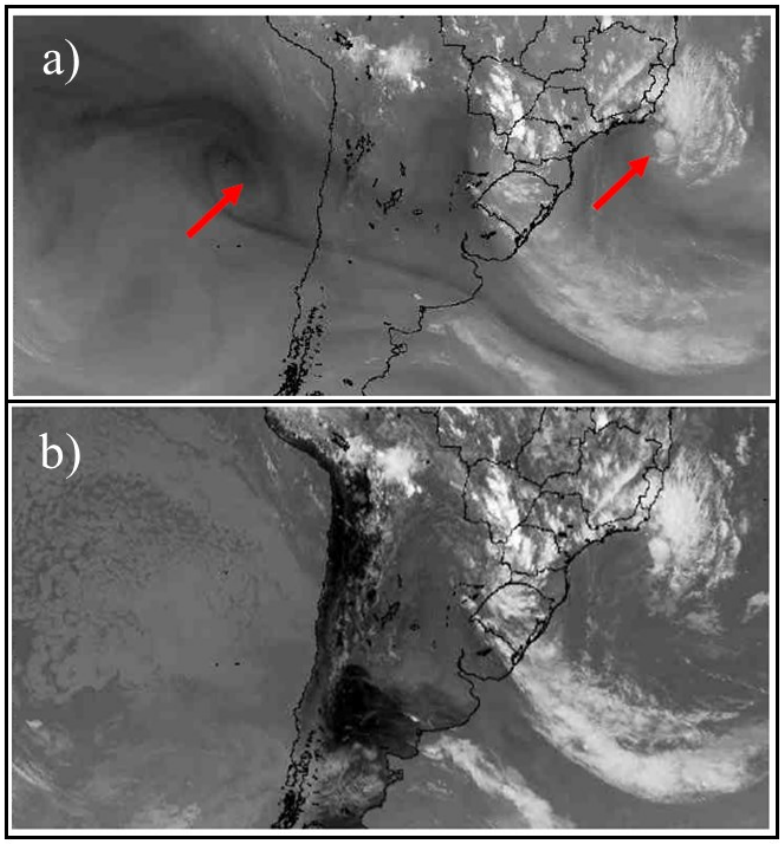


Source: Adapted from Pinheiro (2010).

The contribution of COLs to precipitation has been verified for particular regions such as the Iberian Peninsula and Mediterranean Region (DELGADO et al., 2007; NIETO et al., 2007; PORCÙ et al., 2007; WINKLER; ZWATZ-MEISE, 2001). In the SH, the precipitation associated with COLs has received less attention. An exception is the

study of Favre et al. (2013), which examined the precipitation associated with COLs in southern Africa. This shows that most COL precipitation occurs across the south and east coast of South Africa, corresponding to 25-35% of the annual rainfall. The spring is the season with the greatest COL precipitation (more intense and widespread), although autumn has the largest frequency of COLs.

## 2.5 Coupling with Stratospheric Systems

COLs play an important role in the exchange of air mass between the stratosphere and the troposphere (BAMBER et al., 1984; VAUGHAN; PRICE, 1989). The process associated with the COL formation produces a tropopause deformation, which contributes to the transfer of stratospheric polar air into the troposphere in the subtropics and mid-latitudes (ANCELLET et al., 1994; PRICE; VAUGHAN, 1993). During the tropopause folding, high cyclonic PV values are advected equatorward along isentropic surfaces (HOSKINS et al., 1985), eventually leading to Rossby wave breaking (RWB) (NDARANA; WAUGH, 2010), where RWB is defined as an irreversible overturning of PV on isentropic surfaces (MCINTYRE; PALMER, 1983).

A result of the stratosphere-tropospheric exchange is the increase of the ozone concentration in the lower and middle troposphere (ANCELLET et al., 1994; EBEL et al., 1991; KENTARCHOS, 1999a, 1999b) including the boundary layer (LANGFORD et al., 2012). Ozone is a reactive gas species that can be harmful to human health and vegetation when high concentrations are found near the surface. This also affects the balance of the radiative fluxes between the stratosphere and the troposphere, modifying the radiative forcing in the global climate (RAMASWAMY et al., 1992). Rondanelli et al. (2002) measured the ozone concentration at the mountain location of Cerro Tololo (30º10'S, 70º48'W, 2200 m), in the subtropical Andes Cordillera. They observed that all the sudden changes in ozone are associated with COL events.

## 2.6 Temporal variability

Several studies have shown that the variability of COLs occurs on different time scales. The variations associated with the seasonal cycle have been extensively studied, as will be discussed more detailed in the next section. Some studies have aimed at investigating the interannual variability of the COLs and its relation to low-frequency variability

modes, such as the El Niño Southern Oscillation (ENSO). Fuenzalida et al. (2005) found a weak but statistically significant relationship between the frequency of COLs and the cold phase of ENSO. Favre et al. (2012) also observed that COLs are more frequent during the La Niña episodes, particularly for COLs occurring at lower latitudes. Similar results were found by Singleton and Reason (2007) for COLs in southern Africa. However, none of these studies found a relationship between the frequencies of COLs and the El Niño. One reason for these results could be that during the La Niña, negative anomalies of sea surface temperature (SST) near the equator decrease the meridional pressure gradient between lower and mid-latitudes, weakening the westerlies associated with the subtropical jet, which is found to be favourable for COL development. In addition, there are significant changes in the strength of the jets due to changes in the intensity of the Hadley circulation (and changes in the location of the strongest north/south overturning circulation).

The decrease in intensity of the upper-level westerlies has been associated with an increase in blocking occurrences (TRENBERT; MO, 1985) and COLs (NIETO et al., 2007), and is generally accompanied by negative anomalies of the mean sea level pressure (MSLP) and geopotential height at 500 hPa between 30ºS-40ºS and positive anomalies of these fields between 50ºS-55ºS. This atmospheric pattern reinforces the meridional gradient of pressure and temperature between the middle and high latitudes (~50ºS-65ºS), which is defined as the semi-annual oscillation (SAO) (SIMMONS; JONES, 1998; VAN LOON, 1967). The hypothesis that the SAO affects the variability of COLs was demonstrated by a half-yearly cycle in the number of COLs with two maxima near the equinoxes (FAVRE et al., 2012; NDARANA; WAUGH, 2010; SINGLETON; REASON, 2007). On the global scale, these authors observed an apparent relationship between COLs and the zonal wave 3, which in turn plays a key role for the occurrence of blocking in the SH (MARQUES; RAO, 1999; TRENBERT; MO, 1985).

A quasi-periodic oscillation, known as quasi-biennial oscillation (QBO), is another example of circulation mode that can be related to the COL frequency. Nieto et al. (2008) found a positive correlation (at 90%) between QBO and COL occurrence in summer for a European sector. The lower stratosphere undergoes significant changes in

low frequency which has been found to be driven by the solar activity (APOSTOLOV, 1985).

## 2.7 Differences between previous studies

A variety of climatological studies have been performed for COLs in different parts of the world. The studies differ considerably with regard to methods, criteria, geographical domain and pressure level used for the identification. The objective approaches are often based on the analysis of the geopotential or vorticity on a single or multiple pressure levels. A review of the main characteristics of the studies of climatologies of SH COLs is discussed below and summarized in Table 2.1.

Table 2.1: Summary of the main characteristics of the previuos studies on COL climatologies in the Southern Hemisphere, considering the approach, data, methodology, period and region used in each study.

| References | Approach | Data | Methodology | Period | Region |
|---|---|---|---|---|---|
| Fuenzalida et al. (2005) | Objective/subjective | NCEP-NCAR | Geopotential minimum at 500 hPa | 1969-1999 | Southern Hemisphere (60°S-10°S) |
| Campetella and Possia (2007) | Objective/subjective | NCEP-NCAR | Geopotential minimum at 250 hPa | 1979-1988 | South America (60°S-10°S/100°W-20°W) |
| Singleaton and Reason (2007) | Subjective | NCEP-NCAR | Geopotential charts at 300 hPa | 1973-2002 | Southern Africa (40°S-20°S/10°E-40°E) |
| Ndarana and Waugh (2010) | Objective | NCEP-NCAR | Geopotential minimum at 250 hPa | 1979-2008 | Southern Hemisphere (50°S-20°S) |
| Reboita etl al. (2010) | Objective | NCEP-NCAR ERA-40 | Geopotential minimum at 200, 300, and 500 hPa | 1979-1999 | Southern Hemisphere (50°S-10°S) |
| Favre et al. (2012) | Objective | NCEP-DOE II | Geopotential minimum at 500 hPa | 1979-2008 | Southern Hemisphere (45°S-10°S) |
| Pinheiro et al. (2017) | Objective | ERA-Interim | Vorticity minimum at 300 hPa | 1979-2014 | Southern Hemisphere (50°S-15°S) |

Source: Author's production

The earliest climatologies of SH COLs were performed for particular regions, such as southern Africa (TALJAARD, 1985), South America (KOUSKY; GAN, 1981; LOURENÇO, 1996) and Australia (GRIFFITHS, 1999). These studies are based on relatively old datasets and manual methods using visual inspection of past available charts and satellite images. The first climatology of COLs covering the whole SH was carried out by Fuenzalida et al. (2005). They used a method that combines objective detection with visual inspection for a 31-year period (1969-1999) by using the NCEP - National Center for Atmospheric Research (NCEP-NCAR) Reanalysis (KALNAY, 1996). The COLs are initially identified using the Laplacian of the geopotential (geotrophic vorticity) at 500 hPa and after validated subjectively to guarantee the presence of a cold-core cut-off cyclone equatorward from the main westerlies. They found that COLs are more (less) frequent in winter (summer), preferentially around the main continents.

The study of Campetella and Possia (2007) presented the COL distribution for a 10-year period (1979-1988) for South America (100ºW-20ºW and 50ºS-15ºS) using the NCEP-NCAR reanalysis. The COLs were identified based on the minima of the 250-hPa geopotential (objective detection) and the cold-core and minimum thickness in the middle troposphere (subjective analysis). They found the maximum frequency in autumn, followed by winter, spring and summer, which is similar to the seasonality found by Lourenço (1996) for the same region, where the highest (lowest) frequency occurs in winter (summer).

Singleton and Reason (2007) produced a 30-year (1973-2002) climatology of 300-hPa COLs in southern Africa based on the NCEP-NCAR reanalysis. The COLs were identified subjectively based on the inspection of the geopotential field. They found the largest frequency in autumn, followed by spring, winter and summer, the same seasonality observed by the pioneering study of Taljaard (1985) for a similar domain.

Reboita et al. (2010) used the algorithm developed by Nieto et al. (2005) and adapted to the SH, which is a more sophisticated method based on three restrictive criteria: cut-off, thickness and baroclinicity. The statistics are produced for COLs at three pressure levels (200, 300, and 500 hPa) using two different reanalyses, the NCEP-NCAR and the 40-year Reanalysis of the ECMWF (ERA-40). They found that COLs are more common at

300 hPa, followed by 500 hPa and 200 hPa. The largest frequency was found in summer, autumn and winter at 200, 300 and 500 hPa, respectively. The number of identified COLs were found to be larger in ERA-40 than the NCEP-NCAR reanalysis. The seasonality was also found to differ widely between the two reanalyses, suggesting that the statistics of COLs depends critically on the quality of the datasets such as the reanalyses.

The discrepancies between the ERA-40 and NCEP-NCAR reanalysis observed in previous studies may be result from different causes, such as problems with the components of the hydrological cycle associated with the humidity analysis in ERA-40, as discussed in Bengtsson et al. (2004a). Additionally there are problems with the Australian surface pressure bogus data called PAOBS for the years 1979-1992 (http://www.cpc.ncep.noaa. gov/products/wesley/paobs/ek.letter.html) that are used for both older reanalysis of NCEP and ECMWF, although this problem affects only some variables of the reanalysis mainly south of about 40ºS-60ºS. The fact that the newer reanalyses have been produced using more modern data assimilation methods and models makes the results more confident compared to those obtained using older reanalyses.

Ndarana and Waugh (2010) produced a 30-year (1979-2008) climatology of COLs linked to RWB events, by using the NCEP-NCAR reanalysis. The method is similar to that of Nieto et al. (2005) and Reboita et al. (2010), but with a more explicit imposition of the cold-core condition. They found that COLs are more numerous in summer (maximum in December) and less frequent in winter (minimum in August). However, for the COLs linked to the RWB at 330 K, the peak is found in autumn (maximum in April), which agrees with the findings of Reboita et al. (2010) for the 300-hPa COLs.

The study of Favre et al. (2012) used a 30-year period (1979-2008) of the NCEP-DOE reanalysis to construct a climatology of the mid-tropospheric COLs in the SH. The identification is performed based on the geopotential at 500 hPa and a cold core restriction is imposed on the 500-hPa temperature field. They found that COLs are more frequent from late summer to autumn, with a maximum in March and April. In winter, COLs are less frequent but deeper than other seasons.

More recently, Pinheiro et al. (2017) performed a seasonal climatology of SH COLs for a 36-year period (1979-2014) using a more modern reanalysis product than that used in earlier studies, the ERAI reanalysis (SIMMONS et al., 2007). A wide range of statistics is used to explore the main COL features using a multi-criteria scheme based on the 300-hPa relative vorticity minima, cold-core, PV anomalies, and cut-off circulation. The maximum frequency was found in autumn, but winter has the strongest COLs. They suggest that the differences in seasonality observed between previous studies are due to uncertainties in the reanalyses as well as the method used to identify the COLs. The differences in number found between previous studies are discussed in Pinheiro et al. (2017), and the pros and cons of using more complex criteria are pointed out. In general, methods based on multiple step schemes identify fewer events than simpler methods. However, the use of multiple criteria methods allows the identification of systems presenting specific features, such as cold core and stratospheric air intrusion.

# 3 DATA AND METHODOLOGY

This chapter describes the data and methodology used to identify and analyse COLs. In the methodology, a description of the tracking algorithm and the criteria to identify COLs are described. Details of the techniques used for producing the composites and vertical structure diagnostics of COLs are also included here. Finally, the terms of the EKE budget equation are described.

The study area covers the SH between the latitudinal range of 50ºS and 15ºS (Figure 3.1). Most of the SH is covered by ocean (Pacific, Atlantic and Indian), which corresponds to about 81% of the entire area. The continental areas include South America, parts of Africa, most of Oceania (Australia and some archipelagos) and the Antarctic continent. The western part of South America has the Andes Cordillera that has a narrow width (~150-200 km) in subtropical latitudes and extends meridionally from about 53ºS to 10ºN with an average altitude of 4,000 meters. The high altitude of the Andes affects the large-scale atmospheric circulation causing disruption of the mid-latitude weather systems (SELUCHI et al., 2006). Conversely, Australia and the southern part of Africa have lower altitudes in comparison to South America. Most of the African sector is composed of an extensive plateau, located between the Atlantic and Indian Oceans. This region has in the northern boundary the Kalahari Desert. In Australia, most of the subtropical areas are composed of plains and plateaus of low altitude, where the highest altitude is the Mount Kosciuszko, in southeast Australia (2,228m).

Figure 3.1: Topographic map of altitude (m) using data from the Grid Analysis and Display System (GrADS) Data Server.

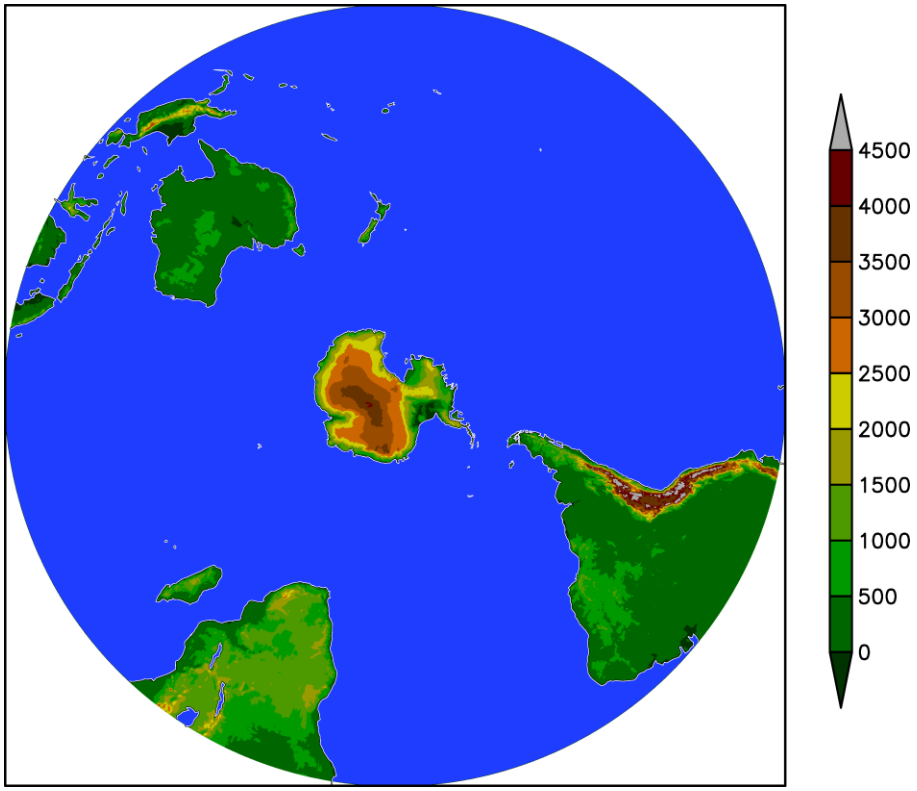


Source: author's production

## 3.1 Data

### 3.1.1 Reanalyses

The five reanalyses investigated in this study for COLs are: the European Centre for Medium-Range Weather Forecasting (ECMWF) Interim Reanalysis (ERAI) (SIMMONS et al., 2007), the National Centers for Environmental Prediction (NCEP) Couple Forecast System Reanalysis (NCEP-CFSR) (SAHA et al., 2014), the National Aeronautics and Space Administration (NASA) Modern Era Retrospective Reanalysis for Research and Applications-2 (MERRA-2) (MOLOD et al., 2015) and the two reanalyses produced by the Japanese Meteorological Agency (JRA), the 25 year (JRA-25) and 55 year (JRA-55) reanalyses (KOBAYASHI et al., 2015; ONOGI et al., 2007). Four of the datasets represent the new generation of reanalyses (ERAI, NCEP-CFSR, MERRA-2 and JRA-55), which are more recent than the reanalyses used in previous studies of COLs in the SH (FAVRE et al., 2012; NDARANA; WAUGH, 2010;

REBOITA et al., 2010), except for Pinheiro et al. (2017) who used the ERAI reanalysis. These reanalyses generally cover the modern satellite period after 1979, though JRA-55 begins in 1958. Other longer reanalyses can provide a longer time range period, such as the ECMWF twentieth century reanalysis (ERA-20C) (COMPO et al., 2011), though these are not appropriate for this study since only surface observations are assimilated which are sparse in the SH so that the reanalyses are not well constrained there. Section 5.5 shows results of the comparison between the five reanalyses for the 30-year period 1980-2009. The reason why we chose this period is because some reanalyses do not cover recent years, such as the NCEP-CFSR which is not available beyond 2010. Except for the results of comparison between different reanalyses (Section 5.5), the ERAI reanalysis will be used as a reference and the discussions will be made based upon results obtained using ERAI for the 36-year period of 1979-2014.

A brief description of each reanalysis and their component systems are given as follows:

(i) **ERAI** uses four-dimensional variational data assimilation (4D-Var) with a 12-hour analysis window to combine all available observations with a short range forecast. Output is available every 6h. It uses a spectral model for the dynamics with an N128 reduced Gaussian grid for the physics packages (corresponding to approximately 79 km or $0.75^{o}$) and 60 vertical hybrid levels, with the model top at 0.1 hPa. ERAI has an improved atmospheric model and assimilation system which reduces some of the problems found in the older ERA-40 reanalysis, in particular for the representation of the hydrological cycle (Simmons et al., 2007). Another important improvement in ERAI is the inclusion of variational bias correction for satellite radiances, which minimizes inconsistencies in the observations (DEE et al., 2011). The period covered by ERAI is from 1979 and is produced with a frozen system, i.e. with an unchanged model and assimilation system.

(ii) The **NCEP-CFSR** produced by NCEP is a global, high resolution coupled atmosphere-ocean-land surface-sea ice model that uses a 6-hour coupled forecast as the first guess. This reanalysis uses the NCEP climate forecast system (CFSv2) model (SAHA et al., 2010) at a resolution of T382 (~38 km) with 64 vertical levels from the surface to 0.26 hPa. The data assimilation system applied for the atmosphere is the three dimensional variational (3D-Var) Gridded Statistical Interpolation (GSI) system which

includes flow dependence for the background error variances (KLEIST et al., 2009), the first-order time extrapolation to the observation (RANCIC et al., 2008), as well as the variational quality control of observations (ANDERSSON; JARVINEN, 1999). The ocean component is the Geophysical Fluid Dynamics Laboratory (GFDL) Modular Ocean Model, version 4p0d (GRIFFIES et al., 2004), at a resolution of ~0.25º with 40 levels to a depth of approximately 4.5 km. The SST analysis has been produced using optimal interpolation to assimilate IR satellite SST data, and in situ data from ships and buoys. NCEP-CFSR is the only reanalysis used in this study which is fully coupled and which assimilates ocean observations as well as atmospheric observations, while the other reanalyses are atmosphere only systems that use prescribed boundary conditions of SSTs and sea ice. The ocean analysis uses the Global Ocean Data Assimilation System (GODAS) to assimilate temperature and salinity profiles at 6-hour intervals (SAHA et al., 2010). Some unprecedented aspects of CFSR are: the interactive GFDL sea-ice model with three layers, including two layers of sea ice and one layer of snow; and the assimilation of satellite radiances instead of derived profiles of fields as previously used in older reanalysis products from NCEP such as the NCEP-NCAR and NCEP-DOE reanalyses.

(iii) **MERRA-2** is the most recent global atmospheric reanalysis, released for use by the NASA Global Modeling and Assimilation Office (NASA GMAO) in 2016 (MOLOD et al., 2015), available from 1980 to the present. The atmospheric model has a grid resolution of 576 points in the longitudinal direction (0.625º) and 361 points in the latitudinal direction (0.5º) which are uniformly distributed on the cubed sphere at all latitudes, unlike the previous version MERRA (RIENECKER et al., 2011). The data assimilation system used in MERRA-2 is the Goddard Earth Observing System, version 5 (GEOS-5) (MOLOD et al., 2012; RIENECKER et al., 2008), which allows much more observations to be assimilated than in MERRA. A wide range of observations are assimilated including conventional data (e.g. radiosondes, surface land observations, aircraft reports) and satellite data (e.g. Special Sensor Microwave Imager (SSM/I), Television and Infrared Observation Satellite (TIROS) Operational Vertical Sounder (TOVS) and Advanced TOVS (ATOVS), Atmospheric Infrared Sounder (AIRS)). The MERRA-2 has substantial advances over the previous version of MERRA (RIENECKER et al., 2011), as described in Molod (2012) and Molod et al. (2015). The

improvements are attributed to changes in the model's physical parameterizations such as the increased re-evaporation of precipitation and cloud condensate, and the improved moist and turbulent processes. This reanalysis also estimates precipitation as forcing for the land surface component of the model, similar to the scheme used in Reichle et al. (2011).

(iv) **JRA-25** uses the global spectral model of the Japan Meteorological Agency (JMA) integrated at T106 horizontal resolution (~120 km or 1.25$^{o}$) with 40 vertical layers with the top level at 0.4 hPa (ONOGI et al., 2007). The data assimilation system is 3D-Var with 6-hourly cycling. In addition to conventional data, JRA-25 uses a full range of observations that includes satellite data from the TOVS and ATOVS, precipitable water and snow coverage data processed by the SSM/I, atmospheric motion vector data retrieved from geostationary satellites, with these observations also used in other reanalyses of this study. JRA-25 is expected to provide the largest contrast between reanalyses since JRA-25 is the oldest and the lowest resolution data set used in this study.

(v) **JRA-55** is the second Japanese global atmospheric reanalysis and employs 4D-Var, a new radiation scheme and forecast model and a new variational bias correction for satellite radiances data (KOBAYASHI et al., 2015). These updates have helped to reduce some of the deficiencies reported in the former JRA-25 such as the large negative temperature bias in the lower stratosphere and the dry bias in the Amazon basin. We use the early release version at a reduced resolution (1.25$^{o}$ x 1.25$^{o}$) for the period 1980-2010, although data back to 1958 is available. Another improvement of JRA-55 over JRA-25 is the introduction of greenhouse gases with time varying concentrations.

The fields used from all reanalyses for the COL tracking and identification are horizontal winds, relative (potential) vorticity, geopotential and temperature. A range of other fields on single levels (e.g. MSLP, precipitation and cloud cover) or on multiple pressure levels and potential temperature surfaces are used to examine the COL properties, such as the potential temperature, divergence, vertical velocity, specific humidity and ozone.

## 3.2 Methodology

### 3.2.1 The Tracking Algorithm

There are a number of ways of constructing a synoptic objective analysis, from the simple grid counting methods (FAVRE et al., 2012; NIETO et al., 2005), which can result in bias due to the rectangular latitude-longitude boxes distributed uniformly (TAYLOR, 1986), to more sophisticated approaches of tracking and statistical estimation on the sphere (HOSKINS; HODGES, 2002, 2005). In this study, we used the TRACK algorithm (HODGES, 1994, 1995, 1996, 1999) together with statistical outputs computed directly on the unit sphere using spherical kernel methods (HODGES, 1996) which are more appropriate for global datasets. The diagnostics for the COL spatial distribution used in this study are the track density and the mean intensity. The track density is computed using the spherical kernels and a single point from each track that is closest to the estimation point, this is then scaled to number density per season per unit area (unit area equivalent to ~$10^6$ km$^2$). The mean intensity is computed from all points along the track using the spherical kernels.

The COL identification is based on the following steps: the pre-processing filtering, the tracking, and the post-tracking filtering. A more detailed description of each step of the COL identification is given in the next section.

### 3.2.2 Identification and tracking of Cut-off Lows

The full process for identifying and tracking COLs is performed objectively in three main stages: a) pre-processing filtering, b) tracking, and c) post-tracking filtering.

a) Before the tracking, the large-scale background is removed by performing a spherical harmonic decomposition of the tracking fields and setting the coefficients of the total wavenumbers less than or equal to five to zero. This does not significantly affect fields such as the vorticity but is considered to be essential for fields such as the MSLP and geopotential (ANDERSON et al., 2003; HOSKINS; HODGES, 2002). For the 300-hPa geopotential ($Z_{300}$) the zonal mean is first removed from the data, i.e., each grid point is subtracted from its mean latitudinal value. The use of the zonal anomaly of geopotential ($Z'_{300}$) for the tracking allows the "weak" extremes to be more easily identified than in the raw geopotential. This is the case for COLs at lower latitudes, where the

geopotential gradient is typically weaker than at higher latitudes. The data are also spectrally truncated to triangular truncation 42 (T42) on a Gaussian grid for vorticity, as this is a very noisy field, whilst T63 is used for the geopotential field, similar to a previous study (PINHEIRO et al., 2017). The filtering focuses the identification on the same spatial scale for each data set which allows a fairer comparison between data with different resolutions. In general, more COLs are identified for $\xi_{300}$ than for $Z'_{300}$ even though a higher resolution data is used for $Z'_{300}$ than for $\xi_{300}$, although this could also be because less of the lifecycle is identified in the relatively short $Z'_{300}$ tracks. Similar results were found for extra-tropical cyclone numbers which is higher for $\xi_{850}$ than for MSLP at the same truncation (HODGES et al., 2003; 2011; HOSKINS; HODGES, 2002, 2005). In addition to the truncation, a spectral tapering is applied to reduce the Gibbs phenomena in exactly the same way as done in Hoskins and Sardeshmukh (1984).

b) The tracking is performed using six hourly data based on the $\boldsymbol{\xi_{300}}$ and $\boldsymbol{Z'_{300}}$ minima in order to present different perspectives. Initially the data is transformed to a polar stereographic projection at similar resolution to the truncated data, and then the grid point minima are identified and refined to the off grid locations (feature points that do not necessarily coincide with the grid point) using B-spline interpolation and steepest descent minimization to produce smoother tracks. The locations are transformed back to the spherical coordinates for the tracking.

A set of tracks is constructed using two main tracking techniques with specific constraints: the nearest neighbour approach and the optimization of a cost function (HODGES, 1999). Feature points are initially linked together using the nearest neighbour search and then refined by minimising a cost function (see Appendix A for more details on this function) for optimal track smoothness which is subject to adaptive constraints, as discussed further in this section. The use of a cost function optimization algorithm is considered to be appropriate when there are a large number of systems per frame. This is more useful especially for global analysis using high resolution data. The nearest neighbour search implies that one point of a track is linked to the nearest grid point for the next time step. However, a possible problem is that the neighbour point

might be another system, resulting in a wrong association. An example of this issue is illustrated in Hodges (1999) in his Figure 1.

In the present study, the COL identification and tracking follow the same method used in Pinheiro et al. (2017) but with some modifications in terms of displacement distances and smoothness. The new modifications concern the implementation of the adaptive tracking constraints, as described in Hodges (1999). These are determined taking into account the type of motion for the observed systems of interest, supported by a limited sensitivity study which showed the different possible matches for the COL tracks. A comparison of the adaptive constraints used in Pinheiro et al. (2017) and in the present study shows the differences in values for each version of the method, as specified in Tables 3.1 and 3.2, respectively.

Table 3.1: Adaptive constraints used in Pinheiro et al. (2017).

| Zonal upper-bound displacements | | | | |
|---|---|---|---|---|
| Zones | 1 | 2 | 3 | |
| Lower (degrees latitude) | -90.0 | -20.0 | 20.0 | |
| Upper (degrees latitude) | -20.0 | 20.0 | 90.0 | |
| $d_{max}$ (degrees) | 6.0 | 3.0 | 6.0 | |
| Adaptive track smoothness | | | | |
| $\bar{d}$ (degrees) | 1.0 | 2.0 | 5.0 | > 8.0 |
| $\psi_{max}$ $(\bar{d})$ | 1.0 | 0.3 | 0.1 | 0.01 |

Source: author's production

Table 3.2: Adaptive constraints used in the present study.

| Zonal upper-bound displacements | | | | |
|---|---|---|---|---|
| Zones | 1 | 2 | 3 | |
| Lower (degrees latitude) | -90.0 | -15.0 | 20.0 | |
| Upper (degrees latitude) | -15.0 | 20.0 | 90.0 | |
| $d_{max}$ (degrees) | 3.0 | 3.5 | 3.0 | |
| Adaptive track smoothness | | | | |
| $\bar{d}$ (degrees) | 1.0 | 3.0 | 6.0 | > 8.0 |
| $\psi_{max}$ $(\bar{d})$ | 1.0 | 0.3 | 0.1 | 0.01 |

Source: author's production

The upper-bound displacement ($\boldsymbol{d_{max}}$) denotes the maximum allowed displacement in a time step in a specific zone generally defined for a latitudinal range, though this could be used to vary with longitude, if required. For the purpose of this study, $\boldsymbol{d_{max}}$ was set at 3.0. This threshold is much smaller than that used in Pinheiro et al. (2017) and is similar to those values generally used to track tropical storms which include depressions and cyclones. An example of $\boldsymbol{d_{max}}$ values used for a tropical application is given in Table 1 of Hodges (1999). Although the use of adaptive constraints helps to reduce the clutter due to the differences in features, there are some systems that do not satisfy the constraints, resulting in unrealistic or spurious tracking. If we make the $\boldsymbol{d_{max}}$ too large, larger changes in velocity would be allowed which could result in incorrect tracking. For example, using $\boldsymbol{d_{max} = 5^o}$ we find some tracks in which a COL weakens at a certain time and intensifies in the next time step, leading to a new COL genesis from the same pre-existing upper-level trough, making the detected track longer than the observed COLs. This explains the larger mean lifetime for the detected $\boldsymbol{\xi_{300}}$ COLs in Pinheiro et al. (2017) (7.3 days) compared to the detected $\boldsymbol{\xi_{300}}$ COLs in the present study (4.1 days). The implementation of new constraints, which are found to be more appropriate for the observed COL motion, makes the tracks closer to the typical observed tracks by excluding possibly more "merged systems" as well as more mobile earlier or later stages of the COL lifecycle. There is no restriction for the minimum displacement distance, but tracks must last at least 24h in order to exclude very short lifecycles.

The track smoothness constraint is measured in terms of changes in direction and speed. This is achieved by specifying values for the upper-bound track smoothness constraint ($\boldsymbol{\psi_{max}}$) which is a function of the mean displacement distances over three time steps. The smoothness constraint is applied adaptively together with the displacement constraint, varying with the local mean separation distance on a track. The values used for the $\boldsymbol{\psi_{max}}$ and for the average displacement over three frames ($\boldsymbol{\bar{d}}$) in each method are shown in Tables 3.1 and 3.2. These values are found to be suitable for the purpose of this study. The smoothness constraint is less restrictive at smaller distances between the track points (and vice-versa). For slow-moving systems, for example, larger changes in velocity (speed and/or direction) are expected to occur in a time step in comparison to faster moving systems.

The potential COLs in the SH are identified as features lower than -1.0 x $10^{-5}$ $s^{-1}$ for $\boldsymbol{\xi_{300}}$ and -50 geopotential meters (gpm) for $\boldsymbol{Z'_{300}}$. Results indicate that the number of tracks obtained are sensitive to these thresholds. In general, increasing the magnitude of these thresholds (making them more negative) reduces the lifetime and the number of COLs detected. In this study the vorticity is the preferred field for the tracking because more systems are identified using $\boldsymbol{\xi_{300}}$ than $\boldsymbol{Z'_{300}}$. A typical problem with vorticity is it is a very noisy field at high resolutions, but the spectral filtering reduces the noise. A particular observation is that the method detects longer tracks using vorticity than those observed in previous studies using geopotential, as the vorticity allows systems to be identified earlier. These differences are minimized when using the cut-off stage instead of the full life cycle. The former counts the time interval between the first and end time steps sampling a cyclonic centre (cut-off stage), and this results similar lifetimes between $\boldsymbol{\xi_{300}}$ and $\boldsymbol{Z'_{300}}$ tracks (more details in Section 4.1).

c) To identify the COLs from amongst all tracked systems additional fields are added to the tracks. The additional field information is used in the post-tracking filtering aimed at detecting a cut-off circulation by sampling along the tracks at one or more offset points from the $\xi_{300}$ or $Z'_{300}$ minima. This is done by referencing the horizontal wind components (u, v) to the tracks at a fixed radial distance of 5° (geodesic distance) from the COL centre in several directions relative to the centre. Similar filters have been previously used as a means of identifying upper tropospheric vortices (COSTA, 2009;

MORAIS, 2016; NIETO et al., 2005). This is accomplished by verifying the sensitivity to three types of filters in detecting the cut-off formation, as shown in Figure 3.2 and described as follows:

- Single-point filter: uses a single sample of zonal wind at a single offset point (similar to Nieto's algorithm) located at 180° relative to the North (Figure 3.2a) where the radial distance is 5º from the $\xi_{300}$ or $Z'_{300}$ minima. If the sample value is negative (easterly direction) for four consecutive steps (1 day), this track is considered a potential COL.
- Four-point filter: uses two samples for each zonal and meridional direction at the four different offset points of 0° (u> 0), 90° (v <0), 180° (u <0), and 270° (v> 0) relative to the North (Figure 3.2b). The radial distance is set as 5º from the $\xi_{300}$ or $Z_{300}$ minima.
- Eight-point filter: uses four samples for each zonal and meridional direction at the four different offset points of 45º (u> 0, v <0), 135º (u <0, v <0), 225º (u <0, v> 0), and 315º (u> 0, v> 0) relative to the North (Figure 3.2c) where the radial distance is 5º from the $\xi_{300}$ or $Z_{300}$ minima.

Figure 3.2: Two-dimensional schematic representation of the horizontal winds in the identification of Southern Hemisphere Cut-off Lows using the a) single-point filter, b) four-points filter, and c) eight-points filter.

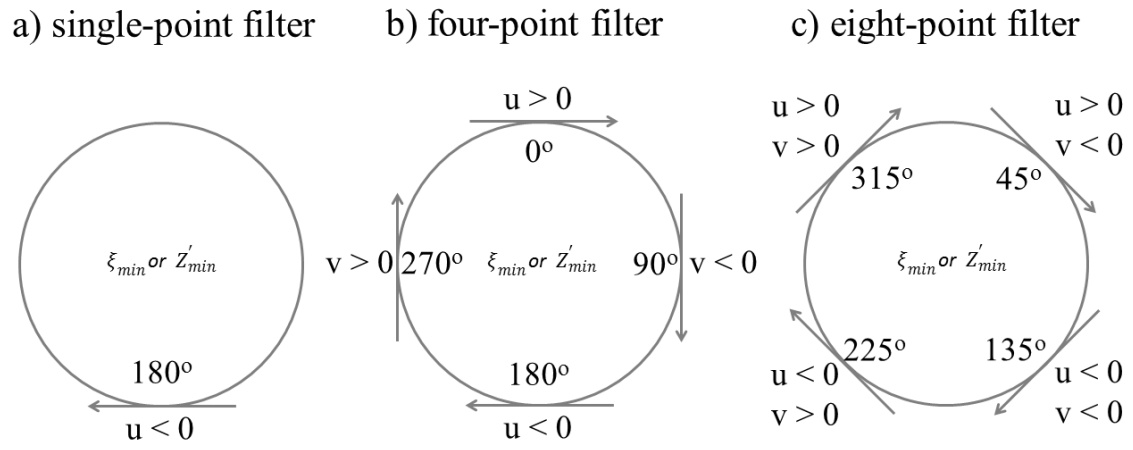


The centre of the spherical cap represents the $\xi_{300}$ or $Z'_{300}$ minimum. Positive and negative values determine the direction of the horizontal wind components (u, v).

Source: author's production.

The four-point and eight-point filters are similar to the criteria used in Coutinho et al. (2010) to identify upper tropospheric cyclones in Northeast Brazil. The track filtering methods described above are applied independently to detect a closed low associated with a $\xi_{300}$ or $Z'_{300}$ minima in the SH, but the eight-point filter is found to be a much more stricter set of criteria than the other filters, since this requires the conditions to be imposed for a greater number of conditions. One problem that concerns the use of the more stricter criteria is that the large-scale circulation varies through the lifecycle, resulting in problems of using fixed criteria. For example, we often find that many of the observed COLs present an elongated trough with significant westward tilt during the early stages of their lifecycle. This problem is illustrated in Figure 3.3 for a Cut-off Low event in South America in two different stages. During the formation (Figure 3.3a), the minimum identified by the method (represented by the symbol "x" in red color) is far offset from the COL centre due to the shear component associated with the upper-level flow, as discussed in Bell and Keyser (1993). On the other hand, objective methods work much better for COLs with more symmetric circulation which is more often found in the mature stage, as shown in Figure 3.3b. The problem described above is minimized by using simpler criteria such as the one-point or four-point filters. For the

four-point filter, in particular, the conditions are not imposed at the same times which make the criteria more flexible. Although it was found that simpler criteria are a good compromise for the identification, some COLs (e.g. short lifetime systems) may not satisfy the criteria even using the simplest methods. One consequence of the shear component effect described above is a larger uncertainty of the mean separation distance for $\xi_{300}$ COLs compared to $Z'_{300}$ COLs, and this aspect will be discussed in Chapter 5.

Figure 3.3: An example of a 300-hPa Cut-off Low identified by the method for an a) earlier stage (18Z 13 Apr 2010) and b) later stage (18Z 15 Apr 2010) of the life cycle.

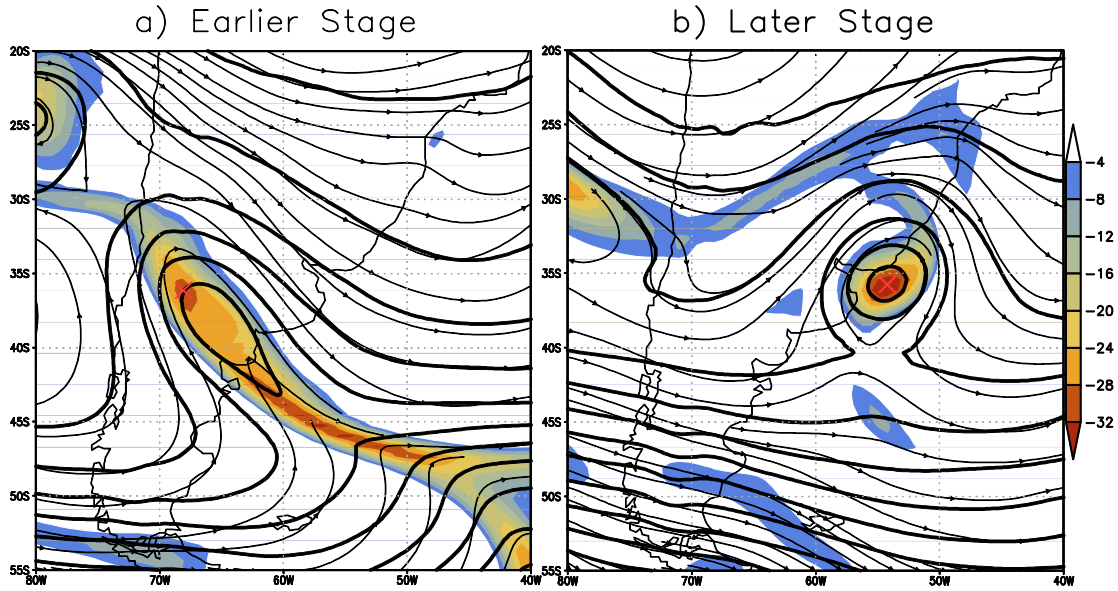


Fields refer to the 300-hPa level for geopotential height for interval contour of 50 gpm (thick line), wind streamlines (thin line), and relative vorticity scale by $10^{-5}$ $s^{-1}$ (shaded). The red color multiplication signs represent the minima identified by method.

Source: author's production.

Previous studies have shown there are two main belts where cyclonic systems are found in the SH: one region is associated with higher latitude disturbances and the other is located more equatorward, as shown in Sinclair (1994) and Hoskins and Hodges (2005). To retain only the tracks located at the more northerly latitudes, the method select only those tracks that move northward and reach at least 40ºS or have their genesis north of 40ºS. This restriction was not used in the original version of the method (PINHEIRO, 2010) and has been introduced to avoid the numerous higher latitude vortices. This

additional criterion does not discriminate between COLs that are essentially formed at upper levels and those associated with frontal occlusions, because it is difficult to separate these using objective methods. In fact, there are no criteria to clearly distinguish the upper-level COLs from those originating with a frontal system since most of the two types of COLs have similar physical characteristics such as a cold centre in the upper troposphere (PINHEIRO, 2010). Additionally, all the tracks that are north of 15ºS are also excluded from this analysis to reject tropical cyclonic vortices (KOUSKY; GAN, 1981).

### 3.2.3 Identification using multiple step schemes

Previous studies show there are various methodologies to identify COLs. The impact of using multiple criteria schemes is investigated here. This additional analysis has been performed by considering PV and temperature as criteria for COL detection. These variables have been widely investigated in case studies (GARREAUD; FUENZALIDA, 2007; LLASAT et al., 2007; SATYAMURTY; SELUCHI, 2007), and used as a tracer to identify COLs (PINHEIRO et al., 2017; WERNLI; SPRENGER, 2007). The analysis is performed on each variable adding one-by-one PV and temperature, as illustrated in Figure 3.4. This allows us to verify how each parameter as well as their combination affects the COL identification. The full set of criteria is exactly the same as used in Pinheiro et al. (2017), where the COL tracks are referenced to zonal anomalies of the 300-hPa PV ($PV_{300}$) and the 300-hPa temperature ($T_{300}$) by searching for the minimum value over a spherical cap region of 5º centered on the $\xi_{300}$ minima. Tracks with $T_{300}$ values lower than -3 Kelvin and $PV_{300}$ values lower than -2 PVU (1 PVU = $10^{-6}$ $m^2$ $s^{-1}$ K $kg^{-1}$) for at least four consecutive steps (1 day) are retained. Additionally, an easterly wind (defined for the zonal wind values lower than -8 m/s) must occur at 5º south from the $\xi_{300}$ minima. A potential COL is defined using a multiple step scheme when the steps described above are satisfied.

Figure 3.4: Flowchart of the methods based on the parameters U (zonal wind), T (temperature), and PV (potential vorticity) at the 300-hPa level.

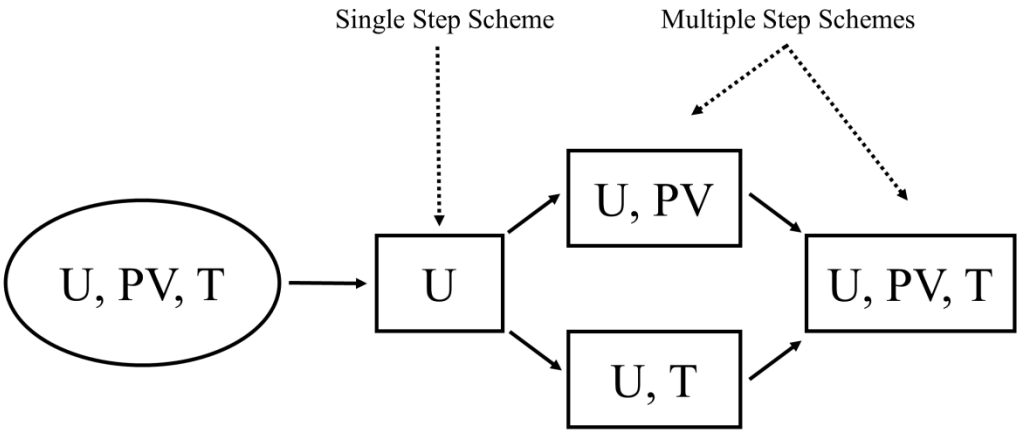


Source: author's production.

### 3.2.4 Method to determine the vertical depth of a Cut-off Low

A new approach is introduced to obtain the vertical depth of COLs by matching the same cyclonic systems between different pressure levels. This is done by first tracking the vorticity minima at a number of levels down to the surface or the lowest pressure level where the match is found. The track matching algorithm is then used to find a corresponding cyclonic centre in the next level down by applying a prescribed value for the mean separation distance and overlaps in time for the corresponding points between the tracks, similar to previous studies to compare tracks between different datasets (BENGTSSON et al., 2009; HODGES et al., 2003; 2011, 2017). There is no constraints on the separation of levels for consecutive levels in the matching The percentage of the number of points that overlap in time is computed using the approach described in Hodges et al. (2003) which defines the formula $\chi = 100[2n_m/(n_1 + n_2)]$, where $n_m$ is the number of points that match in time, and $n_1$ and $n_2$ are the number of points in the track corresponding to different pressure levels, such as the $\xi_{300}$ and $\xi_{400}$ tracks. The track matching between pressure levels are not applied for the same times, because the matches between tracks corresponding to different layers generally occur in different stages of the COL lifecycle. Such aspect will be discussed further in this section and in Chapter 4. The sensitivity of different values for the mean separation distance and the temporal overlap for the vertical depth of COLs will be assessed through verifying the

impact of different choices of either of these two parameters. The procedure to determine the vertical extent of the COL is illustrated in Figure 3.5, and is described in detail as follows:

1) The T42 vorticity tracking is performed at eight pressure levels (1000, 900, 800, 700, 600, 500, 400 and 300 hPa) in the same way and using the same threshold as used in the $\xi_{300}$ tracking (-1.0 x $10^{-5}$ $s^{-1}$). The tracks are then filtered by the wind filtering illustrated in Figure 3.2b to retain only the cyclonic centres generally seen in geopotential maps. Finally, only the tracks that move equatorward and reach latitudes north of 40°S or have their genesis north of 40°S are accepted by the method in order to reject the higher latitude vortices. Also, the COLs with lifetime smaller than 24h are excluded.

2) The track matching algorithm is applied starting at the highest pressure level. If the mean separation distance is less than 5° and overlap in time is by at least 1% of the combined number of track points, the $\xi_{400}$ matched track is retained for next stage. This means the matches between the $\xi_{300}$ and $\xi_{400}$ belong to the same system, but they are at different levels, i.e., the cyclonic system vertically extends over the two pressure levels. Otherwise, the system is labeled as a COL confined at 300 hPa, represented by the non-matched $\xi_{300}$ tracks.

3) Similarly, the tracks retained in the previous step are matched against the next level down, i.e. the $\xi_{400}$ tracks are matched to the $\xi_{500}$ tracks using the same criteria and thresholds. The matches found in this step are stored for the next step, while the non-matches are the COLs that do not extend lower than the 400 hPa level. The overlap threshold, chosen to be 1%, ensures that the matches occur for at least a single time step because the matches eventually can occur in the late stage of the COL life cycle, in particular for matches in the lower levels.

4) This procedure is performed in the same way for the next level down, and so on until the 1000-hPa level or the pressure level where the last match occurs. Hence, the vertical depth of a COL is defined by the lowest pressure level where the last match is found.

Figure 3.5: Flowchart of the approach to obtain the vertical depth of a Cut-off Low.

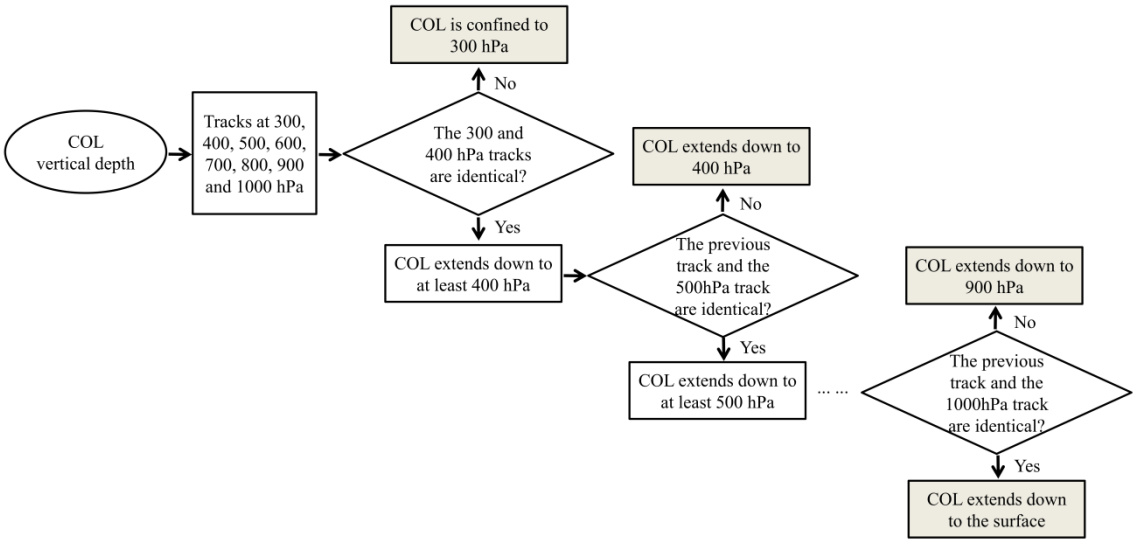


Source: author's production.

The main advantage of the method introduced here is that the vorticity tracking at different pressure levels is not too sensitive to the threshold chosen, as is the case for the geopotential. The method used by Porcù et al. (2007) to obtain the vertical depth of COLs uses geopotential for the tracking, so that the search of the geopotential minima is performed using different thresholds for different levels as the magnitude of geopotential increases with height.

Since our method retains only the tracks that have the mean separation distance less than 5º, it is expected that the vertical tilt between the $\xi_{300}$ and $\xi_{1000}$ minima does not exceed the horizontal mean separation distance of 5º as most of COLs exhibits an almost barotropic structure. Such evidence will be confirmed by the result of the COL vertical tilt presented in Chapter 6. This is important to avoid matching different systems that may be the case when the vorticity is used for the tracking as this variable tends to focus on small spatial scales compared to geopotential. The reason for the time overlap chosen for matching is that COLs generally intensify from upper to lower levels, reaching the surface at a late stage of their life cycle. This means that if we choose a relatively high value for time overlap, some deep COLs that reach lower levels in late stages will likely be missed as a consequence of the too strict criterion, whereas using a low value for time overlap (e.g. 1%) implies the method is more flexible to

capture most of the COL lifecycle. The sensitivity of estimating the COL depth will be discussed in detail in the next chapter.

### 3.2.5 Types of Cut-off Lows based on intensity and vertical depth

COLs can be classified in different ways such as intensity, vertical depth, and duration. To investigate how intensity and vertical depth are related to each other and how they affect the structure and evolution of COLs, the systems identified by the algorithm are divided into three categories according to their intensity and vertical depth. The strength of COLs is obtained based on the $\xi_{300}$ (scaled by -1) as follows:

a) **Weak**: the $\xi_{300}$ maximum along a track is lower than 10.5 x $10^{-5}$ $s^{-1}$.

b) **Moderate**: the $\xi_{300}$ maximum along a track is in the range between 10.5 x $10^{-5}$ $s^{-1}$ and 13.5 x $10^{-5}$ $s^{-1}$.

c) **Strong**: the $\xi_{300}$ maximum along a track is greater than 13.5 x $10^{-5}$ $s^{-1}$.

Besides the fact that the COL tracking is performed at 300 hPa, the peak intensity is measured at the same level where COLs reach their maximum intensity (i.e. 300 hPa). This aspect will be discussed in detail in Chapter 6. The thresholds for $\xi_{300}$ were chosen in order to separate the total number of COLs into groups with similar number, which is important for the production of composites and their comparison, which will be shown in Chapter 7.

The vertical depth of COLs is obtained for different regions as well as for the entire hemisphere. This allows us to see the differences of the vertical structure of COLs between different regions in the SH. The three categories of COLs are defined according to the vertical layer extent organized as follows:

a) **Shallow**: cyclonic centres are confined to 300 hPa or extend vertically downward to 400 hPa.
b) **Medium**: cyclonic centres extend vertically downward to 500 hPa or 600 hPa.
c) **Deep**: cyclonic centres extend vertically downward to 700 hPa, 800 hPa, 900 hPa, or 1000 hPa.

This combination of the chosen levels is somewhat arbitrary, though this could be defined by a histogram in terms of percentiles. The analysis is performed for each intensity and vertical depth group, but the discussion will be focused only on the strong and weak COLs as well as the deep and shallow COLs. We decided to leave out the intermediary groups to show the main differences between the strong/deep and weak/shallow COLs.

### 3.2.6 Compositing methodology

To investigate the typical life cycle and structure of COLs a compositing methodology is used similar to previous studies on tropical cyclones (BENGTSSON et al., 2009) and extratropical cyclones (BENGTSSON et al., 2007; CATTO et al., 2010; DACRE et al., 2012; GUIA, 2010). Firstly, the COLs are identified and selected according to their intensity and vertical depth for the period from 1979 to 2014 as discussed above. The composites will show regional and hemispheric features, produced by selecting the COLs as described below:

a) Hemispheric analysis: the compositing is restricted to the 200 most intense COLs in the SH. The composites were produced using the tracks by matching the identically same COLs between the $\xi_{300}$ and $Z_{300}$ to give a general perspective on the COL structure in the SH. The same COLs are identified by matching the tracks with the mean separation distance less than 4º and overlap in time is by at least 50% of the track points. An extensive analysis of structure and evolution of the strongest COLs are presented in Chapter 6.

b) Regional analysis: the compositing is performed for those tracks whose genesis occurs within a 10º (geodesic) spherical cap centered on specific locations of maxima in genesis density, such as seen in surrounding areas of Australia, Africa and South America as shown in Pinheiro et al. (2017) in their Figure 7. However, this work will focus mainly on the COLs that affect South America, particularly for those with their genesis occurring in the Pacific in a region off Chile (34.5ºS/80.0ºW). The tracks are extracted within a circle of 10º centered on this region (total number is 803 COLs). The composites were constructed separately according to intensity and vertical depth of COLs (defined in Section

3.2.5), and the results are shown in Chapter 7. An additional analysis is performed where the Pacific COLs are contrasted with the Atlantic COLs, i.e. those whose genesis occurred within an arc radius of 10° centered on 35.0°S/80.0°W (total number is 611 COLs). This analysis is done in respect of the EKE, shown in Chapter 8. Therefore, the aims of the regional compositing analysis are twofold: to examine the COL structure for the COLs selected by intensity and vertical depth for the COLs formed in the Pacific, in particular for those that reach the Andes Cordillera, and how the mountains affect the COL structure and precipitation. The other analysis is of interest to examine the mechanisms that dynamically affect the Atlantic and Pacific austral COLs.

The second step in the compositing is to determine the specific time in the COL life cycle used to extract the required field for compositing. In this study, we will consider the time of maximum intensity of COLs, although this may also be done based on the time of maximum precipitation or growth rate. Thus, each COL is centered on the time when the $\xi_{300}$ and $Z'_{300}$ minima are found along each track. Lastly, single level fields such as precipitation, or multi-level fields such as winds are extracted on to a radial grid with maximum radius of 15° centered on the COL centres which is suitable for capturing the COL synoptic features. Because the composites are produced directly on the sphere in a radial coordinate, biases are reduced as compared to composites produced using a latitude-longitude projection. COLs are not rotated to the same direction as done in previous works for extratropical cyclones (e.g. BENGTSSON et al., 2007), as this allows us to view the COL horizontal tilt during its development. A more detailed description of the approach used to produce the composites is given in the appendix of Bengtsson et al. (2007) and the paper of Catto et al. (2010).

The same compositing scheme is used to examine the COL lifecycle by identifying a specific offset time relative to the time of maximum intensity. This is achieved in two ways, by using spatial composites or single-value properties. The former captures specific fields at different stages along the lifecycle, in exactly the same way as described above. The second approach uses single-value variables averaged within some prescribed radius of the COL centre to give a composite lifecycle of the intensity. Here the total lifetime is used for the compositing, computed from the genesis to the

lysis time, which is appropriate for verifying what occurs before and after the time of maximum intensity. The regional composites for the COLs formed in the southeastern Pacific are produced by centering on the time when the COLs cross the Andes, allowing us to verify what happens when COLs are either west or east of the Andes by applying an offset relative to the time they are over the Andes.

### 3.2.7 Energetics of Cut-off Lows

The main mechanisms associated with COL development are analysed here using the EKE equation developed by Orlanski and Katzfey (1991) and modified by Chang (2000). This is done by partitioning the processes associated with the COL development into mean flow and perturbations (eddies), and then analysing individually the components of the EKE. This approach considers the most important processes for the evolution of mid-latitude disturbances such as the baroclinic and the barotropic instabilities, and the downstream development (DSD) (Orlanski and Sheldon, 1995). The EKE terms are represented in Equation 3.1 and described below:

$$\frac{\partial K'}{\partial t} = -\nabla.\vec{V}K' - \nabla.\overrightarrow{V_a'}\phi' - \omega'\alpha' - \overrightarrow{V'}.\left(\overrightarrow{V_3'}.\nabla_3\right)\overrightarrow{\overline{V}} + \overrightarrow{V'}.\overrightarrow{\left(\overrightarrow{V_3'}.\nabla_3\right)V'} - \frac{\partial}{\partial p}\omega K' - \frac{\partial}{\partial p}\omega'\phi' + RES \quad (3.1)$$

In Eq. 3.1, $K$ represents the kinetic energy, $\alpha$ the specific volume, $\vec{V}$ the horizontal wind, $\phi$ the geopotential, $\omega$ the vertical velocity, and $p$ the surface pressure. The overbar denotes the time-mean flow calculated for each season (MAM, JJA, SON and DJF) averaged over ~90 days for the 6-hourly data, similar to the time-mean used in Chang (2000). Alternatively, time-mean could be calculated using a shorter time mean such as in Gan and Piva (2013), or a spatial (zonal) mean such as in Orlanski and Sheldon (1993). The primes represent the terms associated with the eddies (which refer to the deviation from the mean state), the superscript 3 the three-dimensional vector, and the subscript $a$ the ageostrophic component.

The term on the left-hand side of Eq. 3.1 is the local tendency of EKE. The first term on the right-hand side is the EKE flux convergence (KFC) which is associated with advective fluxes (CHANG, 2000). The 2nd term is the ageostrophic flux convergence

(AFC) due to the transfer of energy through the wave dispersion, the so-called DSD (CHANG, 1993). The 3rd term is the baroclinic conversion (BRC) that is associated with the thermally-direct circulation with warm air rising and cold air sinking. The 4th and 5th terms are the Reynolds stress or barotropic conversion (BRT), which are associated with the horizontal wind shear. This mechanism normally contributes to extract energy from the mid-latitude disturbances, i.e. it is directly related to the system dissipation. The 6th and 7th terms are the vertical energy fluxes through the lower and upper boundaries. The 8th term is the budget residual representing the mechanisms not explained in equation 3.1, such as friction, diabatic effects, sub-grid flows and errors introduced by numerical methods, such as interpolation and finite differences.

The tendency of EKE can be calculated using two different methods: the first one uses a centered-time difference between the previous and subsequent time steps on the left-hand side (lhs) of Eq. 3.1, resulting in 12-h differences in EKE. As an alternative to this, a shorter time difference could be calculated by averaging the previous and subsequent time steps with the central time step, but this would require an additional computation. The other way to compute the tendency is by summing all the terms on the right-hand side (rhs) of Eq. 3.1, except the $RES$ term. Note that this is done using all the terms rather than only the dominant terms. In Chang (2000) the first and second methods are called observed and computed tendency, respectively. The $RES$ can be estimated by the difference between the two methods described above, i.e. the lhs minus the rhs.

There are other processes that are not considered here, such as the energy fluxes due to the volume integration displacement and the variation of the mass in the volume. The area of the cylinder used for the calculations is considered to be fixed at a prescribed radius, so the terms regarding to the volume are negligible. A problem concerning the volume used to calculate the quantities is the fact that there are variations in the horizontal dimension between different COLs, resulting in complications when using a fixed volume. However, the differences in structure between COLs tend to be smoothed out by the large number of systems used in the compositing.

Previous studies have used a vertically-integrated approach to examine the energetic components, such as Orlanski and Katzfey (1991), Piva et al. (2010), Gan and Piva (2013), among others. In this study we used this approach but also calculated the EKE

averaged between different levels, expressed per unit mass. This allows us to examine how each term of the EKE equation behaves in specific tropospheric layers. The vertically integrated quantities are calculated using 10 pressure levels from the 1000-hPa level or surface to the top level (100 hPa), where the surface depends on the topography obtained from the reanalysis. This is particularly important over the mountain areas such as the Andes, implying that the energy is computed only above the surface. For the calculations involving the vertically integrated energy, we do not use the mass (area) weighted average as in most of previous studies. Despite the variations of the tropospheric mass with latitude and orography, the vertically integrated EKE distribution for an individual case (Figure 3.6a) is very similar to that using the mass weighted field (Figure 3.6b). The former is the total energy expressed in Joules, while the latter is the total energy divided by the air-mass into a vertical column for each grid, expressed in $m^2.s^{-3}$. Because the distributions are quite similar between the two fields, we decided to use the non mass weighted average to compute the vertically integrated terms.

Figure 3.6: Vertically integrated Eddy Kinetic Energy (EKE) for a Cut-off Low in the southeast Pacific using a) EKE and b) EKE mass weighted average.

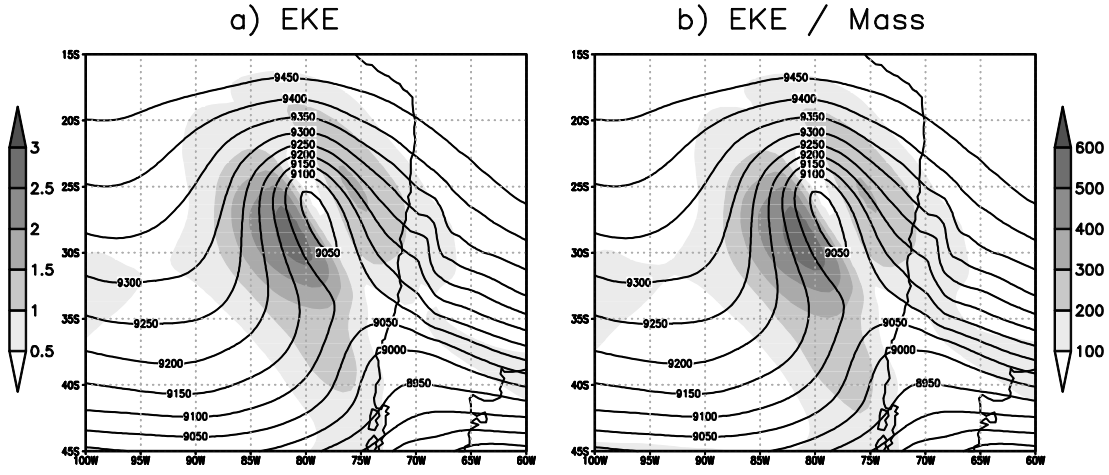


$Z_{300}$ in gpm (solid line), EKE in shaded. Analysis performed using the ERAI reanalysis at 18Z 12 September 2014.

Source: author's production.

The EKE terms are computed for the most intense COLs in the SH, and for COLs formed in specific regions such as in the southeast Pacific and southwest Atlantic (see Section 3.2.6). The same approach was used to investigate the differences from the

strong/deep COLs to the weak/shallow COLs. Perhaps the main difference between the approach used in this study and those used in previous studies is that we use an objective method to identify and track the system of interest, so that the energetics are computed directly over the COL centre, avoiding subjective decisions on the system location. Moreover, the algorithm facilitates using a larger number of systems for the compositing in comparison to manual procedures used to create composites (DANIELSON et al., 2004; GAN; PIVA, 2016).

# 4 VALIDATION AND SENSITIVITY ANALYSIS

This chapter discusses the use of different methodologies to identify COLs. The validation of the post-tracking filtering is divided into two steps. Firstly, the three schemes to separate cut-off lows from open troughs are examined by sampling at different offset radial distances from the cyclone centres (Section 4.1). Also, the sensitivity of identifying COLs using multiple criteria is analyzed in terms of number, seasonality and intensity. Four methods are constructed by combining PV and temperature criteria (Section 4.2). Lastly, a new methodology is used to determine the vertical depth of COLs based on the track matching algorithm (Section 4.3). The analysis presented in this chapter uses the $\xi_{300}$ for the tracking, because the method using this field identifies more COLs than that using the $Z'_{300}$.

## 4.1 Cut-off Low detection

The three different schemes used to separate COLs from upper level troughs, defined in Section 3.2.2, are analysed and discussed here. For the whole period from 1979 to 2014, 540 tracks per year were identified using the single-point filter, 519 tracks with the four-point filter, and 300 tracks with the eight-point filter. Note that the numbers of the detected tracks using the single-point and the four-point filters are similar, however, there is a significant reduction in number of identified COLs for the eight-point filter. This reduction is due to the greater number of constraints, i.e., the larger the restriction the smaller the sample size. A particular issue concerning the use of the eight-point filter occurs when the trough axis tilt is pronounced, generally seen in the earlier stages of the lifecycle, so that the criterion does not fit the upper-level flow associated with a COL. This is typical example of problem that could be more accurately diagnosed using machine learning methods based on recognition pattern techniques. For example, such type of method could offer the possibility to apply a filter that rotates in such a way that it matches the tilt.

The comparison between the three filtering methods is also performed by matching the same tracks as done in Hodges et al. (2003). The tracks are compared using a prescribed value for the mean separation distances, chosen here to be $4^{o}$ geodesic, and overlaps in time by at least 50% of the track points. The largest number of matches is observed between the single-point and the four-point filters (398 tracks per year), which

corresponds to approximately 74% and 77% of the total tracks found in the single-point and the four-point filters, respectively. Comparing the single-point and the eight-point filters, there is a much lower number of matches (244 tracks per year), equivalent to 45% and 81% of the tracks found in the single-point and the eight-point filters, respectively. Finally, the comparison between the four-point and the eight-point filters has 280 matches yearly, which corresponds to 54% and 94% of the tracks observed in the four-point and the eight-point filters, respectively. Surprisingly, the number of matches does not increase for the most intense COLs for each filter, as is the case for the comparison of extratropical cyclones between different reanalyses (HODGES et al., 2011). This means the choice of the filtering method to detect cut-off lows does not affect the distribution of the COL intensities, i.e. the matches occur similarly for both strong and weak systems.

The comparison between the three filtering methods is also performed by analysing the maximum intensity distributions of the 300-hPa COLs, determined by finding the $\xi_{300}$ maximum (scaled by -1) along the detected tracks for each filter, and shown in Figure 4.1. The $\xi_{300}$ maxima are determined searching for the maximum value within 5.0$^{o}$ geodesic radius centered on the 300-hPa COL centre. It is apparent that there is a similar intensity distribution for each of the filters, which have the maximum frequency and number for values around 10 x $10^{-5}$ $s^{-1}$. The extreme tails shown in the top inset graph in terms of frequency (Figure 4.1a) show the tail is marginally longer in the eight-point filter than in other filters. However, the difference in number in respect of the extreme tails (Figure 4.1b) is not significant among the filters. The conclusion is that although there are substantial differences in number, particularly with respect to the eight-point filter, the intensity distribution is similar for each filter. Therefore, the choice of the method to detect the cut-off circulation does not affect the type of detected system.

The visual inspection of the $Z_{300}$ maps (figure not shown) shows that the highest number of COLs is observed in the single-point filter, followed in that order by the four-point and eight-point filters. This means that the single-point filter detects more COLs than the other schemes, but it also detects some upper tropospheric troughs. About 20% of the tracks identified in the single-point filter do not have an associated closed circulation in $Z_{300}$. The results of the four-point filter are similar to the single-

point filter, although the former identifies less troughs than the latter. The eight-point filter retains fewer troughs than the other schemes, but excludes many COLs. This happens, for example, when the axis of the COL tilts westward in the horizontal maps.

Figure 4.1: a) Frequency and b) number distributions for the maximum intensity of the 300-hPa Cut-off Lows obtained with the single-point filter, four-point filter, and eight-point filter.

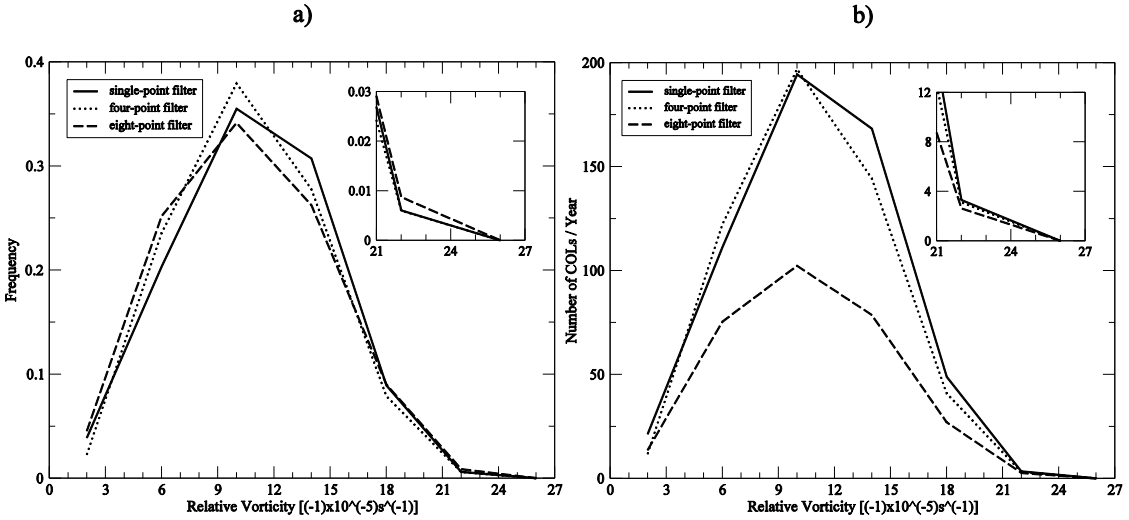


Maximum intensity based on the $\xi_{300}$ scaled by -1 for the single-point filter (solid line), four-point filter (dotted line), and eight-point filter (dashed line). Analysis performed using the ERAI reanalysis for a 36-yr period (1979-2014). The insets represents the high-intensity tails. Unit is $s^{-1}$.

Source: author's production.

By imposing the criteria along the whole track, instead of determining whether four consecutive points satisfy the criteria, it is possible to calculate the time associated with the cut-off stage that starts when the upper tropospheric low becomes completely detached (tear-off) from the westerly winds. If a discontinuity occurs along the track, only the longer part of the track is counted to avoid double counting. Figure 4.2 shows the distribution of COL lifetimes with most COLs lasting one or two days during the cut-off stage, although a few tracks persist for more than 10 days. This result is observed for both $\xi_{300}$ and $Z'_{300}$ tracks. The mean lifetime of the cut-off stage is exactly the same for the $\xi_{300}$ and $Z'_{300}$ COLs (i.e. ~2.9 days), similar to the mean lifetime found in previous studies using geopotential for the COL tracking (CAMPETELLA; POSSIA, 2007; FUENZALIDA et al., 2005; REBOITA et al., 2010).

Figure 4.2: Lifetime distribution in number for the total and cut-off stages identified by the $\xi_{300}$ and $Z'_{300}$ Cut-off Lows in the Southern Hemisphere.

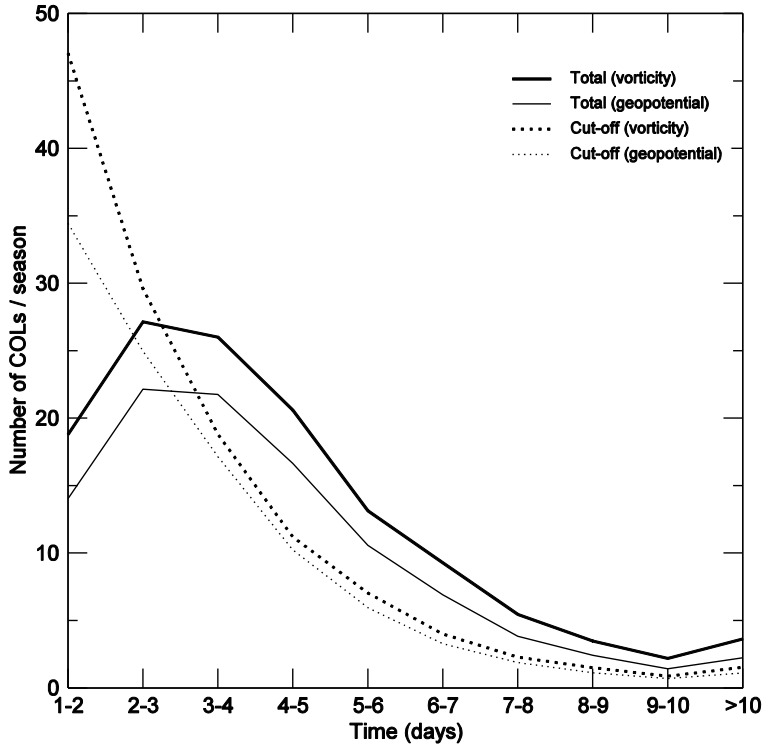


Total duration in solid line, cut-off stage duration in dotted line. Vorticity in thick line, geopotential in thin line. Unit is days. Analysis performed using the ERAI reanalysis for a 36-yr period (1979-2014).

Source: author's production.

## 4.2 Sensitivity of identifying Cut-off Lows to multiple criteria

The sensitivity of the method to identify COLs is assessed with respect to different identification schemes in terms of numbers, seasonality and intensity. The schemes use the T42 $\xi_{300}$ for the tracking and the following additional fields: 1) $U_{300}$; 2) $U_{300}$ and $PV_{300}$; 3) $U_{300}$ and $T_{300}$ ; and 4) $U_{300}$, $PV_{300}$ and $T_{300}$. As expected, the largest number of COLs are found for the simplest methods (e.g. using only the $U_{300}$) with 540 tracks per year, whereas the smallest number of COLs identified is found for the multiple criteria methods (e.g. using $U_{300}$, $PV_{300}$, and $T_{300}$) with 285 tracks per year, i.e, the full set of criteria has about half the number of detected COLs compared to the simplest scheme. The schemes that use $U_{300}/PV_{300}$ and $U_{300}/T_{300}$ found 446 tracks and 327 tracks per year, respectively.

Figure 4.3a shows the monthly distribution, and Figure 4.3b the intensity distribution of the detected COLs for the four different schemes. The single variable scheme, i.e. using only $U_{300}$, is used as a reference as this scheme detects the largest number of COLs. For the single variable scheme compared with the full set of criteria (using $U_{300}$, $PV_{300}$ and $T_{300}$), the seasonality shows relatively small differences as both schemes show the maximum in March and the minimum in August, for the multiple step scheme, and September for the simpler scheme. The frequency of the detected COLs differs between the two schemes, but the difference in number remains roughly constant through the year. However, the intensity distribution shows that the full set of criteria has more of the strongest systems than the method using a single parameter.

Figure 4.3: a) Monthly distribution, and b) maximum intensity distribution (scaled by -1) of Cut-off Lows, obtained with the following criteria: 1) $U_{300}$; 2) $U_{300}$ and $PV_{300}$; 3) $U_{300}$ and $T_{300}$; 4) $U_{300}$, $PV_{300}$ and $T_{300}$.

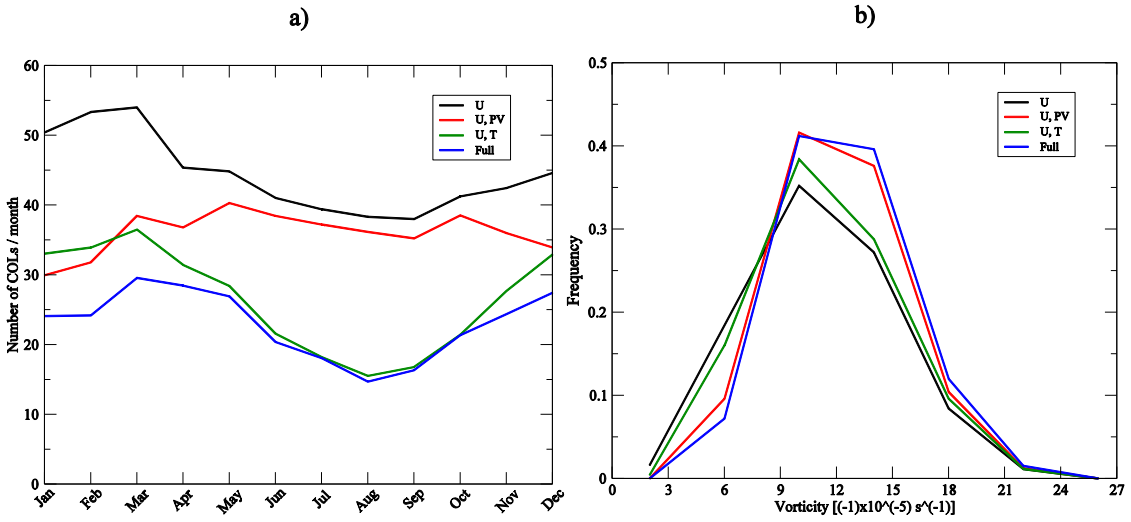


The four schemes for the $\xi_{300}$ Cut-off Lows are: 1) $U_{300}$ (black line); 2) $U_{300}$ and $PV_{300}$ (red line); 3) $U_{300}$ and $T_{300}$ (green line); 4) $U_{300}$, $PV_{300}$, and $T_{300}$ (blue line). The thresholds used in each variable are: $U_{300}$ < -8.0 m/s; zonal anomaly of $T_{300}$< -3.0°C; zonal anomaly of $PV_{300}$ < -2.0 PVU. The zonal anomalies of $PV_{300}$ and $T_{300}$ are determined searching for the minimum value within 5.0° geodesic radius centered on the centre of Cut-off Lows. Analysis performed using the ERAI reanalysis for a 36-yr period (1979-2014).

Source: author's production.

For the comparison of the method using $T_{300}$ together with $U_{300}$, again using the single variable scheme as a reference, the largest discrepancies are found in winter when

typically the strongest COLs occur. Despite this difference, the seasonality and intensity distributions are similar between the two methods, suggesting that the type of the detected COLs does not change much when the cold-core criterion is used. Therefore, the use of the cold-core criterion seems to affect mainly the winter systems when the decrease in numbers occurs.

The largest difference in seasonality occurs for the comparison of the method using $PV_{300}$ together with $U_{300}$ as the maximum frequency is found in May and the minimum in January. The monthly distributions show that the largest differences in number occur in the summer months, but it is relatively small for the period between May and October. The maximum frequency in winter may be as a result of the higher mean intensity of COLs (see Figure 5.2 and Figure 5.9), leading to a more pronounced tropopause folding as well as more efficient transport of cyclonic PV values from the stratosphere into the middle-high troposphere. In contrast, COLs are relatively weak in summer so that the PV intrusion is less effective compared to winter, reducing dramatically the number of detected COLs using the $U_{300}/PV_{300}$ method. An alternative approach to reduce the seasonal variation of PV might be the use of temporal anomalies, similar to the calculation used to produce the perturbation component of energetics (see Section 3.2.7).

Except for the scheme using $PV_{300}$ together with $U_{300}$, the other identification schemes have a similar seasonality of COLs as the peak and trough occurrence are found in a somewhat similar time of year, providing some confidence in how these systems are represented. However, even though the number of COLs identified does change, the number of COLs that occur in reality is unknown. Comparing these results with previous studies of COLs in the SH, Reboita et al. (2010) found substantial differences in frequency when using the NCEP-NCAR and ERA-40 reanalyses finding the annual average of the 300-hPa COLs is 197 using NCEP-NCAR and 349 using ERA-40. These numbers are much greater than the frequency shown by Ndarana and Waugh (2010) for a similar region for COLs at 250 hPa (120 systems per year) using the NCEP-NCAR and a method to identify COLs similar to that used in Reboita et al. (2010), but with a more explicit imposition of the cold-core. The single variable scheme used in the present work identified an annual average of 547 COLs using the $\xi_{300}$ and 355 COLs

using the $Z'_{300}$ in ERAI. However, the frequency reduces to 285 COLs if using the full set of criteria for $\xi_{300}$, i.e. with cold-core and PV restrictions. These results confirm that the number of systems is very sensitive to the criteria and dataset used to identified COLs. It is also worth pointing out that it is difficult to fit the COLs into neat classes because the COLs in nature are more complicated than the typical aspects described in conceptual models.

The conclusion for this comparison is that the four schemes used to identify COLs pick up different types of systems since these criteria impose different constraints. The sensitivity of the method with respect of $PV_{300}$ suggests the $U_{300}/PV_{300}$ scheme is a good choice to detect the strongest systems, but it may be too strict in some cases, particularly for weak summer COLs (for example, most COLs located in the Indian Ocean). The use of the cold-core criterion reduces the number of COLs in all seasons, mainly affecting the winter systems. This may be related to the level used to search for the cold-core, and this aspect is related to the temperature structure which will be discussed in Chapter 6. The full set of criteria results in similar implications for the COL identification since this method combines $PV_{300}$ and $T_{300}$. The single parameter scheme is the preferred method among those analysed here, simply because it is less selective and can detect a larger number of COLs than the other methods. The four-point filter that uses $U_{300}$ and $V_{300}$ has similar implications for the COL identification, as discussed in Section 4.1.

### 4.3 Vertical depth of Cut-off Lows

The sensitivity of the new method to determine the vertical depth of COLs relies on the threshold employed for the mean separation distance and the time overlaps between the matched tracks. Results show that the COL depth is more sensitive in respect of the time overlap rather than the mean separation distance. However, the number of matches significantly increases if we make the mean separation distance too large, but will result in spurious matching of unrelated cyclonic systems. For that reason, the mean separation distance is fixed at 5$^{o}$ geodesic that is suitable for the purpose of this study as the vertical tilt of the COL is normally much smaller than this value (such evidence will be presented in Chapter 6).

The sensitivity analysis to obtain the vertical depth was carried out for 803 COLs, chosen from the systems that have their genesis within a circle of 10º centered on 34.5ºS/80.0ºW, as this region is the focus of the present study. In addition, it is reasonable to analyse the vertical structure of the Pacific COLs separately from those in other regions as the former may be affected by the Andes. The same analysis made for the COLs in the entire hemisphere shows similar results (figure not shown). The sensitivity to the temporal overlap is evaluated by varying the threshold to 1%, 5%, 10%, 25%, 50%, 75%, and 100%, as shown in Table 4.1. Using the overlap threshold of 1% means that the mean separation distance between tracks at different pressure levels must be satisfied and the overlap in time must be at least 1% of the corresponding track points or at least one time step. For this overlap threshold value, 19.4% of the COLs formed at 300 hPa extend throughout the troposphere to the surface. This means that all the levels between 300 hPa and 1000 hPa have cyclonic features which are connected to each other. The percentage of COLs that reach the ground is similar for the overlap thresholds of 5%, 10%, and 25% (that is 19.2%, 18.8%, and 17.4% of the total number, respectively). However, the number of matches decreases markedly for the thresholds greater than 50%. This may be related to the fact that deep COLs intensify from upper to lower levels, reaching the surface at a late stage of their life cycle. This is apparent if we consider, for example, the threshold of 50% because only 11.6% of the cases present a deep structure, roughly half of the amount found using the threshold 1% (19.4% of the total number).

Other studies have been concerned with the depth of COLs in different regions of the southern and northern hemispheres. In Morais (2016), the vertical matching between the vorticity minima is performed over an area of 7.5º starting from the 200 hPa level down to the surface. This study used the ERAI reanalysis at a reduced horizontal resolution (1.5º x 1.5º) to study the upper-tropospheric cyclones in the tropical Atlantic near the northeast Brazil, and found that only 2% of the cases extend vertically toward the surface. The distances for the vertical search used in ours and Morais' algorithms are much smaller than the distance used by Porcù et al. (2007), where the search was performed inside a 5 x 5 grid-point area using the ERA-40 reanalysis at a horizontal resolution of 2.5º x 2.5º. This search area seems to be very large for systems whose tilt is not significant. For a 10-yr period (1992-2001), these authors found that 38% of the

200-hPa COLs identified in Europe and north of Africa (where the total number is 273 events) have a corresponding surface cyclone, a number much greater than that found in ours and Morais studies. Also for the COLs in a European region, Nieto et al. (2005) found that 47% of the 200-hPa COLs over 601 events reach the surface. Unfortunately, they do not detail the procedure used to find this result. Therefore, the criteria used for the vertical matching is probably one of the main reasons for the large differences between the studies. However, perhaps the method used to estimate the vertical depth is not the only reason for the differences as most of studies focus on COLs in different regions. A comparison of the vertical depth of COLs in different regions of the SH will be presented in Chapter 7.

Table 4.1: Sensitivity of the number of $\xi_{300}$ Cut-off Lows to time overlap for each pressure level (hPa), expressed as a percentage of the total number.

| | 1% | 5% | 10% | 25% | 50% | 75% | 100% |
|---|---|---|---|---|---|---|---|
| 300 | 100.0 | 100.0 | 100.0 | 100.0 | 100.0 | 100.0 | 100.0 |
| 400 | 86.4 | 86.4 | 86.3 | 86.2 | 84.2 | 70.4 | 12.7 |
| 500 | 74.7 | 74.6 | 74.3 | 74.1 | 71.1 | 46.3 | 2.2 |
| 600 | 64.0 | 63.9 | 63.5 | 63.1 | 58.0 | 27.6 | 0.2 |
| 700 | 50.1 | 49.8 | 49.6 | 48.3 | 40.3 | 14.9 | 0.0 |
| 800 | 39.4 | 39.1 | 38.9 | 36.9 | 28.9 | 7.7 | 0.0 |
| 900 | 26.5 | 26.2 | 26.0 | 24.3 | 17.4 | 4.1 | 0.0 |
| 1000 | 19.4 | 19.2 | 18.8 | 17.4 | 11.6 | 2.9 | 0.0 |

The overlap thresholds are 1%, 5%, 10%, 25%, 50%, 75%, and 100%. Analysis performed for 803 Cut-off Lows using the ERAI reanalysis for a 36-yr period (1979-2014).

Source: author's production.

The relationship between the different categories for intensity and vertical depth of COLs, (defined in section 3.2.5) is discussed here. Table 4.2 shows the number of tracks that match between the six different groups of COLs according to their intensity (weak, moderate, and strong) and vertical depth (shallow, medium, and deep), again using the set of tracks where their genesis occurred over a circle of 10º centered on 34.5ºS 80.0ºW. This shows that most of the weak COLs match with the shallow COLs (115 tracks), whereas most of the strong COLs match with deep COLs (178 tracks). This

result indicates that there is a significant correspondence between intensity and vertical depth of COLs, although this association is not always observed. For example, a few of the strong COLs do not match with deep COLs, whereas some shallow COLs do not match with weak COLs. This apparent contradiction may be explained by the fact that the intensity of COLs is measured by the $\xi_{300}$ field, while the vertical depth indicates the vertical extension through the troposphere where the cyclonic feature is observed. Different results may be found if using the geopotential minimum as a measurement of intensity. However, the choice of the geopotential to track low-pressure systems in multiple levels would likely require an adjustment to the threshold for each pressure level, as it was the case for the algorithm developed by Porcù et al. (2007). This could be done by filtering the geopotential field to remove the large-scale, resulting in a more level independent threshold.

Table 4.2: Number of Cut-off Lows that match between the categories based on intensity (weak, moderate, and strong) and vertical depth (shallow, medium, and deep).

| | **Shallow** | **Medium** | **Deep** |
|---|---|---|---|
| **Weak** | 115 | 74 | 87 |
| **Moderate** | 48 | 72 | 137 |
| **Strong** | 40 | 52 | 178 |

Analysis performed for 803 COLs using the ERAI reanalysis for a 36-yr period (1979-2014).
Source: author's production.

## 4.4 Summary and discussion

In this part of the study the analysis was performed in order to evaluate the new methodologies to identify COLs. Three schemes to detect the cut-off circulation are assessed in terms of how they affect the frequency and intensity distributions of the detected COLs. Results show that the single-point filter identifies more COLs than the other schemes. However, this approach also identifies more open troughs than the other methods. Using the eight-point filter, the number of troughs identified as COLs reduces dramatically but also the number of COLs is reduced, as this scheme is more selective than the others. The four-point filter seems to be the best compromise for the identification of COLs with an improved performance in comparison to the other

schemes, although similar issues are still found as for the single-point filter in terms of the detection of open troughs.

The sensitivity of identifying COLs to multiple criteria that include $T_{300}$ and $PV_{300}$ is discussed here. The results reveal that the frequency, seasonality and intensity are strongly affected by the choice of criteria. Results using the $PV_{300}$ as a condition for the COL identification indicate that the systems are stronger in comparison to those identified in schemes with no PV restriction. The cold-core condition reduces the number of COLs but the seasonality does not change dramatically as is the case for the scheme with $PV_{300}$. Except for the method that uses $U_{300}$ and $PV_{300}$, all other methods show that COLs are more frequent from late Summer to early Autumn which is in agreement with other studies of upper-level COLs in the SH (FAVRE et al., 2012; REBOITA et al., 2010). The results indicate that using multiple step schemes implies the identification of fewer events than using simpler schemes, but it is difficult to know definitely which is the best scheme due to lack of a respected verification data set of COLs.

A method for determining the vertical depth of COLs is proposed here by using the track matching algorithm (HODGES et al., 2003). Results show that the vertical depth of COLs does not significantly vary by changing the temporal overlap for values from 1% to 25%. For these thresholds, about 50% of 300-hPa COLs extend down to 700 hPa, but only 17%-19% reach the surface. However, increasing the overlap threshold to larger values leads to a marked drop in the matched tracks, in particular for lower levels.

The results presented in the following sections will be made based upon: 1) the four-point filter; 2) the simpler scheme that has only the horizontal winds ($U_{300}$ and $V_{300}$) as additional fields; and 3) the temporal overlap threshold 1% used by the method for obtaining the vertical depth of COLs.

# 5 CHARACTERISTICS OF CUT-OFF LOWS IN THE SOUTHERN HEMISPHERE

In this chapter, the results are produced for the COLs in the SH, using the ERAI reanalysis for the period from 1979 to 2014. The synoptic-scale features associated with the COLs are analysed in Section 5.1 using spatial statistics based on the spherical kernel estimators (HODGES, 1996) for the austral seasons of autumn (March-May), winter (June-August), spring (September-November), and summer (December-February). Section 5.2 shows the results of the comparison between the $\xi_{300}$ and $Z'_{300}$. The vertical structure of COLs is examined in Section 5.3 in terms of spatial and temporal distributions, and the vertical depth is estimated using the new methodology. Section 5.4 shows the seasonal distribution of the intensity and precipitation of COLs. Lastly in Section 5.5, an inter-comparison of COLs using four recent reanalyses (ERAI, NCEP-CFSR, MERRA-2, and JRA-55) and one older reanalysis (JRA-25) is performed, indicating the similarities and differences between the datasets. The results were obtained using the simpler scheme with the four-point filter which has the horizontal winds U and V as additional fields.

## 5.1 Climatology

During the 36 year-period, 18,686 COLs were identified in the latitudinal range between 50ºS and 15ºS, with a seasonal average of about 130 cases. The track density of the $\xi_{300}$ COLs (Figure 5.1) for each austral season shows a pronounced zonal asymmetry, and the most notable feature is the maxima around the continents and the minima over the oceans, although there are large values in the western Pacific throughout the year and in the central Indian Ocean during the summer. For the sector of eastern Australia and New Zealand the high COL activity may be associated with the high-frequency of blocking, as discussed in Trenberth and Mo (1985) and Marques and Rao (2000). Track density minima occur in eastern Africa during the winter, spring and summer, and in western Australia during the summer. A pronounced seasonal cycle is observed with a peak in the summer where the average is 29.6% of the yearly track numbers followed by autumn (28.1%), spring (23.4%), and winter (18.9%). No significant differences in seasonality are observed compared to the track density obtained using the full set of criteria which is based on the $PV_{300}$ and $T_{300}$, as shown in

Pinheiro et al. (2017) in their Fig.1, though this method indicates the highest frequency of COLs in autumn. The use of simpler criteria (e.g. using only winds as additional fields) allows us to pick up the weaker systems which are more often found in summer, so that is the main reason for the highest frequency of the detected summer COLs in this study.

Figure 5.1: Seasonal track density of Southern Hemisphere $\xi_{300}$ Cut-off Lows for a) autumn (MAM), b) winter (JJA), c) spring (SON), and d) summer (DJF).

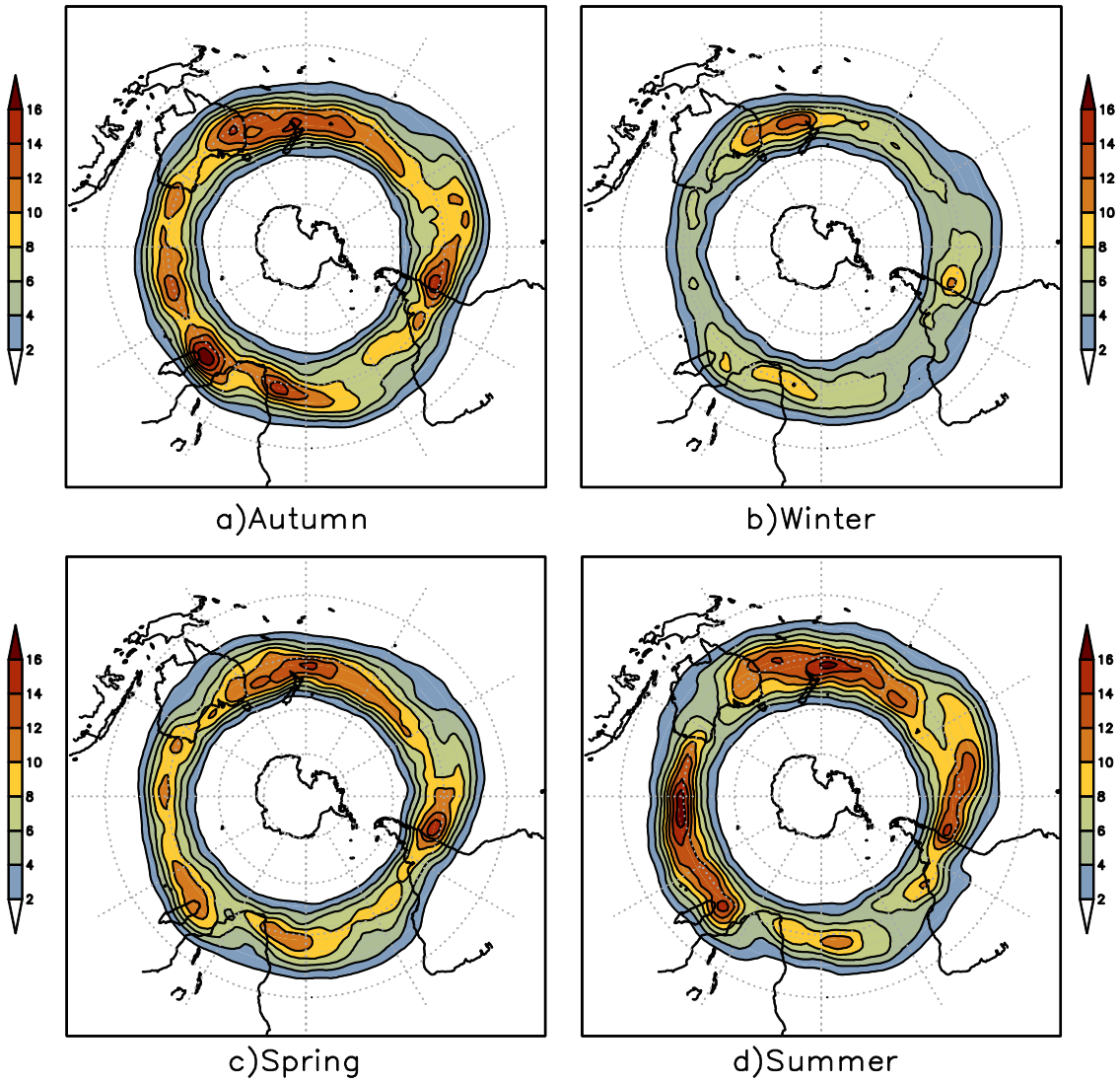


Track density in shaded and solid line for the contour intervals of 2.0 units. Analysis is performed using the ERAI reanalysis for a 36-yr period (1979-2014). Units is number per season per unit area, the unit area is equivalent to a 5° spherical cap ($\cong 10^6$ km$^2$).

Source: author's production

Figure 5.2 shows the mean intensity of $\xi_{300}$ COLs based on the $\xi_{300}$ maxima scaled by -1, the statistic is suppressed where the track density is less than 1.0 per season per unit area, chosen subjectively. The mean intensity of $\xi_{300}$ COLs shows a remarkable geographical and seasonal variability. The lowest intensities occur in the austral summer with values generally between 8 and 12 x $10^{-5}$ $s^{-1}$ in the main track density region, while the most intense summer COLs occur mainly at higher latitudes, where the COL activity is minor. The mean intensity of COLs increases during the autumn and reaches a peak in the winter. The largest values are located more equatorward in winter, reaching the range of 10-12 x $10^{-5}$ $s^{-1}$ along the maximum track density region and the subtropical jet stream location (indicated by the zonal mean winds in Figure 5.2b), and values greater than 12 x $10^{-5}$ $s^{-1}$ near the continents. A relative minimum of the 300-hPa average zonal wind is observed in southeast Australia and New Zealand during autumn, winter and spring, which may contribute to the high frequency of COLs and highs associated with blocking. The mean intensities in spring have a similar behavior as the intensities in winter but with weaker values with values generally not exceeding 10 x $10^{-5}$ $s^{-1}$. These results are comparable to a similar method based on a multiple step scheme using also $PV_{300}$ and $T_{300}$ as in Pinheiro et al. (2017) in their Figure 5. A detailed view of other statistics, such as genesis and lysis densities, growth/decay rate, mean velocity and mean lifetime is presented in Pinheiro et al. (2017).

Figure 5.2: Seasonal mean intensity of the $\xi_{300}$ Cut-off Lows in the Southern Hemisphere and 300-hPa mean zonal wind for a) autumn (MAM), b) winter (JJA), c) spring (SON), and d) summer (DJF).

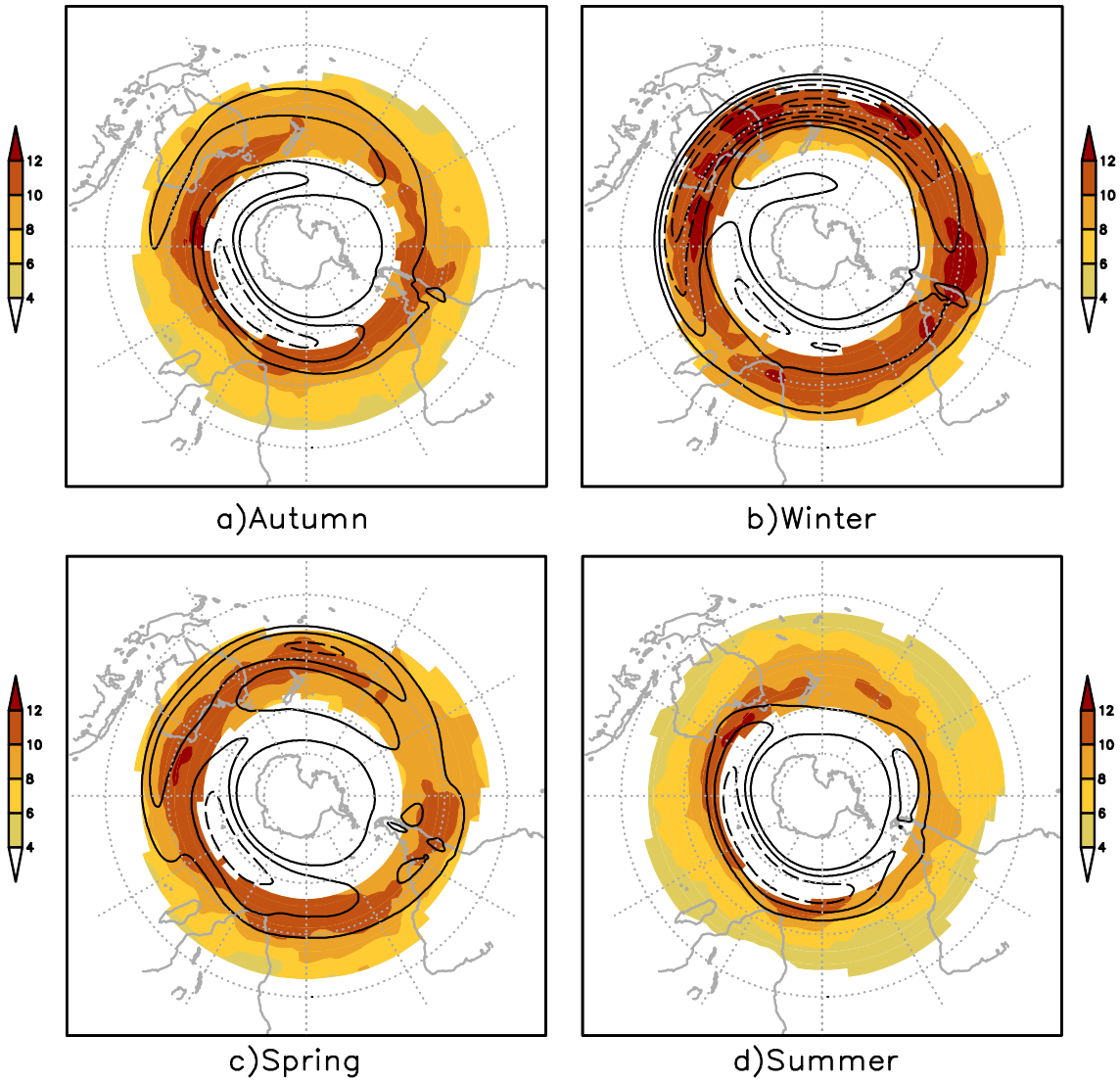


Mean intensity in shaded, and mean zonal wind ≥ 80 km/h (solid line) and ≥ 120 km/h (dashed line) for contour intervals of 20 km/h. Analysis is performed using the ERAI reanalysis for a 36-yr period (1979-2014). Unit for vorticity is $10^{-5}$ $s^{-1}$, scaled by -1. Track density suppression threshold is 1.0.

Source: author's production.

## 5.2 Differences between vorticity and geopotential

In previous studies, COL tracking has been based only on the use of either vorticity or geopotential. Here, both $\xi_{300}$ and $Z'_{300}$ are used separately for the COL tracking in order to provide different perspectives. The annual track densities for $\xi_{300}$ and $Z'_{300}$ COLs in

the SH are shown in Figure 5.3. This shows that the $Z'_{300}$ distribution is very similar to that obtained from the $\xi_{300}$ based on the same tracking methodology and selection criteria. The main areas of COLs are located near the continents for both $\xi_{300}$ and $Z'_{300}$, but the density values differ substantially between the two fields. In general, the $\xi_{300}$ densities are greater than the $Z'_{300}$ densities due to the differences in scales, as discussed in Hoskins and Hodges (2002). In addition to this aspect, there are other remarkable differences between the $\xi_{300}$ and $Z'_{300}$. One is the $\xi_{300}$ track density maximum over the central Indian Ocean which is related to weak summer COLs, as shown in Figs. 5.1 and 5.2. Another difference is that the $\xi_{300}$ COL activity occurs at more northern latitudes in the SH than that observed for the $Z'_{300}$, such as seen in northern Australia and South America. The reason for these differences may be attributed to the fact that the geopotential gradients (and the laplacians) are stronger moving poleward as a consequence of geostrophy. This means that the difference in frequency between vorticity and geopotential is strongly dependent on latitude. Another aspect to consider is that the uncertainties related to the geopotential computation have the same order of magnitude as that of the disturbance in lower latitudes.

Also, methods using fields that emphasise the smaller synoptic scales (e.g. vorticity) tend to identify longer tracks than methods using larger-scale fields (e.g. geopotential). This has important implications for the track density estimation since this statistic is sensitive to the track length. Hence, longer tracks contribute to higher track densities, while shorter tracks contribute to smaller densities. This may be the reason for the track density gaps in the ocean areas observed in the $Z'_{300}$ compared to the $\xi_{300}$. A somewhat similar distribution of the $Z'_{300}$ COLs has been shown in previous studies that use the geopotential for the tracking (FUENZALIDA et al., 2005; REBOITA et al., 2010).

Figure 5.3: Annual track density of Southern Hemisphere 300-hPa Cut-off Lows for a) vorticity and b) geopotential.

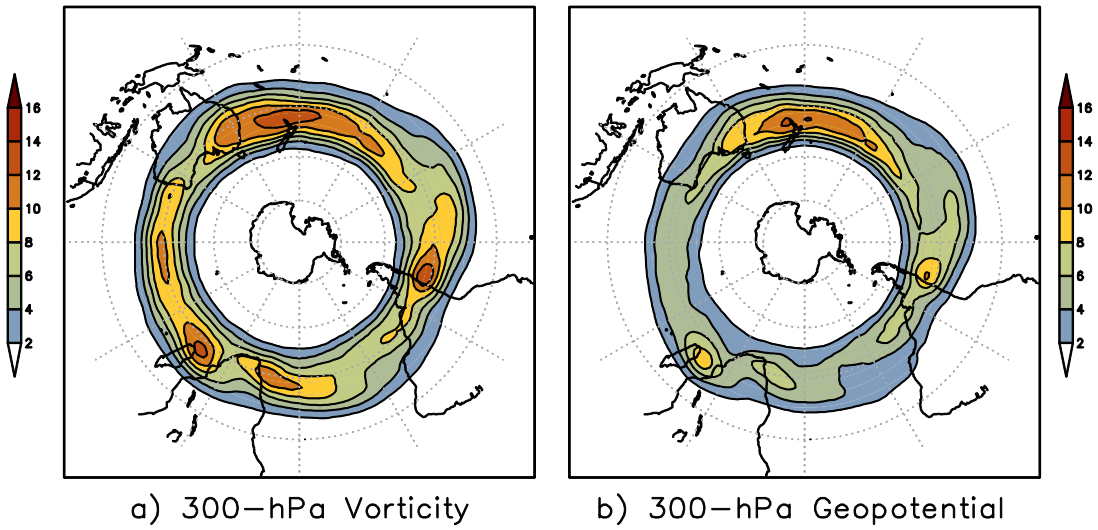


Track density in shaded and solid line for contour interval of 2.0 units. Analysis is performed using the ERAI reanalysis for a 36-yr period (1979-2014). Unit is number per season per unit area, the unit area is equivalent to a 5º spherical cap (≅ $10^6$ km$^2$).

Source: author's production.

Results for the number of $\xi_{300}$ and $Z'_{300}$ COLs and the number of matches between the two fields for each season are shown in Table 5.1. The matches are determined for the tracks with a mean separation distance less than 4º and an overlap in time greater than 50% of their points. This shows that the annual average is 519.1 COLs for $\xi_{300}$ and 407.9 COLs for $Z'_{300}$. The difference in number of COLs between the $\xi_{300}$ and $Z'_{300}$ increases when no additional fields are used as criteria (figure not shown). This means the filter used to separate COLs from upper-level troughs (for instance, the four-point filter) makes the identification more stricter and reduces the spatial differences found between the vorticity and geopotential fields. Despite the differences in numbers, the seasonality is quite similar between the two fields, although it is somewhat more pronounced in $\xi_{300}$. The largest number of matches occurs in autumn with 90.4 tracks (representing 81% (62%) of the $Z'_{300}$ ($\xi_{300}$) tracks), while the lowest number of matches is observed in winter with 61.9 tracks (representing 73%(63%) of the $Z'_{300}$ ($\xi_{300}$) tracks). The reason for the relatively low number of matches in winter will be discussed further in this section.

Table 5.1: Number of $\xi_{300}$ and $Z'_{300}$ Cut-off Lows, and the number of matches between the $\xi_{300}$ and $Z'_{300}$.

| Period | MAM | JJA | SON | DJF | Annual |
|---|---|---|---|---|---|
| **Vorticity** | 146.1 | 98.3 | 121.3 | 153.4 | 519.1 |
| **Geopotential** | 111.0 | 84.7 | 99.6 | 112.6 | 407.9 |
| **Matches** | 90.4 | 61.9 | 80.4 | 87.9 | 320.6 |

The analysis is performed using the ERAI reanalysis for a 36-yr period (1979-2014).

Source: author's production

To verify where the differences in the spatial distribution of the $\xi_{300}$ and $Z'_{300}$ COLs occur, the track matching algorithm is used to construct statistics based on the tracks that match and do not match. Figure 5.4 shows the track density based on (1) the tracks that match between the $\xi_{300}$ and $Z'_{300}$, in white solid line, and (2) the tracks that do not match, i.e., the difference between the $\xi_{300}$ and $Z'_{300}$, in shaded. The results indicate that, in general, the regions of high density of matches coincide with the regions of high density of differences. This result is expected since the regions of matches and non-matches are in the same region as the main track density. This occurs for regions of high COL activity located around the main continental areas, in particular in summer and autumn when the density of matches and differences reach 12 and 10 per season (per unit area), respectively. High values for the matches and difference are also found over the oceans during the summer, such as over the Indian Ocean, mostly due to small-scale weak systems. Positive values for the density of difference means that in general there are more $\xi_{300}$ tracks than $Z'_{300}$ tracks. A surprising opposite result occurs over southeastern Australia and parts of the Pacific in winter where the track density has larger values in $Z'_{300}$ rather than in $\xi_{300}$. The reason for this result is not clear, but it may be explained by the fact that the $Z'_{300}$ tracks are longer than the $\xi_{300}$ tracks in this region (figure not shown), and the longer tracks result in larger values of track density as discussed above. According to Pinheiro et al. (2017), the western Pacific is a preferred region for both COL genesis and lysis, and this aspect may result in uncertainties due to the difficult task of identifying the COL lifecycle. Similar problems are also found over the central Indian Ocean, where the track density values based on the matches are comparable to those based on the non-matches. This occurs particularly

during the winter, and this confirms the relatively small number of matches between the $\xi_{300}$ and $Z'_{300}$ in this period, as shown in Table 5.1.

Figure 5.4: Seasonal track density of Cut-off Lows in the Southern Hemisphere for the matches and the difference between the $\xi_{300}$ and $Z'_{300}$ tracks for a) autumn (MAM), b) winter (JJA), c) spring (SON), and d) summer (DJF).

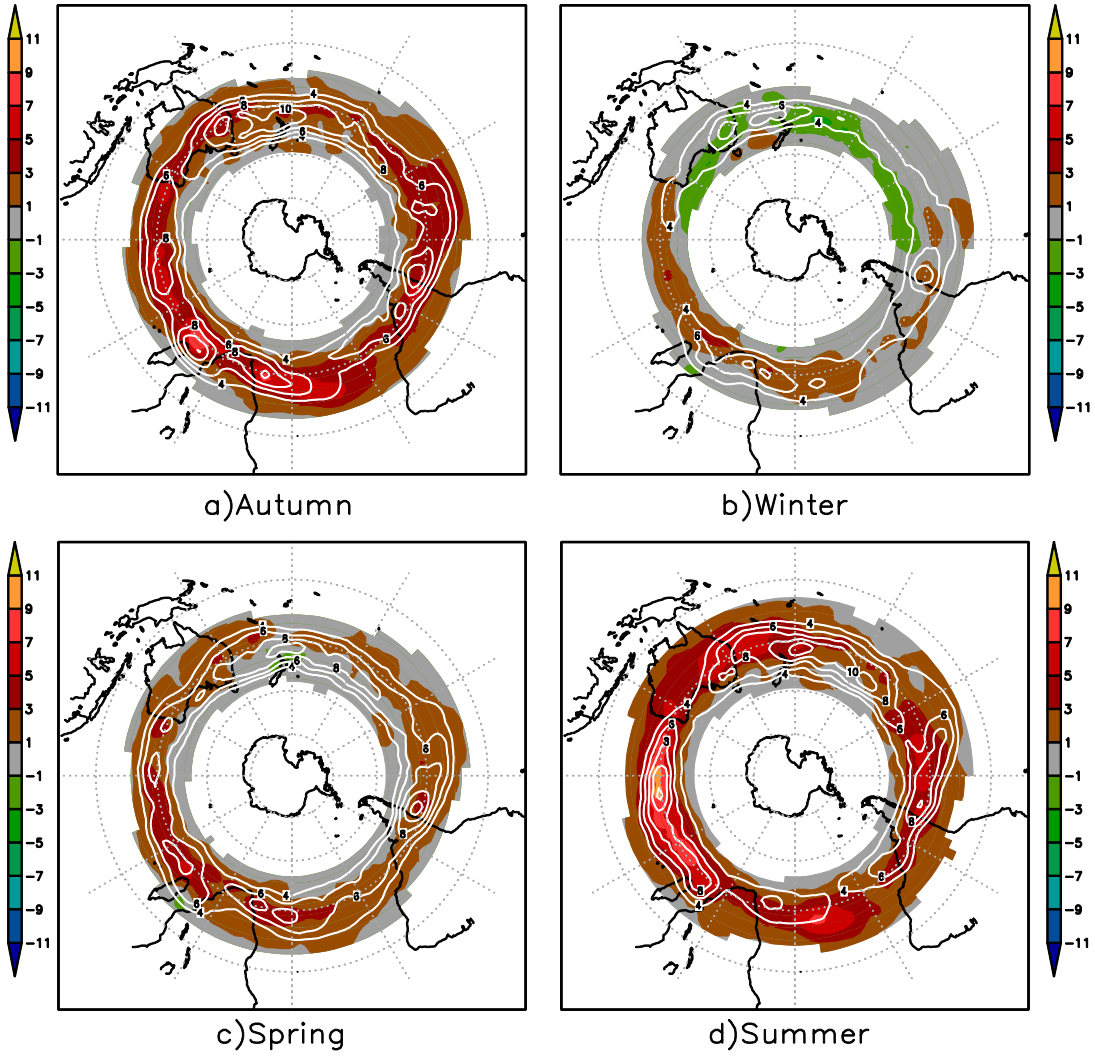


Track density of (1) matches between the $\xi_{300}$ and $Z'_{300}$tracks, represented in white solid line, and (2) difference between the $\xi_{300}$ and $Z'_{300}$ tracks, represented in shaded, both the contour intervals are 2.0 units per season per unit area. The density of matches and difference have been suppressed were the vorticity track density is below 1.0 per season per unit area. The unit area is equivalent to a 5º spherical cap ($\cong 10^6$ km$^2$). Analysis is performed using the ERAI for a 36-yr period (1979-2014).

Source: author's production

To provide a more detailed analysis of the comparison between vorticity and geopotential, a three-month period is used to give a view of how the tracks of COLs look between the two fields. Figure 5.5 shows the $\xi_{300}$ and $Z'_{300}$ tracks plotted for the period of June, July and August 2010. The symbol 'x' indicates the position of the genesis of each COL, and the colored lines indicate the intensity at each 6-hourly time step in units of $10^{-5}$ $s^{-1}$ for vorticity, and in gpm for geopotential, both scaled by -1. The most notable differences between the vorticity and geopotential are as follows: (i) the number of $\xi_{300}$ tracks is greater than the number of $Z'_{300}$ tracks; (ii) weaker systems are likely to be not identified for geopotential, this is the case for some tracks seen in southeastern Brazil and north of Australia; (iii) the $\xi_{300}$ tracks are normally longer than the $Z'_{300}$ tracks since the vorticity allows systems to be identified earlier in their life cycle.

Figure 5.5: Tracks of cut-off lows in the Southern Hemisphere identified in a) $\xi_{300}$and b) $Z'_{300}$.

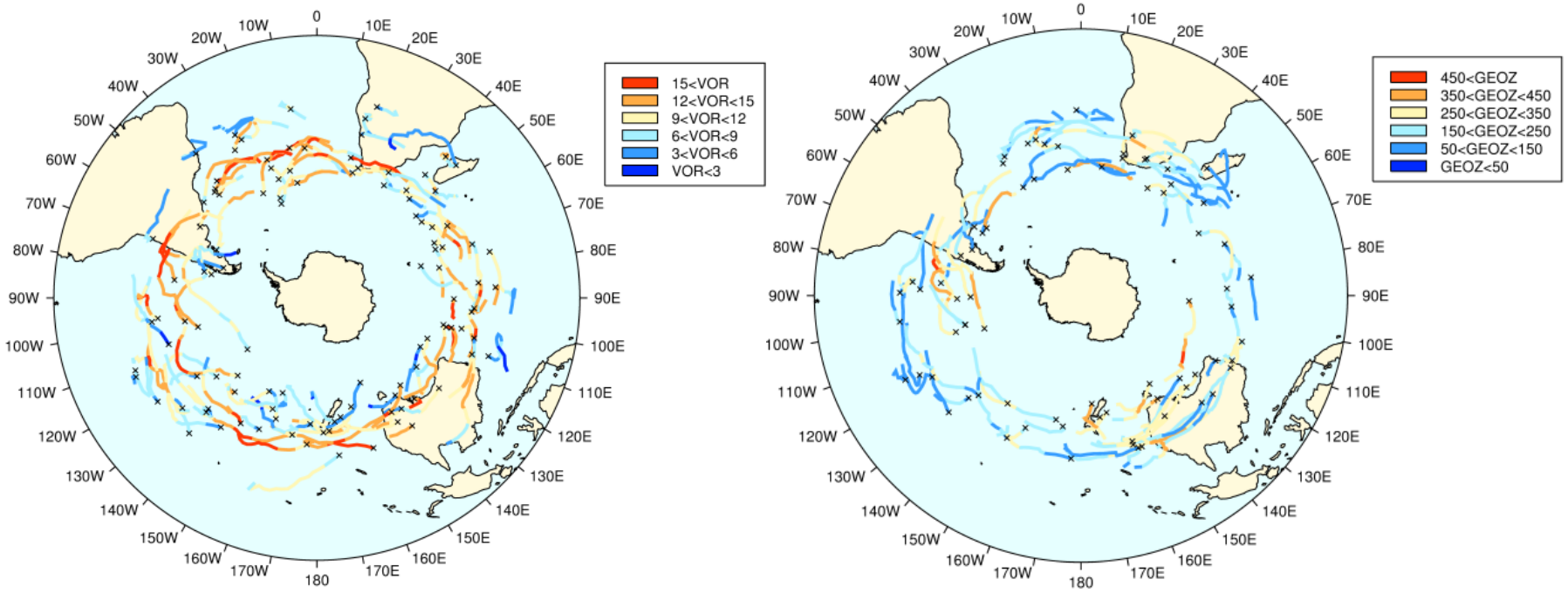


a) 300-hPa vorticity

b) 300-hPa geopotential

The symbol ‘x’ indicates the position of the genesis of COL, the colored lines indicate the intensity at each 6-hourly time step in units of $10^{-5}$ $s^{-1}$ for vorticity and in geopotential meters for geopotential, both scaled by -1. Analysis is performed using the ERAI reanalysis for the period from June to August 2010.

Source: author’s production

## 5.3 Vertical structure of cut-off lows

An extensive body of literature is found on extratropical cyclones since the early study of Bjerknes (1919). Additionally, there have been several studies focusing on mid-upper cyclones as cut-off lows for both the northern and southern hemispheres. However, the literature is very poor concerning the vertical structure of COLs and its relation to surface cyclones. This section explores the vertical structure of COLs in terms of numbers and their spatial and temporal distributions.

### 5.3.1 Number of low-pressure systems at different levels

One of the most interesting aspects of COLs is their vertical structure. Table 5.2 shows the vertical extension of COLs estimated by the methodology described earlier, expressed as the percentage of the detected $\xi_{300}$ COLs. In other words, this shows how much COLs in the SH have a deep structure. COLs generally form earlier at 300 hPa and then intensify toward the surface, and such evidence will be shown in Chapter 7. The approach used for determining the COL depth found that about 75% of the total number extend down to 500 hPa, 50% reach 700 hPa, but less than 20% reach the surface. However, the percentage of deep COLs rises markedly when using the stronger systems. For example, for the 1000 most intense COLs (~5% of the total number) 86.8% of the total number reach at least 500 hPa, but the percentage rises to 90.3% and 91.0% when the COLs are the 300 and 100 strongest systems, respectively. For the deepest COLs, i.e. the systems in which the low-pressure centre reaches the surface, the frequency increases to 61.7% and 66% when the COLs are the 300 and 100 strongest systems, respectively. In general, the more intense is the upper-level circulation, the deeper is the cyclonic feature seen in the $Z_{300}$ charts, though this link does not always occur (see Table 4.2).

It is worth mentioning that the vertical structure of COLs is sensitive to the method chosen and some differences occur when changing the thresholds, as discussed in Section 4.3. The use of geopotential instead of vorticity to estimate the vertical depth could be an alternative for further studies, but some care should be taken to assure an adequate use of the geopotential since the magnitude of this variable generally rises with height.

Table 5.2: Vertical depth of cut-off lows in the Southern Hemisphere for the climatology and for the most intense cut-off lows.

| hPa | Climatology | 1000 COLs | 300 COLs | 100 COLs |
|---|---|---|---|---|
| 300 | 100.0 | 100.0 | 100.0 | 100.0 |
| 400 | 86.4 | 93.5 | 95.7 | 96.0 |
| 500 | 74.7 | 86.8 | 90.3 | 91.0 |
| 600 | 64.0 | 79.1 | 82.0 | 87.0 |
| 700 | 50.1 | 72.9 | 76.7 | 83.0 |
| 800 | 39.4 | 67.8 | 72.7 | 79.0 |
| 900 | 26.5 | 59.5 | 66.3 | 72.0 |
| 1000 | 19.4 | 54.1 | 61.7 | 66.0 |

Number of $\xi_{300}$ Cut-off Lows that reach each pressure level (hPa), expressed as a percentage of the total number for: the climatology (18,868 systems); and the most intense Cut-off Lows (1000, 300, and 100 strongest systems referenced to the $\xi_{300}$). Analysis is performed using the ERAI reanalysis for a 36-yr period (1979-2014).

Source: author's production

### 5.3.2 Vertical distribution of low-pressure systems

In this section the vertical distribution of COLs in the SH is analysed in respect of the track density, and the results are based on the tracks referenced to the following pressure levels: 300, 500, 700, and 1000 hPa. Before the spatial statistics are produced, the method for determining the COL depth is applied just to select the systems according to their vertical extension. For example, the $\xi_{300}$ track density (Figure 5.6a) is exactly the same statistic shown in Figure 5.3a which represents all the detected $\xi_{300}$ COLs. The $\xi_{500}$ track density (Figure 5.6b) is determined from the $\xi_{500}$ tracks (with the same method and criteria as used in the $\xi_{300}$) that match with both $\xi_{300}$ and $\xi_{400}$. The $\xi_{700}$ track density (Figure 5.6c) is obtained from the $\xi_{700}$ tracks that match iteratively with $\xi_{300}$, $\xi_{400}$, $\xi_{500}$ and $\xi_{600}$. Similarly, the $\xi_{1000}$ track density (Figure 5.6d) is based on the $\xi_{1000}$ tracks that match with each track for every pressure level above 1000 hPa, representing the cyclones originated from the deepest COLs. This allows us to see where the deepest COLs are in the SH.

Figure 5.6: Track density of Cut-off Lows in the Southern Hemisphere based on their vertical depth referenced to the following pressure level: a) 300 hPa, b) 500 hPa, c) 700 hPa, and d) 1000 hPa.

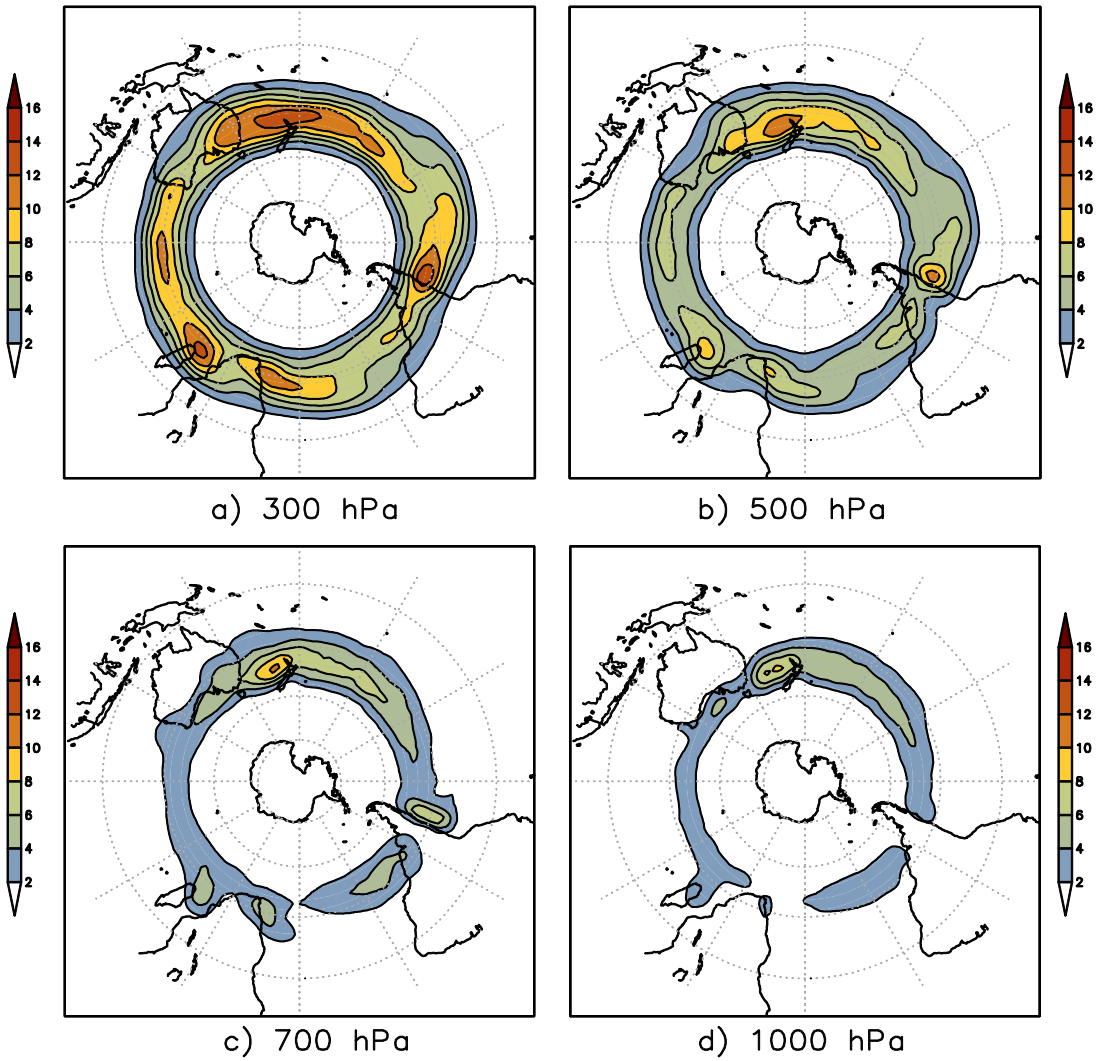


Track density in shaded and solid line for contour interval of 2.0 units. Units is number per season per unit area, the unit area is equivalent to a 5º spherical cap (≅ $10^6$ $km^2$). Analysis is performed using the ERAI reanalysis for a 36-yr period (1979-2014).

Source: author's production.

In Reboita et al. (2010), the spatial distributions of COLs at three pressure levels (200, 300 and 500 hPa) have been obtained using the Nieto algorithm (NIETO et al., 2005) adapted for the SH. However, in the Reboita study it seems that the COLs are identified independently at each level, i.e. the spatial distribution of COLs is not based on the matched tracks obtained from the tracks between different levels, as in the present

study. The advantage of matching the tracks is that statistics are produced using the systems with similar vertical extension, so that it is possible to examine the vertical structure of COLs rather than simply tracking the cyclonic features. If no matching were applied to the systems tracked independently at different levels, the number of tracks for $\xi_{300}$ would be smaller than that for vorticity in lower levels, because there are other types of systems identified by the method as a COL but with different characteristics. This is the case for vortices that originate from a frontal occlusion as discussed in Pinheiro (2010) and Reboita and Veiga (2017). Such systems seem to fit into the classification proposed by Sinclair and Revell (2000) for "Class U cyclones" where a surface cyclone lies directly beneath an amplified upper-level trough that may exhibit a closed geopotential height in the mature stage of the lifecycle (see their Figure 7). For these types of systems, a lower-level cyclone intensifies through the diffluent flow in the poleward exit of the 300-hPa jet stream, and the low-tropospheric features resemble the Norwegian cyclone model. The systems that originate from the described synoptic-scale flow pattern are unlikely to be included in the statistics presented in Figure 5.6 since the matching approach implies the system is identified earlier at upper levels. A more detailed discussion of the coupling between lower and upper level disturbances will be given further in this section and in Chapters 6 and 7.

The comparison of the track density between the $\xi_{300}$ (Figure 5.6a) and $\xi_{500}$ (Figure 5.6b) shows strong similarities in terms of their distributions, because the main $\xi_{300}$ COL regions coincide with those where the $\xi_{500}$ COLs typically are found. The difference of track density between $\xi_{300}$ and $\xi_{500}$ is not too large, suggesting that the most $\xi_{300}$ COLs reach the mid-troposphere, and these results are consistent with Table 5.2. The track density for $\xi_{700}$ (Figure 5.6c) shows reduced values compared to the mid and upper-tropospheric fields, but the main COL regions are still found there. The $\xi_{1000}$ track density (Figure 5.6d) generally shows relatively low values, where the maxima are mainly over the oceans. This indicates that a few COLs reach the surface. However, strong values occur in the north of New Zealand and over the Tasman Sea, indicating that COLs are much deeper in these regions in comparison to other parts of the SH. More details of the vertical structure of COLs in different regions of the SH will be presented in Chapter 7.

To examine the relationship between the upper-level COLs and the surface cyclones, the track density for $\xi_{1000}$ is computed in two different ways. One is to track the $\xi_{300}$ COLs and match them with the corresponding vorticity minima in the next level down, and so on, until the lowest pressure level, as shown in Figure 5.6d. The other way is to compute the track density directly from the $\xi_{1000}$ without association with the upper-tropospheric fields (Figure 5.7). This is done using the same method, criteria, and domain as used in the $\xi_{300}$. The results show two fields completely different to each other. The track density produced directly from the $\xi_{1000}$ shows much larger values than that produced using the matching approach. The differences are particularly large in specific locations such as in western Africa, southern Madagascar, and southwest Australia. This means that most of cyclones in these regions do not originate from a pre-existing upper-level COL. In contrast, a distinct pattern is seen for the maximum track density in the western Pacific where the cyclones are more connected with upper-level COLs. These results are in agreement with Sinclair (1994) in his Figure 6, despite the differences observed near the Andes Cordillera and southern Africa. Indeed, the representation of surface cyclogenesis near large mountain ranges by using more modern reanalysis products (e.g. ERAI, MERRA and NCEP-CFSR) has been improved compared to older datasets (HODGES et al., 2011).

Figure 5.7: Track density of the $\xi_{1000}$ cyclones in the Southern Hemisphere (50ºS-15ºS).

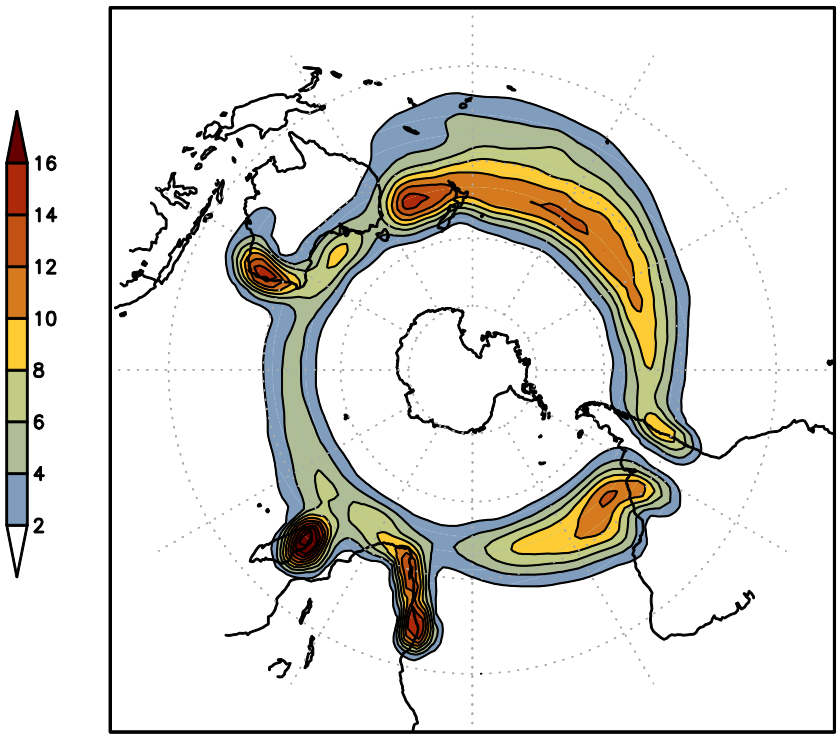


Track density in shaded and solid line for contour interval of 2.0 units. No matching is used to produce this track density. Units is number per season per unit area, the unit area is equivalent to a 5º spherical cap (≅ $10^6$ km$^2$). Analysis is performed using the ERAI reanalysis for a 36-yr period (1979-2014).

Source: author's production

### 5.3.3 Temporal distribution of cyclonic features

COLs show a seasonal variation in terms of number and intensity, as discussed in Pinheiro et al. (2017). One reason for the differences between studies is the level chosen to search for the cyclonic features. The monthly distributions of the COLs according to their vertical depth are shown in Figure 5.8. The COLs were obtained in exactly the same way as in Figure 5.6. This means, for example, that the $\xi_{500}$ COLs represent the upper-level COLs that reach 500 hPa. For the $\xi_{300}$ comparison with $\xi_{500}$, there are relatively small differences in terms of seasonality, because the maximum frequency occurs in autumn and summer months, and minimum frequency is observed during the winter and spring months for both type of COLs. As is expected the number of $\xi_{300}$ COLs is greater than the number of $\xi_{500}$ COLs because some COLs remain confined to

the upper-troposphere. The largest differences in number is found in the summer months, when the differences are generally about 20 cases per month, whereas the winter shows the smallest differences (~10 cases per month). This means the winter COLs are deeper than the summer COLs which is consistent with Figure 5.2. COLs that reach 700 hPa or 1000 hPa have a monthly distribution much less pronounced in comparison to the upper-levels COLs. Therefore, the results indicate that the typical vertical structure of COLs varies spatially and seasonally.

Figure 5.8: Monthly distribution of Cut-off Lows in the Southern Hemisphere based on their vertical depth referenced to the following pressure levels: a) 300 hPa, b) 500 hPa, c) 700 hPa, and d) 1000 hPa.

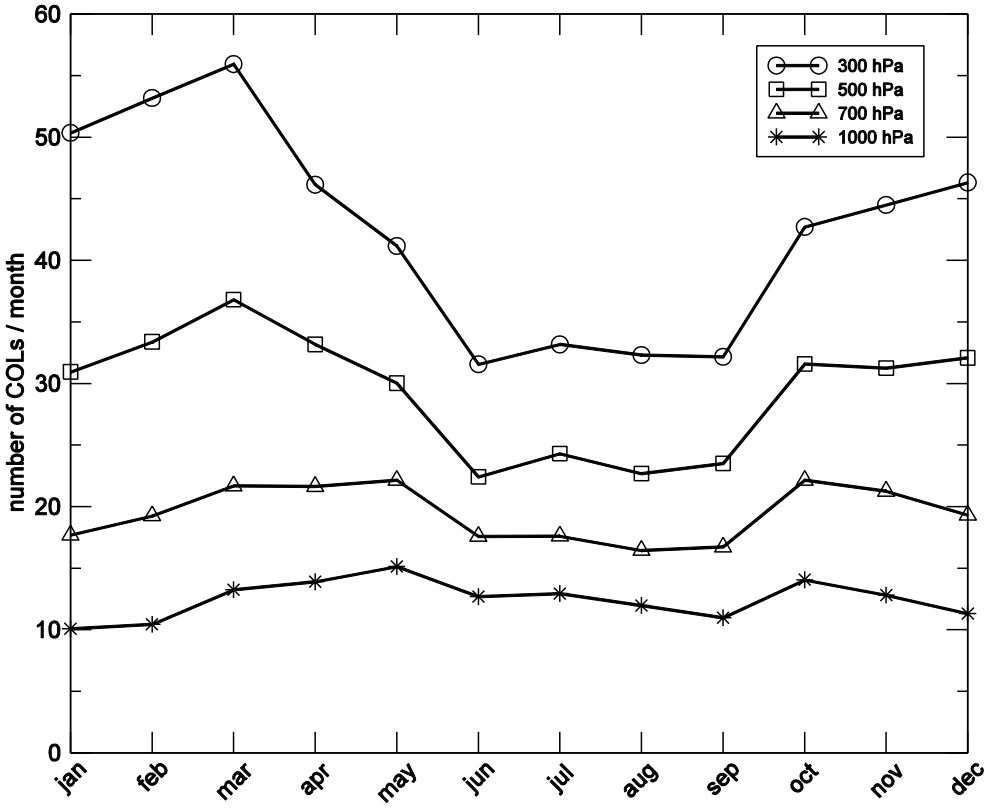


Solid line for each symbol denotes the number of tracks identified at 300 hPa (circle), 500 hPa (square), 700 hPa (triangle), and 1000 hPa (star). Analysis performed using the ERAI reanalysis for a 36-yr period (1979-2014).

Source: author's production

## 5.4 Seasonality of intensity and precipitation

The seasonal intensity distribution of the $\xi_{300}$ and $Z'_{300}$ COLs, computed from the full-resolution of $\xi_{300}$ and $Z'_{300}$, is shown in Figure 5.9. Values are determined from the maximum area averaged within a 5° geodesic radius (scaled by -1), centered on the $\xi_{300}$ and $Z'_{300}$ maxima. The probability density distribution for $\xi_{300}$ COLs, referenced to the $\xi_{300}$, provides a similar perspective to that shown in Pinheiro et al. (2017) in their Figure 6 who used a multiple criteria scheme. The most intense $\xi_{300}$ COLs are found in winter, followed by spring, autumn and summer. Similarly the $Z'_{300}$ distribution, referenced to the $Z'_{300}$ tracks, also shows a broad range of values and significant differences between the seasons, with the strongest COLs occurring in winter. This last result contradicts what was observed by Fuenzalida et al. (2005) since these authors found no significant seasonal and geographical variations of intensity for 500-hPa COLs based on the Laplacian of 500-hPa geopotential. It is difficult to say what field is best at representing the intensities of COLs because vorticity and geopotential are very different, although the geostrophic vorticity is proportional to geopotential vorticity (HOLTON, 1992). However, the results in the next chapter will show which of these fields detects the strongest systems.

Figure 5.9: Probability density function of seasonal maximum intensity for the a) $\xi_{300}$ Cut-off Lows, and b) $Z'_{300}$ Cut-off Lows in the Southern Hemisphere.

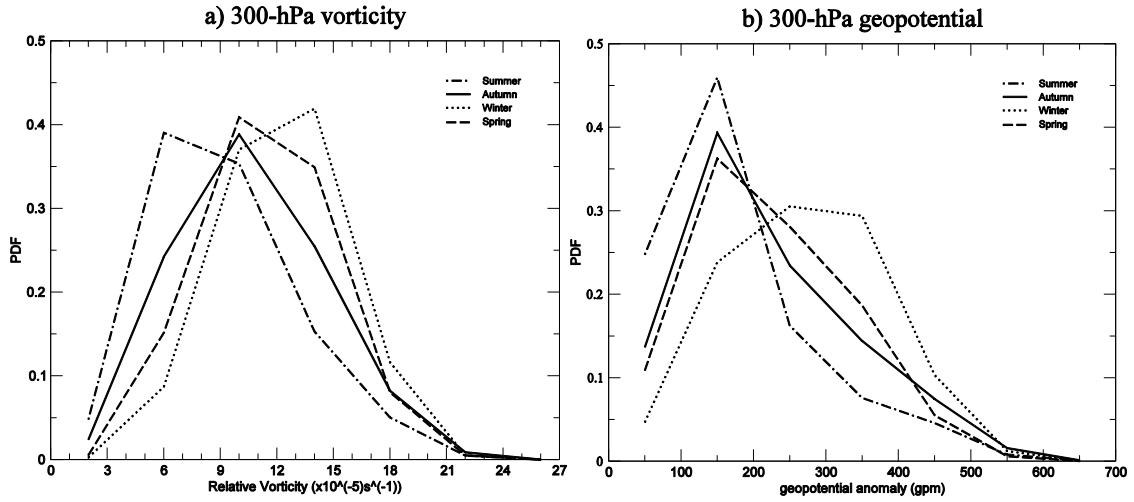


$\xi_{300}$ and $Z'_{300}$ values are determined from the maximum area averaged within a 5° geodesic radius (scaled by -1), centered on the $\xi_{300}$ and $Z_{300}$ maxima. The vorticity (geopotential) distribution is referenced to the $\xi_{300}$ ($Z'_{300}$) tracks. Units is $10^{-5}$ $s^{-1}$ for vorticity and gpm for geopotential. Analysis is performed using the ERAI reanalysis for a 36-yr period (1979-2014), for autumn (MAM) in solid line, winter (JJA) in dotted line, spring (SON) in dashed line, and summer (DJF) in dashed-dotted line.

Source: author's production

To verify the differences in precipitation associated with COLs between the seasons, the area-average total precipitation is computed over a 5° spherical cap region centered on the maximum $\xi_{300}$ for all $\xi_{300}$ COLs. The precipitation is not the instantaneous value, it is the precipitation obtained from the forecast model accumulated over a 6h period with 12 hour forecast lead time. It is expected that the precipitation in COLs may extend to regions with larger radius than that chosen here, so different radii were used to calculate the area-average precipitation such as 10° and 15°. In general, the seasonality does not change when varying the search radius of the maximum precipitation values. As can be seen in Figure 5.10a, there are more COLs with larger values of maximum precipitation (> 2.0 mm/h) in autumn and summer than in other seasons. Conversely, there are more COLs with smaller values of maximum precipitation (< 0.5 mm/h) in winter and spring than in other seasons. These results were also verified for the precipitation referenced to the $Z'_{300}$ tracks, and the results are similar to that using the $\xi_{300}$ (figure not shown).

Figure 5.10: Probability density distribution for seasonal a) maximum precipitation, and b) cumulative precipitation, of Southern Hemisphere $\xi_{300}$ cut-off lows.

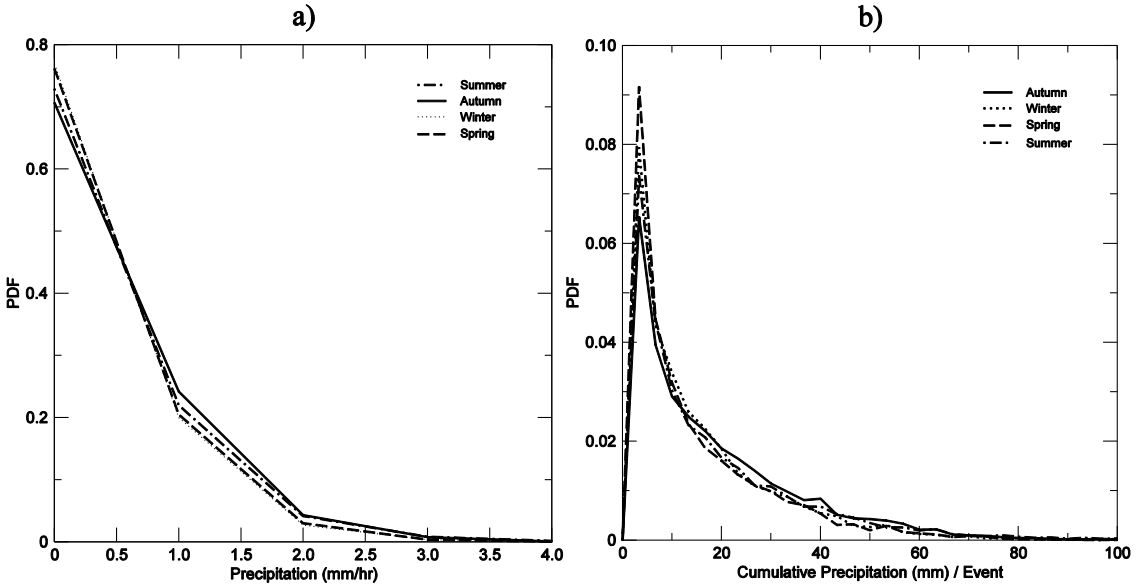


a) Maximum precipitation (mm/h) computed at the time of maximum precipitation accumulated over 6h, and b) cumulative precipitation (mm/event) obtained by accumulating all values between the first and last track points. Area-average precipitation computed over a 5° spherical cap region centered on the $\xi_{300}$ maximum. Analysis for autumn (MAM) in solid line, winter (JJA) for dotted line, spring (SON) for dashed-line, and summer (DJF) for dashed-dotted line, for the period from 1979 to 2014.

Source: author's production

The distribution of the cumulative precipitation of COLs, measured along each $\xi_{300}$ track, has also produced and shown in Figure 5.10b. The cumulative precipitation is obtained by accumulating all values between the first and last track points, computed over a 5° spherical arc radius centered on the $\xi_{300}$ maxima. This information is useful since the slow-moving COLs can cause excessive rainfall amounts over a particular area. On a first look at the cumulative precipitation distribution, it is not apparent that there are differences in densities between the seasons. However, if the extreme events are considered, for example, when the cumulative precipitation is larger than 50 mm (Table 5.3), the largest number of COLs is found in summer (349), followed by autumn (318), spring (155), and winter (126). For values larger than 100 mm, again more COLs are found in summer than other seasons. For the 36-year period, the largest extreme cumulative precipitation in a single event occurred in summer (280.5 mm), followed by

autumn (244.4 mm), spring (129.9 mm), and winter (115.0 mm). Similar results are found for the $Z'_{300}$ COLs, though more winter COLs with cumulative precipitation larger than 50 mm and 100 mm are found compared to $\xi_{300}$ COLs.

Table 5.3: Seasonal number of $\xi_{300}$ and $Z'_{300}$ Cut-off Lows with cumulative precipitation larger than 50 mm and 100 mm, and the maximum precipitation value for a single event.

| Method | Prec. (mm) | MAM | JJA | SON | DJF |
|---|---|---|---|---|---|
| $\xi_{300}$ | >50 | 318 | 126 | 155 | 349 |
| | >100 | 20 | 2 | 3 | 47 |
| | Max. Prec. | 244.4 | 115.0 | 129.9 | 280.5 |
| $Z_{300}$ | >50 | 221 | 160 | 141 | 197 |
| | >100 | 5 | 5 | 1 | 15 |
| | Max. Prec. | 133.5 | 136.1 | 114.5 | 324.3 |

The number of systems with cumulative precipitation larger than 50 mm and 100 mm are shown in the first and second rows, respectively. The third row indicates the maximum precipitation value in a single event. Analysis is performed for the austral seasons of Autumn (MAM), Winter (JJA), Spring (SON), and Summer (DJF), using the ERAI reanalysis for a 36-yr period (1979-2014).

Source: author's production

## 5.5 Intercomparison of Cut-off Lows in the Southern Hemisphere using recent reanalyses ERAI, NCEP-CFSR, MERRA-2, JRA-55, and JRA-25

This section presents results of the comparison of the SH 300-hPa COLs between different reanalyses, contrasting the performance of the new generation of reanalyses with an older reanalyses. The reanalyses investigated here for the newest reanalyses are: ERAI, NCEP-CSFR, MERRA-2, and JRA-55; and for the older reanalyses is JRA-25. The analysis will be performed based on the $\xi_{300}$ and $Z'_{300}$ for the 30-year period (1980-2009). The discussion of the spatial statistics will be focused on austral autumn (MAM) and winter (JJA) which present respectively the largest frequencies and intensities of the $\xi_{300}$ COLs in the SH (PINHEIRO et al., 2017). The other diagnostics, such as the frequency, the temporal and intensity distributions, and the mean separation distances, are examined for the COLs in all seasons.

### 5.5.1 Differences in number

The number of COLs based on $\xi_{300}$ and $Z'_{300}$ for each reanalysis for each season is summarized in Table 5.4. The difference in number of COLs identified in the reanalyses are generally small (<5 events per season) for both $\xi_{300}$ and $Z'_{300}$, except in the case of JRA-25, where the number of COLs is much smaller than in either of the recent reanalyses. It is noticeable that the number of $\xi_{300}$ COLs is greater than the number of $Z'_{300}$ COLs for all reanalysis, due to the difference in scale as previously discussed. This is the case even if the highest resolution reanalysis is contrasted with the lowest resolution reanalysis, that is, the NCEP-CFSR and JRA-25 reanalyses, respectively. The only exception occurs in winter, when the number of $Z'_{300}$ COLs for NCEP-CFSR (84.9 COLs) is slightly higher than the number of $\xi_{300}$ COLs for JRA-25 (84.8 events). For the annual average, the largest number of systems is found in JRA-55 for $\xi_{300}$ (518.1), and in ERAI for $Z'_{300}$ (407.0), while the smallest number of systems is found in JRA-25 for both $\xi_{300}$ (485.1) and $Z'_{300}$ (372.4). The reason why the ERAI and JRA-55 have more tracks than NCEP-CFSR and MERRA-2 is unclear, even though the former reanalyses do not have the highest resolutions.

If considering only the most recent reanalysis the results are very impressive since the differences in number is generally less than three tracks per season (~3% of total number) for both $\xi_{300}$ and $Z'_{300}$. The exception is the comparisons between JRA-55 and MERRA-2 in winter, when the differences in values reach 5.9 systems in $\xi_{300}$. In contrast, the differences in number of COLs between JRA-25 and the newest reanalyses are much larger, reaching 11.0 events in spring for $Z'_{300}$ and 13.4 events in winter for $\xi_{300}$, which corresponds to approximately 12.2% and 15.8% of the total number of $Z'_{300}$ and $\xi_{300}$ in JRA-25, respectively.

Table 5.4: Number of $\xi_{300}$ and $Z'_{300}$ Cut-off Lows in the Southern Hemisphere per season for each reanalysis.

| | | MAM | JJA | SON | DJF | YEAR |
|---|---|---|---|---|---|---|
| ERAI | $\xi_{300}$ | **143.9** | **98.0** | **121.4** | **153.5** | **516.8** |
| | $Z_{300}$ | 109.9 | 84.4 | 100.9 | 111.8 | 407.0 |
| NCEP-CFSR | $\xi_{300}$ | **144.2** | **95.6** | **119.8** | **154.3** | **513.9** |
| | $Z_{300}$ | 107.2 | 84.9 | 101.3 | 109.7 | 403.1 |
| MERRA-2 | $\xi_{300}$ | **142.3** | **92.3** | **119.0** | **155.6** | **509.2** |
| | $Z_{300}$ | 110.6 | 83.8 | 100.6 | 111.0 | 389.6 |
| JRA-55 | $\xi_{300}$ | **145.0** | **98.2** | **119.0** | **155.9** | **518.1** |
| | $Z_{300}$ | 107.6 | 83.1 | 98.8 | 109.0 | 398.5 |
| JRA-25 | $\xi_{300}$ | **137.0** | **84.8** | **110.3** | **153.0** | **485.1** |
| | $Z_{300}$ | 102.5 | 76.2 | 90.3 | 103.4 | 372.4 |

Number of COLs is obtained from the $\xi_{300}$ and $Z'_{300}$. The reanalyses used are ERAI, NCEP-CFSR, MERRA-2, JRA-55, and JRA-25, for the Southern Hemisphere subtropics (15ºS-50ºS) for the 30-yr period (1980-2009).

Source: author's production.

### 5.5.2 Differences in spatial distribution

To investigate the differences in the spatial distribution of $\xi_{300}$ COLs, the differences in track density between the reanalyses datasets are shown in Figures 5.11 and 5.12, using ERAI as a reference. The periods analysed here are the austral autumn (MAM) and winter (JJA), which have the most frequent and intense COLs (PINHEIRO et al., 2017). The frequency of COLs in summer is comparable to the frequency observed in autumn, but summer COLs are much weaker than the systems in other seasons.

For the comparison between ERAI and NCEP-CFSR (i.e. ERAI - NCEP-CFSR, Figure 5.11a-b), the track density shows there are relatively small differences, typically less than 3-5 per season per unit area. Positive values indicate that the track density has larger values in ERAI than in NCEP-CFSR. The largest values occur in autumn for

regions where the COL activity is high (see Figure 5.1), such as in the western Pacific and southern Africa where the values reach 3-5 per season per unit area in both autumn and winter periods. For the ERAI comparison with MERRA-2 (Figure 5.11c-d), the differences are similar to those seen in the NCEP-CFSR comparison with the largest differences in regions of high values of track density. Comparing ERAI with JRA-55 (Figure 5.11e-f), it is noticeable that in general the differences are much smaller than those observed in NCEP-CFSR and MERRA-2. Most regions present values ranging between -1 and 1 in both autumn and winter. The largest differences are observed south of Madagascar in autumn and through the Pacific in winter, but the values do not exceed 1-3 per season per unit area. The largest differences in track density are observed for the JRA-25 (Figure 5.12a-b), with in many areas there are values ranging from 3 to 5 between 25$^{o}$S and 35$^{o}$S, and reaching values up to 5-7 on the southwest coast of Africa and near Madagascar for both autumn and winter.

Figure 5.11: Differences of track density for the $\xi_{300}$ Cut-off Lows in the Southern Hemisphere, between ERAI and NCEP-CFSR (top), ERAI and MERRA-2 (middle), and ERAI and JRA-55 (bottom) for the austral autumn (left panel) and winter (right panel).

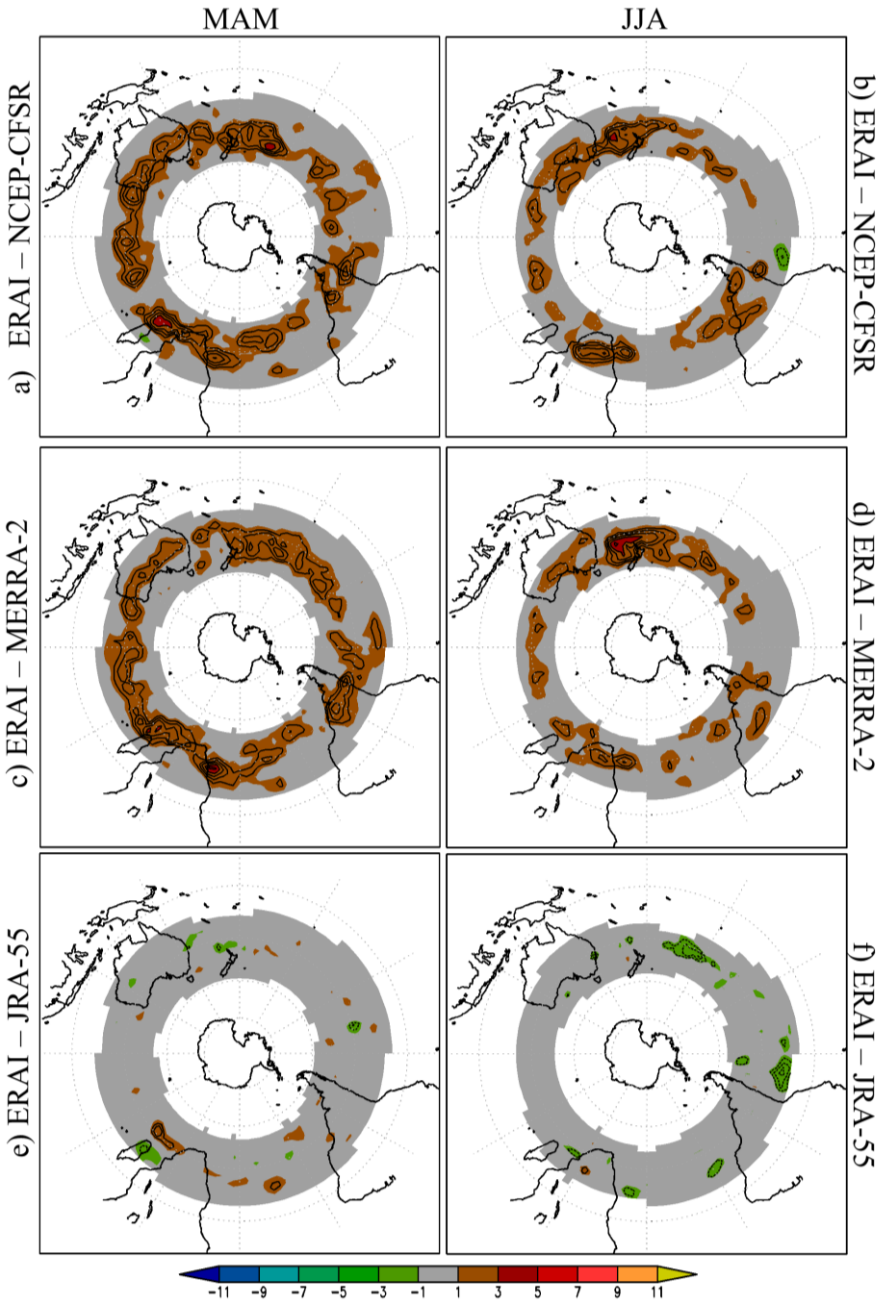


Values indicate the difference of track density for the contour interval of 2.0 units for austral autumn (left) and winter (right) for the 30-yr period (1980-2009): ERAI-NCEP-CFSR (top), ERAI-MERRA-2 (middle), and ERAI-JRA-55 (bottom). Units is number per unit area, the unit area is equivalent to a 5° spherical cap ($\cong 10^6$ km$^2$).

Source: author's production.

Figure 5.12: As Figure 5.11, but for the differences ERAI - JRA-25 (top), and NCEP-CFSR - MERRA-2 (bottom).

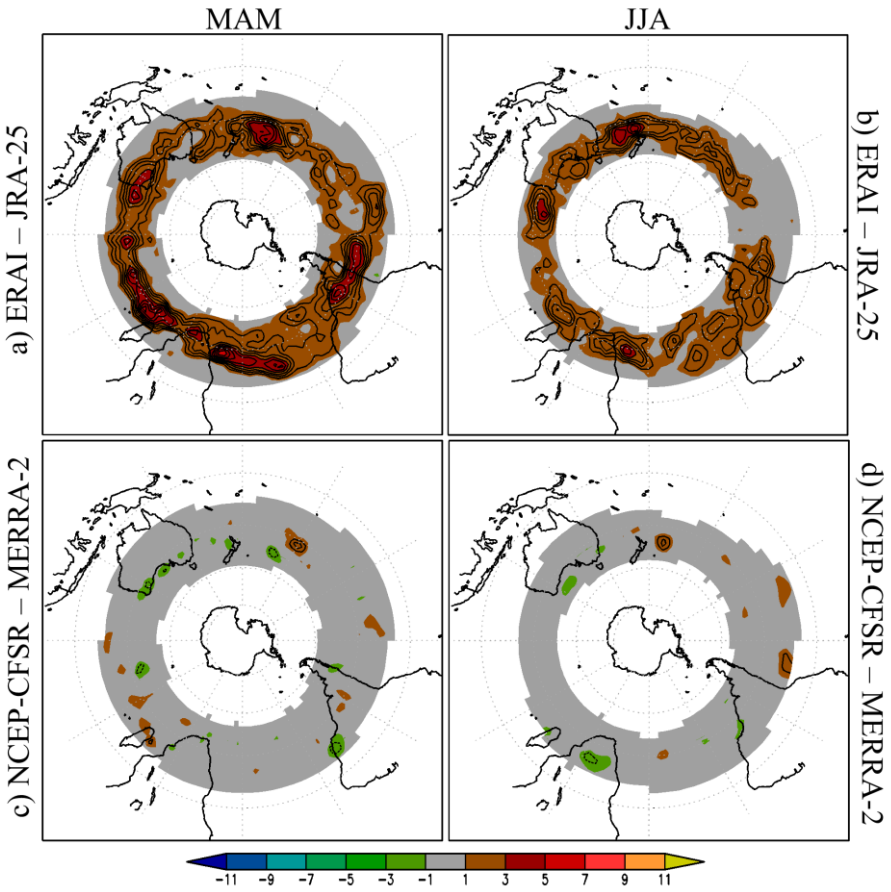


Source: Author's production

For another perspective, the track density between NCEP-CFSR and MERRA-2 is compared (Figure 5.12c-d). Results show that there is an improvement in the agreement compared to ERAI. In general the differences between NCEP-CFSR and MERRA-2 are close to zero in the main COL region for both autumn and winter, similarly to the comparison between ERAI and JRA-55. These results suggest that the similarities between ERAI and JRA-55 as well as between NCEP-CFSR and MERRA-2 are likely related to the way the data are assimilated in each reanalysis system. The data assimilation used in the ERAI and JRA-55 reanalyses is the 4D-Var, whereas the data are assimilated by the 3D-Var GSI system in the NCEP-CFSR and MERRA-2 reanalyses. It is worthwhile mentioning that the differences in numbers of COLs between the more recent reanalyses are relatively small as shown in Table 5.4. The differences in the track density are mainly due to the differences in the track length,

which is larger in ERAI and JRA-55 reanalysis than in NCEP-CFSR and MERRA-2 (figure not shown). The longer tracks lead to an increase in overlapping tracks and consequently an increase in the track density. The comparison of the differences of track density based on geopotential show similar results (figure not shown).

It is interesting to compare the results of the track densities quantitatively by performing significance tests for a pair of reanalyses rather than quantifying subjectively the differences. The main difficulty here is that the data are serially correlated due to the data being organised into tracks, this typically requires the use of non-parametric methods. One approach is the Monte Carlo method that has been widely used for meteorological and climatological applications (HODGES et al., 2011; LIVEZEY; CHEN, 2006; XU, 2006). However, the use of the Monte Carlo approach to compute the sampling distribution is quite expensive computationally.

### 5.5.3 Monthly distribution

Figure 5.13 shows the monthly distribution of the 300-hPa SH COLs based on the $\xi_{300}$ and $Z'_{300}$ for each reanalysis. This shows that there is a well-defined cycle with the peak in March and the minimum in June, July or August, with small differences in numbers between reanalyses. For most reanalyses the minimum occurs in June for $\xi_{300}$ and in August for $Z'_{300}$. The more pronounced seasonal cycle in $\xi_{300}$ rather than in $Z'_{300}$ may be as a consequence of a higher number of $\xi_{300}$ small-scale weak systems in summer, as observed in all reanalyses. The largest difference occurs in the JRA-25 distribution, in particular during winter and spring months when the numbers of $Z'_{300}$ COLs are significantly less than those observed with the newest reanalyses. However, if considering only the four newest reanalyses, the differences are relatively small, which is consistent with the results found through comparative studies for extratropical cyclones (HODGES et al., 2011) and tropical cyclones (HODGES et al., 2017) in the NH. It is then plausible that the newer reanalyses have improved over the older ones in their representation of cyclones and COLs in both hemispheres.

Figure 5.13: Monthly distribution of the $\xi_{300}$ and $Z'_{300}$ Cut-off Low number for the reanalysis ERAI, NCEP-CFSR, MERRA-2, JRA-55, and JRA-25.

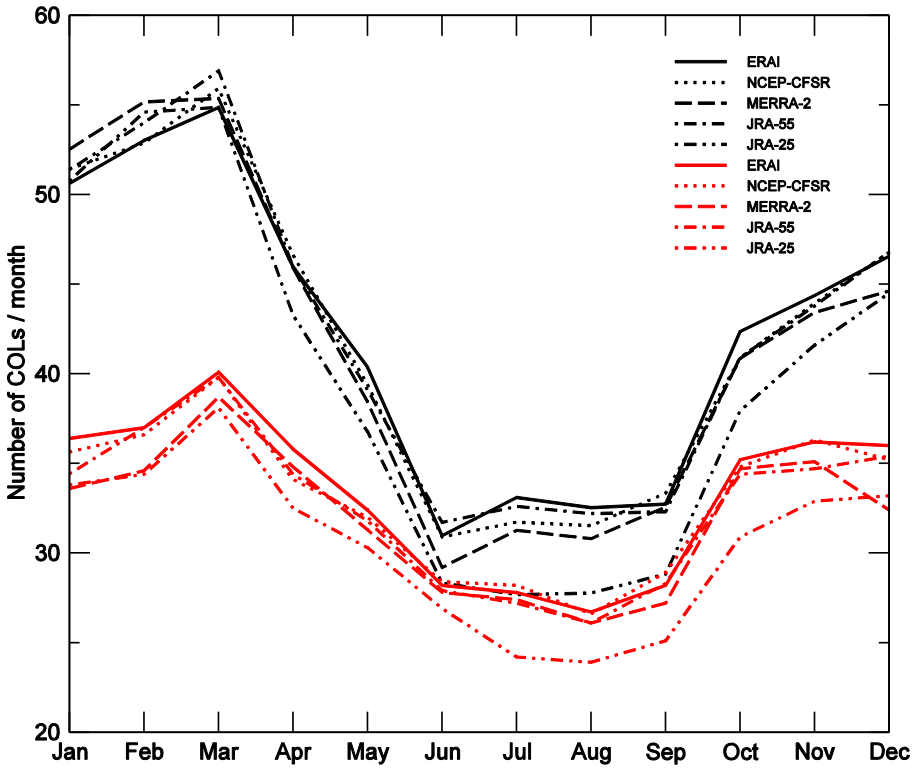


Vorticity in black lines and geopotential in red lines. The reanalyses used are ERAI (solid line), NCEP-CFSR (dotted line), MERRA-2 (dashed line), JRA-55 (dashed-dotted line), and JRA-25 (dashed-double-dotted line), for the Southern Hemisphere subtropics (15ºS-50ºS) for the period from 1980 to 2009.

Source: Author's production

### 5.5.4 Interannual variability

The interannual variability of the $\xi_{300}$ and $Z'_{300}$ COLs in terms of frequency is shown in Figure 5.14. During the 30-year period 1980-2009, there seems to be no obvious trend in the number of $\xi_{300}$ and $Z'_{300}$ COLs represented in each reanalyses, but there is clearly a considerable variation over this period, with noticeable peaks and troughs. The highest standard deviation of the COL number is found in NCEP-CFSR for both $\xi_{300}$ (26.6) and $Z'_{300}$ (24.7), whereas ERAI has the lowest standard deviation (21.0, 19.8). It is not surprising that the largest differences between reanalyses occur throughout the first half of period, when the uncertainties are larger than the more recent years due to the quality and available observations that are assimilated. In contrast, the period that started from

the start of the 21st century is particularly marked by reducing differences between the reanalyses, performing better with respect to the COL variability.

Figure 5.14: Interannual distribution of the COLs number based on $\xi_{300}$ and $Z'_{300}$ for the reanalysis ERAI, NCEP-CFSR, MERRA-2, JRA-55, and JRA-25.

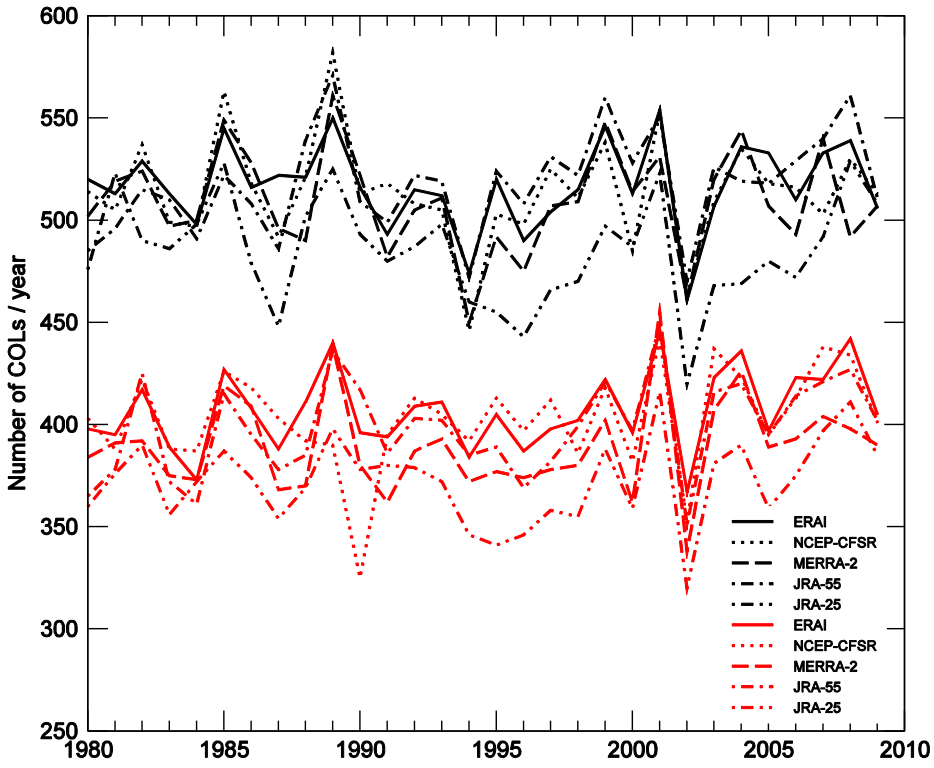


Vorticity in black lines and geopotential in red lines. The reanalyses used are ERAI (solid line), NCEP-CFSR (dotted line), MERRA-2 (dashed line), JRA-55 (dashed-dotted line), and JRA-25 (dashed-double-dotted line), for the Southern Hemisphere subtropics (15°S-50°S) for the period from 1980 to 2009.

Source: author's production

Interestingly, there are a number of studies that have reported a positive trend of the cyclonic activity in terms of interannual and interdecadal scales for both southern (FAVRE et al., 2012; FUENZALIDA et al., 2005; PEZZA et al., 2007; PIVA et al., 2008) and northern hemispheres (NIETO et al., 2007; WANG et al., 2006). Fuenzalida et a. (2005), using the NCEP-NCAR reanalysis for a 31 year-period (1969-1999), found a positive trend for the COL number in the African and South American sectors, in particular from the 1990's, but a decrease in number occurred for COLs in Australia. For the same regions, similar results have been found by Favre et al. (2012) using the

NCEP-DOE reanalysis, also known as NCEP 2 reanalysis (KANAMITSU et al., 2002) for the period 1979-2008, who suggested the positive trend may be as a result of the temperature and pressure rising in mid-latitudes as reported by the Intergovernmental Panel on Climate Change assessment (IPCC 2007), concerning the period from 1979 to 2001. Hence more highs and cut-off lows pressure systems associated with blocking patterns are generated, as suggested by Favre et al. (2012). Also for the SH, positive trends have been found for upper-tropospheric troughs (PIVA et al., 2008), and for surface cyclones (PEZZA et al., 2007), while Pezza and Ambrizzi (2003) found a decrease in number of cyclones but an increase for the strongest systems. The findings of the present work do not show an obvious trend, and even slight negative trends occur in the NCEP-CFSR and MERRA-2 reanalyses for the $\xi_{300}$ tracks (figure not shown). No noticeable trend is apparent for all five reanalyses for both $\xi_{300}$ and $Z'_{300}$ tracks even though a simpler method is used (without filter to detect a cut-off circulation), which results that about 70% of the detected tracks are open troughs (figure not shown). Also, our study did not analyse the interannual variability in terms of the COL intensity which may be interesting to examine in future work.

It is also important to remark that some discrepancies observed between studies are related to the different types of weather systems and regions chosen in addition to the dataset used for the analysis, as pointed out by Wang et al. (2006). For the large number of studies that have found a positive trend, it is reasonable to consider this aspect may be related to the increase in quality of available observations and how they are assimilated (SIMMONDS; KEAY, 2000). The studies that found a positive trend, as commented before, used relatively old reanalyses with low resolution in which the reanalyses have some problems in observations in the SH, as discussed in Pinheiro et al. (2017). Therefore, the use of the more recent reanalyses, which have more modern atmospheric models and assimilation systems, and with some known problems found in previous versions have been corrected, provides much more confidence in the analysis of weather systems in the SH.

An interesting aspect of the COL distribution is the abrupt decrease in occurrence in 2002, represented for all the reanalysis in both $\xi_{300}$ and $Z'_{300}$. The reduction in the number of COLs is well defined in spring (figure not shown) and may be associated

with the anomalous event of a Sudden Stratospheric Warming (SSW) in 2002, as discussed in many studies (CHARLTON et al., 2005; NEWMAN; NASH, 2005; ORSOLINI et al., 2005; THOMPSON et al., 2005; VAROTSOS, 2002). A SSW is characterized by an abrupt disruption of the westerly winds associated with the winter stratospheric polar vortex. For the NH, numerous studies have shown evidence of the stratosphere-troposphere coupling (ANDREWS et al., 1987; LIMPASUVAN et al., 2004; THOMPSON et al., 2005), suggesting the deceleration of the stratospheric polar vortex impacts the tropospheric circulation. In particular, a SSW event is often accompanied by a shifting of the jet stream and storms tracks equatorward (BALDWIN; DUNKERTON, 2001). However, SSW events are very rare in the SH due to the smaller planetary wave amplitude (BONATTI, 1979; VAN LOON et al., 1973). The exception is the unique and remarkable case of September 2002 (KRUGER et al., 2005), the only SSW event detected in the SH since the satellite observations began in 1979 (BUTLER et al., 2017). Despite the evidence of the importance of the SSW in positioning the main mid-latitude storms tracks, it is unclear what the influence of SSWs are in the subtropics. A hypothesis for the decrease in number of COLs is that during the extraordinary event of SSW in 2002 that the equatorward displacement of the jet stream would strengthen the subtropical zonal flow which it is not favorable for COL formation.

Although the main focus of this study is not on the low-frequency variability, some large-scale modes have been investigated. The possible association between the El Niño/Southern Oscillation (ENSO) and the frequency of COLs is examined, this found that the annual mean Southern Oscillation Index (SOI) is temporally correlated with the annual number of $\xi_{300}$ and $Z'_{300}$ COLs in each reanalysis in respect of El Niño and La Niña events. Table 5.5 shows the correlation coefficients between the SOI and $\xi_{300}$ and $Z'_{300}$ COL numbers. The one-tailed student's *t*-test is used to test the significance of the correlation coefficients. The most highly correlated reanalyses are found in the JRA-55 and JRA-25 for the $\xi_{300}$ COLs with values of 0.58 and 0.45, respectively, which are statistically significant at a 99% confidence level. In contrast, the correlation coefficients for the $Z'_{300}$ COLs identified by the NCEP-CFSR are low compared with those in other reanalyses (about 0.09), indicating these systems are less correlated with the SOI. The reason for this relatively weak correlation is unclear, but it may be related

with the high variation in number of COLs found in the NCEP-CFSR throughout the period as discussed above. A common aspect between the reanalyses is the positive correlation coefficients for both $\xi_{300}$ and $Z'_{300}$ COLs, indicating the increase in number of systems may be related to the La Niña episodes, which corroborates the findings of Favre et al. (2012) and Singleton and Reason (2007). During the cold phase of ENSO, negative anomalies of SST near the equator decreases the meridional pressure gradient between lower and mid-latitudes, weakening the westerlies associated with the subtropical jet which is found to be favourable for COL genesis. Other indices used to characterize the SST anomalies in different sectors of the tropical Pacific as well as the correlation for seasonal frequencies could be interesting to be considered for further works.

Table 5.5 Correlation coefficient and statistical significance (student's *t*-test) for the number of $\xi_{300}$ and $Z'_{300}$ Cut-off Lows with the Southern Oscillation Index for a 30-yr period (1980-2009).

| Reanalyses | correlation coefficient r | | student's *t* values | |
|---|---|---|---|---|
| | $\xi_{300}$ | $Z_{300}$ | $\xi_{300}$ | $Z_{300}$ |
| ERAI | 0.38 | 0.38 | 2.14 | 2.18 |
| NCEP-CFSR | 0.34 | 0.09 | 1.91 | 0.48 |
| MERRA-2 | 0.28 | 0.26 | 1.55 | 1.43 |
| JRA-55 | 0.58 | 0.27 | 3.73 | 1.50 |
| JRA-25 | 0.45 | 0.34 | 2.66 | 1.88 |

Source: author's production

There are other patterns of large-scale atmospheric variability that might affect COLs such as the Southern Annular Mode (SAM) or Antarctic Oscillation, the Pacific South American mode (PSA), and the Semi-annual Oscillation (SAO). For the SAO, in particular, a few studies have found a half-yearly cycle of COLs and a positive correlation with the COL frequency (FAVRE et al., 2012; NDARANA; WAUGH, 2010; SINGLETON; REASON, 2007). However, the four methods analysed in the present study do not show a semi-annual cycle of COLs (see Figure 4.3a). The exception is the method that uses the PV that shows two peaks (May and October), although they are not sharp enough to be considered as a semi-annual cycle. Chapter 7 will show whether the semi-annual cycle is apparent from a regional perspective.

### 5.5.5 Intensity distributions

The maximum intensity distributions of the $\xi_{300}$ and $Z'_{300}$ COLs referenced to the full resolution for $\xi_{300}$ and $Z'_{300}$, scaled by -1, are shown in Figure 5.15 as a probability density function. These values are computed for all tracks identified in each reanalysis over an area averaged within a 5$^{o}$ (geodesic) radius. If the direct search for absolute maxima is performed within the same area the results are very similar to the distribution produced using an area average. The distribution for the $\xi_{300}$ tracks shows that there is a broad range of values and significant differences between the reanalyses. NCEP-CFSR and MERRA-2 have stronger COLs (higher-intensity tails) than the other reanalysis, and JRA-25 has the weakest extremes. It is plausible to suppose that the higher resolution reanalyses help to produce the most intense systems, although a larger number of COLs is not always found (see Table 5.4). For the intensities based on the $Z'_{300}$, the distribution shows much smaller differences between the reanalyses than that shown for $\xi_{300}$. Again, MERRA-2 and NCEP-CFSR have the deeper COLs in comparison to the other reanalyses, whereas the JRA-25 consistently underestimates the intensities compared to the higher resolution datasets. Smaller differences are expected between the $Z'_{300}$ distributions since the geopotential tends to focus on the large-scale features, which are less influenced by the reanalysis resolution.

Figure 5.15: Probability density function of the intensity for the a) $\xi_{300}$ and b) $Z'_{300}$ obtained from the reanalyses ERAI, NCEP-CFSR, MERRA-2, JRA-55, and JRA-25.

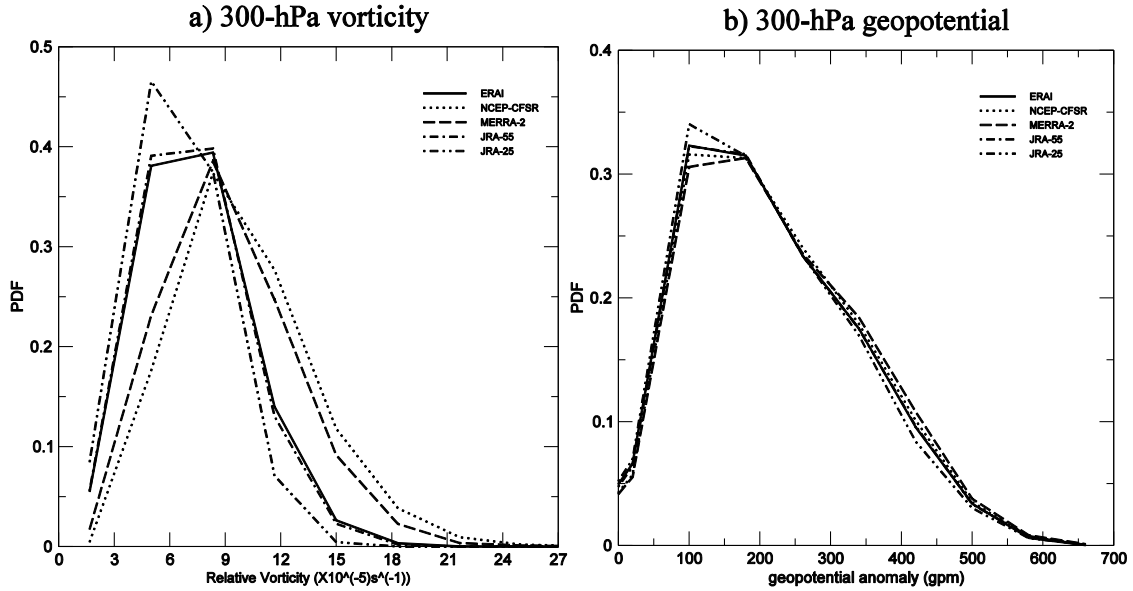


The reanalyses used are ERAI (solid line), NCEP-CFSR (dotted line), MERRA-2 (dashed line), JRA-55 (dashed-dotted line), and JRA-25 (dashed-double-dotted line), for the Southern Hemisphere subtropics (15°S-50°S) for the period from 1980 to 2009. Units is $10^{-5}$ $s^{-1}$ for vorticity and gpm for geopotential.

Source: author's production.

### 5.5.6 Track matching

A more detailed comparison of COLs between the reanalyses is performed by matching the identically same COLs. The matches are determined in exactly the same way as done in Section 5.2. The number of matches for each pair of reanalysis for both the $\xi_{300}$ and $Z'_{300}$ tracks are shown in Table 5.6. Percentages are defined as the number of matches divided by the largest number between each pair of reanalysis. This shows that ERAI has the largest number of matches for both $\xi_{300}$ and $Z'_{300}$ with about 78% of matches in $\xi_{300}$ (83% in $Z'_{300}$) for each modern reanalysis, whereas the worst comparison occurs for JRA-25 with about 67% of matches in $\xi_{300}$ (75% in $Z'_{300}$). Using ERAI as a reference, the largest number of matches occurs for JRA-55 in both $\xi_{300}$ (79.8%) and $Z'_{300}$ (84.5%), followed by NCEP-CFSR (77.1%; 83.9%), MERRA-2 (76.9%; 81.6%), and JRA-25 (67.5%; 75.4%). For the 10% most intense COLs, the number of matches in $\xi_{300}$ ($Z'_{300}$) increases to 92.5% (87.8%) for JRA-55, 91.3%

(89.4%) for NCEP-CSFR, 90.3% (89.3%) for MERRA2, and 85.5% (83.4%) for JRA-25. This result is expected since the strongest COLs are more easily identified in reanalyses. Also, the comparison between reanalyses show lower percentages of matches in winter than in other seasons for both $\xi_{300}$ and $Z'_{300}$. This result contradicts the fact that the number of matches increases for the most intense systems, which are typically found in winter. The exception occurs for the MERRA-2 comparisons in $Z'_{300}$ that have the lowest percentages of matches in summer.

Table 5.6: Number of $\xi_{300}$ and $Z'_{300}$ Cut-off Lows per season that match between the reanalyses ERAI, NCEP-CFSR, MERRA-2, JRA-55, and JRA-25.

| | | MAM | % | JJA | % | SON | % | DJF | % | YEAR | % |
|---|---|---|---|---|---|---|---|---|---|---|---|
| ERAI-NCEP | $\xi_{300}$ | **111.6** | **77.4** | **72.3** | **73.8** | **93.8** | **77.2** | **120.8** | **78.3** | **705.2** | **77.1** |
| | $Z_{300}$ | 90.7 | 82.6 | 69.9 | 82.3 | 85.6 | 84.5 | 95.2 | 85.1 | 341.3 | 83.9 |
| ERAI-MERRA2 | $\xi_{300}$ | **111.5** | **77.5** | **70.9** | **72.4** | **95.6** | **78.7** | **119.7** | **76.9** | **703.2** | **76.9** |
| | $Z_{300}$ | 91.3 | 83.1 | 69.1 | 81.9 | 83.9 | 83.1 | 87.9 | 78.6 | 332.3 | 81.6 |
| ERAI-JRA55 | $\xi_{300}$ | **115.3** | **79.5** | **76.4** | **77.8** | **97.2** | **80.1** | **124.4** | **79.8** | **730.4** | **79.8** |
| | $Z_{300}$ | 93.7 | 85.3 | 70.1 | 83.1 | 86.0 | 85.2 | 94.1 | 84.1 | 343.9 | 84.5 |
| ERAI-JRA25 | $\xi_{300}$ | **98.8** | **68.5** | **61.5** | **62.8** | **81.9** | **67.5** | **106.5** | **69.4** | **616.8** | **67.5** |
| | $Z_{300}$ | 83.7 | 78.1 | 62.9 | 74.5 | 75.3 | 74.6 | 84.9 | 75.9 | 306.8 | 75.4 |
| NCEP-MERRA2 | $\xi_{300}$ | **110.5** | **76.6** | **70.0** | **73.2** | **92.9** | **77.5** | **117.6** | **75.6** | **693.9** | **76.1** |
| | $Z_{300}$ | 88.9 | 82.6 | 68.8 | 81.1 | 83.8 | 82.7 | 87.0 | 79.3 | 328.4 | 81.5 |
| NCEP-JRA55 | $\xi_{300}$ | **107.6** | **74.2** | **69.1** | **70.4** | **89.2** | **74.5** | **117.3** | **75.2** | **677.4** | **74.0** |
| | $Z_{300}$ | 88.1 | 82.2 | 67.0 | 78.9 | 82.4 | 81.4 | 90.4 | 82.4 | 327.9 | 81.4 |
| NCEP-JRA25 | $\xi_{300}$ | **97.2** | **67.4** | **59.6** | **62.4** | **79.3** | **66.2** | **103.7** | **67.2** | **603.1** | **66.1** |
| | $Z_{300}$ | 80.2 | 74.5 | 60.8 | 71.6 | 72.8 | 71.9 | 81.6 | 74.4 | 295.4 | 73.3 |
| MERRA2-JRA55 | $\xi_{300}$ | **107.5** | **74.1** | **68.1** | **69.4** | **90.6** | **76.1** | **117.0** | **75.1** | **677.9** | **74.0** |
| | $Z_{300}$ | 87.8 | 82.7 | 65.7 | 79.1 | 81.3 | 82.3 | 84.1 | 77.1 | 318.8 | 80.0 |
| MERRA2-JRA25 | $\xi_{300}$ | **96.3** | **67.6** | **58.4** | **63.3** | **79.8** | **67.0** | **103.7** | **66.6** | **602.8** | **66.4** |
| | $Z_{300}$ | 80.9 | 75.1 | 59.6 | 72.0 | 72.4 | 73.9 | 78.0 | 75.4 | 290.9 | 74.7 |
| JRA55-JRA25 | $\xi_{300}$ | **100.3** | **69.1** | **60.5** | **61.6** | **81.1** | **68.1** | **107.6** | **69.1** | **617.4** | **67.5** |
| | $Z_{300}$ | 84.2 | 78.2 | 61.8 | 74.4 | 75.1 | 76.1 | 83.9 | 76.9 | 304.9 | 76.5 |

Percentage is defined as the number of matches divided by the largest number between each pair of reanalysis. Analysis for the period from 1980 to 2009.

Source: author's production.

From the tracks that match, the distribution of the mean separation distances between each pair of reanalysis is constructed as shown in Figure 5.16. This shows a very left-skewed distribution with the best matches occurring for the newest reanalyses. Most of tracks in the more recent reanalysis have separation distances less than 0.5º (geodesic)

for $Z'_{300}$ and 0.7º for $\xi_{300}$. The smallest values of separation distances in general occur for ERAI, NCEP-CFSR, and MERRA-2. In contrast, JRA-25 has a broader distribution for separation distances than in the other reanalyses, indicating greater uncertainties in location of COLs which is consistent with the statistics shown in Figure 5.11 and Figure 5.12. The reason for the larger uncertainties in vorticity compared to geopotential is closely related to the position of the $\xi_{300}$ centres in COLs. For symmetric systems, the $\xi_{300}$ maximum tends to appear near the low-pressure centre, as typically seen in surface extratropical cyclones. However, an elongated upper-level COL may shift the $\xi_{300}$ maximum equatorward as a consequence of the shear component (BELL; KEYSER, 1993), resulting in differences in location of $\xi_{300}$ centres.

Figure 5.16: Probability density function for mean separation distances for the tracks that match between the reanalyses ERAI, NCEP-CFSR, MERRA-2, JRA-55, and JRA-25, for a) $\xi_{300}$ and b) $Z'_{300}$.

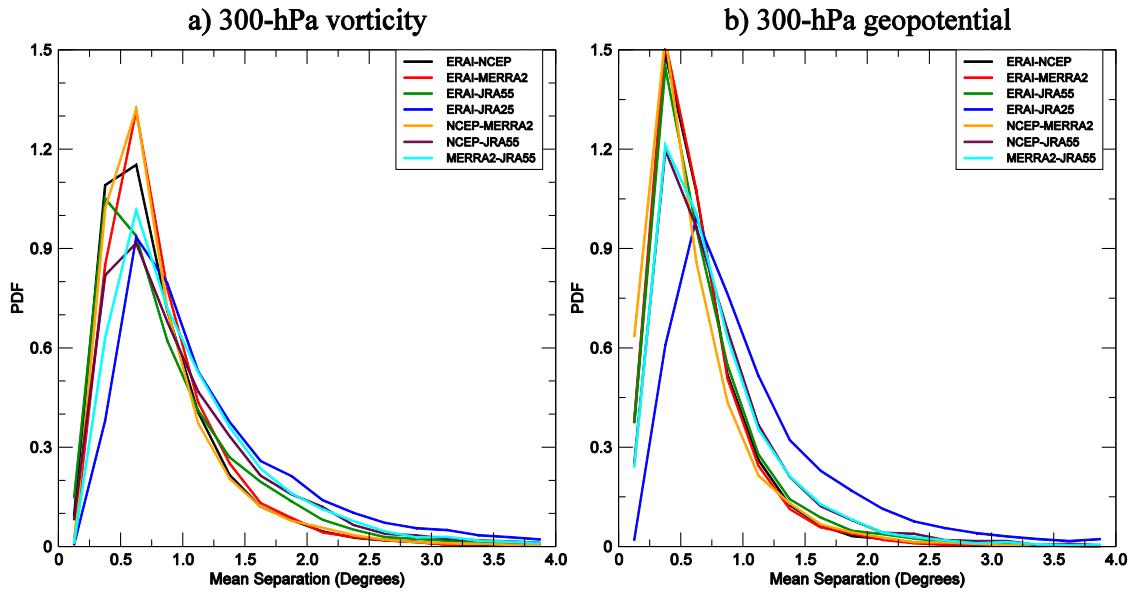


Analysis is for the Southern Hemisphere subtropics (15ºS-50ºS) for the period from 1980 to 2009. Unit is degree geodesic.

Source: author's production

## 5.6 Summary and discussion

A detailed analysis of the seasonal variability of the $\xi_{300}$ COLs in the SH is provided here using the ERAI reanalysis for a 36-year period (1979-2014). The most notable

features are the peak activity of COLs around the continents (Australia, South America, and Africa) and the minor activity over the oceans, which are in close agreement with previous studies. However, the maximum values of track density seem to migrate to oceanic areas in summer, and this aspect may likely be related to diabatic processes over the continents. During the austral summer, deep moist convection is most active inland over subtropical latitudes in South America and Africa, which may be important to reduce the frequency and/or lifetime of COLs due to the latent heat release (KOUSKY; GAN, 1981; HOSKINS et al., 1985). Conversely, it is fairly dry over most parts of Australia, where the latent heat effect is found to be less important (FUENZALIDA et al., 2005). The latent heat released by the deep convection seems to be one of the most important mechanisms to dissipate COLs since this process is able to produce a distinct warming of the COL cold-core, as discussed previously (GARREAUD; FUENZALIDA, 2007; KATZFEY; MCINESS, 1996; KOUSKY; GAN, 1981). This process destroy Eddy Available Potential Energy (EAPE) inhibiting the baroclinic conversion. Another reason is the sign of the divergent component of wind, which tends to produce upper level divergence in the trough (or upper level low), destroying EKE. A more detailed discussion of how the diabatic processes affect the COL lifecycle will be discussed in the next chapter.

In previous studies, the COL tracking has been based only on the use of either vorticity or geopotential. Here, a twofold perspective of the COL activity is presented using both $\xi_{300}$ and $Z'_{300}$ for the tracking. The results show that the track density of $Z'_{300}$ is comparable with the track density of $\xi_{300}$ in terms of location and seasonality. However, the values for $\xi_{300}$ are substantially larger than for $Z'_{300}$ due to the differences in scale, as discussed in Hoskins and Hodges (2002). This particular aspect has important implications for the identification of weak smaller-scale COLs, since these systems are generally not identified by the method based on the $Z'_{300}$. In addition, the tracks identified in $\xi_{300}$ are generally longer than in $Z'_{300}$, since the $\xi_{300}$ allows systems to be tracked from earlier in their lifecycle. For the comparison between the tracks performed by matching the same COLs, the largest matches between $\xi_{300}$ and $Z'_{300}$ occur in autumn (81%), whereas winter has the lowest number of matches with 73% of matches, indicating larger uncertainties.

A new approach was used to estimate the vertical depth of COLs, indicating that only about 20% of the total number reach to the surface. However, the proportion of deep COLs rises markedly when they are restricted to the strongest systems, suggesting a strong relationship between intensity and vertical depth. The spatial and temporal distributions of COLs were analysed in respect of different pressure levels. Results indicate that COLs are generally deeper in the western Pacific, Australia and New Zealand in comparison to those in other regions of the SH. In terms of monthly distributions, COLs were found to be deeper in winter and shallower in summer, which is consistent with the seasonal intensity distribution. Also, the results indicate that the spatial and temporal distributions of $\xi_{300}$ COLs are comparable with those of $\xi_{500}$ COLs. This contradicts the findings of Fuenzalida et al. (2005) and Reboita et al. (2010) who found a larger number of 500-hPa COLs in winter than in other seasons. However, in these studies the mid-tropospheric COLs were identified directly from the pressure level of interest, without matching with the upper-level COLs as done in the present study, so there is no guarantee that the systems are connected between the levels. Therefore, the discrepancies in seasonality reported in different studies may be explained by the criteria and dataset used to identify COLs which differ considerably from study to study. The main differences between previous studies on COL climatologies are summarized in Pinheiro et al. (2017) in their Table 1.

The seasonal variability of the $\xi_{300}$ and $Z'_{300}$ COLs is investigated in terms of the intensity measured by the $\xi_{300}$ and $Z'_{300}$ fields, and the precipitation for the maximum rate and the cumulative distributions. For the intensity distributions, a broad range of values is observed for both $\xi_{300}$ and $Z'_{300}$, agreeing with the results shown in Pinheiro et al. (2017) who analysed the COLs in terms of the $\xi_{300}$. The precipitation distributions show that the highest precipitation occurs in summer and autumn. This result was verified for the maximum precipitation rate and for the cumulative precipitation along the tracks using the thresholds of 50 mm and 100 mm. Therefore, these results indicate that the most intense COLs in terms of dynamical intensity occur in winter and spring, while the COLs that produce the most precipitation are commonly found in autumn and summer. This suggests the importance of factors other than the intensity for the precipitation in COLs. Chapter 6 will show how both intensity and moisture affect the precipitation in the COLs.

An intercomparison between five different reanalysis have been made based on the $\xi_{300}$ and $Z'_{300}$ COLs, allowing us to determine the differences and similarities between the reanalyses as well as the improvements of the newer reanalyses over the older JRA-25. The main findings of the comparisons between reanalyses are outlined below:

- The numbers and spatial distribution of COLs compare much better in the newer reanalyses than with the older reanalysis JRA-25. For the $\xi_{300}$ track density, in particular the smallest differences were found for the comparison between ERAI and JRA-55 as well as between NCEP-CFSR and MERRA-2. These results are likely associated with the method of data assimilation used in each reanalysis with ERAI and JRA-55 both using 4D-Var, whereas NCEP-CFSR and MERRA-2 use the 3D-Var GSI system.

- Previous studies have shown large differences of the COL seasonality between different reanalysis for both SH (REBOITA et al., 2010) and NH (NIETO et al., 2008). However, the results presented here show a strong similarity in seasonality between the reanalyses, in particular for the more recent reanalyses. These results highlight the improvements of the newer reanalyses over the older reanalyses. Also, these results suggest that the set of criteria used to identify a COL is the most important factor in determining the seasonality.

- A large variability of $\xi_{300}$ and $Z'_{300}$ COLs in terms of annual numbers is shown, although no significant trends were observed. The best comparison occurs for the new reanalyses, in particular for the period from 2000. An absolute minimum in 2002 is observed for all reanalyses, which may be related to the anomalous event of Sudden Stratospheric Warming, reported in previous studies. A positive but weak correlation between COLs and La Niña was found, i.e. COLs are found to be more common during La Niña events. However, no evidence has been found between the El Niño and the COL activity.

- For the distribution of maximum intensity of COLs, small differences in the $Z'_{300}$ values occur between the reanalyses. This is the case even if the newer reanalyses are compared with JRA-25. In contrast, the $\xi_{300}$ distributions have larger differences between the reanalyses. NCEP-CFSR and MERRA-2 have the

strongest COLs, and JRA-25 has the weakest COLs. This shows that the intensities of vorticity seem to be closely linked to the resolution of the reanalysis.

- For the matching, the largest number of matches was found for the comparison between ERAI and JRA-55 with 79.8% for $\xi_{300}$ and 84.5% for $Z'_{300}$. For the 10% most intense COLs, the number of matches increases to 92.5% and 87.8% for $\xi_{300}$ and $Z'_{300}$, respectively. This is much better than the comparison of the older reanalysis JRA-25, which the largest number of matches occurs for JRA-55 with only 67.5% for $\xi_{300}$ and 76.5% for $Z'_{300}$.

- The analysis of the mean separation distances between the matches shows that the four recent reanalyses have the best matches with separation distances less than 0.5° (geodesic) in $Z'_{300}$ and 0.7° in $\xi_{300}$. However, JRA-25 has a broader distribution and larger number of matches with distances greater than 1.0°, indicating large uncertainties in location of COLs.

# 6 STRUCTURE AND LIFE CYCLE OF CUT-OFF LOWS

This chapter provides a detailed analysis of the spatial structure and lifecycle of the SH COLs by using a more modern reanalysis (ERAI) than those used in previous studies. The composites are based on large samples of systems that make results more statistically robust compared to earlier case studies. The focus is on extreme COLs obtained from the 200 most intense systems. This is done using the identical COLs that can be found in both $\xi_{300}$ and $Z'_{300}$. The reason for this choice is to give a generic view of the structure of COLs using both $\xi_{300}$ and $Z'_{300}$. The main synoptic features and life cycle of the strongest COLs are examined such as the cold core, high-PV intrusion, baroclinic zones, vertical tilt and the cloud and precipitation patterns. Sections 6.1 and 6.2 focus on the upper-level features and vertical features of COLs, respectively. The sensitivity of compositing COLs that are identified using multiple criteria is investigated in Section 6.3. Composites of the cloud cover and precipitation are shown in Section 6.4. Lastly, the lifecycle of COLs is presented in Section 6.5.

## 6.1 Upper-level features

This section examines the main upper-level features of the COL composites by analysing horizontal fields such as geopotential height, winds, temperature, specific humidity, potential vorticity, and specific parameters for frontal analysis such as the temperature gradient and the thermal frontal parameter (TFP), defined in Appendix. For some analyses that require anomaly fields two methods are used to calculate the anomaly fields (such as done for temperature and geopotential height): the zonal anomaly and the area-average anomaly. The first one is computed by removing the zonal mean at each time step and for each latitude, as described in Section 3.2.2. The second method of computing an anomaly is obtained directly during the calculation of the spatial composites by removing the area average for a prescribed radius value from the grid for each storm. There are similarities and differences between the fields obtained using the two filters. The zonally averaged quantities (Figure 6.1a) are used to highlight the longitudinal gradients, which are often found in a baroclinic upper-level wave along the ridges and troughs. Temperature and geopotential height show an inverted shape with respect to each other along the $y$ axis. For the area-average over the COL centres using a 15$^{o}$ radius cap (Figure 6.1b), distributions are much more similar to

the original parameters, and this type of anomaly is highly influenced by the latitudinal gradients within the spherical region used to compute the average. However, it is difficult to say which filter is the best option to analyse the structure within COLs. For this reason, the two filtering methods to calculate the anomaly are used for further analysis. Since the COLs move preferentially eastward and we aim to examine the horizontal tilt, all composites that will be presented use a non-rotated spherical cap to extract the regions around the COL centres referred to cardinal points relative to the north (see Figure 6.1): north (0º), east (90º), south (180º), and west (270º). Composites are produced for the 200 most intense $\xi_{300}$ COLs occurring in the SH.

Figure 6.1: Composites of Cut-off Lows in the Southern Hemisphere for temperature at 500-300 hPa and geopotential height at 300 hPa based on the a) zonal anomaly and b) area-average anomaly.

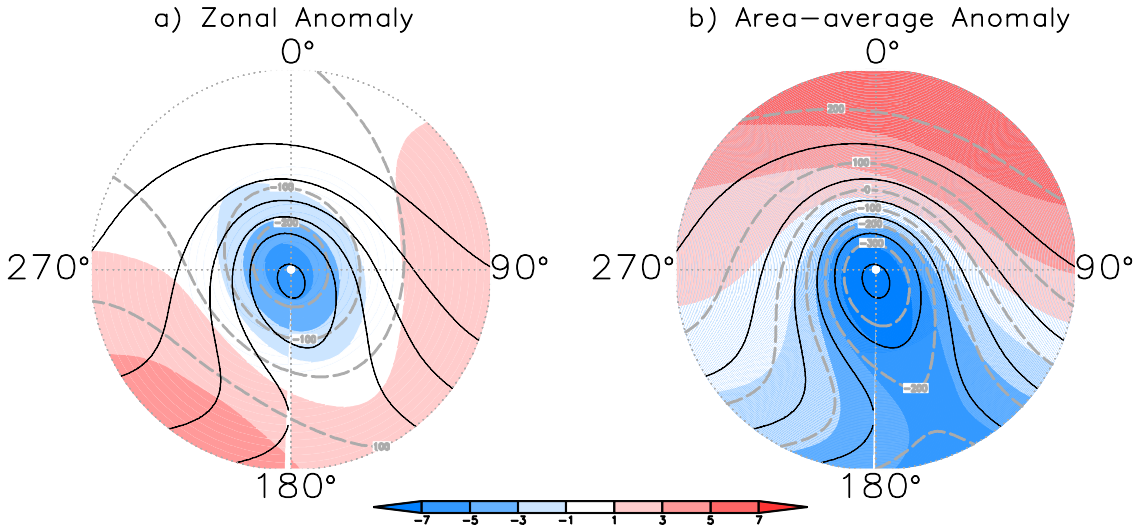


Composites for the 200 most intense Cut-off Lows that match between the $\xi_{300}$ and $Z'_{300}$. Unit is geopotential meters (gpm) for $Z_{300}$ height (black solid line) from 8900 to 9400 gpm for contour intervals 100 gpm, $Z'_{300}$ (dashed grey line) for contour intervals 100 gpm, and temperature anomaly (shaded) in K. Analysis using the ERAI reanalysis for a 36-yr period (1979-2014).

Source: Author's production.

The zonal and meridional circulation and the $Z_{300}$ height associated with the upper-level COLs are shown in Figure 6.2. The $Z_{300}$ height (Figure 6.2c) shows an amplifying upper-level trough with a deep centre of 8900 gpm located slightly displaced south of

the composite centre, i.e. the $\xi_{300}$ minimum. The difference in location for the geopotential and vorticity minima occurs because the vorticity is influenced by the shear component associated with elongated upper-level troughs (BELL; KEYSER, 1993), as commented in Chapter 5. This circulation pattern contrasts with the more symmetrical vortices originating in tropical regions (COUTINHO, 2010; KELLEY; MOCK, 1982; MORAIS, 2016; SATYAMURTY; SELUCHI, 2007). Additionally, the upper-level trough represented in the $Z_{300}$ height shows a discrete westward tilt at the time of maximum intensity of the COLs. The magnitude of the zonal and meridional wind components at 300-hPa show two maxima: the stronger centre is on the east side where the magnitude of winds is greater than 50 m/s mainly attributed to the meridional component (Figure 6.2b); the other centre is on the west side of the trough with a smaller extent than the former. However, the wind intensity for the two centres varies widely with the stage of the COL since the kinetic energy moves downstream throughout the life cycle. Evidence of the downstream development in COLs will be shown in Chapter 8.

Figure 6.2: Composites of Cut-off Lows in the Southern Hemisphere for a) zonal component of wind, b) meridional component of wind, and c) $Z_{300}$ height combined with magnitude of the zonal and meridional winds, all fields referred to 300 hPa.

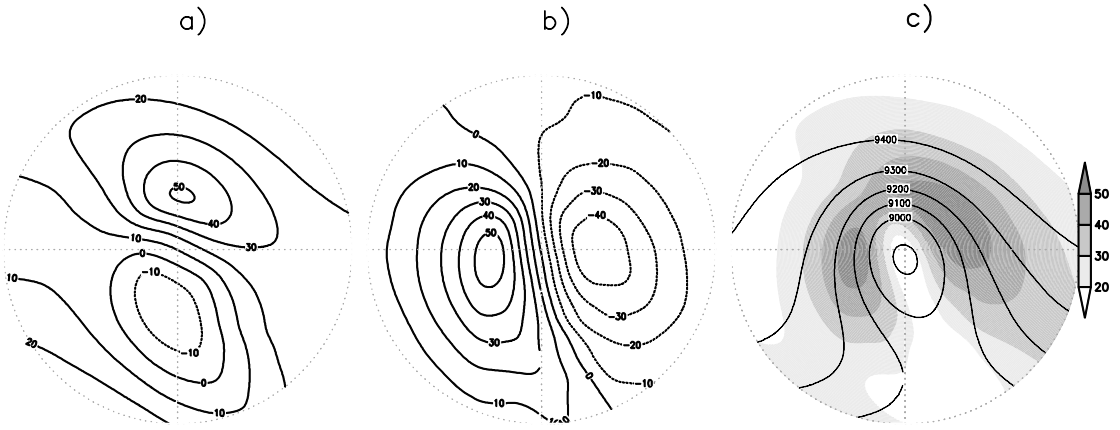


Composites for the 200 most intense Cut-off Lows that match between the $\xi_{300}$ and $Z'_{300}$ . Unit is m/s for winds (interval is 10 m/s) and geopotential meters for $Z_{300}$ height (black solid line). Winds are in black line in (a) and (b), and shaded in (c). Analysis performed using the ERAI reanalysis for a 36-yr period (1979-2014).

Source: Author's production.

The classical formation of a COL begins when a cold trough in mid-latitudes deepens toward lower latitudes (sequence not shown), so that the cold-air in the northern part of the trough is cut-off from its polar source, leading to the formation of a cold low-pressure system embedded in a subtropical mass, the so-called “cold pools”. This aspect is well represented in the composite of temperature in the layer 500-300 hPa (Figure 6.3a) determined from the maximum intensity. It is apparent that the cold core is located exactly on the COL centre, i.e. where the geopotential minimum occurs. Similar results were found using the thickness between the same pressure levels used to calculate temperature, as a result of the hypsometric equation (HOLTON, 1992). The specific humidity depicted in Figure 6.3b shows there is relatively dry air near the COL centre, but the values rapidly increase eastward. This means that a moisture front is typically observed east of the COL centre.

Figure 6.3: Composites of Cut-off Lows in the Southern Hemisphere for $Z_{300}$ height combined with a) temperature averaged between 500 hPa and 300 hPa, b) specific humidity at 300 hPa, and c) thermal frontal parameter and potential temperature gradient, averaged between 500 hPa and 300 hPa.

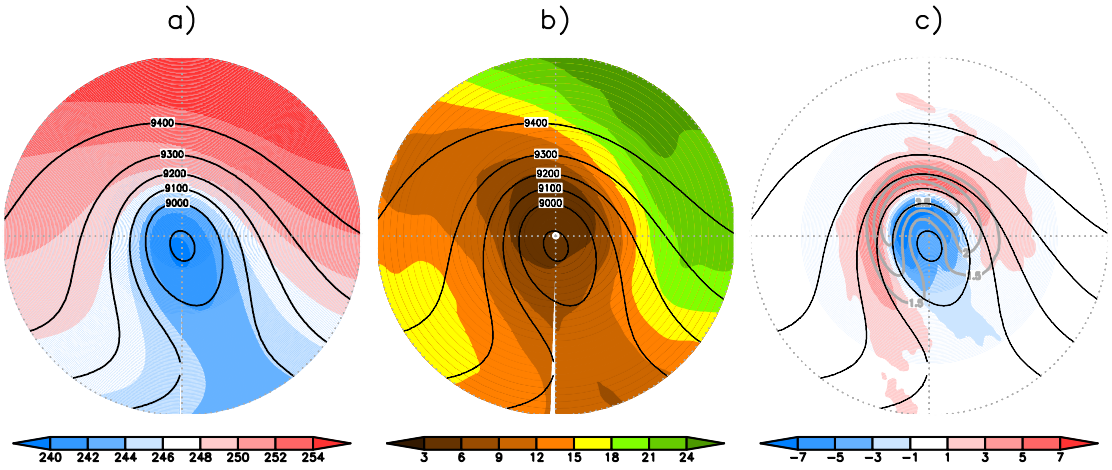


Composites for the 200 most intense Cut-off Lows that match between the $\xi_{300}$ and $Z'_{300}$ . Unit is gpm for $Z_{300}$ height (black solid line), a) K for temperature (shaded), b) $10^{-5}$ kg kg$^{-1}$ for specific humidity (shaded), c) $10^{5}$ K/(100km) for temperature gradient (grey solid line), and $10^{11}$ K/(100km)$^{2}$ for thermal front parameter (shaded). Temperature, thermal frontal parameter, and potential temperature gradient are averaged over three pressure levels (500, 400 and 300 hPa). Analysis performed using the ERAI reanalysis for a 36-yr period (1979-2014).

Source: Author’s production.

It is well-known that COLs are characterized by strong baroclinicity in the mid-upper troposphere, as documented in many studies (HOSKINS, 1971; PALMEN, 1949; SHAPIRO, 1970). The identification of baroclinic zones around the COLs with the TFP has been done by Sabo (1992) over a European region, and in the present study the same parameter will be used as a guide to identify the frontal zones of the COLs in the SH. The TFP has been seen as a valuable tool to identify fronts since it takes into account the changes of temperature in the direction of the temperature gradient. In other words, a front is located where the maximum TFP occurs, that it is offset from the maximum temperature gradient. More details about the TFP and its usage for frontal analysis are available in the Appendix B.

The TFP can be computed for potential temperature (RENARD; CLARKE, 1965) as well as for temperature (CLARKE; RENARD, 1966). This study uses only temperature to obtain the TFP. Figure 6.3c shows the $Z_{300}$ height combined with the TFP and the temperature gradient both derived for three pressure levels (500, 400, and 300 hPa) because the baroclinic zones of COLs usually cover a deep layer in the troposphere, as will be shown in Section 6.2. A visible distinction is made between the cold and warm regions. The temperature gradient maximum is located at the northern boundary of the COL and nearly coincides with zero TFP, indicating the start of the baroclinic zone. The region of the COL where the temperature gradient varies more rapidly in the direction of the gradient represents the maximum TFP (positive values), that is referred to as the frontal zone, i.e. the region where the warm and cold boundaries of the upper-level front are located.

Results of the composite of TFP differs from those reported by Sabo (1991) who found two baroclinic zones, one in front of the COL centre (i.e. east of the low-pressure minimum) which is connected with the frontal cloud band, and the other behind the COL centre associated with a baroclinic boundary. Furthermore, Nieto et al. (2005) has used the TFP as a criterion to identify COLs (see Step 3 of their methodology) based on the baroclinic zone located downstream of the trough axis. One reason for the differences found between previous studies and this study is that the composite is produced for the time when the individual COLs reach their maximum intensity. The analysis of the TFP for individual cases often shows the two baroclinic regions

discussed in the Sabo and Nieto's studies (see Appendix C) but they do not exist simultaneously as suggested by these authors. In most of the cases, the TFP maximum originates upstream of the trough axis and moves cyclonically downstream along the northern boundary of the COLs. Thus, it seems that the baroclinic zones propagate from the western side to the eastern side of a COL during their development, similar to the energy dispersion through the ageostrophic fluxes in the upper-troposphere as discussed in many studies (ORLANSKI; KATSFEY, 1991; CHANG, 2000; DANIELSON et al., 2006; GAN; PIVA, 2013, 2016).

To give an idea of how the PV distributions vary at different levels, composites of COLs in respect of PV have been constructed on three isobaric levels (400, 300 and 200 hPa) and three isentropic levels (315, 330 and 350 K) as shown in Figure 6.4. Also shown in this figure is the geopotential height at 400, 300 and 200 hPa (from left to right). An advantage in using isentropic surfaces in addition to isobaric surfaces is that the PV is conserved following adiabatic and frictionless flow. The isentropic surface at 350 K generally samples stratrospheric PV values, while the 330 K and 315 K surfaces sample both stratospheric and tropospheric values since these surfaces intersect the tropopause in the subtropics and mid-latitudes (HOSKINS et al., 1985). An analogous interpretation can be given for the 400, 300 and 200 hPa isobaric levels. For COLs in the SH, the most prominent feature of the PV are the regions of negative values near the COL centre which nearly coincide with the $\xi_{300}$ minimum. It can be seen that the tongues of cyclonic PV stretch into narrow streamers that extend equatorward, leading to the formation of isolated stratrospheric air cut-off from its origin, the so-called "stratospheric reservoir". Additionally, the PV streamers and cut-offs associated with the COL formation are often linked with Rossby wave breaking which has been discussed in many studies (HOSKINS et al., 1985; NDARANA; WAUGH, 2010; WERNLI; SPRENGER, 2007). Such wave breaking is accompanied by an irreversible deformation of PV which can be manifested by the reversal of the meridional PV gradient. This aspect is seen in the composites COLs with PV reversal more pronounced if the composites are produced for COLs only associated with blocking, which occur for relatively high PV values in lower latitudes and low PV values in higher latitudes.

Figure 6.4: Composite of Cut-off Lows in the Southern Hemisphere for geopotential height and potential vorticity for the isobaric levels at a) 400 hPa, b) 300 hPa, and c) 200 hPa, and for the isentropic surfaces on d) 315 K, e) 330 K, and f) 350 K.

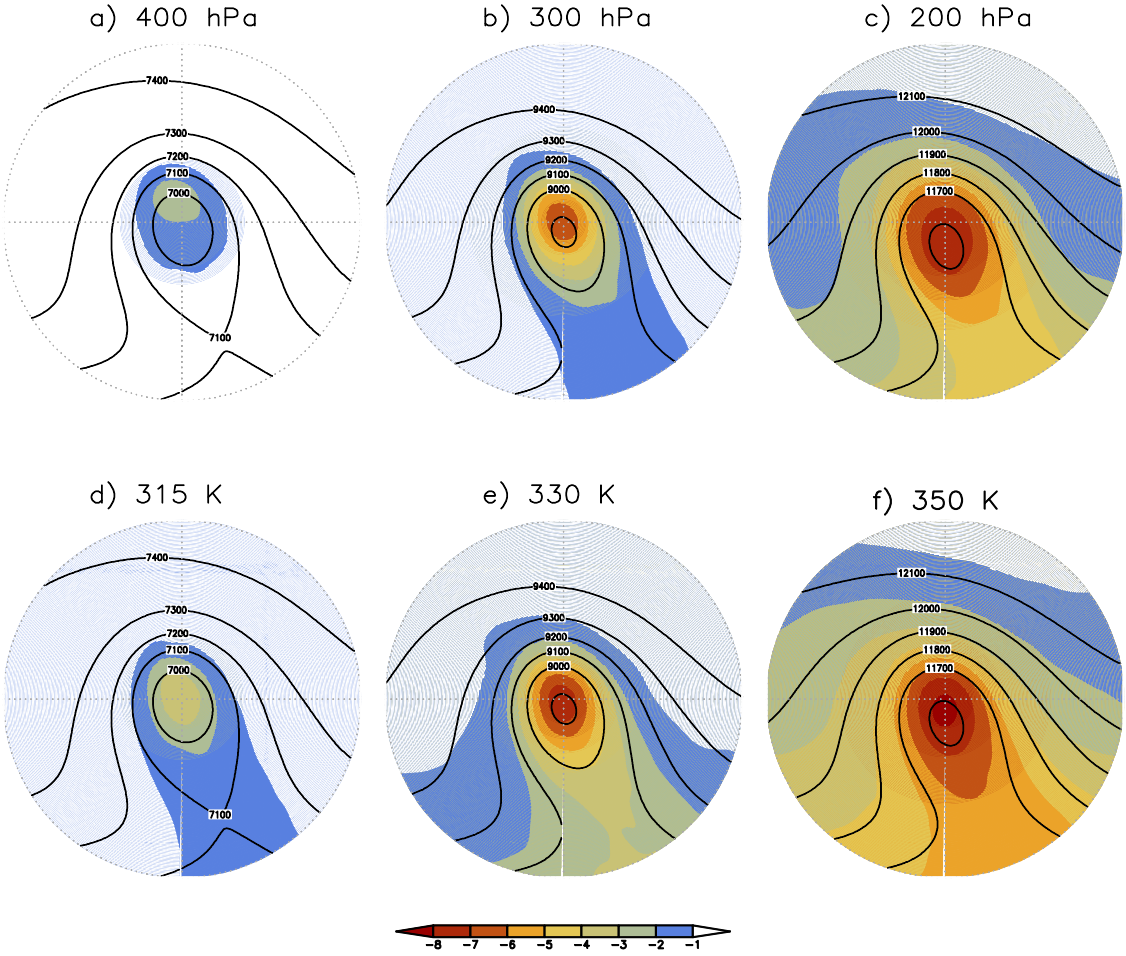


Composites for the 200 most intense Cut-off Lows that match between the $\xi_{300}$ and $Z'_{300}$. Unit is $10^{-6}$ $m^2$ $s^{-1}$ K $kg^{-1}$ for potential vorticity (shaded) Analysis using the ERAI reanalysis for a 36-yr period (1979-2014).

Source: Author's production.

There is a clear correspondence between the composites when viewing the PV structure for COLs using the isobaric or isentropic surfaces. Comparing the COL PV composite at 200 hPa level with that on the 350 K isentropic surface, the distributions and values are relatively similar to each other, in general values lower than -2.0 PVU cover almost the entire composite plots. It is noticeable that the PV values on the 350 K isentropic surface are greater than the PV values at the 200 hPa level. The main reason for the differences may be the level where the PV is measured rather than the fact that the

isentropic surface intersects the isobaric surfaces, because the distributions are similar. In addition, the comparison between the 300-hPa PV and the 330-K PV show similarities between each other, and the stratospheric influence is mainly restricted to the vortex area and its surroundings. For the comparison between the PV at 400 hPa and that on the 315 K isentropic surface, it can be noticed that the stratospheric intrusion is much less apparent in the COLs, though the two surfaces still intersect the tropopause near the COL centre. Also, the analysis of the geopotential height confirms that the 300-hPa COLs are stronger than the COLs at the other levels. The results presented here are consistent with the PV structure found in earlier studies (BASSET; GAHEIN, 2003; BELL; KEYSER, 1993; KENTARCHOS et al., 1999a). Therefore, the composites of PV using the isentropic coordinate are found to be comparable with those viewed from the isobaric levels, suggesting that both coordinates are appropriate and equivalent for the diagnostics of PV properties in the COLs. Other interesting parameters of the upper-level structure of COLs, such as relative vorticity, divergence, and ozone ($O_3$) mass mixing ratio will be shown in the following section.

## 6.2 Vertical features

The vertical structure of COLs is investigated for several fields and analysed through the west-east (W-E) and south-north (S-N) vertical cross sections. The 15º spherical cap region is extracted for ten pressure levels from 1000 up to 100 hPa using the track point at 300 hPa as the reference. Thus, the vertical tilt of COLs is not taken into account for this specific analysis, but it will be examined further in this chapter. Vertical composites could be produced using the vorticity or geopotential minimum at each pressure level to extract the region centered on the minimum referred to each level, but the results will likely not change since tilt is minor in the mature stage (time of maximum intensity). The vertical composites are exhibited only within 10º of radius, that it is where synoptic-scale processes dominate. Composites are produced at a specified offset time relative to the time of maximum intensity of COLs, but the COL temporal evolution will be discussed in Section 6.5.

Some parameters such as wind magnitude, geopotential and vorticity are conveniently discussed together in order to provide a typical dynamic structure of COLs, these are shown in Figure 6.5. Large contrasts are seen for the W-E cross section (Figure 6.5a)

because COLs move preferentially eastward, and as a consequence of the quasi-geostrophic theory (PETTERSSEN, 1956; SUTCLIFFE, 1947; TRENBERTH, 1978) rising air due to negative vorticity advection is expected to occur downstream of the COL motion and sinking air due to positive advection upstream of the COL motion in the SH. This shows a nearly symmetric circulation in the mid and upper troposphere. The centres of maximum wind speed are located about $4^{o}$-$6^{o}$ west and east of the COL centre, with the eastern centre a little stronger and higher than the western centre. The magnitude of the winds is greatly reduced vertically and horizontally away from the maxima, indicating a region of strong wind shear in the mid and upper troposphere. However, the S-N cross section (Figure 6.5b) shows an asymmetric circulation with stronger winds in the northern part of the COL, associated with the westerly winds (baroclinic zone). Similar results have been observed for a COL in North America by the pioneering study of Palmén (1949). However, that study attributed the asymmetry of the N-S cross section to a lack of observations in the southern United States and Mexico. Further studies such as Hsieh (1949) and Kelley and Mock (1982) confirmed the asymmetry does exist with stronger winds on the equatorward side of the COL. The results of this study are consistent with previous findings as the relatively weak winds appear poleward from the low centre and occur due to the weakening of westerlies and reversal of winds associated with the cut-off process.

Figure 6.5: Composite vertical cross-sections along the a) west-east and b) south-north lines of Cut-off Lows in the Southern Hemisphere. The fields are wind magnitude, relative vorticity, and geopotential height anomaly.

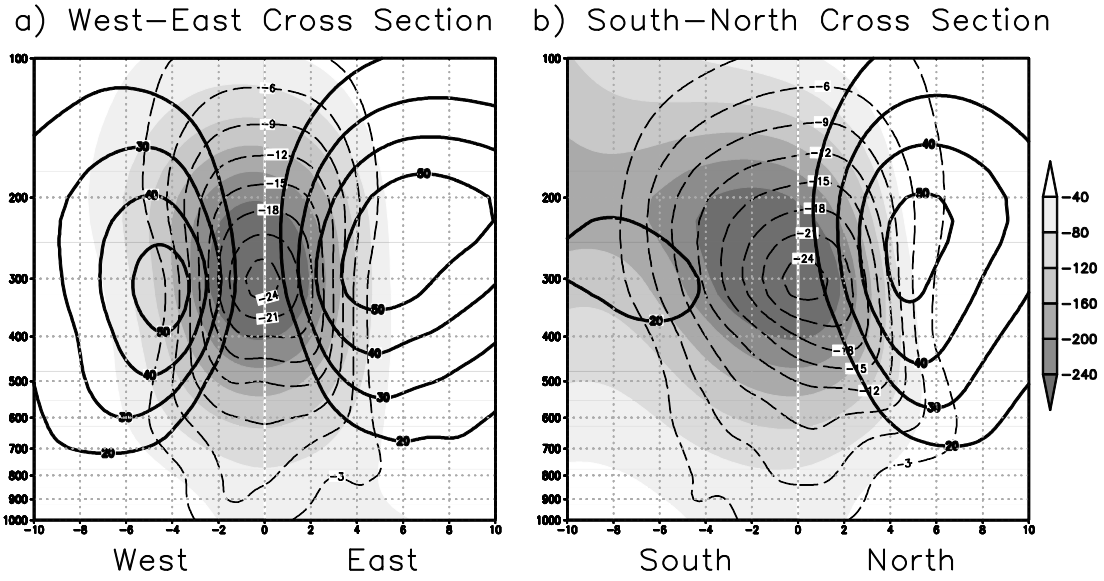


Composites for the 200 most intense Cut-off Lows that match between the $\xi_{300}$ and $Z'_{300}$, centered on the time and space relative to the $\xi_{300}$ minimum. The total distance in the $x$ axis is 20º geodesic. Magnitude of horizontal winds (thick solid line) from 20 m/s for the contour intervals 10 m/s. Geopotential height anomaly for negative values (shaded) for the contour intervals 40 gpm, where the anomaly is determined based on the area average within a 15º spherical arc radius. Relative vorticity (dotted lines) for contour intervals 3.0 $10^{-5}$ $s^{-1}$. Analysis using the ERAI reanalysis for a 36-yr period (1979-2014).

Source: Author's production.

The full resolution of relative vorticity and geopotential height anomaly are taken to demonstrate the vertical structure of COLs in terms of intensity. It is expected that the maximum intensity occurs where the wind (shear) magnitude is maximum, i.e. near the tropopause. For the W-E and S-N cross sections, the largest intensities are found in the upper troposphere and the values gradually weaken toward the surface, though cyclonic features are still found in the lower troposphere. It can be noticed that the largest geopotential anomalies (-240 gpm) coincide in location with the vorticity minimum (-24.0 x $10^{-5}s^{-1}$) in the W-E cross section, but the geopotential minimum is offset from the vorticity minimum in the S-N cross section, which is consistent with the results discussed in Section 6.1. Similar results would be obtained if the compositing were

performed referencing to the $\xi_{500}$ tracks (figure not shown). This means the maximum intensity of COLs is expected to be at about 300 hPa even if the tracking were performed at a level other than 300 hPa. In general, our results agree closely with previous studies such as Quispe and Avalos (2006) who found a very similar vertical structure for winds and vorticity (see their Figure 3). However, some differences are found when compared with the structure typically seen in upper-tropospheric vortices of lower latitudes (GAN, 1982; KOUSKY; GAN, 1981; KELLEY; MOCK, 1982; MORAIS, 2009) where the tropopause is higher than that in the subtropics and mid-latitudes.

The thermal structure of COLs is examined in terms of isentropes and isotherms and is shown in Figure 6.6. In the W-E cross section, the isentropes and isotherms appear to be almost completely symmetric, but the S-N cross section exhibits a discernible asymmetry. The tropospheric cold-core is apparent through the isotherms folding in the COL centre where it is surrounded by warmer air, while the stratospheric warm-core is marked by cooler temperatures in the COL periphery. Contrary to the temperature profile, the potential temperature increases with height, thus the cold core is depicted by a reversal of the lapse rate in the lower troposphere. The thermal structure of the COL composites is in close agreement with previous studies (CAMPETELLA; POSSIA, 2006; GRIFFITHS et al., 1998; PALMEN, 1949; SATYAMURTY; SELUCHI, 2007). However, the discontinuity of (potential) temperature typically seen along the tropopause is smoothed out by the compositing process.

Figure 6.6: Composite vertical cross-sections along the a) west-east and b) south-north lines of Cut-off Lows in the Southern Hemisphere. The fields are wind magnitude, temperature, and potential temperature.

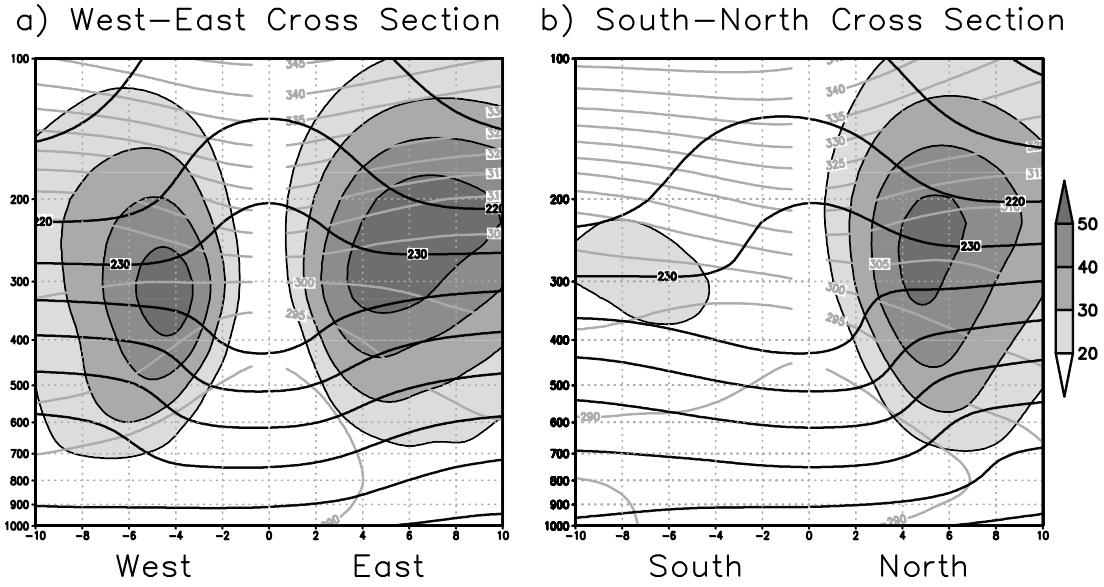


Composites for the 200 most intense Cut-off Lows that match between the $\xi_{300}$ and $Z'_{300}$, centered on the time and space relative to the $\xi_{300}$ minimum. The total distance in the $x$ axis is 20º geodesic. Magnitude of winds from 30 m/s for the contour intervals 10 m/s (shaded). Temperature in K for the contour intervals 10 K (thick black line). Potential temperature in K for the contour intervals 5 K (grey solid line). Analysis using the ERAI reanalysis for a 36-yr period (1979-2014).

Source: Author's production.

The analysis of the three-dimensional structure of COLs continues by assessing other parameters such as the vertical velocity, divergence, and specific humidity anomaly (Figure 6.7). Similar to previous results of this section, the largest contrasts are seen in the W-E cross section (Figure 6.7a). This shows that the lower and middle troposphere are dominated by convergence downstream and divergence upstream of the storm centre, and the opposite holds for the upper troposphere and lower stratosphere. As a consequence of the convergence in the lower troposphere, the maximum uplift takes place on the eastern side of COL at 500-400 hPa (~5º from the COL centre), then the moist air indicated by the positive values of specific humidity anomaly is transported to higher levels by the ascent. On the western side of the COL, a strong subsidence can be found at a distance of about 5º from the centre, with values that are comparable to the

ascent. It can be seen that the ascent and descent influence almost the entire troposphere, but the maximum values occur at the level of non-divergence, which is approximately at 500 hPa for the descent and somewhat higher for the ascent. Therefore, cloud formation and precipitation are expected downstream of the COL centre, whereas the subsidence upstream tends to suppress the precipitation, even when a thermodynamically unstable condition occurs. Also, the western side of the COLs is associated with downward movement and stratospheric intrusions as the result of ageostrophic flow (KENTARCHOS et al., 1999a). The results for the COL vertical structure are in close agreement with earlier studies for subtropical and mid-latitude COLs (MIKY FUNATSU et al., 2004; GODOY et al., 2011; KNIPPERTZ; MARTINS, 2005; SIQUEIRA et al., 2013), but differ from the structure typically found in the upper tropospheric vortices of lower latitudes. According to Gan (1982), the upper-tropospheric vortices that affect the northeast Brazil are characterized by a symmetric thermodynamic structure consisting of cold air descending in the centre and warmer air rising at the periphery. The dynamics in the upper tropical troposphere differ from those of midlatitudes, where the disturbances seem to be driven by the mechanism of mixed Rossby-gravity waves, as discussed earlier.

Figure 6.7: Composite vertical cross-sections along the a) west-east and b) south-north lines of Cut-off Lows in the Southern Hemisphere. The fields are divergence, vertical velocity, and specific humidity zonal anomaly.

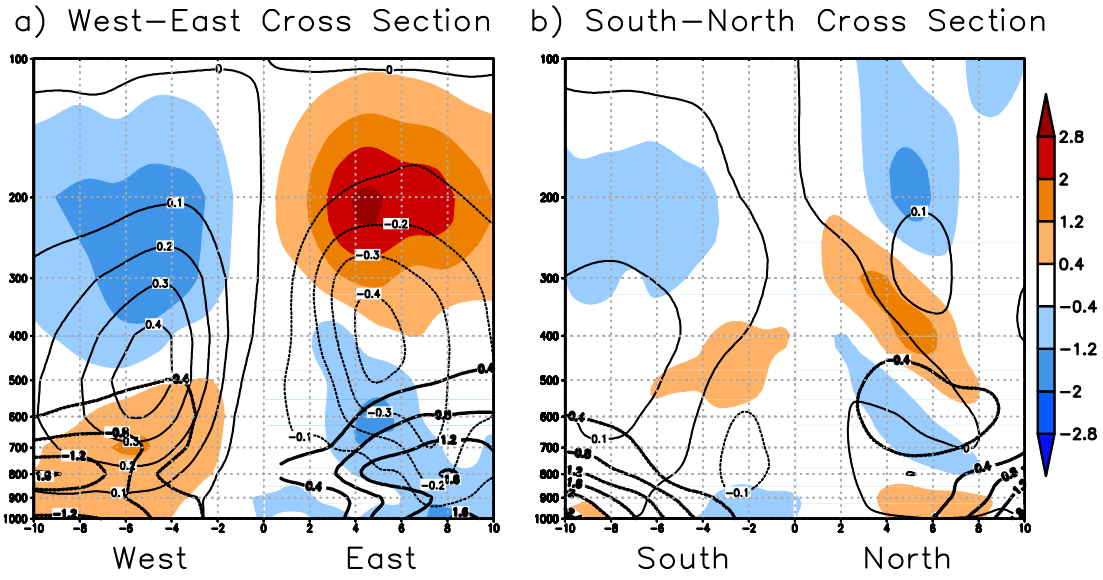


Composites for the 200 most intense Cut-off Lows that match between the $\xi_{300}$ and $Z'_{300}$, centered on the time and space relative to the $\xi_{300}$ minimum. The total distance in the $x$ axis is 20º geodesic. Divergence in $10^{-5}$ $s^{-1}$ for contour intervals 0.8 (shaded), vertical velocity in Pa $s^{-1}$ for contour intervals 0.1 (thin black line), specific humidity anomaly in $10^{-3}$ kg $kg^{-1}$ (thick black line), where the anomaly is determined based on the area average within a 15º spherical arc radius. Analysis using the ERAI reanalysis for a 36-yr period (1979-2014).

Source: Author's production.

In Section 6.1, the analysis of upper-level fronts associated with the strongest COLs was carried out using horizontal plots, while this section presents similar fields, such as the temperature anomaly and the TFP, but for vertical cross-sections. The W-E and S-N cross sections (Figure 6.8) show that the baroclinic zones are not restricted to a narrow surface but they extend through a deep layer in the troposphere and stratosphere associated with cold and warm cores, respectively. Focusing on the tropospheric cold-core, the W-E cross section (Figure 6.8a) indicates the existence of two main baroclinic zones which are located approximately between 700 and 300 hPa on the edges of the cold core. The maximum (minimum) TFP occurs on the western side of the COL with positive (negative) values up to 9 (12) × $10^{-11}$ ºC/(100 $km^2$). Similar results are found for composites produced using earlier stages, while in the decaying stage the maximum

TFP occurs downstream of the COL centre (figure not shown). These results are in agreement with the conceptual model proposed by Keyser and Shapiro (1985) shown in their Figure 19, since the upper-level frontal zones propagate downstream throughout the COL lifecycle. However, there are significant differences from case to case which is smoothed out by the compositing (see Appendix C). In the S-N cross section (Figure 6.8b), a single well-defined maximum is observed on the northern side of the COL, which is consistent with Figure 6.3c. The zero isoline between the maximum and minimum values (black thick line) denotes the largest temperature gradient.

Figure 6.8: Composite vertical cross-sections along the a) west-east and b) south-north lines of Cut-off Lows in the Southern Hemisphere. The fields are temperature anomaly and thermal frontal parameter.

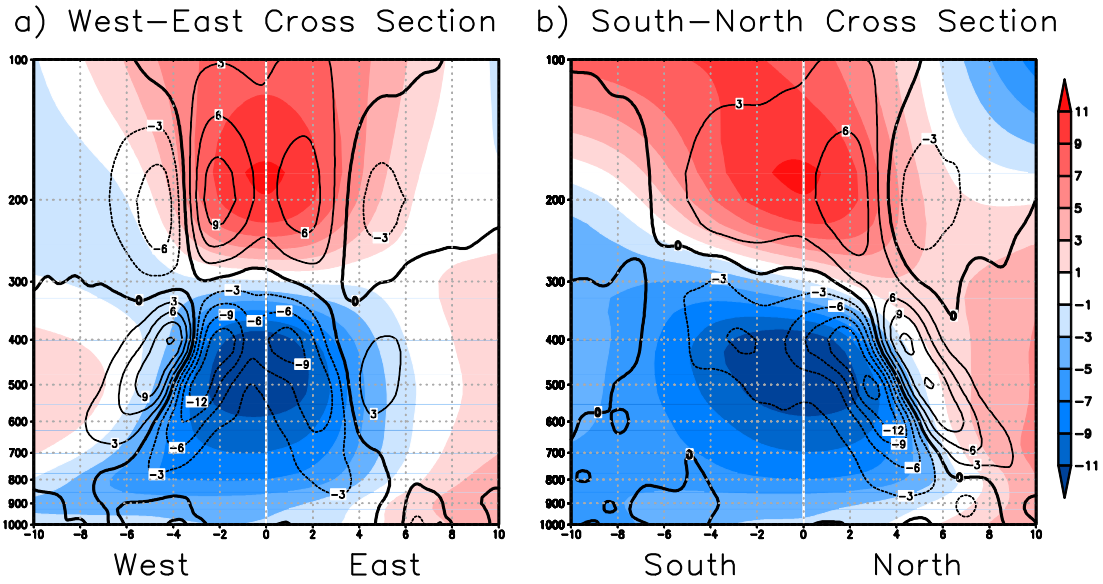


Composites for the 200 most intense Cut-off Lows that match between the $\xi_{300}$ and $Z'_{300}$, centered on the time and space relative to the $\xi_{300}$ minimum. The total distance in the $x$ axis is 20º geodesic. Temperature anomaly in K (shaded), where the anomaly is determined based on the area average within a 15º spherical arc radius. Thermal front parameter in $10^{-11}$ K/(100 km)$^2$ for contour intervals 3.0 (black line). Analysis using the ERAI reanalysis for a 36-yr period (1979-2014).

Source: Author's production.

The greatest extent of the tropospheric cold-core as well as the maximum TFP are observed during the development and mature stages, while in the decaying phase the

cold core reduces horizontally and vertically, and the maximum TFP shifts toward the COL centre (figure not shown). Since the aspects described above are typical of the strongest COLs and assuming that numerical models are capable to capture these, meteorologists could use models in practice to predict the COL evolution. On another note, these results suggest that during the decaying phase the COL cold-core is warmed uniformly over the entire area of the system. This differs somewhat from the numerical experiment reported by Garreaud and Fuenzalida (2007), shown in their Figure 15b, who found that, using a reduced topography, the COL core warming by the latent heat is more effective on the eastern side. Their result is explained by the presence of the moisture influx from the continental warm air into the COL area. A hypothesis for the symmetric dissipation of the cold core observed in our results is attributed to the flow inside the COL that moves cyclonically distributing the warm air from the latent heat source region to other parts of the system. In addition to this, as the COL intensifies the subsidence (uplift) in the west (east) side of the COL (see Figure 6.7) becomes stronger causing adiabatic warming (cooling) in the periphery of the COL, and this may contribute to weaken the horizontal temperature gradient. These mechanisms have received much less attention than the diabatic effects on the COL dissipation. Therefore, further studies should be undertaken to evaluate both diabatic and adiabatic effects for the COL development.

Another typical aspect of COLs is the troposphere-stratosphere exchange as a consequence of the tropopause fold as briefly discussed in Section 6.1. This is examined in terms of the vertical distribution of PV and $O_3$ in the W-E and S-N cross sections (Figure 6.9). A peculiar feature of the COL composite is the anomalous tropopause that descends to lower than 400 hPa in the COL centre, depicted by the 2.0 PVU surface in the W-E cross-section (Figure 6.9a). Another way to represent the dynamic tropopause is based on the isentropic PV gradient (KUNZ et al., 2011), but the conclusions are not altered. The deepest intrusion takes place at the time of maximum intensity induced by the cyclonic PV anomalies. The tropopause descent is more marked in the S-N cross-section (Figure 6.9b), where the asymmetry is quite apparent due to the deepest intrusion and the abrupt variation on the northern side of the COL. As the tropopause is lowered, high-PV stratospheric air is drawn down into the troposphere. For very intense

systems, the tropopause can reach lower levels (e.g. 600 hPa) as seen in Hoskins et al. (1985) and in Appendix D.

Figure 6.9: Composite vertical cross-sections along the a) west-east and b) south-north lines of Cut-off Lows in the Southern Hemisphere. The fields are ozone mass mixing ratio anomaly and potential vorticity.

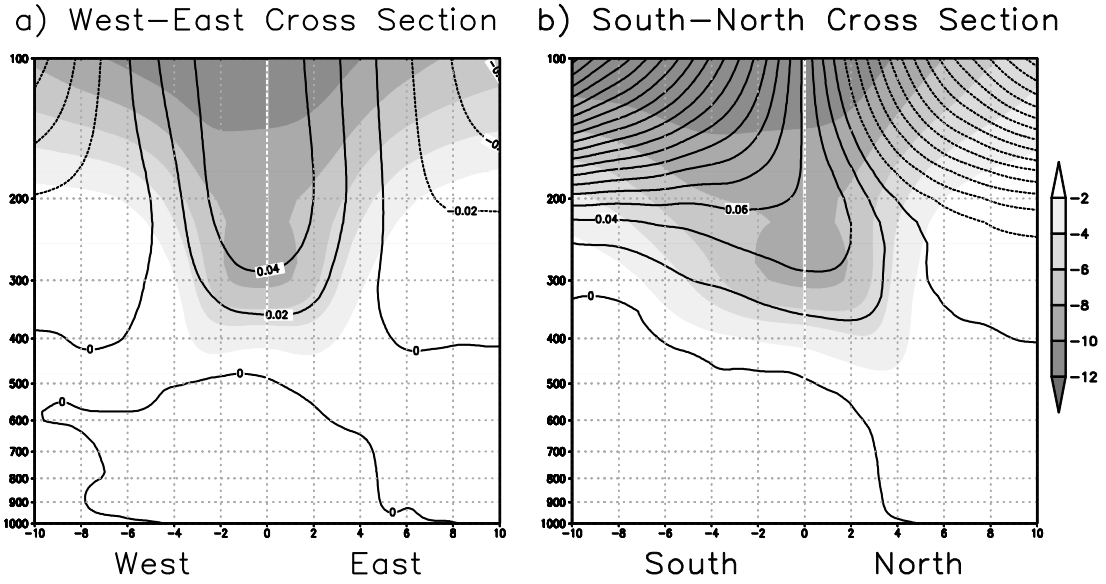


Composites for the 200 most intense Cut-off Lows that match between the $\xi_{300}$ and $Z'_{300}$, centered on the time and space relative to the $\xi_{300}$ minimum. The total distance in the $x$ axis is 20º geodesic. Potential vorticity in $10^{-6}$ m$^2$ s$^{-1}$ K kg$^{-1}$ (shaded), ozone mass mixing ratio anomaly in kg kg$^{-1}$ for the positive (solid line) and negative (dashed line) values, where the anomaly is determined based on the area average within a 15º spherical arc radius. Analysis using the ERAI reanalysis for a 36-yr period (1979-2014).

Source: Author's production.

The transport of stratrospheric $O_3$ into the troposphere is investigated in terms of the $O_3$ anomaly distribution for the vertical cross sections produced from the ERAI reanalysis. The $O_3$ anomaly is preferred instead of $O_3$ because the latter has a smoother distribution (figure not shown). Figure 6.9 shows that the tropopause descent is followed by a vigorous transport of stratospheric $O_3$ into the troposphere, as denoted by the positive $O_3$ anomalies near the COL centre. In general, the high $O_3$ coincides with the high PV, i.e. both fields are dynamically linked to each other and are frequently used as indicators of the depth of stratospheric air penetration (BASSET; GAHEIN, 2003). Similar to PV,

the $O_3$ distribution is almost symmetric in the W-E cross section, but an asymmetry is seen in the S-N cross section since the positive (negative) $O_3$ anomalies are found poleward (equatorward) of the COL centre. This illustrates how the $O_3$ rich air associated with the COL is connected to the high-latitude stratospheric reservoir as the large $O_3$ values are found south of the COL centre.

There is a considerable body of studies on stratospheric intrusion affecting the lower troposphere and the boundary layer (HUSAIN et al., 1977; KENTARCHOS et al., 1999b; KNOWLAND et al., 2015; LEVY II et al., 1985, RONDANELLI et al., 2002). The results from the present study show a clear tongue of $O_3$ rich-air observed near the COL centre, but no sign of change in $O_3$ detected in the lower troposphere. This might be due to the smoothed distribution of $O_3$ as a result of the compositing. Similar results were found for the composite of $O_3$ from the Monitoring Atmospheric Composition and Climate (MACC) reanalysis (figure not shown), which is based on the global model and data assimilation system provided by the ECMWF, combining more observations (e.g. reactive gases, aerosols, green house gases) than the conventional reanalyses, such as the ERAI (INESS et al., 2013). However, for an eight-year period (2003-2010) the MACC reanalysis comparison with the ERAI does not show much difference in terms of $O_3$ concentration.

An important aspect concerns how upper-level COLs interact with lower-level cyclones. According to the quasi-geostrophic theory (SUTCLIFFE, 1947), cyclogenesis occurs when either or both of the following conditions exist: (i) low-level baroclinicity (often a frontal system), and (ii) an upper-level precursor (which could be a strong upper-level trough or COL). Other factors such as latent heat release (DAVIES et al., 1993; MARTÍNEZ-ALVARADO et al. 2014), surface fluxes (KUO et al., 1991; NOGUÉS-PAEGLE; MO, 1997; PIVA; GAN. 2011), and the topography (BUZZI et al, 1987; HAYES et al, 1987; GAN; RAO, 1994; MIKY FUNATSU et al., 2004) are also important for cyclogenesis. The contribution of upper-level disturbances to the generation of extra-tropical cyclones has been studied from different perspectives. One view has considered the upper-level flow signatures to classify different types of cyclones (PETTERSSEN; SMEBYE, 1956; SINCLAIR; REVELL, 2000). Other studies have used the PV perspective and how the PV structure is modified by the latent heat

(GRAFT et al., 2017; PLANT et al., 2003), and a height-attributable diagnostic of the quasi-geostrophic omega equation to determine the contribution of both thermal advection at low levels and vorticity advection at upper levels (DEVESON et al., 2002). The composites of the strongest COLs shown in Figure 6.10 suggest a possible link between the upper-level COL and the surface (frontal) cyclone at the mature stage, resulting in a vertically-aligned vortex. The coupling between the upper and lower level disturbance frequently occurs when the low-level thermal advection has initiated (DEVESON et al. 2002) hinting to a possible synergetic interaction of the two features. However, the variability of observed COL structure and lifecycle is too large to represent their features with a single conceptual model.

## 6.3 Sensitivity of compositing Cut-off Lows to multiple criteria

The sensitivity of identifying COLs to different criteria was extensively discussed in Chapter 4. In the present section, we show how the set of criteria to identify COLs impacts their vertical structure based on the simpler method using only the horizontal winds (Figure 6.10a), i.e. the same method used to produce the composites above, and the more sophisticated method using zonal wind, temperature and PV (Figure 6.10b). Composites are produced for the 200 most intense COLs occurring in the SH, in exactly the same way as in the previous sections. The fields used for the compositing are horizontal winds, temperature (zonal anomaly), and PV, for ten pressure levels from 1000 hPa to 100 hPa. Only the W-E cross section is shown because in that direction the symmetry is better defined. It is interesting to note that both methodologies show similar distributions of the cold and warm cores which are located at about 500-400 hPa and 100 hPa, respectively. The sharper horizontal and vertical thermal gradients are found in the mid and upper troposphere, but they weaken with decreasing and increasing (higher than 200 hPa) height. This result is consistent with earlier findings (MIKY FUNATSU et al., 2004; HOSKINS et al., 1985; KOUSKY; GAN, 1981; MORAIS, 2016; PALMEN, 1949; SAKAMOTO; TAKAHASHI, 2005; SELUCHI; SATYAMURTY, 2007), corroborating that the stratospheric warm-core lies just above the tropospheric cold-core. For the PV and winds, both single and multiple step schemes present similar structures, and the dynamical tropopause (represented by the 2 PVU, orange line) coincides with the maximum winds. Similar results have been observed in case studies such as Palmén (1949) and Hoskins et al. (1985), and for the study of

Thorpe (1985) who examined the COL structure using an idealized theoretical model. Despite the similar structures of PV and winds, the full set of criteria represents the stronger COLs because the composite using this method has the stronger winds, cold core, and deeper tropopause fold than the composite obtained using the simpler method. It can be noticed that the cold core in both composites superimpose on a region of weak temperature anomalies (anomalies close to zero) in the lower troposphere, in particular on the eastern side of the COL centre. In this sector, the vertical temperature gradient between the lower and mid troposphere is enhanced due to the cold core which implies instability.

Figure 6.10: Composite vertical cross-sections along the west-east line of Cut-off Lows in the Southern Hemisphere based on the a) single step scheme and b) multiple step scheme.

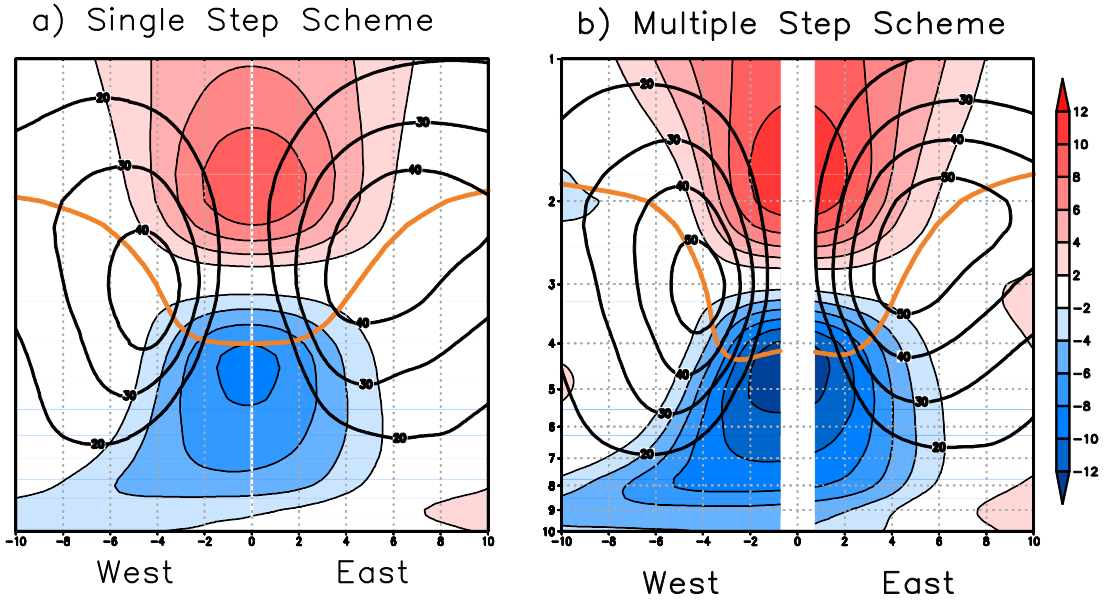


Composites for the 200 most intense Cut-off Lows that match between the $\xi_{300}$ and $Z'_{300}$, centered on the time and space relative to the $\xi_{300}$ minimum. The total distance in the $x$ axis is 20º geodesic. Magnitude of horizontal winds (thick solid line) from 20 m/s for the contour intervals 10 m/s. Temperature zonal anomaly in K (shaded). Potential vorticity for the 2 PVU (1 PVU = $10^{-6}$ m$^2$ s$^{-1}$ K kg$^{-1}$) (orange line). The gap in the centre of the composite using the multiple step scheme is due to the missing data which it requires to be interpolated. Analysis using the ERAI reanalysis for a 36-yr period (1979-2014).

Source: Author's production.

## 6.4 Cloud cover and precipitation structures

The main aspects of the cloud and precipitation structures of COLs are examined in this section. The primary focus is to understand how the intensity and available moisture affect the precipitation in COLs. The composites of precipitation are produced using the 6-hourly accumulations at 12-hour forecast lead times to avoid the spin-up during the first hours of the forecast (KALBERG, 2011; SIMMONS et al., 2010). Composites were also produced using the precipitation at 24h forecast lead time as a means of comparison, indicating strong similarities compared to those produced using the 12 hour lead time (figure not shown). Composites are produced using the $\xi_{300}$ tracks in order to reduce the number of diagnostics presented.

### 6.4.1 Cloud cover structure

The analysis of clouds associated with COLs is performed using the cloud fraction of low, medium and high clouds obtained from the ERAI reanalysis. These diagnostics are calculated using the Geleyn and Hollingsworth (1979) computation method. The composites of cloud cover are performed for different time steps during the COL lifecycle, but only the time 24h after to maximum intensity is shown. This is the time when the cloud features are more discernible, which coincides with the time of maximum precipitation (see Figure 6.15). The level used to plot geopotential height together with the cloud cover is not necessarily representative of the level at which the cloud occurs. Figure 6.11 shows relatively similar distributions in the medium and high cloud cover, where the peak cloud fraction extends southeast (east) of the $\xi_{300}$ minimum for high (medium) clouds. The patterns of cloud obtained with the medium and high clouds are similar to an inverted comma-shaped cloud pattern, which is typical of austral extratropical cyclones. In contrast, low clouds are predominatly found in the southwest quadrant of the composite with values exceeding 60% of cloud fraction. The large amount of low cloud occurs where the relatively cold air in the lower troposphere lies (figure not shown), which may be composed predominantly of stratiform clouds. Similar results are found in Field and Wood (2007) who observed cumulus and stratocumuls clouds behind the cold front for a composite of mid-latitude cyclones. However, these types of clouds are not relevant to characterize the COL. In general, we may expect that the precipitable clouds are found where the medium and high clouds

are, i.e. preferentially east of the COL centre, which is consistent with previous studies on COLs (DELGADO et al., 2007; FRANK, 1970).

Figure 6.11: Composite of Cut-off Lows in the Southern Hemisphere for a) high cloud cover, b) medium cloud cover, and c) low cloud cover.

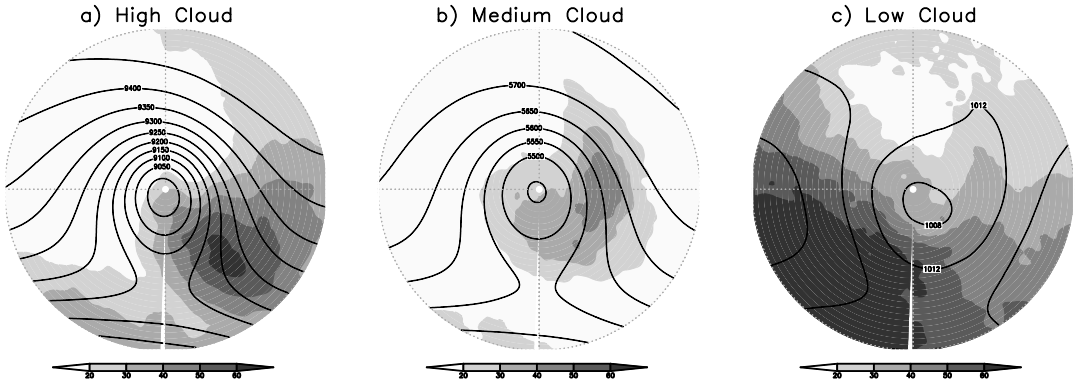


Composites for the 200 most intense Cut-off Lows that match between the $\xi_{300}$ and $Z'_{300}$, relative to 24h after the time of $\xi_{300}$ minimum. Clouds in shaded for the fractional coverage in percentage. Geopotential height in geopotential meter at a) 300 hPa and b) 500 hPa, and c) mean sea level pressure in hPa. Analysis using the ERAI reanalysis for a 36-yr period (1979-2014).

Source: Author's production.

Altought the products from reanalyses are created to facilitate climate studies, they are subject to errors since the cloud cover is not assimilated into the reanalyses, but instead is predicted by a short range forecast using the same atmospheric model used by the reanalysis. In particular, the product of cloud cover derived from the ERAI reanalysis have some deficiencies related to the interface between two cloud layers which means the lower cloud is underestimated if there are clouds in the profile either side of the medium and low cloud boundary (https://software.ecmwf.int/wiki/display/CKB/ERAI+issues+with+cloud+cover). This is also the case for the interface between high and medium cloud cover. The implication of this uncertainty in our results is the underestimation of the low cloud cover, but this is less important to characterize the cloud pattern associated with COLs. The use of remote sensing data, such as the International Satellite Cloud Cimatology Project data set (ISCCP), could be further studied in the future to examine the COL cloud features,

such as has been performed more generally for extratropical cyclones (HAWCROFT et al., 2012; 2017)

### 6.4.2 Precipitation

#### 6.4.2.1 Seasonality of precipitation

The seasonal variation of precipitation is determined for the 200 most intense $\xi_{300}$ COLs detected in each season of Autumn, Winter, Spring, and Summer. The composite precipitation is produced for the time of maximum intensity ($\xi_{300}$ minimum) of the $\xi_{300}$ COLs for each austral season. Figure 6.12 shows that the precipitation gives a spatial distribution similar to the composites of medium and high cloud cover, but remarkable differences occur for values between the seasons. Autumn and summer have the largest values as well as the maximum coverage of precipitation. In particular, autumn has clearly the highest rainfall exceeding 6.0 mm/h on the eastern side of COLs. In contrast, spring has the lowest values with local maximum about 4.2 mm/h. In terms of the cumulative precipitation per event, computed in exactly the same way as given in Figure 5.10b, the largest average value is found in autumn (33.2 mm), followed by summer (29.5 mm), winter (28.1 mm), and spring (27.6 mm).

An important difference between seasons is that the precipitation in autumn increases substantially near the COL centre in the mature stage. This is not clearly seen in other seasons, even if the composites were performed relative to the time of maximum precipitation (figure not shown). Results of this study have previously shown that winter COLs are less frequent than COLs in other seasons (see Table 5.4), but the magnitude of rainfall associated with the strongest systems is comparable to those found in the high frequency seasons of summer and autumn. Contrasting winter with summer, it is noticeable that the differences in terms of precipitation values are not that significant, although the precipitation in summer covers a more extensive area than in winter. Possible reasons for the differences between seasons suggest that the moisture availability may be a contributing factor to generate more precipitation in summer than in other seasons. However, this hypothesis will have to be verified by analyzing the moisture availability during the development of COLs. In a regional analysis of COLs, Favre et al. (2013) found that the largest contribution of precipitation along the south and east coasts of South Africa occurs between summer and winter, which is consistent

with our results. However, spring has the most important contribution for the precipitation inland, and this suggests that the seasonality of precipitation may depend on the region.

Figure 6.13: Composites of Cut-off Lows in the Southern Hemisphere for precipitation in a) autumn, b) winter, c) spring, and d) summer.

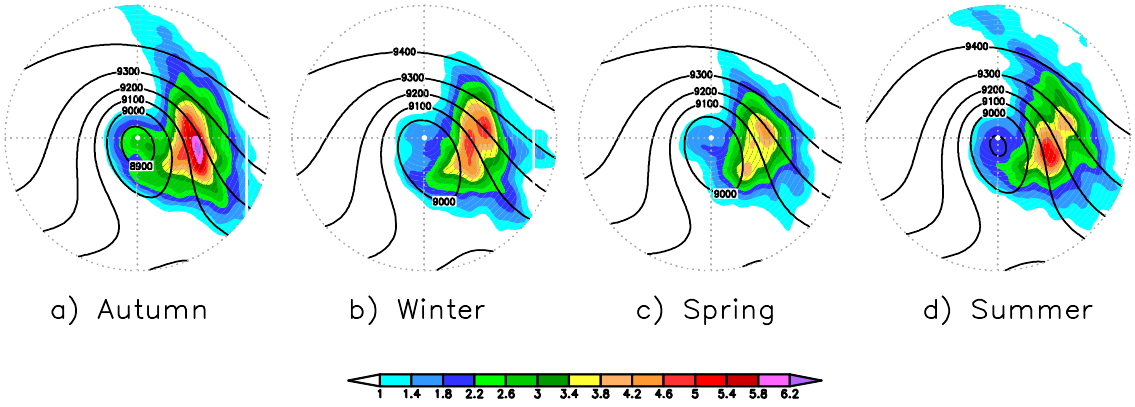


Composites for the 200 most intense Cut-off Lows that match between the $\xi_{300}$ and $Z'_{300}$, centered on the time relative to the $\xi_{300}$ minimum. Fields are the $Z_{300}$ height in gpm (solid line) and the hourly accumulated precipitation in mm (shaded) both relative to the time of $\xi_{300}$ minimum. Analysis using the ERAI reanalysis for a 36-yr period (1979-2014).

Source: Author's production.

### 6.4.2.2 Relationship between precipitation and intensity/moisture of Cut-off Lows

Figure 6.13 shows composites of precipitation for the COLs conditioned on $\xi_{300}$ (increasing from left to right) and precipitable water (increasing from bottom to top). Mean values of the nine composites were calculated for the $\xi_{300}$ COLs relative to the time of maximum intensity averaged within 5º spherical arc radius (about 555 km) centered on the $\xi_{300}$ minimum. As is expected, the precipitation increases simultaneously with both intensity and moisture. The wetter composites are associated with the most intense widespread precipitation, while the drier composites have precipitation occurring over reduced areas. The precipitation structure in composites with the greatest moisture content are similar to the composites of precipitation for autumn and summer in terms of spatial distribution (Figure 6.12a,d), while the precipitation in the drier composites looks more similar to those composites for winter

and spring (Figure 6.12b,c). These results suggest that moisture is an important factor for producing precipitation over larger areas, though the intensity of COLs seems to influence the magnitude of the precipitation. Composites produced relative to the time of maximum precipitation (figure not shown) indicate similar results.

It can be seen that the composite with most precipitation (top right) does not have the deepest pressure centre, but instead the three driest composites have a deeper centre than the three composites with greatest moisture content. The reason for a weaker intensity of COLs with high precipitation may be explained by the modification of the dynamical structure of COLs due to diabatic latent heating, which induces an anticyclonic PV in the upper-troposphere (AHMADI-GIVI, 2002; DAVIES; EMANUEL, 1991; REED et al., 1992; STOELINGA, 1996). A more detailed discussion of the interaction between lower and upper level disturbances and the associated diabatic effect in the COLs will be presented in Chapter 7.

Figure 6.13: Composites of Cut-off Lows in the Southern Hemisphere for precipitation as a function of intensity and moisture.

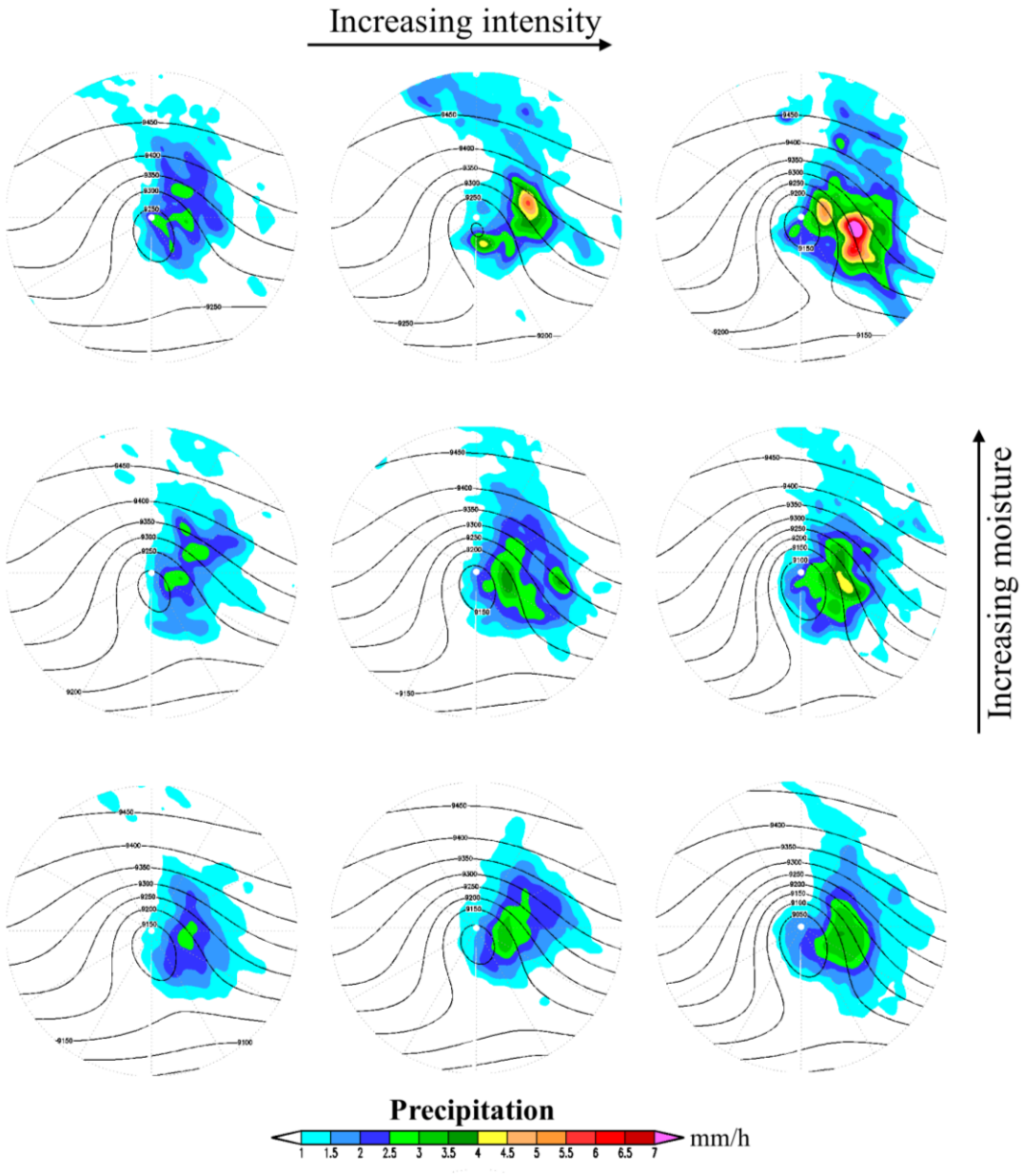


Plots are precipitation in mm/h (shaded) and $Z_{300}$ in gpm (solid line). Composites are determined as a function of intensity ($\xi_{300}$, increasing from left to right) and moisture (total column water, increasing from bottom to top). The two fields are calculated using the $\xi_{300}$ tracks for the time of $\xi_{300}$ minimum. Precipitation is calculated using area average within 5° spherical arc radius centered on the $\xi_{300}$ minimum. The categories are: [intensity]: 9.3-10.5, 10.5-12.0, 12.0-19.0 $s^{-1}$ (scaled by -1 x $10^{-5}$); and [moisture]: 27.6-30.8, 30.8-34.7, 34.7-40.0 kg $m^{-2}$. Analysis using the ERAI reanalysis for a 36-yr period (1979-2014).

Source: Author's production.

To examine in more detail how intensity affects precipitation, the number of tracks is varied to produce different composites, as shown in Figure 6.14. The compositing is done for the 250, 125, 50 and 20 most intense $\xi_{300}$ COLs, centered on the time of maximum intensity. This shows that precipitation is sensitive to intensity because the composites with smaller number of tracks produce higher values of precipitation, whereas the composites with lager number of tracks are smoothed out. The large contrast occurs for the comparison between the composites with the lowest and highest number of tracks, i.e. the composites with 20 and 250 tracks respectively. While the maximum precipitation values are strongly dependent upon the intensity, the structure and distribution for all composite are reasonably similar. For all composites, most of the precipitation occurs east of the COLs centre, normally associated with the diffluent flow that leads to rising air and precipitation. The precipitation structure of COLs looks quite similar to that seen in extratropical cyclones as the precipitation wraps around the COL centre, exhibiting an inverted comma shape (BENGTSSON et al., 2009; GUIA, 2010).

Figure 6.14: Composites of Cut-off Lows in the Southern Hemisphere for precipitation as a function of intensity based on a) 250, b) 125, c) 50, and d) 20 most intense systems.

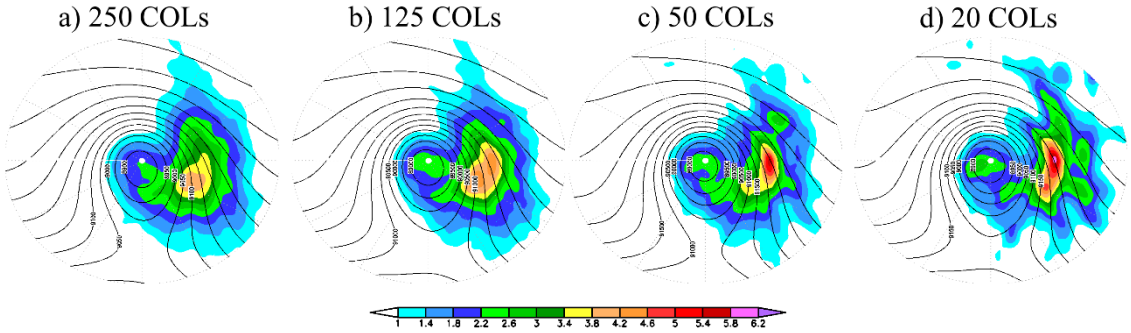


Composites of $Z_{300}$ and precipitation are determined using the $\xi_{300}$ tracks centered on the time relative to the $\xi_{300}$ minimum. $Z_{300}$ height in geopotential meter (solid line) and the hourly accumulated precipitation in mm (shaded). Analysis using the ERAI reanalysis for a 36-yr period (1979-2014).

Source: Author's production.

## 6.5 Life cycle of Cut-off Lows

This section focuses on the COL life cycle by compositing particular fields offset from the time of maximum intensity. This allows us to verify what occurs before and after the time when COLs reach their maximum intensity, namely, time zero (Figure 6.15). Firstly, the $Z_{300}$ height and precipitation are used to show each stage of the COL lifecycle (for the 200 strongest $\xi_{300}$ COLs) and compare with the conceptual model proposed by Nieto et al. (2008), outlined as follows:

1) Upper-level trough (-48h): the initial stage of the COL development starts with a deepening upper-level trough that tilts westward, which is consistent with earlier reports (PALMÉN, 1949). This amplifying synoptic wave is associated with a band of precipitation orientated northwest-southeast that looks like a cold-frontal structure. Most of precipitation does not exceed the precipitation rate of 2.0 mm/h

2) Tear-off stage (-24h): as the trough deepens, the northern part of the wave detaches from the westerly flow, leading to the formation of an isolated cyclonic vortex. Simultaneously, the band of precipitation gradually rotates cyclonically taking on a comma shape typical of mid-latitude cyclones. Maximum precipitation values increase to 2-3 mm/h in some areas northeast from the low-pressure centre.

3) Cut-off and mature stages (0 and +24): the low-pressure system becomes completely detached from the westerly current as the COL reaches its maximum intensity. The intensification of the COL can be seen through the increase of the geopotential gradient. The precipitation structure of COLs shows an asymmetrical distribution where the maximum values are located on the eastern side about $5^{o}$-$7^{o}$ (geodesic) from the centre of the composite. The precipitation rapidly increases during this stage, reaching the peak about 24h after the maximum intensity. At the eastern side, the maximum values are greater than 6.0 mm/h.

4) Decay (+48h): the decaying stage is characterized by the horizontal eastward tilt until the cyclonic vortex dissipates through diabatic effects (HOSKINS et al.,

1985; PRICE; VAUGHAN, 1993; SATYAMURTY; SELUCHI, 2007) or merges into the large-scale upper-level flow (GAN, 1982; NIETO et al., 2008; RAMAGE, 1962; SIMPSON, 1952). This stage is marked by a significant decrease in precipitation.

It is interesting to note that the absolute $Z_{300}$ minimum (~8850 gpm) associated with a cyclonic centre occurs in the tear-off stage, which is 24h before the maximum intensity in the $\xi_{300}$. The minimum of the $Z_{300}$ height gradually increases in the later stages (e.g. 8900 gpm in the time "zero"), indicating that most of the COLs reach their deepest value in terms of the $Z_{300}$ before the maximum intensity as a measure of the $\xi_{300}$. This means there are differences in the COL lifecycle with respect to the vorticity and geopotential.

The atmospheric circulation during the initial stages of the COL lifecycle shows an elongated appearance, while the more symmetrical structure occurs in the mature stages. In terms of precipitation, the lifecycle composite shows a large variation in time and a different behaviour of COLs in comparison to that found in extratropical cyclones where the peak occurs before the time of maximum intensity (BENGTSSON et al., 2009). Comparing our results with other studies on COLs, similar findings have been reported by Godoy et al. (2011) who showed that most of precipitation is found from the mature to the decay stages of a COL in South America. In contrast, in a study of cloud structure for NH COLs, Delgado et al. (2007) suggest the probability of heavy precipitation decreases considerably after the peak intensity of COLs. They also observed convective clouds in the rearward zone (western flank) as described in the conceptual model of Nieto et al. (2008). These results suggest that there may be some differences in the cloud/precipitation life cycle of COLs between the Northern and Southern Hemispheres or how COLs are defined in each region.

Figure 6.15: Life cycle composite of Cut-off lows in the Southern Hemisphere for the precipitation for the period between two days before and two days after the time of maximum intensity.

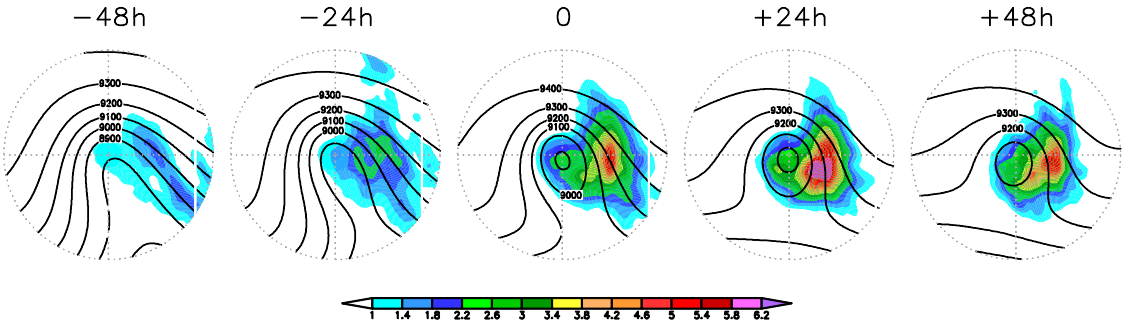


Composites are determined using the $\xi_{300}$ COLs centered on the time relative to the $\xi_{300}$ minimum (day zero). $Z_{300}$ height in gpm (solid line) and hourly accumulated precipitation in mm (shaded). Analysis using the ERAI reanalysis for a 36-yr period (1979-2014).

Source: Author's production.

The study of the lifecycle of COLs continues by analysing the vertical tilt, as shown in Figure 6.16. Tilt is determined for different stages before and after the time of maximum intensity. The composite represents the 200 most intense $\xi_{300}$ COLs in the SH, but not necessarily the deepest COLs, as some intense COLs may not present a cyclonic centre in the lower troposphere, as shown in Table 4.2. The maximum vertical tilt is observed at the first step (60h before the time of maximum intensity) and at low levels (900-700 hPa) when the distance between the 900 and 300 hPa centres is slightly higher than 2º. The westward vertical tilt observed during the early stages is typical of baroclinic systems, though this tilt is much less than that found in extratropical cyclones, as shown in Bengtsson et al. (2009) in their Figure 7. The vertical tilt reduces as the system approaches its maximum intensity, when the distance for vorticity centres between lower and upper levels is less than 1.0º. Once COLs start decaying, their structure becomes quasi-barotropic and exhibits even a reverse tilt, i.e. an eastward vertical tilt. An important feature is the maximum tilt at lower levels observed particularly in the early and late stages. Similar results were found by Randel and Stanford (1985), in their Figure 13, for the lifecycle of baroclinic waves at mid-latitudes in the SH.

Figure 6.16: Vertical tilt life cycle composite for Cut-off Lows in the Southern Hemisphere.

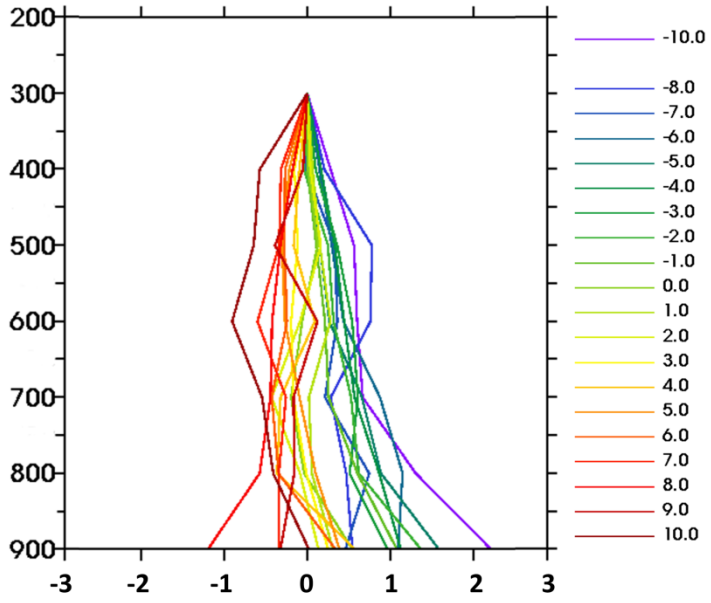


Composite is obtained using the $\xi_{300}$ Cut-off Lows. The time steps are for 6-hour interval, shown up to 60h on either side of the $\xi_{300}$ minimum (time zero). Tilts are in geodesic angle from the 300 hPa centre. Analysis using the ERAI reanalysis for a 36-yr period (1979-2014).

Source: Author's production.

To understand the differences in the life cycle of COLs based on the $\xi_{300}$ and $Z'_{300}$, the identical same COLs found in both fields are used to produce the composites of $\xi_{300}$, $Z'_{300}$, zonal anomaly of temperature in the layer 500-300 hPa ($T'_{500-300}$), and precipitation for different times throughout the lifecycle (Figure 6.17). The composites are created using the matching approach in two different ways. First, a number of $\xi_{300}$ COLs for the strongest systems are matched against the $Z'_{300}$ COLs to produce the 200 most intense COLs detected in both $\xi_{300}$ and $Z'_{300}$ (Figure 6.17a). Another way to create composites using the identical COLs is first selecting the strongest $Z'_{300}$ COLs and then matching them against the $\xi_{300}$ COLs (Figure 6.17b). Note that the only difference is the field chosen ($\xi_{300}$ or $Z'_{300}$) to select the most intense systems since the number of matches are the same in Figure 6.18a and Figure 6.17b. The parameters that were used to create the composites ($\xi_{300}$, $Z'_{300}$, $T'_{500-300}$, and precipitation) are determined for the area average within a 5º (geodesic) radius centered on the minimum of $\xi_{300}$ for the $\xi_{300}$ COLs and the minimum of $Z'_{300}$ for the $Z'_{300}$ COLs. Each storm is centered on the time

at which it reaches the minimum $\xi_{300}$. First, using the $\xi_{300}$ COLs as reference (Figure 6.17a), there is no obvious differences in the lifecycle obtained using the $\xi_{300}$ and $Z'_{300}$ COLs. The composites of $\xi_{300}$ and $Z'_{300}$ have minimum values for the $\xi_{300}$ COLs slightly lower than those obtained using the $Z'_{300}$ COLs. This is also the case for the $T'_{500-300}$ , i.e. no significant differences are found between the distributions using $\xi_{300}$ and $Z'_{300}$. The precipitation on the other hand indicates large discrepancies in the decay stage, when the peak precipitation obtained with the $\xi_{300}$ COLs is offset in time from that obtained with the $Z'_{300}$ COLs. The largest difference in precipitation occurs in the interval between +24h and +36h. This is because the precipitation is an estimated parameter produced by the forecast model, while the other parameters are directly assimilated into the ERAI reanalysis (DEE et al., 2011).

The composites created using the $Z'_{300}$ COLs as reference for the same parameters ($\xi_{300}$, $Z'_{300}$, $T'_{500-300}$, and precipitation) are shown in Figure 6.17b. This indicates that the minimum of $Z'_{300}$ obtained with the $Z'_{300}$ COLs is much deeper than that obtained with the $\xi_{300}$ COLs. It can be seen that the $Z'_{300}$ minimum in the $Z'_{300}$ COLs occurs exactly at the time of the $\xi_{300}$ minimum, while the $Z'_{300}$ minimum in the $\xi_{300}$ COLs occurs just before the $\xi_{300}$ minimum. In terms of precipitation, it is interesting to note that the peak value in the $Z'_{300}$ COLs occurs nearly at the time of maximum intensity, while the maximum precipitation in the $\xi_{300}$ COLs still happens between +24h and +36h. The reason for the differences in precipitation obtained between $\xi_{300}$ and $Z'_{300}$ is not clear, but it is likely due to the differences in the lifecycle of the $\xi_{300}$ and $Z'_{300}$ COLs. In fact, such differences occur simply because the two variables are different to each other, since the minimum of $\xi_{300}$ is often found offset in time relative to the minimum of $Z'_{300}$. The overall impression is that the $\xi_{300}$ is more related to the smaller-scale circulation, while the $Z'_{300}$ is much more dependent on the background field of "average conditions" used for calculating the $Z'_{300}$.

Some aspects of the COL lifecycle can be identified irrespective of the variable used to create the composite. One example is given by the $T'_{500-300}$ associated with the cold core, which is well-defined during the development stages, and weakens as the precipitation increases, suggesting that the COL dissipation may be related to diabatic effects. It is worthwhile mentioning that the radius chosen to average each parameter

may result in differences in values and distribution, in particular for precipitation which does not have a symmetric distribution. Composites for the same parameters discussed above have been created using the $\xi_{300}$ and $Z'_{300}$ COLs independently, i.e. without using the matches for the compositing. The results do not change the conclusions, since the distribution for either $\xi_{300}$ or $Z'_{300}$ is similar to that using the matches.

Figure 6.17: Life cycle composites of the 200 most intense Cut-off Lows in the Southern Hemisphere identified in the a) $\xi_{300}$ and b) $Z'_{300}$. The parameters are $\xi_{300}$, $Z'_{300}$, $T'_{500-300}$, and precipitation.

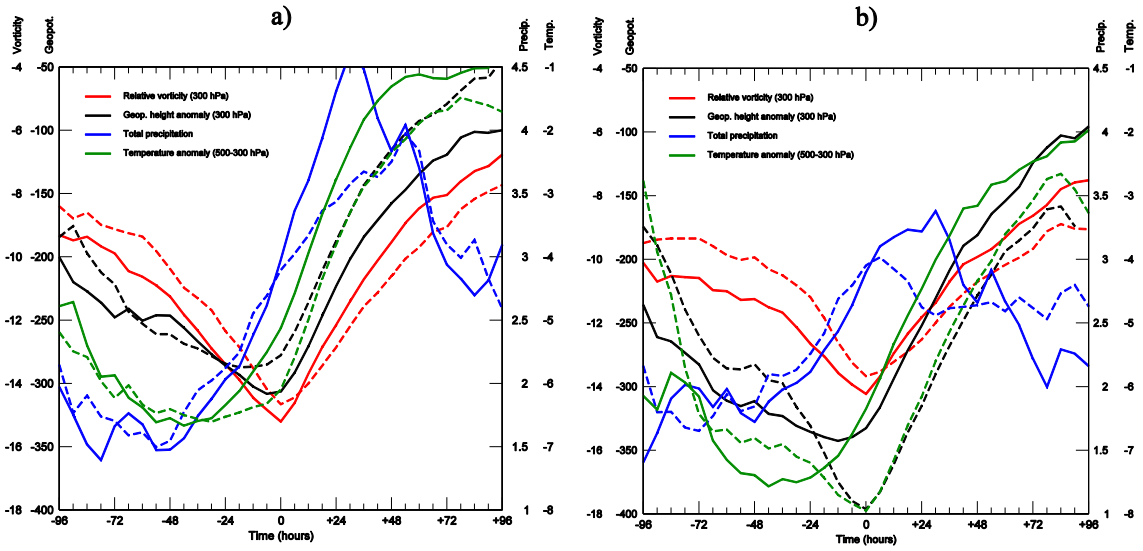


Vorticity fields are referenced to the $\xi_{300}$ Cut-of Lows (solid line), geopotential fields are referenced to the $Z'_{300}$ Cut-off Lows (dashed line). Parameters shown are $\xi_{300}$ ($10^{-5}$ $s^{-1}$, red line), zonal anomaly of geopotential height at 300 hPa (gpm, black line) and temperature in the 500/300 layer (K, gree line); and area-average total precipitation (mm/h, blue line). Each parameter is determined over area average within a 5º spherical arc radius.. Analysis using the ERAI reanalysis for a 36-yr period (1979-2014).

Source: Author's production.

## 6.6 Summary and discussion

This chapter describes in great detail the main aspects of the structure and evolution of the most intense COLs in the Southern Hemisphere. For the upper-level features, a well-defined cold and dry core is represented by the composites which is connected to frontal zones in its surroundings. The baroclinicity associated with COLs is analysed using the

thermal frontal parameter (TFP) which was found to be a useful tool for locating the warm and cold boundaries of the upper level fronts. A conceptual model was proposed to explain the propagation of baroclinic zones through the COL life cycle, similar to the schematic depiction for the upper-level frontal evolution discussed in Keyser and Shapiro (1986).

A number of composites for the vertical cross-sections W-E and S-N of COLs have been created by combining different fields. The vertical circulation structure based on U and V reveals an almost symmetrical structure in the W-E direction, and a close association of geopotential with vorticity with respect to the spatial distribution. The maximum intensity of vorticity/geopotential occurs in the upper troposphere but it gradually weakens both up and down. These results are in close agreement with previous studies (HSIEH, 1949; KELLEY; MOCK, 1982; PALMEN, 1949), confirming that COLs reach their maximum intensity at about 300 hPa in the subtropics and mid-latitudes. This is the case even if the tracking is performed for other levels such as 500 hPa. This synoptic feature differs in comparison to the upper-level vortices at lower latitudes, e.g. such as in the South Atlantic (GAN, 1982; KOUSKY; GAN, 1981) and North Pacific (KELLEY; MOCK, 1982) where the maximum intensity is near 250 hPa.

The analysis of the thermal structure of COLs in respect of the isotherms and isentropes suggests an unstable profile due to the very cold air in the mid upper troposphere. The cold core is located between 500 and 400 hPa, just below the warm core (~100 hPa). Another interesting feature of COLs is the tropopause fold whereby the stratospheric air is transported into the troposphere, as denoted by the vertical distribution of PV and $O_3$. A comparison of the COL structure using different methods for the identification has been made, indicating similarities and differences. The differences are mainly associated with the magnitude of particular fields such as winds, PV and temperature, where the stronger composite is obtained using the full set of criteria (which uses U, PV and temperature) in comparison to the simpler method (which uses only U and V). Despite the differences in values, the spatial structure obtained using the two methods are not altered, i.e. both composites have similar structural features. The similarities provide confidence in the representation of the synoptic aspects of COLs.

Composites of cloud cover and precipitation demonstrate a clear relationship between the medium and high clouds with the precipitation. In general, the large fraction of medium/high cloud cover coincides in location with the large precipitation, since these features are commonly found east of the COL centre. The cloud and precipitation exhibit an inverted comma-shaped similar to that associated with extratropical cyclones. These aspects are strongly related to the horizontal and vertical distributions of the vertical velocity and divergence. In a seasonal perspective, it was found that Autumn and Summer have the largest values and coverage of precipitation, although winter has peaks of precipitation limited to smaller areas. In addition, a possible link between intensity/moisture and precipitation was proposed, suggesting that moisture is an important factor for controlling the areal coverage of precipitation, while the magnitude of precipitation is more dependent on the intensity.

The conceptual description of precipitation and its evolution in time has been formulated based on the conceptual model of COLs proposed by Nieto et al. (2005), as described by the following stages (relative to the time of maximum intensity): upper-level trough (-48h), tear-off stage (-24h), cut-off and mature stages (0 and +24h), and decay (+48h). Results indicate that the precipitation is highly dependent on the stage of the COL lifecycle, varying from smaller values in the developing stage (< 2.0 mm/h) to larger values in the mature stage (> 6.0 mm/h). The warming of the cold core denoted by the increase in $T'_{500-300}$ is possibly linked to the precipitation increase and its associated diabatic effects. Additionally, other mechanisms may be important to dissipate COLs such as the adiabatic warming associated with the subsidence on the west side of the COLs, but this has not been investigated. Finally, particular fields were used to assess the COL lifecycle by comparing the composites obtained using $\xi_{300}$ and $Z'_{300}$. The results suggest that the difference between $\xi_{300}$ and $Z'_{300}$ COLs is likely related to the differences in the lifecycle of the $\xi_{300}$ and $Z'_{300}$ COLs, as indicated by Figs. 6.16 and 6.18. Despite the differences between the two fields, the results of this chapter demonstrate that compositing is a useful tool for studying the typical aspects of the structure and evolution of COLs. Further effort is needed to compare different datasets, such as the other recent reanalyses (e.g. NCEP-CFSR, MERRA-2, JRA-55, and ERA-5), and assess weather and climate models.

# 7 REGIONAL FEATURES OF CUT-OFF LOWS

This chapter outlines regional aspects of austral COLs for three main sectors located in the neighborhood of subtropical Africa, Oceania and South America. Section 7.1 compares the spatial and temporal distribution of COLs and their vertical structure in eight different genesis regions around the SH (two in South America, two in Africa and four in Oceania). In Section 7.2, different synoptic scale aspects are analysed in particular detail for the COLs originating in the southeastern Pacific near South America. The discussion will be limited to groups of COLs based on the intensity and vertical depth. The last section considers the potential effect of the Andes Cordillera on the vertical structure of the COLs coming from the South Pacific Ocean.

## 7.1 Cut-off Lows in the three main sectors: America, Africa and Oceania

Assuming that COLs have a distinct type due to the geographical characteristics, the COL activity is examined for three main sectors with respect to kernel spatial statistics based on the track, genesis and lysis densities. The main genesis areas are identified and the tracks are selected over a spherical region (radius=10$^{o}$) centered on the maxima for eight regions around the SH, as described in Chapter 3. The spatial statistics are shown for both $\xi_{300}$ and $Z'_{300}$, although the discussion is focused on the $\xi_{300}$ to be consistent with previous chapters.

### 7.1.1 South America

The COL activity is analysed for a subtropical region of South America (~20$^{o}$S-45$^{o}$S) that covers part of this continent, the western Atlantic and the southeast Pacific. The statistics show a similar distribution between $\xi_{300}$ and $Z'_{300}$ (Figure 7.1), despite the differences in spatial scale between the two fields. A genesis region is found for the COLs in the eastern Pacific Ocean (hereafter region A) and the Río La Plata estuary on the western South Atlantic coast (hereafter region B). During the 36-year period (1979-2014), the method identified 803 COLs in region A, while 611 COLs were detected in region B. The difference in number is not too larger between the two regions, although the genesis density indicates the values in the Pacific sector are much larger than those in the Atlantic sector, because the systems are more concentrated in the former region. The systems used to produce the statistics could be selected by using both genesis and

lysis constraints, but this would result in a smaller number of tracks than when using only the genesis region.

The COLs whose genesis occurs in region A and their associated lysis over the Andes seem to be strongly related to the topographic Rossby wave and the blocking activity in this sector. This occurs when a moving disturbance approaches the Andes, leading to the superposition of the transient upon a steady mountain wave, as discussed in Hayes et al. (1987, 1993) and observed by Miky Funatsu et al. (2004). Another consequence of the presence of the Andes is the "protective" effect that obstructs the inflow of warm and moist air from the interior of South America, delaying the COL dissipation that would occur if deep convection develops (GARREAUD; FUENZALIDA et al., 2007). This aspect can also be found in regions with similar geographic characteristics, such as upstream of the Rocky Mountains (subtropical northeast Pacific) and the South African plateau (subtropical southeast Atlantic). This means that the presence of a mountain chain may be an important factor for the development of COLs.

The relatively short distance between the genesis and lysis maxima suggests most of the COLs have very short tracks due to their slow movement. This feature is a consequence of the nature of stationary waves (NASCIMENTO; AMBRIZZI, 2002) and the mechanical effect associated with the mountains that retard the eastward propagation of COLs, as observed by Pinheiro et al. (2017) in their Figure 10. However, some COLs develop far from the continent and travel toward the west cost of Chile until they die out approaching or crossing the mountains. The existence of long-lived systems is verified by inspecting the detected tracks and analysing the spatial statistics that show the maximum lysis over the Andes is much higher than the nearest maximum genesis upstream of the mountains.

Figure 7.1: Annual statistics (track, genesis and lysis densities) of Cut-off Lows in South America based on the a) $\xi_{300}$ and b) $Z'_{300}$.

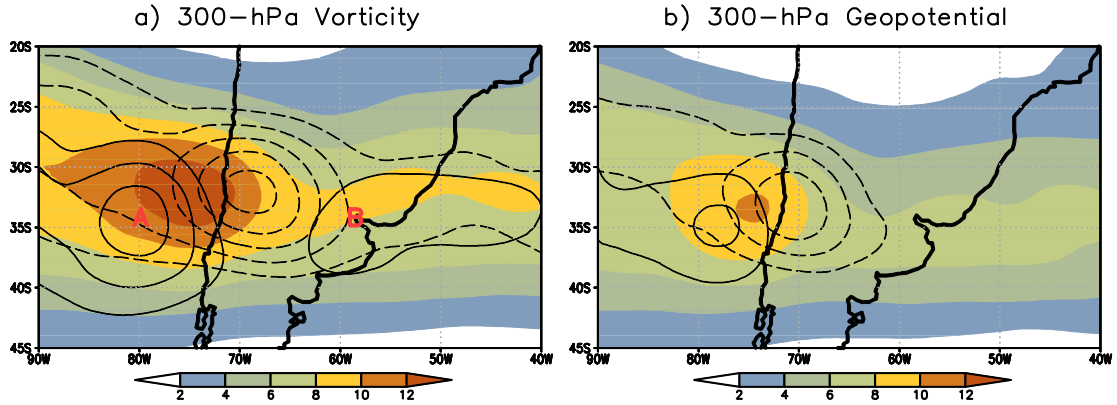


The densities are track (shaded), genesis (solid line), and lysis (dashed line). The maximum genesis are denoted by A and B. Analysis performed using the ERAI reanalysis for a 36-yr period (1979-2014). Unit is number per season per unit area, the unit area is equivalent to a 5º spherical cap ($\cong 10^6$ km$^2$).

Source: Author's production.

According to Pinheiro et al. (2017), the seasonality of COLs are quite similar for the three main areas, observed as maxima in the COL activity (see their Figure 3). However, some features can be distinguished from a regional perspective. The monthly distribution of COLs captured in the two genesis areas around South America (regions A and B) are shown in Figure 7.2 together with the average distribution over a set of eight different regions (namely regions A, B, C, D, E, F, G and H). Statistics regarding the COLs in other regions of the SH (including the southern Africa and Oceania) will be discussed further in this section. Note that the distribution of COLs in region A is similar to that obtained for the average (red line) in terms of number and shape, as the peak activity occurs in March followed by a decrease in number until the minimum frequency observed in winter. For region B, COLs also exhibit a high occurrence in January and February but the frequency begins to decrease from March to May, and then remains almost constant until September. Satyamurty (1990) also found in a similar region the highest frequency of cyclonic vortices during the summer, although this study is mostly based on satellite imagery, which does not mean the observed cyclonic feature represents the upper-tropospheric flow.

It is well known that COLs often form within a synoptic-scale blocking pattern consisting of a cut-off high in higher latitudes and a cut-off low in lower latitudes. Several studies have reported a high frequency of blocking in the southeast Pacific (CASARIN; KOUSKY, 1986; LEJEÑAS, 1984; MARQUES, 1996; MARQUES; RAO, 1999, 2000; MENDES et al., 2012). However, most of these studies found that the highest frequency of blocking occurs in winter, which is the less common season for the occurrence of COLs in this region. These apparently contradictory results may be attributed to the different blocking signatures, since blocking episodes with an inverted omega (Ω) type, such as observed by Marques and Rao (1999), do not have an associated COL located at lower latitudes. The other reason is the criteria used to define blocking, which requires a certain time persistence of the event. In general, a blocking episode is defined when the blocking index is satisfied for at least five days (MARQUES; RAO, 2000; MENDES et al., 2012; TRENBERTH; MO, 1985; VAN LOON, 1956; WRIGHT, 1974). Indeed, most summer COLs in the SH are short-lived systems (PINHEIRO et al., 2017), while winter COLs tends to have longer lifetimes, although they are less frequent than in summer.

Figure 7.2: Monthly distribution of $\xi_{300}$ Cut-off Lows in South America and the average of eight different regions in the Southern Hemisphere.

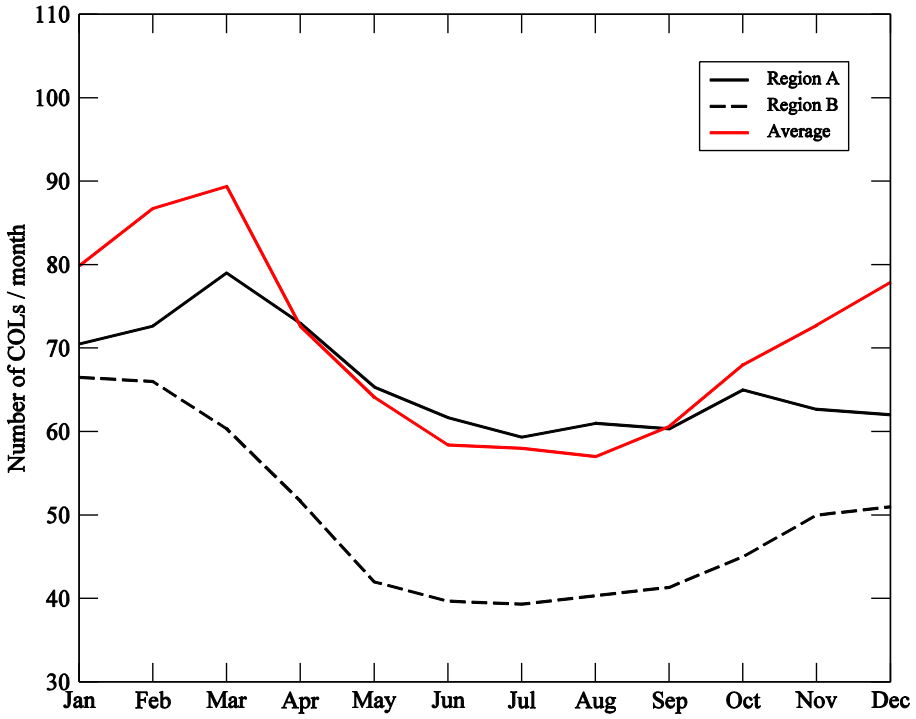


Solid line for region A, dashed line for region B, red line for the average of the eight regions. The $\xi_{300}$ COLs are selected over a spherical cap (r=10º) centered on the maximum genesis, denoted by regions A (34.5ºS 80.0ºW) and B (35.0ºS 57.0ºW). Analysis performed using the ERAI reanalysis for a 36-yr period (1979-2014).

Source: Author's production.

Table 7.1 shows the vertical depth of the Atlantic and Pacific COLs. This is analysed with respect to the vertical depth averaged over the whole hemisphere (values in parentheses in Table 7.1), so positive (negative) values indicate that COLs are generally deeper (shallower) than the average for a specific level. This shows that both the Atlantic and Pacific COLs are deeper than the average in all levels. The only exception is for the Pacific COLs reaching the surface that are slightly less common than the average. The comparison of COLs between regions A and B shows that the percentage of systems extending between 300 hPa and 600 hPa is quite similar, but larger differences occur at lower levels (generally below ~700 hPa), where the Atlantic COLs are found to be much deeper than the Pacific COLs. The largest difference occurs for the COLs that reach the surface, which corresponds to 19.4% and 30.9% of all the cases

formed in regions A and B, respectively. Campetella and Possia (2007) found that about 25% of the upper-level COLs observed in subtropical South America and surroundings have a corresponding surface cyclone. In a sector in the southwest Atlantic Ocean, Reboita et al. (2012) observed that 35% of the COLs reach the surface.

The deepest systems observed in the Atlantic sector coincide with the well-known cyclogenesis region over southeast South America (GAN; RAO, 1991; HOSKINS; HODGES, 2005; SINCLAIR, 1994), which may be the reason for the more frequent coupling between the upper and lower-level cyclones in comparison to the Pacific sector. The COL activity in the Pacific sector on the other hand is not located over a cyclogenesis region but instead decaying systems are frequently found there (HOSKINS; HODGES, 2005).

Table 7.1: Vertical depth of Cut-off Lows in South America as a percentage of the $\xi_{300}$ Cut-off Lows.

| hPa | Region A | Region B |
|---|---|---|
| 300 | 100.0 (-) | 100.0 (-) |
| 400 | 84.6 (3.7) | 85.6 (4.7) |
| 500 | 74.7 (9.2) | 74.6 (9.1) |
| 600 | 64.0 (12.9) | 63.3 (12.2) |
| 700 | 50.1 (12.4) | 51.6 (13.9) |
| 800 | 39.4 (10.6) | 42.1 (13.3) |
| 900 | 26.5 (3.4) | 34.7 (11.6) |
| 1000 | 19.4 (-0.9) | 30.2 (9.9) |

The $\xi_{300}$ COLs are selected over a spherical cap (r=10$^{o}$) centered on the maximum genesis, denoted by regions A (34.5$^{o}$S 80.0$^{o}$W) and B (35.0$^{o}$S 57.0$^{o}$W). Values in parentheses represent the deviation from the average of the whole hemisphere. Analysis performed using the ERAI reanalysis for a 36-yr period (1979-2014).

Source: Author's production.

### 7.1.2 Southern Africa

Other regions of high COL genesis are found in the neighborhood of subtropical southern Africa (Figure 7.3). One genesis maximum is located in the eastern Atlantic, just southwest of South Africa (hereafter region C). Most COLs in this region do not cross the central plateau and dissipate near the west coast of South Africa and Namibia.

This is similar to what occurs for COLs in region A in South America, as discussed above. The rainfall regime in the western South Africa and Namibia (NICHOLSON et al., 1981; 2000) has similarities to that observed in northern Chile and southern Peru (REBOITA et al., 2010) where both regions are characterized by a semi-arid climate. The second region affecting the African continent in the austral latitudes (hereafter region D) has the maximum genesis in the Mozambique Channel. The COLs in this sector are found at lower latitudes compared to COLs in other regions of the SH. The COL activity in this region has previously been observed by Favre et al. (2012) and Pinheiro et al. (2017), but it is not apparent in other studies (FUENZALIDA et al., 1995; NDARANA; WAUGH, 2010; REBOITA et al., 2010). There are some reasons that can explain the observed differences. One is the level used for the tracking. The pioneering objective climatology of Fuenzalida et al. (2005) uses the Laplacian of 500-hPa geopotential as the feature point to track the mid-tropospheric COLs, while the other studies are based on features at higher levels. The other reason is the criteria chosen for the identification. Except for the Fuenzalida et al. (2005) study, the thickness used to detect the cold-core is much higher than the observed cold-core in the most intense austral COLs, as shown in Chapter 6. Also, the dataset used in the Favre study (NCEP-DOE II) and in this study (ERAI) are more recent than the dataset used in the earlier studies. This highlights the improvements that have been made since the last decade with the new generation of reanalyses, as extensively discussed in Section 5.5. Table 1 in Pinheiro et al. (2017) summarizes the main differences between studies on COL climatologies considering the dataset, method, period and region used in each study.

Figure 7.3: Annual statistics (track, genesis and lysis densities) of Cut-off Lows in southern Africa based on the a) $\xi_{300}$ and b) $Z'_{300}$.

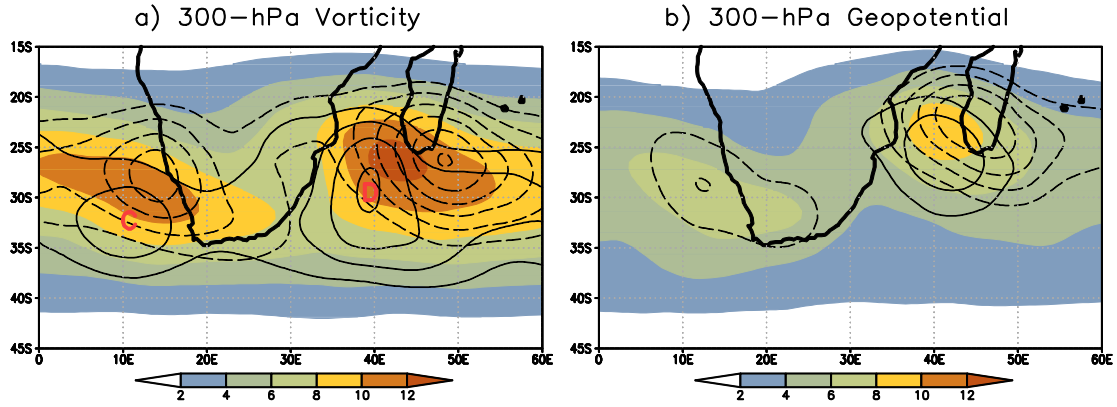


The densities are track (shaded), genesis (solid line), and lysis (dashed line). The maximum genesis are denoted by C and D. Analysis performed using the ERAI reanalysis for a 36-yr period (1979-2014). Unit is number per season per unit area, the unit area is equivalent to a 5° spherical cap ($\cong 10^6$ km$^2$).

Source: Author's production.

The monthly distribution of COLs in the two regions near Africa is shown in Figure 7.4. It is apparent that COLs from region C have a semi-annual cycle with relative peaks in April and November and a trough in August, whereas COLs from region D have larger frequencies in late summer and early autumn and smaller frequencies in winter. Although the seasonality of COLs from region D is similar (despite the large amplitude) to those of COLs near South America, the seasonality with respect to region C is somewhat different from the others since the COLs in this sector presents a semi-annual cycle, confirming previous results (FAVRE et al., 2012; SINGLETON and REASON, 2007) which suggests a possible association with the SAO, as briefly discussed in Chapter 5. The SAO is characterized by a dominant half-yearly component of the (second harmonic) temperature gradient in the middle troposphere in high latitudes in the SH, which reaches a maximum in the equinoxes with the strongest contrast in Autumn (VAN LOON, 1967). However, the semi-annual cycle is not evident in other regions of the SH, therefore, it is unclear why such distributions were found by Singleton and Reason (2007) and later by Favre et al. (2012).

Figure 7.4: Monthly distribution of $\xi_{300}$ Cut-off Lows in southern Africa and the average of eight different regions in the Southern Hemisphere.

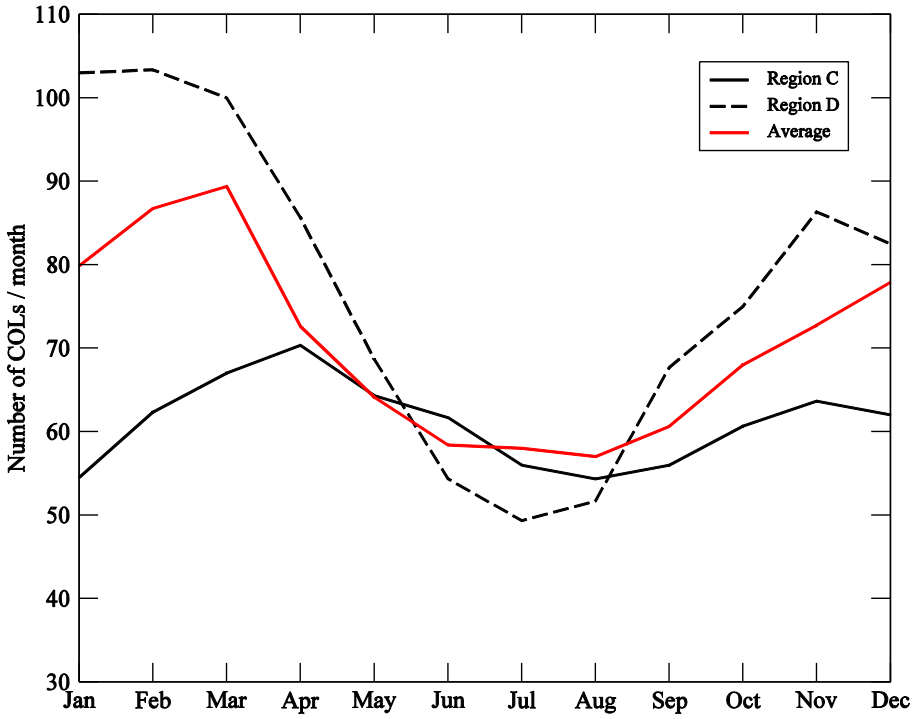


Solid line for region C, dashed line for region D, red line for the average of the eight regions. The $\xi_{300}$ COLs are selected over a spherical cap (r=10º) centered on the maximum genesis, denoted by regions C (32.0ºS 10.0ºE), and D (29.0ºS 39.0ºE). Analysis performed using the ERAI reanalysis for a 36-yr period (1979-2014).

Source: Author's production.

Table 7.2 shows there are differences in terms of vertical depth of COLs from regions C and D. The COLs formed in region C have deeper systems than the average in most levels. The exception occurs at 900 and 1000 hPa where deeper systems are less frequent than the average with 15.8% of the COLs extending down to the surface. The smallest vertical depth of COLs in the SH is observed for COLs from region D where only 14.0% of the total reach the surface.

Table 7.2: Vertical depth of Cut-off Lows in southern Africa as a percentage of the $\xi_{300}$ Cut-off Lows.

| hPa | Region C | Region D |
|---|---|---|
| 300 | 100.0 (-) | 100.0 (-) |
| 400 | 87.9 (7.0) | 80.6 (-0.3) |
| 500 | 71.5 (6.0) | 62.3 (-3.2) |
| 600 | 56.9 (5.8) | 43.9 (-7.2) |
| 700 | 42.1 (4.4) | 29.6 (-8.1) |
| 800 | 30.0 (1.2) | 22.2 (-6.6) |
| 900 | 19.8 (-3.3) | 16.1 (-7.0) |
| 1000 | 15.8 (-4.5) | 14.0 (-6.3) |

The $\xi_{300}$ COLs are selected over a spherical cap (r=10$^o$) centered on the maximum genesis, denoted by regions C (32.0$^o$S 10.0$^o$E) and D (29.0$^o$S 39.0$^o$W). Values in parentheses represent the deviation from the average of the whole hemisphere. Analysis performed using the ERAI reanalysis for a 36-yr period (1979-2014).

Source: Author's production.

The relatively short distances between the location of maximum genesis and lysis around South America (region A and B) and southern Africa (regions C and D) suggests the COLs are slow-moving systems. The results indicates a northeast movement through the COL life cycle since the maximum of lysis is located in more northerly latitudes than the corresponding maximum of genesis. The possible mechanism associated with the northeast displacement is the relative vorticity advection while the divergent terms are important to make the COLs quasi-stationary systems, as observed by Godoy et al. (2011). A more detailed discussion of the dynamics associated with the COL displacement will be presented in Chapter 8.

### 7.1.3 Southern Oceania

The primary location of COLs in the SH is found over southern Australia (particularly across the south-eastern part) and western Pacific including the Tasman Sea and the extreme north of New Zealand, as shown in Figure 7.5. The more western genesis maximum is located near the southwestern coast of Australia (hereafter region E). The pioneering regional climatology of Qi et al. (1999) found the highest incidence in the southwest sector of Australia (their Area 1 in Figure 1) which covers the longitude

range 110-120ºE. This result contradicts recent findings which have found the highest frequency of COLs in southeastern Australia (FUENZALIDA et al., 2005; FAVRE et al., 2012; REBOITA et al., 2010; NDARANA and WAUGH, 2010; PINHEIRO et al., 2017). Because Qi et al. (1999) used weather charts from the Australian Bureau of Meteorology data for a 14-yr period (1983-1996) that have missing data, and assuming older observations are not as reliable compared to recent datasets (as shown in Section 5.5), the quality of observations is likely to be the main reason for the differences described above, although significant interannual variability has been observed with respect to COLs in southern Australia (FUENZALIDA et al., 2005; POOK et al., 2006; QI et al., 1999).

The highest track density in the SH is located north of New Zealand and is associated with the maximum in genesis observed in regions F, G and H (Figure 7.5). Kousky and Gan (1981) also observed a high frequency of 200-hPa COLs across the central-southwestern Pacific. The high COL activity in these regions coincides with the principal location of persistent anomalies (MARQUES; RAO, 2000) due to a local feature of the climatological split in the mean westerlies and the presence of multiple blocking associated with the zonal wave 3 (TRENBERTH and MO, 1985). The high correlation between COLs and blocking associated with a dipole-blocking pattern has been observed by POOK et al. (2012) where a cut-off high is found in higher latitudes than a cut-off low. This atmospheric pattern can also be linked to the Rossby wave breaking, as discussed in Berrisford et al. (2007) and Ndarana and Waugh (2010).

The spatial statistics shown in Figure 7.5 indicate larger differences between $\xi_{300}$ and $Z_{300}$ in the region of southern Oceania compared to the statistics of COLs in South America and southern Africa. For example, the COL activity associated with region E in $\xi_{300}$ is not apparent in $Z'_{300}$. This difference was previously observed in Figure 5.3, and is mostly related to the presence of weak summer COLs that are difficult to identify in $Z'_{300}$. Another difference occurs in southeastern Australia where two maximum in genesis are found in the $Z'_{300}$, but only one maximum occurs in the $\xi_{300}$ (region F). In fact, the COL distribution in southern Oceania is more different from those observed in other regions of the hemisphere. As discussed above, the peak activity of COLs in South America and southern Africa seems to be highly influenced by the topography,

resulting in a discontinuity over these continents, which have high altitude terrains, and maximum occurrence over adjacent oceans. On the other hand, most of Australia lies on an extensive plateau with averages between 200 and 500 m in elevation above sea level, making this place unique. The nature of the COLs occurring in southern Oceania is evidently quite different from the COLs in other regions of the hemisphere because an extensive area including the southeastern Australia, the Tasman Sea, north of New Zealand and the western part of the Pacific Ocean is found to be favorable for both genesis and lysis.

Figure 7.5: Annual statistics (track, genesis and lysis densities) of Cut-off Lows in southern Oceania based on the a) $\xi_{300}$ and b) $Z'_{300}$.

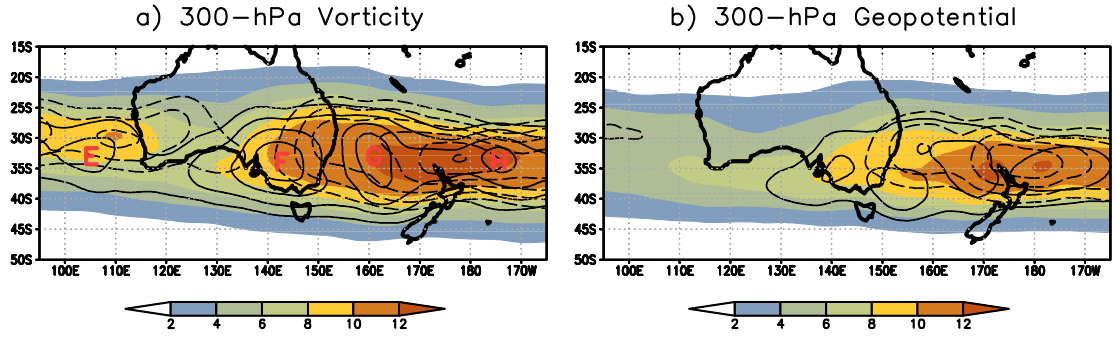


The densities are track in shaded, genesis in solid line, and lysis in dashed line. The maximum genesis are denoted by E, F, G and H. Analysis performed using the ERAI reanalysis for a 36-yr period (1979-2014). Unit is number per season per unit area, the unit area is equivalent to a 5º spherical cap ($\cong 10^6$ km$^2$).

Source: Author's production.

The seasonal cycle of the COL occurrence for regions E, F, G and H is shown in Figure 7.6. For COLs in regions G and H the shape of the seasonal curve differs little from each other as the maximum occurs in January-February followed by an abrupt decrease to a minimum in May. This is different from the seasonal distribution averaged over all regions (red line), in which the minimum occurs in August. The monthly distribution of COLs in region F, apart from the greater frequency, is quite similar to the average distribution since the maximum is found in February-March and the minimum in August. The most marked difference in the seasonal cycle is encountered for the COLs from region E. These systems have the peak occurrence in November-December, but a secondary maximum appears in April, while July-August is the period with the

minimum frequency. Another remarkable difference is the relatively low frequency of COLs in region E compared to those in other regions in Oceania.

Figure 7.6: Monthly distribution of $\xi_{300}$ Cut-off Lows in southern Oceania and the average of eight different regions in the Southern Hemisphere.

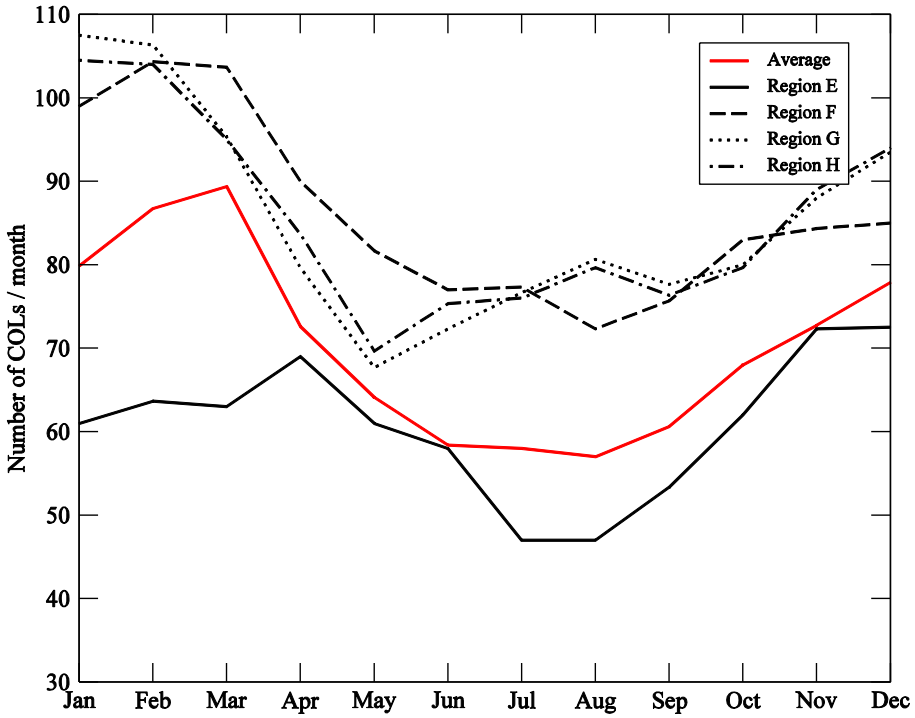


Solid line for region E, dashed line for region F, dotted line for region G, dashed-dotted line for region H, red line for the average of eight regions. The $\xi_{300}$ COLs are selected over a spherical cap (r=10º) centered on the maximum genesis, denoted by regions E (33.0ºS 105.0ºE), F (34.0ºS 142.0ºE), G (33.0ºS 161.0ºE), and H (34.0ºS 166.0ºE). Analysis performed using the ERAI reanalysis for a 36-yr period (1979-2014).

Source: Author's production.

Table 7.3 shows the vertical depth of COLs in the four regions locating in southern Australia and western Pacific. It is apparent that the majority of COLs in these regions are deeper than the global average. Deeper COLs are particularly common in regions G and H where 30.2% and 31.3% of the total reach the surface, respectively. In fact, the vertical depth of COLs in the two regions is comparable with that observed for COLs in region B, in South America. Despite the lack of studies investigating the vertical structure of COLs, there are some studies that did observe COLs interacting with frontal systems in southern Australia (QI et al., 1999) and eastern Australia (MCINNES and

HUBBERT, 2001). However, how COLs are linked to lower-level synoptic systems is not fully understood.

Table 7.3: Vertical depth of Cut-off Lows in southern Oceania as a percentage of the $\xi_{300}$ Cut-off Lows.

| | Region E | Region F | Region G | Region H |
|---|---|---|---|---|
| 300 | 100.0 (-) | 100.0 (-) | 100.0 (-) | 100.0 (-) |
| 400 | 86.0 (5.1) | 84.1 (3.2) | 81.3 (0.4) | 82.7 (1.8) |
| 500 | 71.3 (5.8) | 70.9 (5.4) | 70.6 (5.1) | 71.9 (6.4) |
| 600 | 55.0 (3.9) | 60.0 (8.9) | 59.8 (8.7) | 60.6 (9.5) |
| 700 | 42.5 (4.8) | 47.6 (9.9) | 47.8 (10.1) | 48.6 (10.9) |
| 800 | 35.0 (6.2) | 38.6 (9.8) | 38.2 (9.4) | 39.2 (10.4) |
| 900 | 26.1 (3.0) | 31.8 (8.7) | 32.8 (9.7) | 33.6 (10.5) |
| 1000 | 22.4 (2.1) | 27.2 (6.9) | 30.2 (9.9) | 31.3 (11.0) |

The $\xi_{300}$ COLs are selected over a spherical cap (r=10$^{o}$) centered on the maximum genesis, denoted by regions E (33.0$^{o}$S 105.0$^{o}$E), F (34.0$^{o}$S 142.0$^{o}$E), G (33.0$^{o}$S 161.0$^{o}$E), and H (34.0$^{o}$S 166.0$^{o}$E). Values in parentheses represent the deviation from the average of the whole hemisphere. Analysis performed using the ERAI reanalysis for a 36-yr period (1979-2014).

Source: Author's production.

## 7.2 Synoptic-scale features of Cut-off Lows in the Subtropical Andes

In this section, different aspects are analysed in particular detail for the COLs formed in region A (803 cases). The first part will show how the spatial distribution, velocity, lifetime, precipitation and lysis of the COLs is related to their vertical depth and intensity. In the second part, a discussion will be given on the interaction between the upper and lower tropospheric flow within the structure of the deepest COLs.

### 7.2.1 Relationship between intensity and vertical depth

The results of this section are based on the classification of COLs with regard to intensity and vertical depth. The number of COLs in each group is shown in Table 7.4. Most of results were created using the frequency instead of the total number in order to avoid wrong conclusions given that the number of COLs is distinct for each of the four categories analysed here.

Table 7.4: Number of $\xi_{300}$ Cut-off Lows based on intensity (first column) and vertical depth (second column).

| Category | Strong/Deep | Moderate/Medium | Weak/Shallow |
|---|---|---|---|
| Number | 270 / 402 | 257 / 198 | 276 / 203 |

The $\xi_{300}$ COLs are selected over a spherical cap (r=10º) centered at 34.5ºS 80.0ºW (Region A). Analysis performed using the ERAI reanalysis for a 36-yr period (1979-2014).

Source: Author's production.

Figure 7.7 shows the frequency of COLs in the four groups (strong, deep, weak and shallow) with respect to the latitude (through the zonal mean of the track density averaged over the entire longitude range), lifetime and maximum speed distributions. It is well-known that the highest COL activity occurs at lower mid-latitudes of the SH (<40ºS), as observed in many studies (FAVRE et al., 2012; FUENZALIDA et al., 2005; PINHEIRO et al., 2017; REBOITA et al., 2010). The maximum frequency of COLs is found at about 32ºS in the four groups (Figure 7.7a), although strong and deep COLs are slightly more frequent at higher latitudes compared to weak and shallow COLs. This result differs from that found by Fuenzalida et al. (2005) in which the highest density of COLs occurs at about 38ºS. The reason for the differences is unknown, but could be a result of the criteria and level chosen to identify the cyclonic features, as discussed in previous chapters.

Figure 7.7: Distribution of $\xi_{300}$ Cut-off Lows in four groups (deep, shallow, strong and weak) with respect to the a) latitude, b) maximum speed, and c) lifetime.

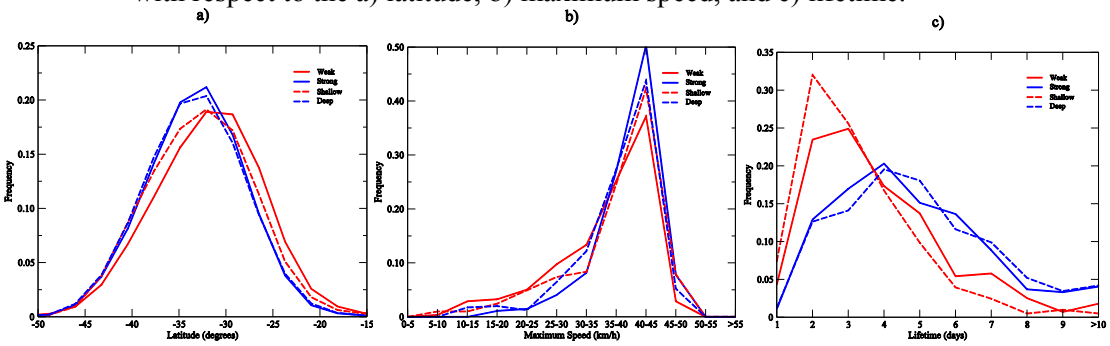


The four groups are: deep in blue-solid line, shallow in red-solid line, strong in blue-dashed line, and weak in red-dashed line. The $\xi_{300}$ COLs are selected over a spherical cap (r=10º) centered at 34.5ºS 80.0ºW (Region A). Analysis performed using the ERAI reanalysis for a 36-yr period (1979-2014).

Source: Author's production.

The distribution of maximum speed (Figure 7.7b) shows the highest frequency of COLs occurs for the range 40 to 45 km/h. This result is observed in all four groups, which means that apparently the maximum speed of the system does not depend on either intensity or vertical depth. However, a recent study shows there are significant differences in the COL velocity between different regions in the SH (PINHEIRO et al., 2017). The Pacific COLs, for example, decelerate as they approach the Andes

There are large differences in the total lifetime distribution (Figure 7.7c) since the strong and deep COLs are found to be longer than the weak and shallow COLs. Most of weak or shallow COLs last 2 or 3 days, although a few can persist longer than one week. However, about half the stronger or deeper systems last more than 5 days. The reason for this is that stronger COLs generally have more kinetic energy than weaker systems which may extend their lifetime (a more detailed analysis of the EKE budget will be shown in next chapter). Longer-lived systems have been previously observed by Hoskins et al. (1985) and Price and Vaughan (1992) for regions in the NH, particularly for COLs occurring in higher latitudes. Price and Vaughan (1992) suggest that persistent polar COLs are periodically intensified due to the injection of stratospheric PV air through the jet stream. Other authors suggest that the moisture supply is an

important factor to destroy the COL (FUENZALIDA et al., 2005; HOSKINS et al., 1985).

An interesting regional feature is the maximum lysis found over the Andes such as observed by Fuenzalida et al. (2005) and confirmed in Pinheiro et al. (2017). This can be explained by the fact that "when a COL approaches the mountain it weakens because of the superposition of the COL with the steady mountain wave ridge", also called a topographic Rossby wave as discussed in Pinheiro et al. (2017). This aspect is observed in all four groups of COLs (Figure 7.8). However, some COLs are able to cross the Andes and dissipate on the lee side. This is more frequent for the stronger and deeper COLs, in which a few dissipate in southeast South America and the southwestern Atlantic, and is consistent with the fact that the duration of strong or deep COLs is generally longer than the duration of weak or shallow COLs. This is a topic that could be studied from the point of view of modal decomposition by the interaction among vertical and horizontal modes in the vicinity of the mountains. The high topography certainly excites the gravity waves and poses a barrier for the horizontal displacement of Rossby waves that compose the COL (GAN; RAO, 1994; SATYAMURTY et al., 1980).

Figure 7.8: Lysis density of $\xi_{300}$ Cut-off Lows based on a) vertical depth (deep and shallow) and b) intensity (strong and weak).

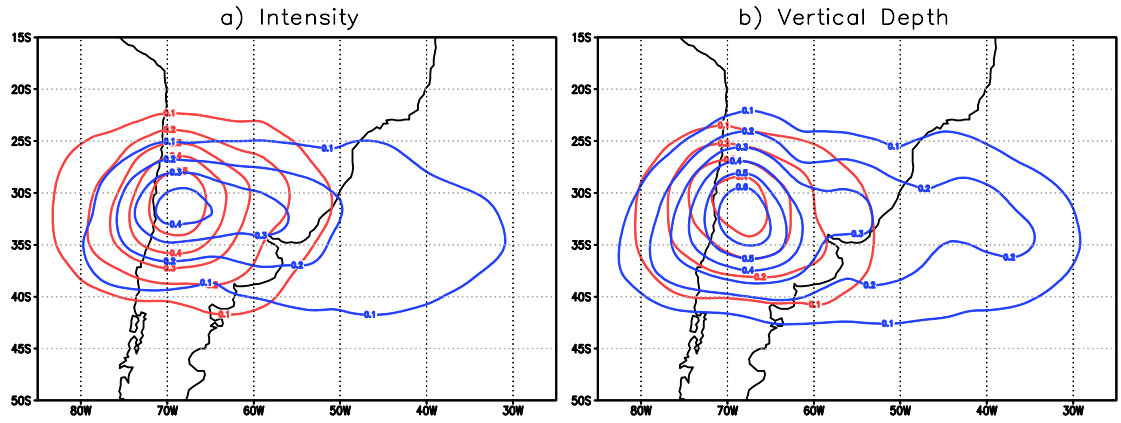


Strong and deep cases in blue line, weak and shallow cases in red line. The $\xi_{300}$ COLs are selected over a spherical cap (r=10°) centered at 34.5°S 80.0°W (Region A). Unit is number per unit area per season, the unit area is equivalent to a 5° spherical cap (~$10^6$ km$^2$). Analysis performed using the ERAI reanalysis for a 36-yr period (1979-2014).

Source: Author's production.

The zonal distribution of the lysis density of COLs is shown in Figure 7.9. As expected the highest frequency of lysis is found exactly over the Andes (mountain is indicated by the orange rectangle) irrespective of the category of COL. However, there are more strong and deep COLs decaying on the eastern side of the Andes, while there are more weak and shallow COLs decaying on the western slope. This means that if the COL is strong enough it may succeed in crossing the mountain ridge axis, and then reintensify on the lee side of the mountains which can favor the lee cyclogenesis, as observed by Miky Funatsu et al. (2004). A more detailed analysis of the mountain effect on the vertical structure of COLs will be discussed later.

Figure 7.9: Zonal distribution of the lysis location of $\xi_{300}$ Cut-off Lows for groups based on intensity and vertical depth.

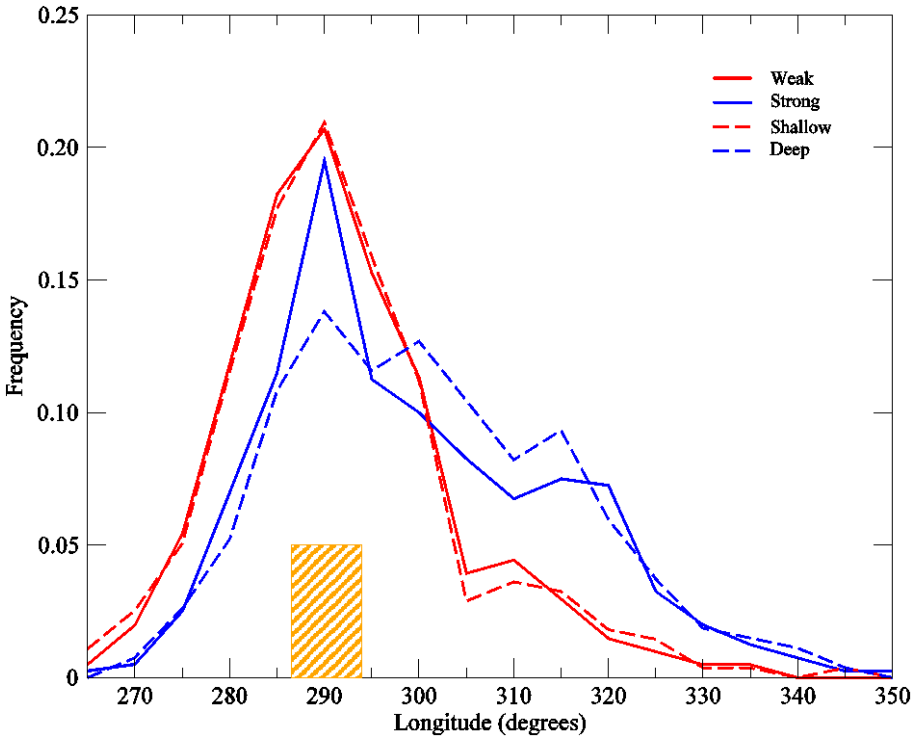


The four groups of COLs are deep (blue-solid line), shallow (red-solid line), strong (blue-dashed line), and weak (red-dashed line). The $\xi_{300}$ COLs are selected over a spherical cap (r=10°) centered at 34.5°S 80.0°W (Region A). Orange bar denotes the Andes position. Analysis performed using the ERAI reanalysis for a 36-yr period (1979-2014).

Source: Author's production.

To investigate how the vertical depth of a COL affects the precipitation, the maximum and cumulative precipitation distributions were obtained for the two groups which are the deep and shallow COLs, as shown in Figure 7.10. The results obtained as a measure of intensity are not discussed here given the strong association between the strong and deep COLs as well as the weak and shallow COLs. This means that the precipitation statistics based on the deep (shallow) COLs are very similar to those of the strong (weak) COLs. The results of precipitation were produced in exactly the same way as in Figure 5.10. Using the radius of $5^{o}$ centered on the cyclone, it can be seen that there are more deep COLs with relatively large precipitation (>1.0 mm/h) than shallow COLs (Figure 7.10a). This means that the maximum rainfall rate for COLs with deep structure is generally higher than that for COLs with shallow structure. Another noticeable difference between the two groups is the increased cumulative precipitation for deep COLs in comparison to shallow COLs, as shown in Figure 7.10b. The relatively long lifetime of COLs with deep structure may contribute to larger precipitation compared to shorter shallow COLs. However, the increase of precipitation and the associated diabatic effects may lead to the faster decay after the COL reach the mature stage, as shown in Figure 6.15. The aspects of the precipitation discussed here was also examined using larger radii to extract the average values (e.g. $10^{o}$ and $15^{o}$), but the conclusions are not changed (figure not shown).

Figure 7.10: Distribution of a) maximum rainfall and b) cumulative precipitation for deep and shallow $\xi_{300}$ Cut-off Lows.

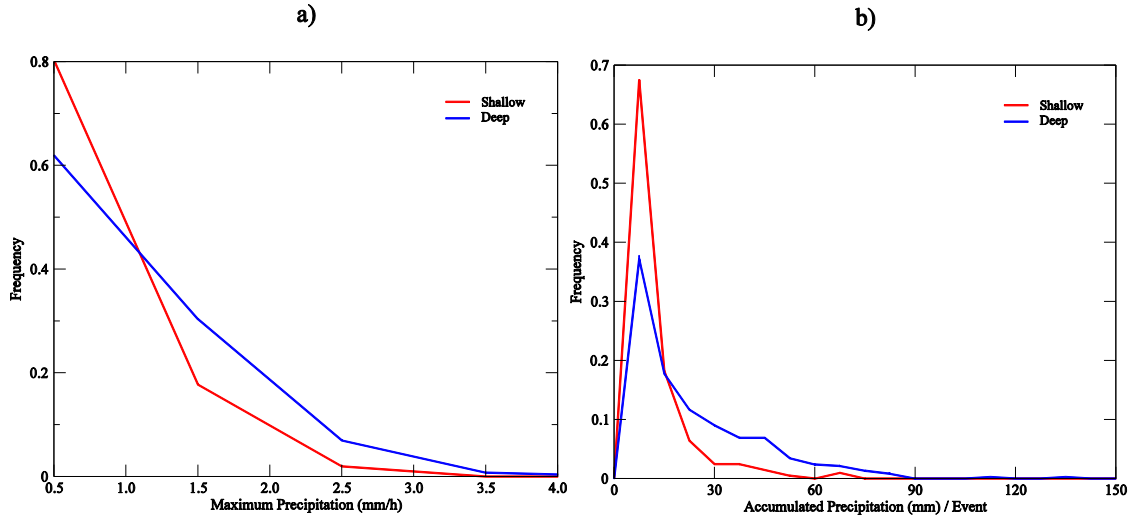


Groups are deep (blue-solid line) and shallow (red-solid line). The $\xi_{300}$ COLs are selected over a spherical cap (r=10°) centered at 34.5°S 80.0°W (Region A). Unit is mm/h for the maximum precipitation, and mm per event for the cumulative precipitation. Analysis performed using the ERAI reanalysis for a 36-yr period (1979-2014).

Source: Author's production.

The cumulative precipitation associated with each event is also undertaken for the COLs with deep and shallow structures, as shown in Figure 7.11. The set of all events for the two groups refers to the distributions presented in Figure 7.10b. It is evident that the greatest precipitation events are associated with the deepest COLs, despite the fact that this class of systems is more frequent (402 cases) than the shallow COLs (203 cases). The highest absolute value of cumulative precipitation is 132.4 mm for a deep COL and 66.2 mm for a shallow COL. Considering the events accumulating more than 50.0 mm, it was found that 29 cases have a deep structure (7.2% of the total number of deep COLs) while only 2 events have a shallow structure (1.0% of the total number of shallow COLs). The average value per event is found to be 18.9 mm in the deep COLs and 7.2 mm in the shallow COLs, as represented by the red line in Figure 7.11.

Figure 7.11: Cumulative precipitation per event for a) shallow and b) deep $\xi_{300}$ Cut-off Lows.

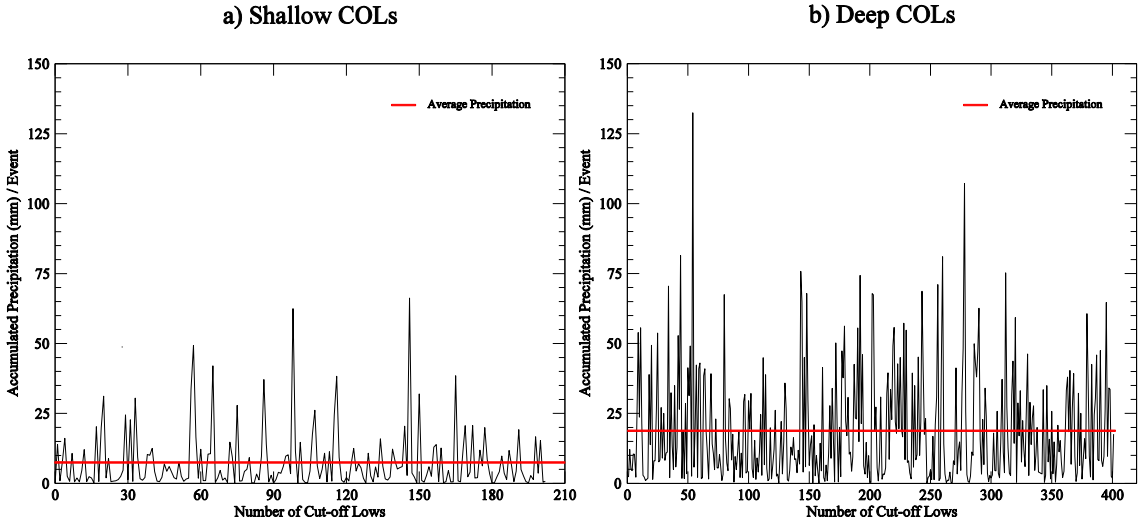


The $\xi_{300}$ COLs are selected over a spherical cap (r=10º) centered at 34.5ºS 80.0ºW (Region A). Unit is mm per event. Analysis performed using the ERAI reanalysis for a 36-yr period (1979-2014).

Source: Author's production.

Results of Chapter 6 have shown that precipitation is highly variable within the COL lifecycle. A similar analysis is performed regionally by compositing the COLs with respect to their time evolution (Figure 7.12). These are created by centering on the time when the COLs cross the Andes which differs from the composites shown in Chapter 6 that are centered on the maximum intensity[1]. The area-average precipitation is obtained using three different radii which are 5, 10, and 15 degrees in geodesic distance. This shows that the precipitation associated with the COL is highly sensitive to the size of the radial cap. For example, using a smaller radius such as 5º the contribution to the precipitation for the peak values in the lifecycle is much higher than using a larger radius such as 10º or 15º, but the difference is not significant in the early stages. Note that there is a marked increase in precipitation as the COL crosses the Andes. The increase is by a factor of approximately 8.0 in the COLs with deep structure and 16.0 in the COLs with shallow structure, which are much higher than the increase observed in

[1]The verification found that 7% of the total number of COLs formed in region A does not reach the Andes in the longitudinal range from 92.5ºW to 87.5ºW. These systems are not included in the lifecycle composites.

the strongest COLs of the SH (see Figure 6.17). The large contrast in precipitation between the western and eastern sides of the Andes suggests that the mountains play an important role in the development of the COL. The mountain effect is manifested by blocking the warm moist air from the Amazon region (GARREAUD; FUENZALIDA, 2007) when the COL is on the upslope and triggering deep convection when the COL is east of the Andes (MIKY FUNTASU et al., 2004). The peak precipitation occurs between three and four days after the deep COL passes the Andes. For the shallow COLs, there are two maxima of precipitation, one at +2.5 days, and the second in +4.5 days after the systems reach the mountains, even though it is not clear if this is real or just noise. This occurs later than the peak precipitation of COLs in the whole hemisphere (see Figure 6.17), suggesting the mountains may delay the onset of deep convection in the interior of South America.

Figure 7.12: Lifecycle composite of deep and shallow $\xi_{300}$ Cut-off Lows with respect to the precipitation.

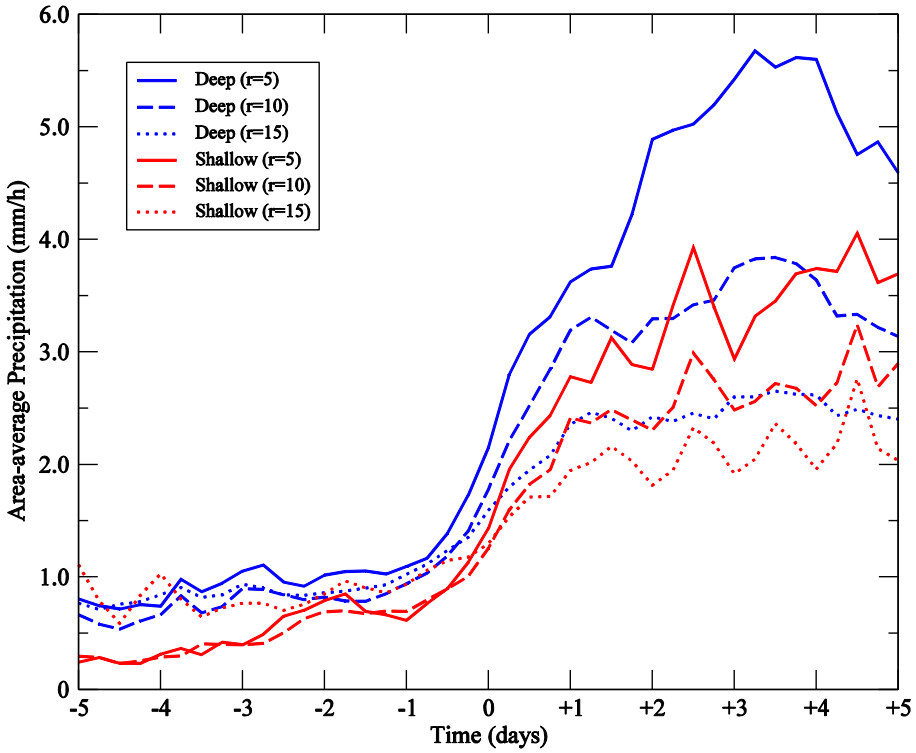


The groups are deep (blue lines) and shallow (red lines). Values are averaged over a spherical cap region with 5º (solid line), 10º (dashed line), and 15º (dotted line). The $\xi_{300}$ COLs are selected over a spherical cap (r=10º) centered at 34.5ºS 80.0ºW (Region A). Each COL are centered on the time that the system crosses the Andes, defined for the longitudinal range from 92.5ºW to 87.5ºW. Unit is mm/h. Analysis performed using the ERAI reanalysis for a 36-yr period (1979-2014).

Source: Author's production.

### 7.2.2 The coupling between upper and lower level disturbances

One particular aspect concerns where the COLs start and end at each pressure level. Statistics of COLs based on the genesis and lysis densities are assessed at eight pressure levels (from 300 to 1000 hPa) by using the systems that reach the surface which are represented by 156 cases (19.4% of the total). Figure 7.13 indicates that the maximum genesis at 300 hPa is followed downstream by the maximum genesis at lower levels, indicating strong evidence of vertical mode interaction. In general, the horizontal distance between the maxima increases with the increase of vertical distance between

the pressure levels. There are two reasons that may explain this result. First, the vertical tilt of the typical COLs toward the west with height in the development stages, thus it is expected that the maximum genesis of upper-level COLs locate upstream from the corresponding genesis at lower-levels. However, this explains only partially the horizontal distance between the maxima genesis because the vertical tilt generally does not exceed 2 degrees during the early stages of COLs, as shown in Figure 6.16. The other part of the horizontal distance is probably the result of COLs moving preferentially north-eastward in this region. This may indicate that, at least for this particular region, the COL genesis at 300 hPa occurs earlier than the corresponding genesis at lower levels. The mean lifetime of the COLs at each pressure level (Figure 7.14) provides evidence that the genesis occurs earlier in the upper troposphere, because longer lifetimes are observed at 300 hPa than at lower levels. The duration of COLs reduces with decreasing height, but a lifetime reversal is observed with a secondary peak at 800 hPa. This is approximately the level where the lower-troposphere cyclonic features are normally more prominent in the extratropics of the SH (HOSKINS; HODGES, 2005). The longer lifetime of cyclones at 800 hPa may be a consequence of the COLs penetrating from the South Pacific and inducing more intense warm advection at low levels east of the Andes (MIKY FUNATSU et al., 2004). The mountain effect promotes an intensification of the northerly winds along the Andes eastern slope, with frequent low-level jet episodes (CAMPETELLA; VERA, 2002; SALIO et al., 2002), and affects the cyclone activity in southeast South America (GAN; RAO, 1991, 1994; GAN, 1992; SELUCHI; SAULO, 1998; VERA; VIGLIAROLO, 2000).

A second region of COL generation is found on the east side of the Andes such as shown in the density of genesis at 600 hPa or lower levels. This is associated with the COLs that cross the mountains and couple with lower-level disturbances. The results suggest that the coupling between the upper and lower level vortices can occur in two different regions, one in the southeast Pacific and the other in the southeast South America and adjacent ocean.

Figure 7.13: Genesis density of the deepest Cut-off Lows at different pressure levels.

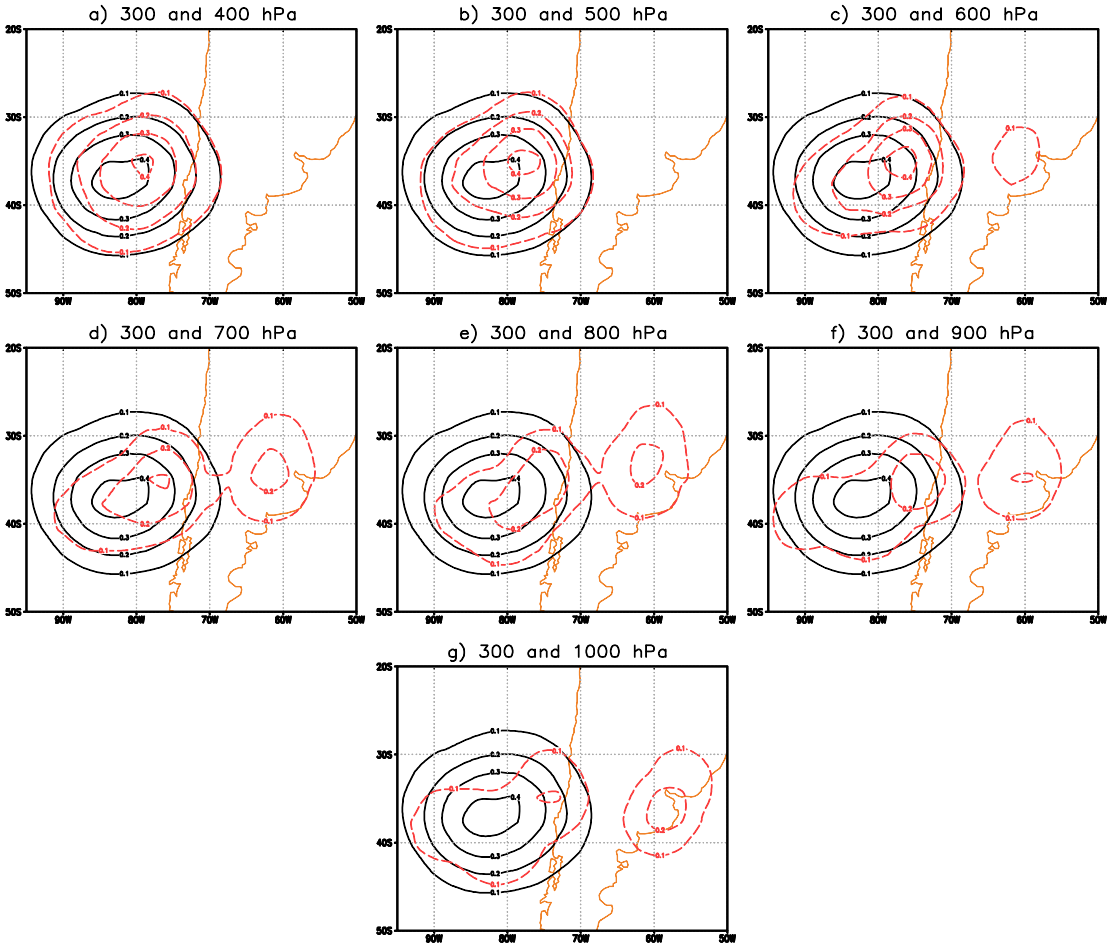


Genesis density is in black solid line at 300 hPa and red dashed line at other levels. The deepest systems are $\xi_{300}$ COLs that reach the surface, selected over a spherical cap (r=10º) centered at 34.5ºS 80.0ºW (Region A). Unit is number per unit area per season, the unit area is equivalent to a 5º spherical cap (~$10^6$ km$^2$). Analysis performed using the ERAI reanalysis for a 36-yr period (1979-2014).

Source: Author's production.

Figure 7.14: Mean lifetime of cyclonic features at different levels in the deepest $\xi_{300}$ Cut-off Lows.

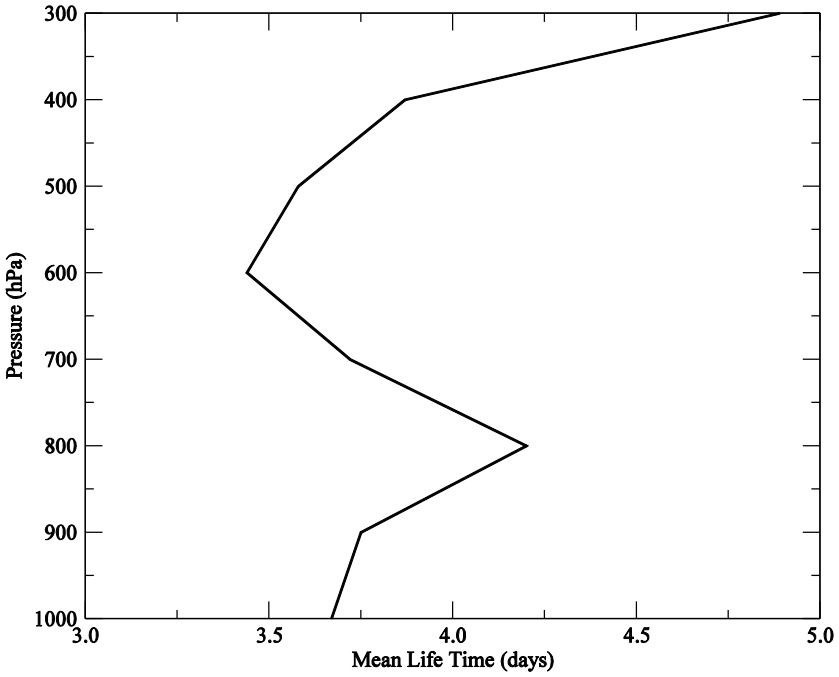


The deepest systems are $\xi_{300}$ COLs that reach the surface, selected over a spherical cap (r=10$^o$) centered at 34.5$^o$S 80.0$^o$W (Region A). Unit is day. Analysis performed using the ERAI reanalysis for a 36-yr period (1979-2014).

Source: Author's production.

A similar analysis is carried out on the lysis density of COLs at the same pressure levels as those used for genesis density. Figure 7.15 shows that most of the deepest COLs at 300 hPa dissipate near or over the Andes. The COLs that cross the mountains are likely to dissipate over the western Atlantic, at approximately 36$^o$S 38$^o$W. A similar distribution is observed for lysis at 400 hPa and 500 hPa. However, there is no lysis in the Atlantic Ocean at 600, 700 and 800 hPa. This means that the systems do not cross the mountains if the cyclonic feature is between 600 hPa and 800 hPa, leading to the decay on the upslope side. There is a large variation in the region where the COLs dissipate between 600 and 800 hPa, because some systems move northward before they disappear. Interestingly, lysis reappears in the Atlantic sector at 900 and 1000 hPa, which is associated with the lower-level cyclogenesis near the Río La Plata estuary as shown in Figure 7.13.

Figure 7.15: Lysis density of the deepest Cut-off Lows at different pressure levels.

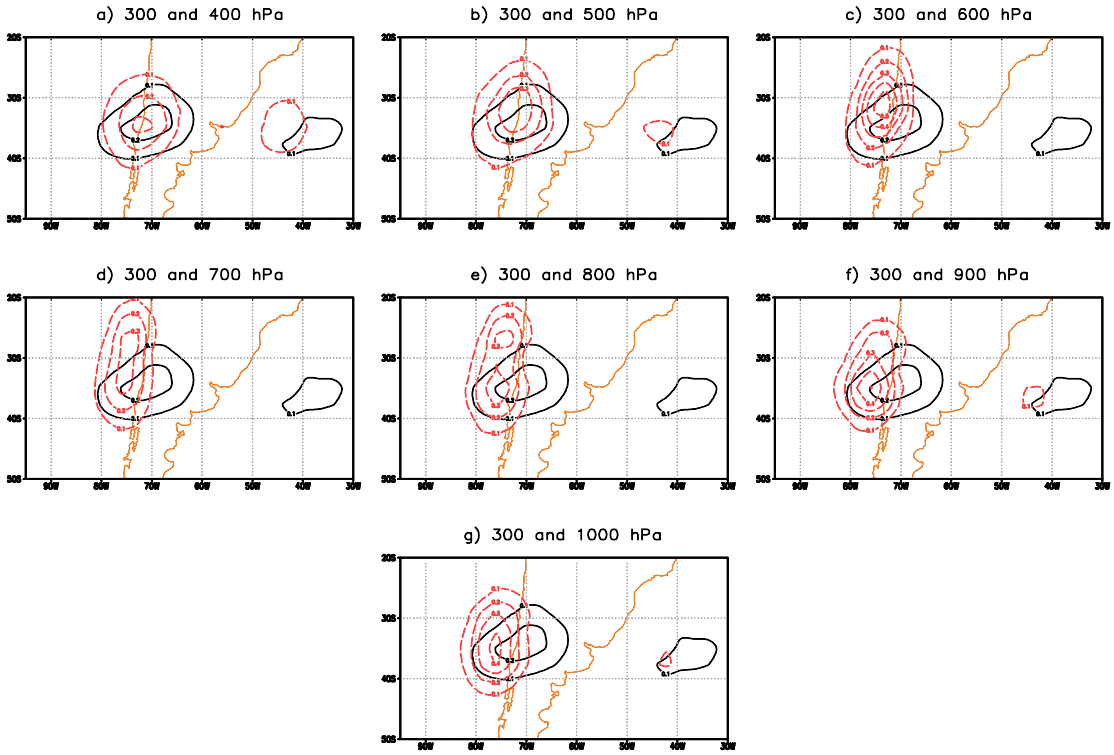


Lysis density is in black solid line at 300 hPa and red dashed line at other levels. The deepest systems are $\xi_{300}$ COLs that reach the surface, selected over a spherical cap (r=10°) centered at 34.5°S 80.0°W (Region A). Unit is number per unit area per season, the unit area is equivalent to a 5° spherical cap (~$10^6$ km$^2$). Analysis performed using the ERAI reanalysis for a 36-yr period (1979-2014).

Source: Author's production.

The development of COLs affecting South America can be viewed as a manifestation of interactions between upper and lower tropospheric disturbances and the regional features that affect those responses. Such interaction is demonstrated in Figure 7.16 that depicts the composite lifecycle of the tropospheric vorticity and geopotential anomaly associated with the deep and shallow COLs. This is done by first determining the minimum $\xi_{300}$ or $Z'_{300}$ and then the corresponding cyclonic minimum at each pressure level at a number of levels down to the surface. The search is performed over a spherical cap region of 5° centered on the minimum of $\xi_{300}$ or $Z'_{300}$. Values at pressure levels ≤ 600 hPa within the time interval between -12h and +12h were rejected, because of the discontinuity due to the mountains, and assuming that COLs typically take about one day to cross the Andes. As in Figure 7.12, composites are centered on the time

when the COLs cross the Andes. The early stages of the COL development is marked by a strengthening of vorticity and deepening of geopotential for both shallow and deep COLs, but the variation within the COL lifecycle is much more pronounced in the deepest systems. The evolution of vorticity and geopotential during the initial stages seems to be driven by the baroclinic dynamics where the upper and lower tropospheric disturbances reinforce each other. The mechanism of mutual amplification is described by Hoskins et al. (1985) using a PV framework to explain the effect of upper-tropospheric flow on the cyclogenesis process. The peak intensity in the upper troposphere occurs between one and three days before the COL reaches the Andes, followed by a sharp decrease because of the superimposition of the COL with the mountain wave ridge, as discussed above.

The decay process is more prominent in the COLs with a deep structure, particularly from the geopotential perspective (Figure 7.16d). If the COL reaches the east side of the mountains, a new intensification phase may initiate, as indicated by the evolution of vorticity and geopotential. However, differences are found between the composites of deep and shallow COLs. The upper-tropospheric flow associated with the deepest COLs seems to be more affected by the mountains in comparison to the shallow cases. If an intense and deep COL crosses the Andes, it tends to weaken in the lee side of the mountains but a lower-tropospheric perturbation intensifies just beneath the decaying COL. It is possible that the cyclonic feature near the surface is strengthened by the inflow of warm moist air from the tropics of South America, increasing the ascent and inducing cyclogenesis events. During this process, the cyclone near the surface may present two distinct peaks of intensity (occurs earlier in $\xi_{300}$ than in $Z'_{300}$), suggesting the existence of a two-phase growth, though it is not clear that this is real or just noise. Thus, the intensification of cyclones with COLs as an upper-level precursor could be forced earlier by the orography, and then making a transition to a more usual "baroclinic development" phase. Such theory is supported by experimental studies on cyclogenesis in the lee side of the Alps, as earlier discussed by Buzzi and Tibaldi (1978) and Smith (1986).

The competing effects of an increased intensity at the surface and a decreased intensity in the upper troposphere may be related to diabatic processes that modifies the structure of mid-latitude disturbances. In fact, numerous studies (AHMADI-GIVI et al., 2004;

DAVIES; EMANUEL, 1991; REED et al., 1992; STOELINGA, 1996) have shown the direct effect of the moisture generated by the mid-tropospheric latent heat release on the cyclogenesis by inducing cyclonic PV at lower levels and anticyclonic PV aloft. Therefore, the vorticity and geopotential views are consistent with one another, as each perspective emphasizes different aspects of the same circulation.

Figure 7.16: Lifecycle composite of the tropospheric fields of (a, c) relative vorticity and (b, d) geopotential height anomaly, for the (a, b) shallow and (c, d) deep $\xi_{300}$ Cut-off Lows.

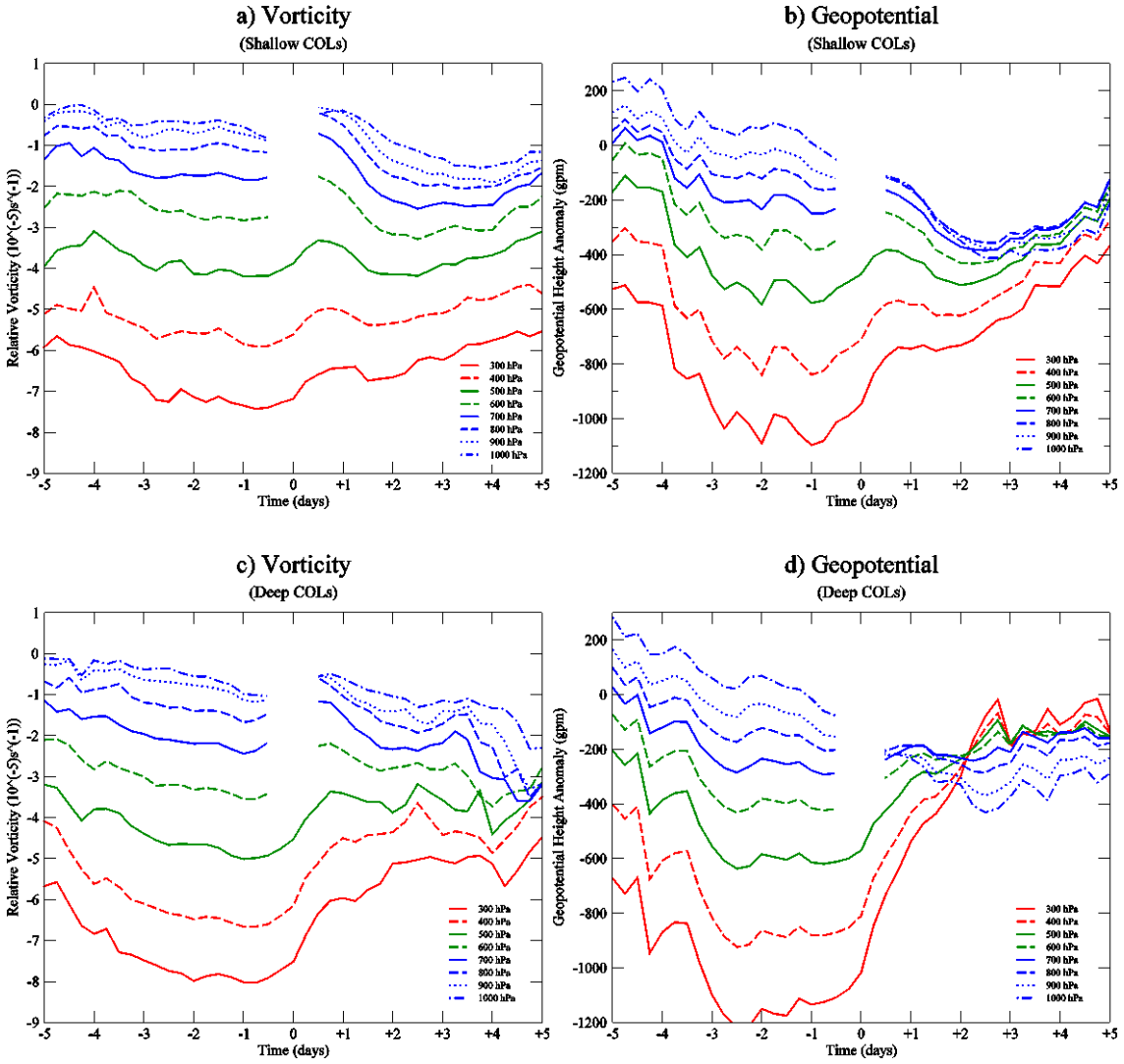


The pressure levels are in hPa: 1000 (blue dashed-dotted line), 900 (blue dotted line), 800 (blue dashed line), 700 (blue solid line), 600 (green solid line), 500 (green dashed line), 400 (red dashed line), and 300 (red solid line). The $\xi_{300}$ COLs are selected over a spherical cap (r=10º) centered at 34.5ºS 80.0ºW (Region A). Unit is $10^{-5}$ $s^{-1}$ for vorticity and gpm for geopotential height anomaly. Analysis performed using the ERAI reanalysis for a 36-yr period (1979-2014).

Source: Author's production.

One purpose of separating the COLs into deep and shallow groups is to understand the main differences in structure between the two types. Our understanding of the structure of COLs is due to case studies of individual systems, but little is known about the effect

of vertical depth of COLs on their structure. This is studied here by creating composites of the deep and shallow COLs and examining the vertical cross-sections in the W-E direction (Figure 7.17). The fields examined are the horizontal winds, temperature and PV for ten pressure levels from 1000 hPa to 100 hPa, similar to Figure 6.10. The temperature anomaly is calculated by removing the area-average for a $15^{o}$ radius cap from the grid for each COL at each level. The key features of COLs shown in Figure 6.10 are also identified in the regional analysis (Figure 7.17), such as the typical circulation, cold core, and PV intrusion. The deep COLs have stronger winds and a deeper circulation, and the tropopause folding is clearly more pronounced compared to the shallow COLs. However, even for the deep COLs, the circulation is not as strong as the 200 most intense COLs in the whole SH (Figure 6.10). The cold and warm cores have similar extension and are located in relatively similar positions, but the temperature anomaly is clearly more visible in the deeper COLs. The fact that the temperature anomaly appears at the surface, even for the shallow COLs, contradicts earlier results obtained with relatively old observations (ERICKSON, 1971) that suggested the COLs modify only the features in the upper troposphere. These results can be useful for the characterization of COLs with respect to their vertical structure.

Figure 7.17: Composite vertical cross-sections along the west-east line of the a) shallow Cut-off Lows and b) deep Cut-off Lows. Fields are zonal and meridional winds, temperature anomaly and potential vorticity.

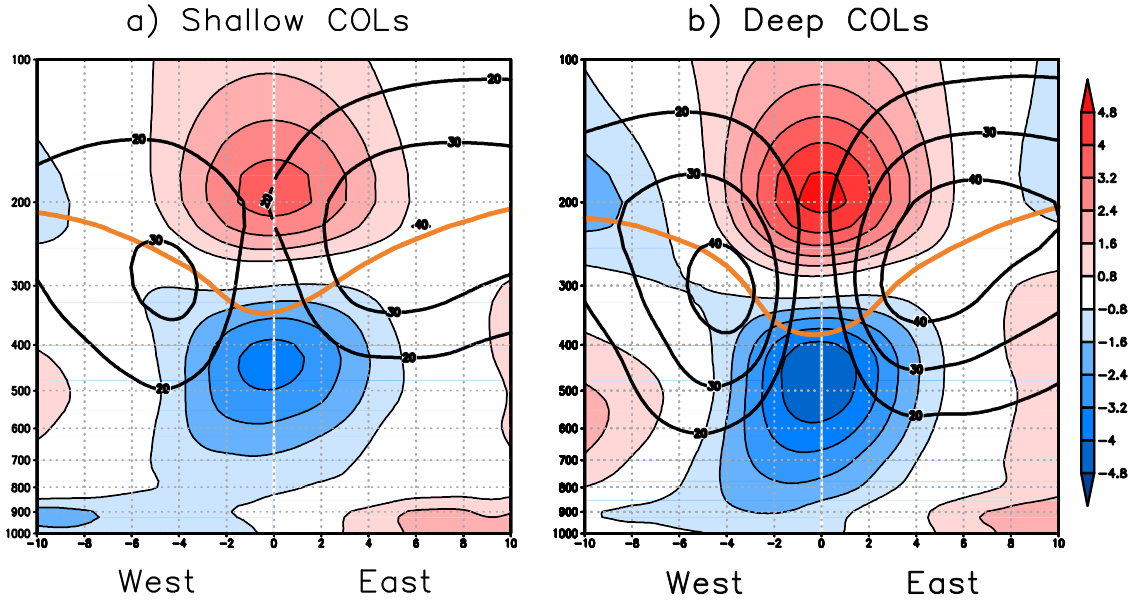


The $\xi_{300}$ COLs are selected over a spherical cap (r=10º) centered at 34.5ºS 80.0ºW (Region A). Composites are centered on the time and space relative to the $\xi_{300}$ minimum. The total distance in the $x$ axis is 20º geodesic. Magnitude of horizontal winds (thick solid line) from 20 m/s for the contour intervals 10 m/s. Temperature area-average anomaly in K (shaded). Potential vorticity for the 2 PVU (1 PVU = $10^{-6}$ $m^2$ $s^{-1}$ K $kg^{-1}$) (orange line). Analysis using the ERAI reanalysis for a 36-yr period (1979-2014).

Source: Author's production.

## 7.3 Summary and discussion

The results of this chapter reveal that COLs differ considerably across eight distinct regions, because of the particular geographical and orographical conditions in the SH. In general, COLs prefer to form near but off the continents. The exception is the maximum genesis in southeast Australia (region F) which is the only region of significant genesis over a continent. COLs generate both upstream and downstream of elevated terrain, such as observed in the subtropics of South America and southern Africa (referred to regions A, B, C and D). However, a different behavior is seen in southern Oceania where there are peaks of genesis and lysis close to each other, resulting in the highest occurrence of COLs in the whole SH. In this sector, the frequency of COLs is above the

hemispheric average throughout the year. The COL generation in this part of Oceania occurs simultaneously with the split of the upper-level jet stream and is frequently associated with blocking and zonal wave 3 such as a modon-type structure (TRENBERTH; MO; 1985), and with Rossby wave breaking events (NDARANA; WAUGH, 2010).

Regional differences are particularly notable in terms of the vertical depth of COLs. In the southeast Australia and western Pacific, COLs are deeper than the average and about 30% of the total reach the surface. These systems contrast with those observed in southern Africa where only about 15% of them reach the surface. The COLs formed in the southeastern Pacific are normally deep in the mid-troposphere, weakening toward the surface. In contrast, much deeper COLs are found in the lee side of Andes, affecting directly the precipitation.

The results of the regional analysis show that precipitation depends on both intensity and vertical depth. The strong and deep classes have the COLs with the largest maximum rainfall rates and cumulative precipitation in a single event (that is 132.4 mm). The presence of the Andes represents a major obstacle for the transport of moisture from the interior of the continent onto the eastern side of the COLs, inhibiting precipitation even under a strong upper-level COL. However, on the lee side of Andes a jump in the precipitation to values above average is observed. In fact, the increased precipitation seems to be a result of the latent heat release, which weakens the disturbance in the upper troposphere but strengthens that in the lower troposphere. Hence, surface cyclogenesis is induced due to the possible existence of two relevant mechanisms, one is the mechanical effects associated with the Andes, the other is baroclinic instability.

# 8 NEW PERSPECTIVES ON THE DOWNSTREAM BAROCLINIC DEVELOPEMT

This chapter examines the eddy kinetic energy (EKE) budget of the SH COLs by using a well-established EKE budget methodology developed by Orlanski and Katzfey (1991) and modified by Chang (2000) and described in Section 3.2.7. Section 8.1 discusses the impact of the sampling radius, chosen to compute the EKE budget on the residual. The major dynamical mechanisms typically controlling the development of COLs, such as the ageostrophic flux convergence (AFC), known as Downstream Development (DSD), and the baroclinic (BRC) and barotropic (BRT) conversions, are examined in Section 8.2. Since there are a wide variety of development scenarios, an investigation of individual cases with respect to their evolution is shown in Section 8.3. In Section 8.4, the energetics of COLs is discussed for particular regions of the SH. The last section summarizes the main results and concludes the discussion.

## 8.1 Sensitivity of the area (volume) to the residue

The residual exists mainly because there are energy forcings that are not included in Eq. 3.1, such as the friction and diabatic processes (including the radiative, latent and sensible heat fluxes). In addition, there are errors introduced by numerical methods due to the reanalysis time interval. The residual is first assessed to determine its magnitude for COLs using different radial distances from the vortex centre, such as $5^o$, $10^o$, $15^o$, $20^o$ and $25^o$ in geodesic distances (Figure 8.1a) in order to find the more appropriate size to calculate the energetics of COLs. It can be seen that the estimation of the residual in COLs depends on the size of the measurement volume in which the values are calculated. In general, the larger the horizontal area the smaller the amplitude of the residual throughout the COL life cycle. The largest amplitude of the residual is observed using $5^o$ and $10^o$, but it decreases with increasing area. The fact that the amplitude of the residual reduces with increasing volume may be related to the transfer of energy across the boundaries (MICHAELIDES, 1987; MUENCH, 1965), where part of this transfer is represented by the AFC. The transport of energy inside and outside the bounds (defined as the area around the COL) are not directly calculated in Eq. 3.1. Thus, for relatively small regions (e.g. $5^o$ or $10^o$ geodesic radius) the boundary

transports of energy within the COL are likely more important than in the outer regions where the energy fluxes are weaker.

Note that the residual is negative (rhs larger than lhs) for almost the whole life cycle, with larger values found in the decay stage of the lifecycle (Figure 1a). One of the main reason for this "energetic imbalance" is the unknown contribution of the frictional dissipation, which represents an important energy sink for the disturbance. In a brief period of the COL development (from 'day -2' to zero), the residual remains positive for the small radii (e.g. $5^o$, $10^o$, $15^o$) which means there are other mechanisms that act as energy sources but are not directly computed, such as the latent heat release. However, it is important to note that the residual may also be due to computational errors associated with the numerical methods such as the analysis increment and other unknown mechanisms. Despite the large variation in amplitude, the average residual computed along the whole life cycle does not depend on the radius, as shown in the inset of Figure 8.1a.

The EKE tendency is calculated using two different methods based on the Eq. 3.1: the first is obtained by using a centered time difference for the lhs of Eq. 3.1 using the previous and subsequent time steps; and the second is obtained by using the rhs terms (except the residual term), as described in Section 3.2.7. These are shown in Figure 8.1b, where it can be seen that there is a significant correspondence for the tendency obtained with the rhs terms and the lhs terms during the growth phase of the COLs, but marked differences are found in the decay phase resulting in the higher residual. The difference between the lhs and rhs is negative when the COLs are decaying, and this is probably related to effects associated with the friction and diabatic heating near the COL centre. This energetic inconsistency is clearly evident in the curve of EKE tendency obtained with the rhs when positive values appear during the decay phase, indicating that there are dissipative mechanisms that are not included in the formulation. The temporal evolution of the total EKE in the COLs (Figure 8.1b) indicates that the peak EKE coincides in time with the maximum intensity of the $\xi_{300}$ COLs, which is consistent with our expectation. Further results involving quantities averaged over a spherical cap will be determined using $15^o$ as a radius, because this is appropriate to represent the main energy centres that control the development of COLs.

Figure 8.1: Temporal evolution of the a) residual and b) total EKE and EKE tendencies in the strongest Cut-off Lows.

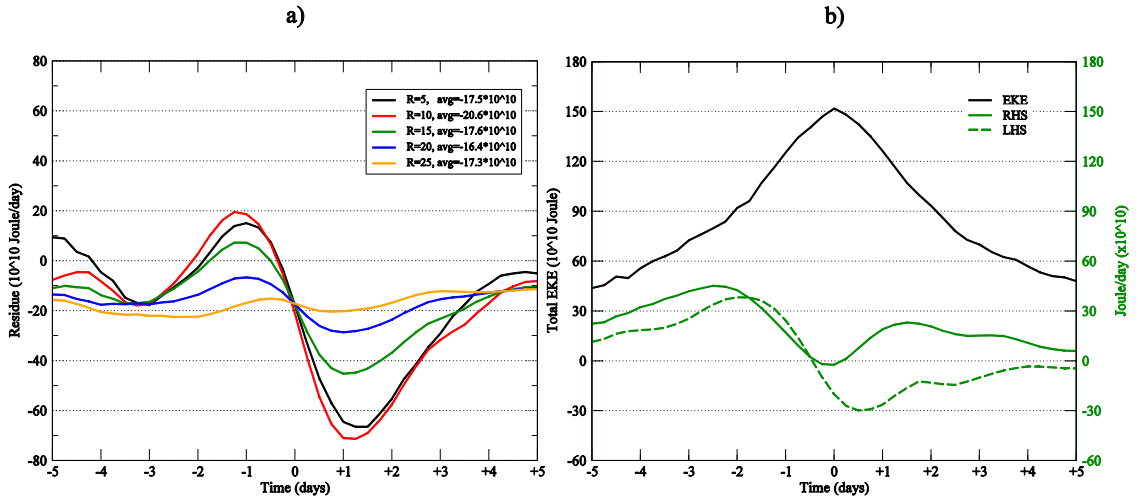


Composites of the 200 most intense SH COLs that match between the $\xi_{300}$ and $Z'_{300}$, relative to the time of maximum intensity. a) Residual values are determined using different spherical cap regions (r=5º, 10º, 15º, 20º, and 25º) centered on the COL location. The inset indicates the average of residue within the corresponding area. b) EKE values determined within a 15º spherical cap region centered on the COL location. Tendencies are computed using rhs (solid line) and lhs (dashed line). Unit is Joule/day for residuals and tendencies, and Joule for the total EKE, both scaled by $10^{10}$. All these quantities are vertically averaged from surface to 100 hPa. Analysis performed using the ERAI reanalysis for a 36-yr period (1979-2014).

Source: Author's production.

## 8.2 The strongest Cut-off Lows

The relative contribution of the most important mechanisms for the development of the 200 strongest SH COLs is shown in Figure 8.2. It can be seen that the AFC is by far the most important contributor to the EKE growth. The transport of energy due to ageostrophic fluxes occurs with a group velocity of Rossby waves and represents the radiative part of the total energy flux that exists due to the dispersive nature of the atmospheric waves (CHANG, 2000; PEDLOSKY, 1987). The AFC acts to import EKE from an upstream system in the early stage of the COL lifecycle, while strong dispersive EKE fluxes occur in the decay phase (Fig 8.2), resulting in the primary source of energy for the COL. The AFC decreases as the COL approaches its maximum intensity. At this time, the BRC becomes the most important mechanism to maintain the COL, converting

EAPE to EKE (OORT; PEIXOTO, 1983). The EAPE is also generated by diabatic heating, particularly during the mature and decay stages of an upper-level COL, which is the time of the peak precipitation (see Figs. 6.16 and 6.18). The major source of diabatic heating is generally found in the warm sector of mid-latitude cyclones (CARLSON, 1991). This is similar to what happens in the COLs, where most precipitation occurs on the east side, and this may contribute to enhance the horizontal temperature gradient. However, when the convection occurs near the COL centre, which is typically observed during the decay stage (see Figure 6.15), the diabatic heating tends to destroy the cold-core leading to the dissipation of the COL. The composite of the BRC term shows (Figure 8.2) two peaks, which occur in the growth and decay phases. This is basically due to the cold air sinking and warm air rising within the COL. A more detailed analysis of the spatial distribution of the BRC conversion within the COL will be presented later.

The other part of the total energy flux is the advective flux (KFC) that has a large magnitude, but only contributes to displace the EKE (CHANG, 2000; DECKER; MARTIN, 2005; GAN; PIVA, 2013). This is attributed to the movement of energy centres rather than the intensification of the system, where its movement is given by the phase velocity (CHANG; ORLANSKI, 1993). This means that the KFC does not contribute to the redistribution of energy within the COL, as happens with the ageostrophic fluxes. Positive (negative) values of KFC imply that the EKE centre propagates eastward (westward). The composite of KFC denotes that most of the EKE moves eastward during the development phase and westward during the decay phase. The BRT term remains negative during the whole development phase, representing the main sink of energy. Note that this mechanism acts in opposition to the EKE growth, but this is not enough to prevent the intensification of the COL. In the decay, the BRT is nearly zero, thereby the AFC and other dissipative mechanisms such as friction and diabatic heating are the most important mechanisms to dissipate the COLs. These results confirm that the growth (decay) of COLs is dominated by the ageostrophic flux convergence (divergence) (GAN; PIVA, 2013, 2016), where the sum of the energy gain over the entire life cycle corresponds to 3248 Joule for the composite COL. However, despite the smaller amplitude, the BRC conversion is crucial for the formation and

maintenance of COLs, amounting to approximately 3670 Joule for the whole life of the composite COL.

Figure 8.2: Temporal evolution of the main EKE terms in the strongest Cut-off Lows.

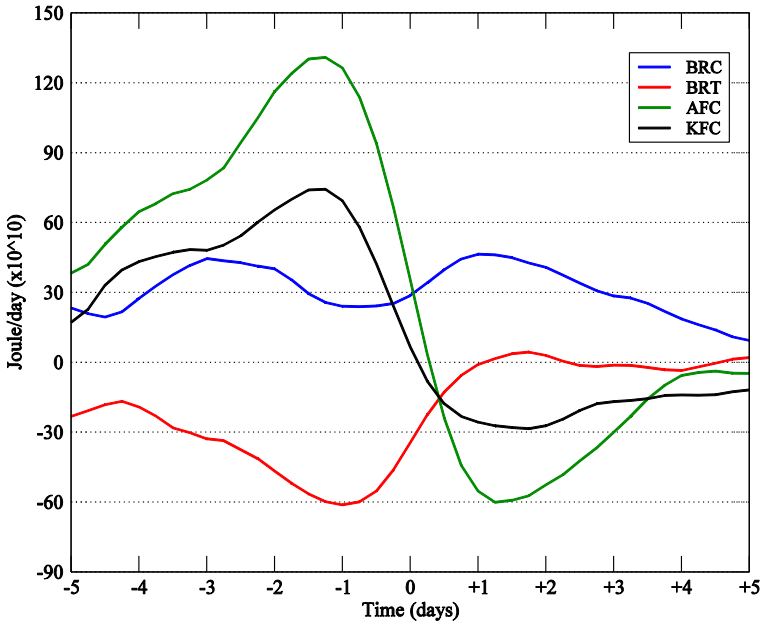


Composites of the 200 most intense SH COLs that match between the $\xi_{300}$ and $Z'_{300}$, relative to the time of maximum intensity. The terms are BRC (blue line), BRT (red line), AFC (green line) and KFC (black line). Fields are vertically averaged within a 15° spherical cap region centered on the COL location. Unit is Joule/day, scaled by $10^{10}$. Analysis performed using the ERAI reanalysis for a 36-yr period (1979-2014).

Source: Author's production.

The spatial distribution of the EKE associated with the strongest COLs is shown for the horizontal composite in Figure 8.3 which depicts the vertically averaged energy together with the $Z_{300}$ height. The initial stage of the COL lifecycle ($T = -48h$) begins with a pre-existing upper-level trough associated with a fairly broad EKE centre on the west side and a weaker EKE centre on the east side of the COL. The upstream energy centre grows vigorously over the next day ($T = -24h$) mainly due to the convergence of ageostrophic fluxes (Figure 8.2). As this EKE centre matures, it loses energy just downstream to intensify the EKE centre to the east side of the COL. The upstream EKE centre starts decaying just before the maximum intensity in the $\xi_{300}$, when there is no longer a supply of energy from an upstream system (see Figs. 8.4 and 8.5), and also as a

consequence of its own export of energy downstream. At the mature stage ($T = 0$), the eastern EKE centre is stronger than the western EKE centre in the COL. The decaying stage ($T \geq 24h$) is marked by an overturning flux as the EKE centres on the east and west sides merge with each other to form a single centre in the southern sector of the COL, which is in agreement with previous studies (DANIELSON ET AL., 2006; GAN; PIVA, 2013; ORLANSKI; SHELDON, 1995). The reversed ageostrophic flux in the decay phase (i.e. westward propagation) is consistent with the evolution of KFC (Figure 8.2), and is likely a manifestation of Rossby wave breaking (MCINTYRE; PALMER, 1985; WILLMOTT, 1985).

Figure 8.3: Temporal evolution of the vertically averaged EKE in the strongest Cut-off Lows.

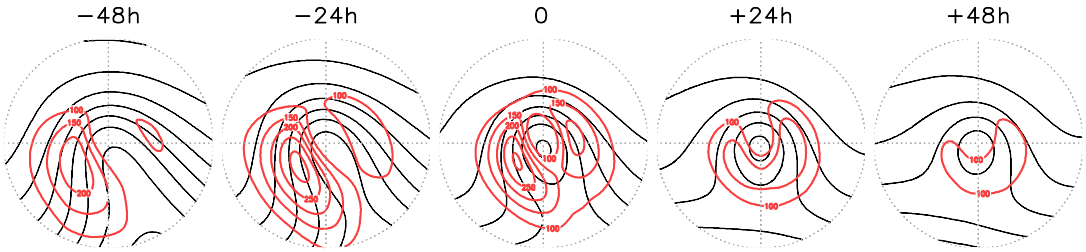


Composites of the 200 most intense SH COLs that match between the $\xi_{300}$ and $Z'_{300}$, relative to the time of maximum intensity. The distance from the centre of the composite to the edge is 15º. Unit is $10^{10}$ Joule for the total EKE (red line), and gpm for the $Z_{300}$ height (black line) with 50 gpm intervals. Analysis performed using the ERAI reanalysis for a 36-yr period (1979-2014).

Source: Author's production.

After the different components of the EKE budget equation have been computed, the composite evolution of the EKE components in the COLs is examined separately for the three main terms (AFC, BRC and BRT) using horizontal composites of the vertically averaged fields (Figure 8.4) and vertical cross-sections in the W-E direction (Figure 8.5) for the 200 most intense SH COLs. The horizontal and vertical cross-sections are conveniently discussed together. In the development phase the AFC maximizes immediately upstream from the COL centre. The divergence of the ageostrophic flux on the western side indicates that the EKE is strongly exported to the eastern side of the COLs during the whole lifecycle (Figure 8.4 first line). This contributes to the decay of the upstream EKE centre and growth of the downstream EKE centre. The vertical cross-sections show that the energy transfer occurs preferably at high levels where the

ageostrophic winds have a major contribution. However, when the COLs are considered individually, the largest values of AFC can be found at mid-levels simultaneously with enhanced baroclinicity. This configuration was observed in mid-latitude disturbances, such as in the mature stage of the Storms *Friedhelm* and *Klaus* in the North Atlantic Ocean (RIVIÈRE et al., 2015) where the ageostrophic fluxes are found to be larger at ~500 hPa. An examination of individual COLs will be discussed in the next section.

The EKE growth in the COLs is also enhanced by the BRC conversion (Figure 8.4 second line). During the development and mature stages, the BRC term is positive on the west side of the COLs due to the sinking motion in the cold air, which implies generation of EKE through thermally direct circulation. Subsequently, the eastern EKE centre also expands through the BRC conversion, associated with the ascending warm air further east. During this stage, positive values of BRC conversion are found at higher levels due to the presence of the warm-core (~200 hPa). Positive values of the BRC term seem to be spatially correlated with negative values of AFC, since the energy produced via the BRC conversion is dispersed through the ageostropic fluxes.

The spatial composite of BRT conversion (Figure 8.4, third line) indicates that most of the COL region is dominated by negative values, particularly upstream from the COL centre in the growth phase. This means that the horizontal shear upstream from the COL contributes to the zonal flow that extracts kinetic energy from the COL. However, a minor contribution associated with barotropic instability (positive values) occurs on the eastern EKE centre in the late stages, although this is much less important than both the AFC and BRC terms. It is important to say that, despite the poor efficiency in generating kinetic energy, the barotropic instability was found to be the dominant mechanism for the development of upper-level disturbances in the tropics (COLTON, 1973; MISHRA et al., 2001, 2007; RAO; BONATTI, 1987).

Figure 8.4: Lifecycle of the strongest Cut-off Lows with respect to the vertically average AFC, BRC and BRT.

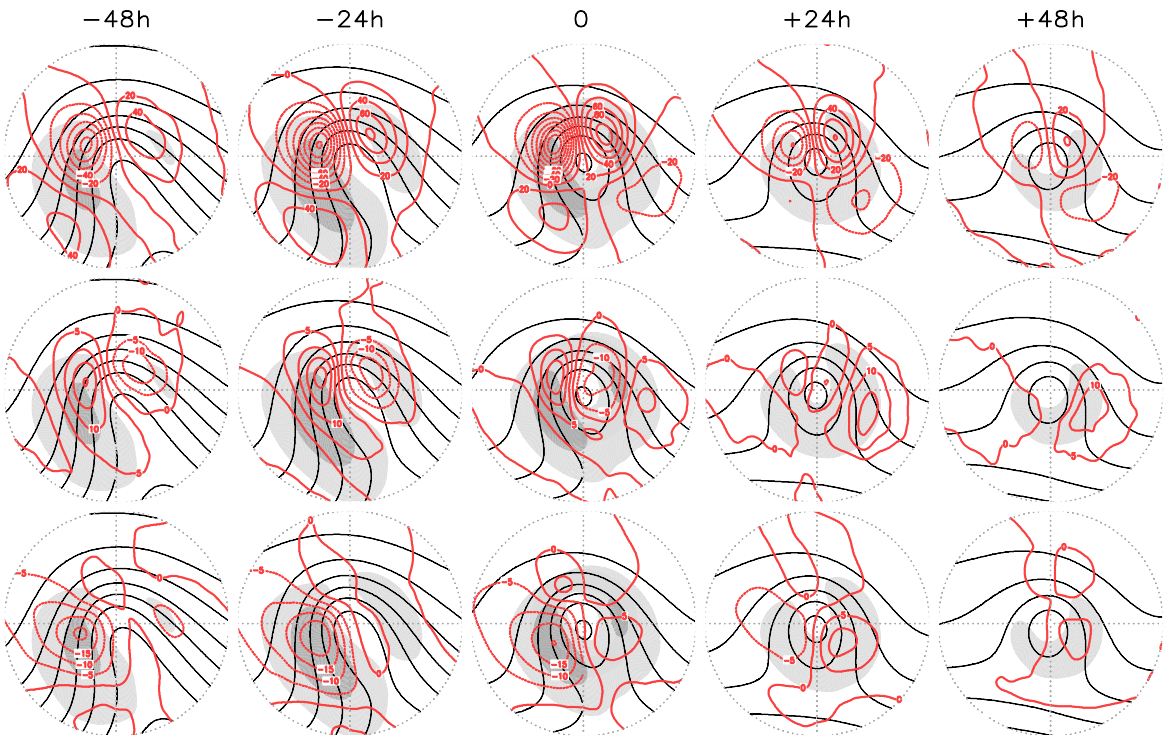


Composites of the 200 most intense SH COLs that match between the $\xi_{300}$ and $Z'_{300}$, relative to the time of maximum intensity. The fields are the total EKE (in shaded) for 100 x $10^{10}$ and 150 x $10^{10}$ Joule intervals, the $Z_{300}$ height (black line) for 100 gpm intervals, combined with vertically average fields of AFC for 20 x $10^{10}$ Joule/day intervals (top), the BRC for 5 x $10^{10}$ Joule/day intervals (middle), and the BRT for 5 x $10^{10}$ Joule/day intervals (bottom). Analysis performed using the ERAI reanalysis for a 36-yr period (1979-2014).

Source: Author's production.

Figure 8.5: Lifecycle of the strongest Cut-off Lows with respect to the vertical cross section (W-E direction) of the AFC, BRC and BRT.

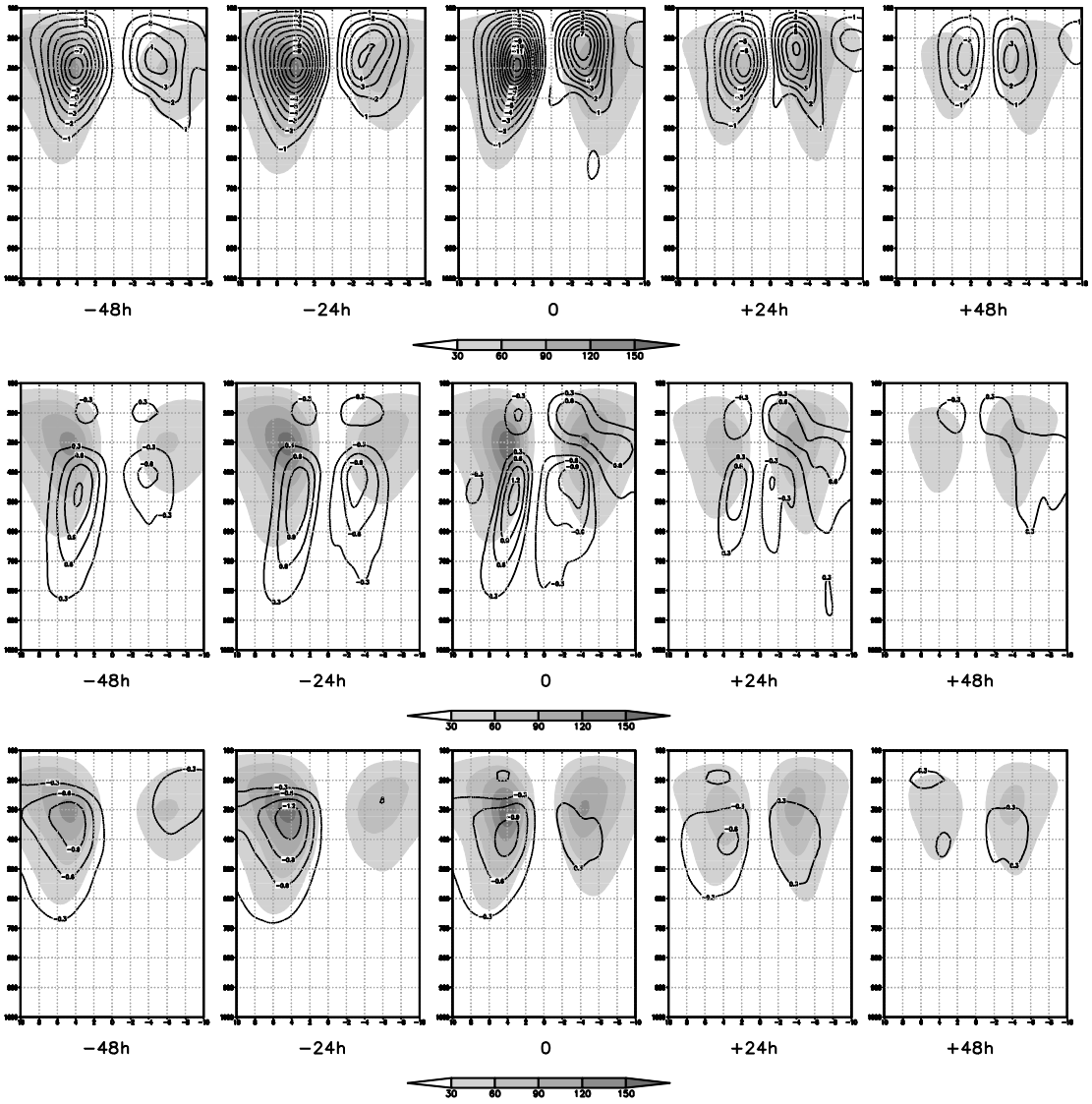


Composites of the 200 most intense SH COLs that match between the $\xi_{300}$ and $Z'_{300}$, relative to the time of maximum intensity. The fields are the total EKE (in shaded) in Joule combined with AFC for 1.0 x $10^{10}$ Joule/day intervals (top), the BRC for 0.3 x $10^{10}$ Joule/day intervals (middle), and the BRT for 0.3 x $10^{10}$ Joule/day intervals (bottom). Analysis performed using the ERAI reanalysis for a 36-yr period (1979-2014).

Source: Author's production.

Figure 8.4 depicts the temporal evolution of the main terms of the EKE budget (AFC, BRC and BRT) where the values are vertically averaged within three tropospheric layers: upper, middle, and lower. The EKE budget with respect to the upper layer

indicates a similar distribution of the main terms compared to those averaged over the entire troposphere (see Figure 8.2). This is consistent with the results above since the largest contribution to the EKE growth is achieved through mechanisms acting at higher levels, such as the AFC. However, in the lower and middle troposphere the BRC is the primary energy source for the COLs, while the contribution from the AFC has a secondary role. The BRT is generally negative and is maximized in the middle troposphere.

Figure 8.6: Temporal evolution of the main EKE terms in the lower, middle and upper troposphere in the strongest Cut-off Lows.

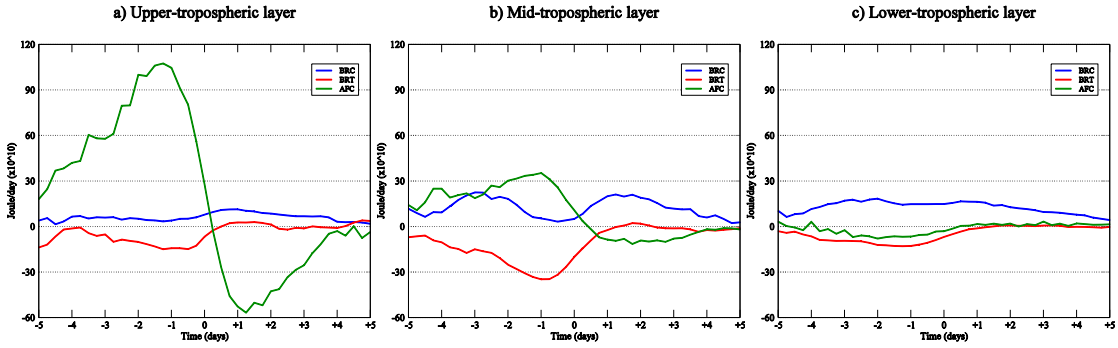


Composites of the 200 most intense SH COLs that match between the $\xi_{300}$ and $Z'_{300}$, relative to the time of maximum intensity. The terms are BRC (blue line), BRT (red line) and AFC (green line). The chosen levels are: 100, 200 and 300 hPa for the upper layer; 400, 500 and 600 hPa for the middle layer; 700, 800, 900 and 1000 hPa for the lower layer. Fields are vertically averaged within a 15º spherical cap region centered on the COL location. Unit is $10^{10}$ Joule/day. Analysis performed using the ERAI reanalysis for a 36-yr period (1979-2014).

Source: Author's production.

To demonstrate more clearly how the dominant mechanisms behave at each pressure level, the temporal evolution of the AFC, BRC and BRT terms in the strongest COLs are given in Figure 8.7. In this figure, the AFC has two distinct phases: the first is dominated by imported energy by ageostrophic fluxes from the upstream system that feed the EKE growth of the COL; the second is marked by the activity of dispersive fluxes that weakens the system. The two phases are clearly seen at high levels, where the largest contribution takes place at 200 hPa, but the effect of the AFC becomes less apparent above and below this level. Note that the amplitude of the AFC in the growth

is larger than that in the decay, suggesting that friction and/or other dissipative mechanisms are important in this stage. This is consistent with Figure 8.1, which indicates that the residual reaches a maximum amplitude (values more negatives) subsequent to the maximum intensity of the COLs.

Figure 8.7: Temporal evolution of the AFC at different levels in the strongest Cut-off Lows.

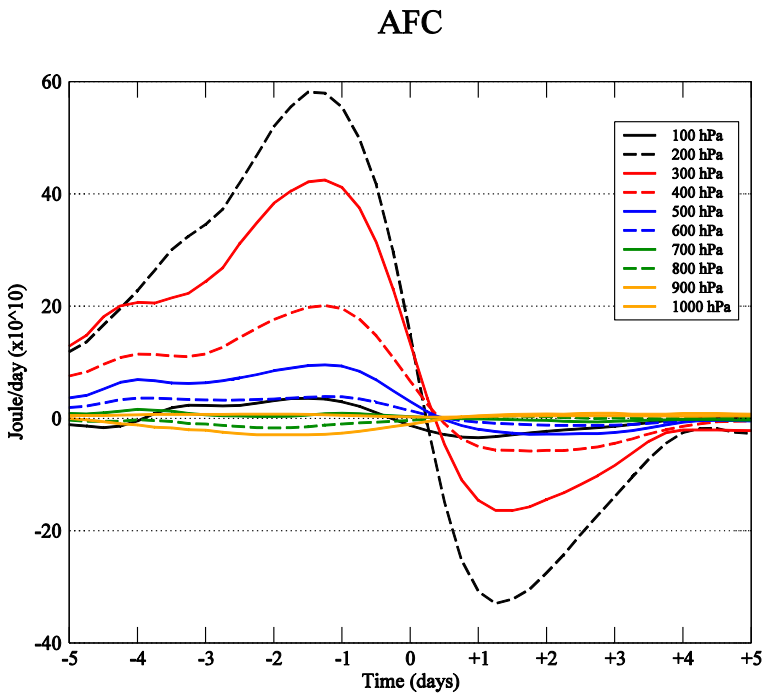


Composites of the 200 most intense SH COLs that match between the $\xi_{300}$ and $Z'_{300}$, relative to the time of maximum intensity. The levels are 1000 hPa (yellow dashed line), 900 hPa (yellow solid line), 800 hPa (green dashed line), 700 hPa (green solid line), 600 hPa (blue dashed line), 500 hPa (blue solid line), 400 hPa (red dashed line), 300 hPa (red solid line), 200 hPa (black dashed line), and 100 hPa (black solid line). Unit is $10^{10}$ Joule/day. Analysis performed using the ERAI reanalysis for a 36-yr period (1979-2014).

Source: Author's production.

The separation of the BRC according to the different vertical levels allows us to examine the variation of this conversion throughout the COL lifecycle. It can be clearly seen from Figure 8.8 that the production of energy via BRC conversion occurs in a deeper layer than that for AFC. The vertical distribution of BRC can be defined into three major classes. One is composed of two high levels (300 and 400 hPa) where the primary and secondary peaks occur in the decay and growth, respectively. The second

class is represented by the 500, 600 and 700 hPa levels, where the primary and secondary maxima are found in the growth and decay phase, respectively. In the third class (800 and 900 hPa), a maximum is not particularly apparent and the EKE produced by BRC conversion remains almost constant during the COL life cycle. Interestingly, the BRC term is positive in the whole troposphere. The exception occurs at 100 hPa in which the BRC is negative, although these values are not significant compared to those at the other levels. This result conflicts with previous studies (GAN; PIVA, 2013; 2016) in which negative values of BRC were observed during the midlife stage of southeast Pacific COLs. The reason for the differences in the BRC values may be attributed to the size of the volume for the integration ($25^{o}$ lat x $30^{o}$ long) used by Gan and Piva (2013; 2016) that is much larger than that used in this study. Thus, mechanisms that operate outside the system may affect the EKE budget when using a larger domain to perform the volume integration. Moreover, the results shown in Figure 8.8 are based on a uniform set of COLs selected from the most intense systems in the whole SH, while the set of events used in Gan and Piva (2016) are not based on an intensity threshold, but instead a common region was used to perform the selection of cases, suggesting the results may be region-dependent. The second maximum of the BRC term observed in Figure 8.8 may be the result of the large precipitation in the decay phase, which is consistent with Figs. 8.4 and 8.5. This promotes more latent heat release that increases the EAPE and consequently the BRC conversion. However, when the precipitation occurs near the COL centre, the latent heat reduces the horizontal temperature gradient contributing to the COL decay.

Figure 8.8: Temporal evolution of the BRC at different levels in the strongest Cut-off Lows.

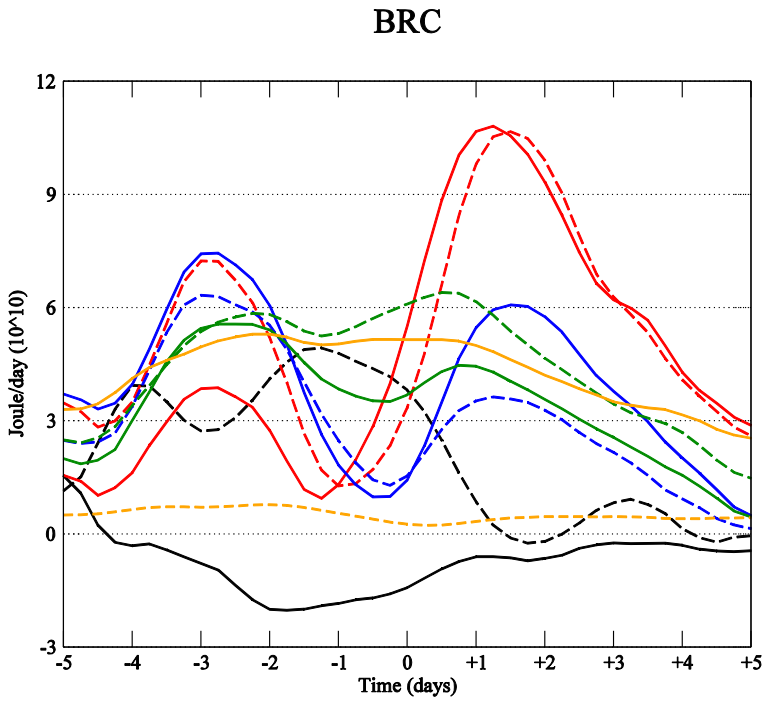


Composites of the 200 most intense SH COLs that match between the $\xi_{300}$ and $Z'_{300}$, relative to the time of maximum intensity. The levels are 1000 hPa (yellow dashed line), 900 hPa (yellow solid line), 800 hPa (green dashed line), 700 hPa (green solid line), 600 hPa (blue dashed line), 500 hPa (blue solid line), 400 hPa (red dashed line), 300 hPa (red solid line), 200 hPa (black dashed line), and 100 hPa (black solid line). Unit is $10^{10}$ Joule/day. Analysis performed using the ERAI reanalysis for a 36-yr period (1979-2014).

Source: Author's production.

The BRT conversion is closely related to the horizontal wind shear resulting from the interaction between the COL and the large-scale flow. This mechanism contributes negatively during the development phase at all levels (Figure 8.9). The exception occurs at 200 hPa where weak values are found. The largest values of BRT are found at 300 and 400 hPa, reducing with increasing and decreasing height. This mechanism apparently does not contribute to the COL decay, thus the theory consisting of baroclinic growth and barotropic decay of mid-latitude baroclinic disturbances is not appropriate to explain the development of the COLs.

Figure 8.9: Temporal evolution of the BRT at different levels in the strongest Cut-off Lows.

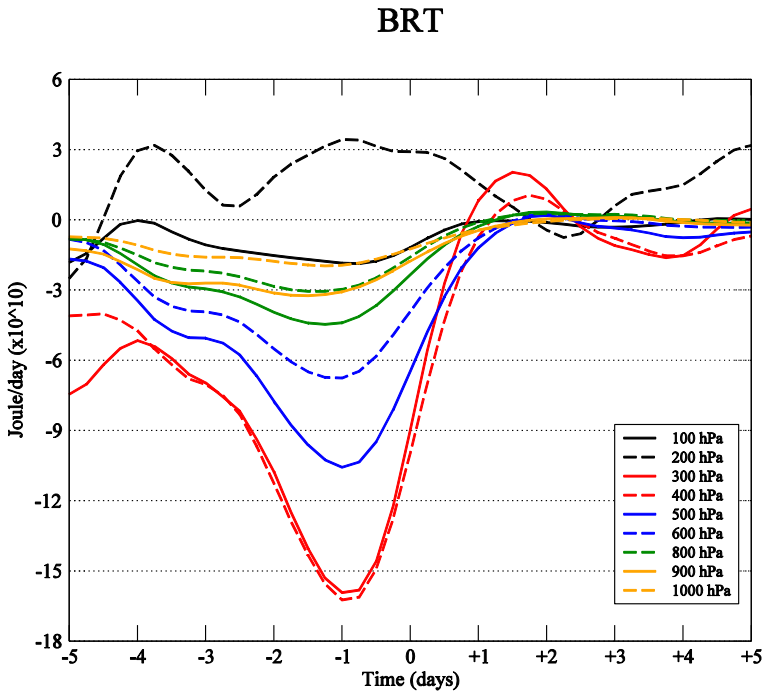


Composites of the 200 most intense SH COLs that match between the $\xi_{300}$ and $Z'_{300}$, relative to the time of maximum intensity. The levels are 1000 hPa (yellow dashed line), 900 hPa (yellow solid line), 800 hPa (green dashed line), 700 hPa (green solid line), 600 hPa (blue dashed line), 500 hPa (blue solid line), 400 hPa (red dashed line), 300 hPa (red solid line), 200 hPa (black dashed line), and 100 hPa (black solid line). Unit is $10^{10}$ Joule/day. Analysis performed using the ERAI reanalysis for a 36-yr period (1979-2014).

Source: Author's production.

## 8.3 Analysis of individual cases

To understand the more relevant variations from case-to-case, an examination of two particular COL events, chosen from among the 200 most intense systems, is shown in Figure 8.10. These cases were chosen as they represent the two most typical COL lifecycle in terms of the EKE propagation based on empirical evidence, although a cluster analysis would be able to identify the cases through similarities. The first case, shown at the top of Figure 8.10, shows a similar evolution to that seen in Figure 8.3, where the downstream development occurs through the export (import) of EKE immediately upstream (downstream) from the COL centre. The decay stage is characterized by an overturning flux of EKE in the poleward region of the COL, until it

disappears due to the friction and dispersive radiative fluxes. In the second case (bottom of Figure 8.10), the EKE grows in exactly the same way as it does in the first case, but differs in terms of the decay, since the energy is exported downstream and will possibly contribute to the formation of another system downstream from the decaying COL (not shown). It can be seen that the COL centre does not tilt toward the east in the decay phase, as happens with most COLs. This synoptic configuration seems to facilitate the natural dispersion of the EKE through the propagation of wave packets in the upper-tropospheric troughs as initially proposed by Orlanski and Sheldon (1995) and observed by other authors (CHANG, 2000; DANIELSON et al., 2006; PIVA et al., 2010). Although compositing is a useful technique to investigate the typical aspects of COLs, a better understand of the case-to-case variability in terms of the ageostrophic fluxes and conversions is needed to yield improved insights into the different nature of the COLs.

Figure 8.10: Temporal evolution of the vertically averaged EKE in two different Cut-off Lows.

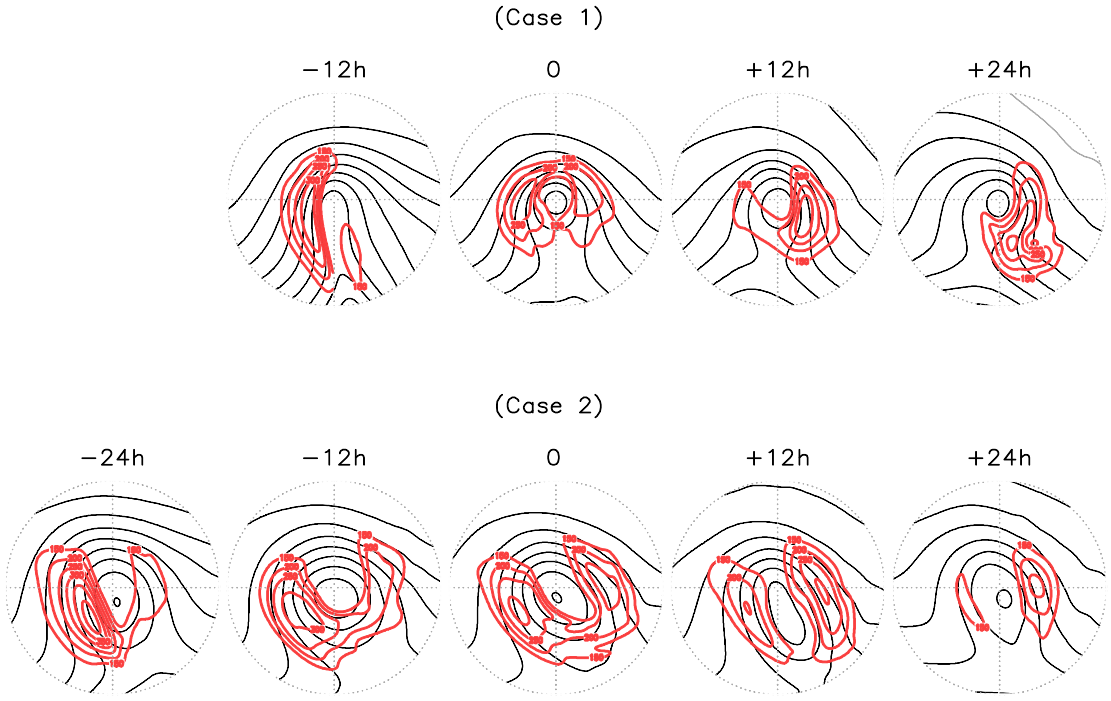


The sequence is relative to the time of maximum intensity. The distance from the centre of the plot to the edge is 15º. Unit is $10^{10}$ Joule for the total EKE (red line), and gpm for the $Z_{300}$ height (black line) with 50 gpm intervals. Analysis performed using the ERAI reanalysis for a 36-yr period (1979-2014).

Source: Author's production.

## 8.4 Regional features

This section focuses on the energetics of COLs formed in particular regions of the SH, such as the COLs whose genesis occurs in the southeast Pacific, namely region A, as in Figure 7.2. Figure 8.11 shows the evolution of the AFC, BRC and BRT for two groups of COLs which are classified according to their vertical depth (deep or shallow). The COLs are centered on a particular range over the subtropical Andes (92.5ºW-87.5ºW and 50ºS-15ºS) in exactly the same way as described in Chapter 7. The two distinct phases of AFC associated with the import and export of EKE are well represented in the regional analysis. It is not surprising that the amplitude of the AFC is much more relevant in the deep COLs than in the shallow COLs, since the circulation associated with the former is generally stronger than that of the latter. The BRC term reproduces the two peaks observed in Figure 8.2, but the peak associated with the decay is clearly much more prominent than that related to the growth. The rapid increase of the BRC conversion after the COL crosses the Andes is more apparent in the deeper cases. On the lee side of the Andes, warm advection at low levels induces a disturbance near the surface, enhancing the vertical motion (which is consistent with Figure 7.16), and consequently, the efficiency of the BRC. This suggests an important local effect of the mountains on the generation of EKE via the BRC conversion. The BRT conversion acts in a similar manner as it does in the strongest COLs. The negative values in the growth phase are more significant in the deep COLs due to their stronger circulation that contributes to the maintenance of the zonal mean flow through the transport of momentum from the COL.

Figure 8.11: Temporal evolution of the main EKE terms in the deep and shallow Cut-off Lows.

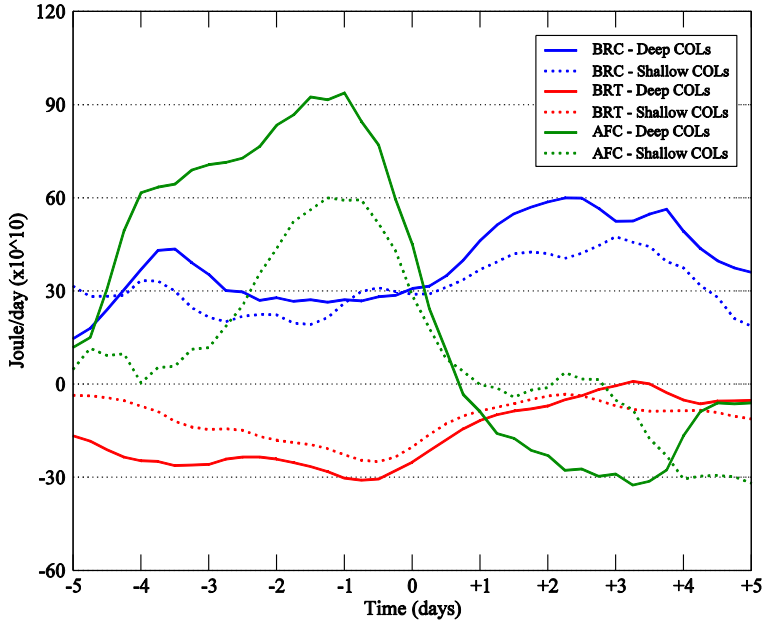


Groups are deep (solid line) and shallow (dotted line). The $\xi_{300}$ COLs are selected over a spherical cap (r=10º) centered at 34.5ºS 80.0ºW (region A). Each COL are centered on the time that the system crosses the Andes, defined for the longitudinal range from 92.5ºW to 87.5ºW. The terms are BRC (blue line), BRT (red line) and AFC (green line). Fields are vertically averaged within a 15º spherical cap region centered on the COL location. Unit is Joule/day, scaled by $10^{10}$. Analysis performed using the ERAI reanalysis for a 36-yr period (1979-2014).

Source: Author's production.

A comparative analysis is performed between the COLs whose genesis occurs in the southeast Pacific and the southwest Atlantic (namely regions A and B, respectively), as in Figure 7.2. The composites shown in Figure 8.12 are constructed by centering the COLs on the time of maximum intensity as measured by the $\xi_{300}$. Perhaps the most interesting difference between the two genesis regions is the BRC term. While the Pacific COLs have a curve consisting of two peaks, the COLs whose genesis occurs in the Atlantic sector show only a single peak, which coincides with the maximum intensity of the COLs. It is not clear the reasons associated with these differences, but there are some factors that may explain the gap in the BRC phase with respect to the two regions. First, assuming that some COLs coming from the southeast Pacific reach the lee side of the Andes, it is possible that the corresponding second maximum BRC (at approximately day +2) occurs in the region where the Atlantic also COLs have the

maximum BRC. The evolution of the BRC associated with the Atlantic COLs indicates that there is a rapid intensification compared to the Pacific COLs. Indeed, the Atlantic COLs are generally deeper than the COLs in other regions of the hemisphere (see Figure 7.1), where the genesis location coincides with the main cyclogenesis region in subtropical South America (GAN; RAO, 1991). Another aspect concerning the Atlantic COLs is the magnitude of the BRC term, which is well above that observed in the strongest COLs. This result suggests that the contribution of the BRC conversion to the EKE growth differs regionally, and is possibly related to the vertical structure of COLs.

Figure 8.12: Temporal evolution of the main EKE terms in the Cut-off Lows formed in southeast Pacific and southwest Atlantic.

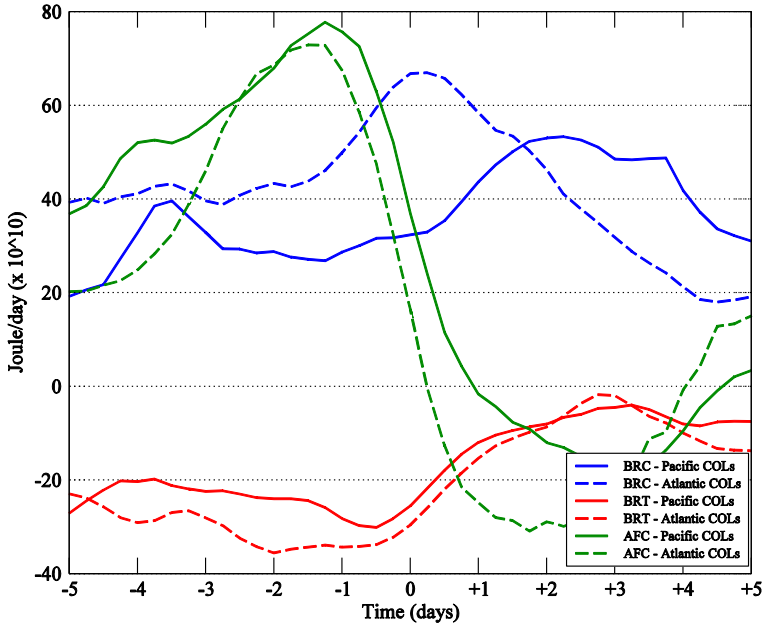


Pacific COLs (region A) in solid line, and Atlantic COLs (region B) in dashed line. The $\xi_{300}$ COLs are selected over a spherical cap (r=10$^{o}$) centered at 34.5$^{o}$S 80.0$^{o}$W (35.0$^{o}$S 57.0$^{o}$W) for region A (region B). Each COL are centered on the time of maximum intensity in the $\xi_{300}$. The terms are BRC (blue line), BRT (red line) and AFC (green line). Fields are vertically averaged within a 15$^{o}$ spherical cap region centered on the COL location. Unit is Joule/day, scaled by $10^{10}$. Analysis performed using the ERAI reanalysis for a 36-yr period (1979-2014).

Source: Author's production.

## 8.5 Discussion and conclusions

The EKE budget for the COLs was assessed by examining the most important mechanisms, such as the DSD and the energy conversions (BRC and BRT). The results confirm previous findings (GAN; PIVA, 2013, 2016) that the evolution of COLs is not dominated by the baroclinic-barotropic conversions, but instead most COLs are governed by the AFC, due to the dispersive nature of the atmospheric waves (CHANG, 2000; PEDLOSKY, 1987). The ageostrophic fluxes act to import EKE from an upstream system in the early stages and export EKE to a downstream system in the late stages, with higher efficiency in the upper troposphere (~200-300 hPa).

In summary, the effect of the AFC within the COLs can be illustrated schematically in Figure 8.13. The direction of the fluxes are represented by orange arrows, while the red (blue) color region represents where the import (export) of energy typically occurs in the COLs. The initial preconditioning mechanism takes place southwest of the COL centre, where the horizontal fluxes converge to nearly the same region to intensify the EKE centre on the west side of the COL. In the northeast sector, strong divergent ageostrophic fluxes act to export the energy eastward, resulting in the growth of the downstream EKE centre and decay of the upstream EKE centre. Immediately downstream of the COL centre, the energy grows due to the strong convergence of the fluxes. Lastly, dispersive fluxes southeast of the COL operate to export the energy out of the system, leading to the COL decay. The configuration described above remains but the magnitude of the AFC varies through the COL lifecycle. Thus, the contribution of the AFC will generally be positive in the growth and negative in the decay of COLs.

Figure 8.13: Two-dimensional schematic representation of the generation of EKE by the upper-level ageostrophic fluxes in an idealized Cut-off Low in the Southern Hemisphere.

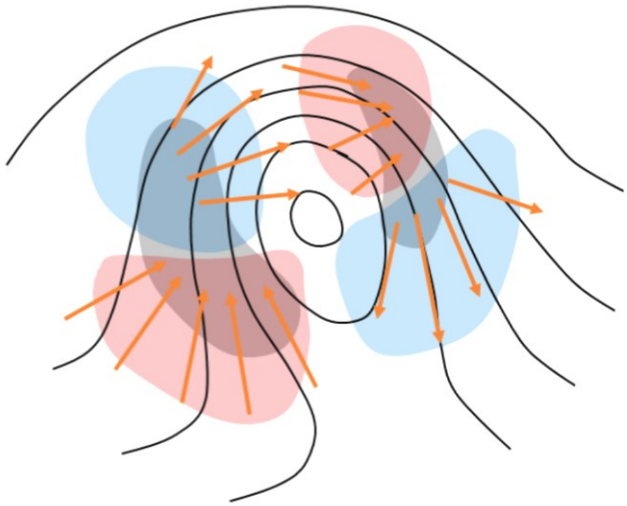

The red (blue) color region represents the import (export) of EKE, the orange arrows represent the direction of ageostrophic fluxes. Solid line is the $Z_{300}$ height.

Source: Author's production.

While the AFC plays the most important role in the EKE growth, the BRC is crucial for the maintenance of the COL. The production of EKE via the BRC occurs due to the descent in the cold sector during the development and the ascent in the warm sector during the decay. A strong interaction between the BRC and AFC was observed, where the area with positive (negative) values of BRC coincides with the area with negative (positive) values of AFC. This means that the energy produced by the BRC is dispersed downstream by the AFC, consistent with the theory of "downstream baroclinic development" proposed by Orlanski and Sheldon (1995). The BRT contributes negatively to the COL development by transferring EKE to the zonal flow. This occurs more frequently in the early stages, whereas dispersive ageostrophic fluxes and frictional effects are conducive for the COL decay in the late stages.

Important insights are gained by examining individual cases that reveal a broad spectrum of possible types of development in which particular aspects are generally masked by the compositing methodology. In general, two different sequential evolutions of the EKE in the COLs are observed (Figure 8.14), which differ only in the

decay stages. The most typical configuration of decaying COLs consists of an eastward tilt and overturning fluxes of EKE (westward propagation), as reproduced by the composite of the strongest COLs. However, some COLs show a synoptic pattern that resembles the upper-level troughs in mid-latitudes, with a more elongated vortex circulation and the dominance of the westward tilt throughout the life cycle. This situation contributes to the downstream development, while the first situation results in an interruption of the wave packet propagation. The technique used in this study shows there is a large case-to-case variability due to the nature of the individual systems. An alternative investigation for such cases could be a vorticity budget due to its nonlinearity, which was found be less case dependent (AZAD; SORTEBERG, 2014).

Figure 8.14: Different stages in the evolution of two typical idealized Cut-off Lows.

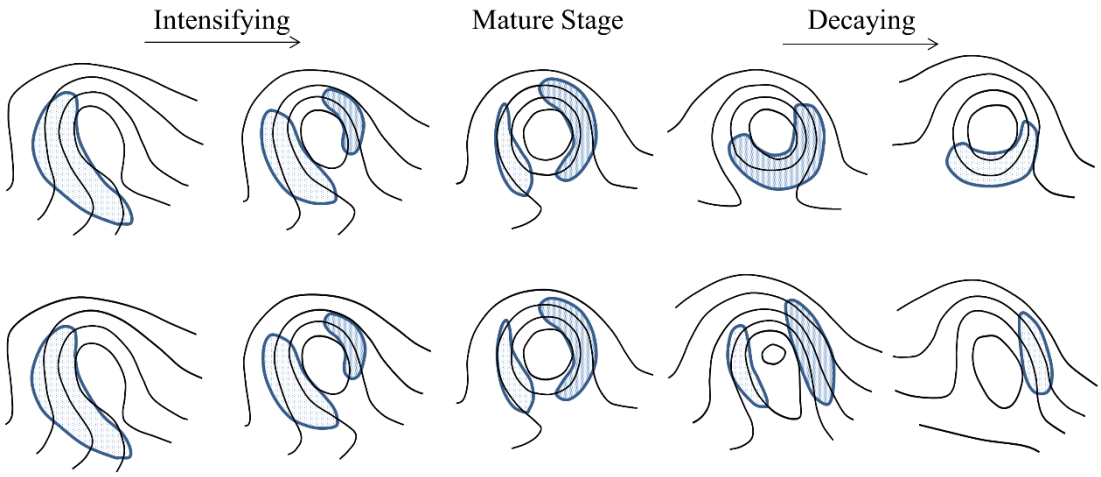


Solid line is the $Z_{300}$ height. Shaded regions are the vertically average EKE, where dark and light represent growing and decaying energy. Interval between the stages is about one day.

Source: Author's production.

An important aspect is the possible interaction between COLs and wavetrains of troughs and ridges. The direct effect of upstream systems on the COL energetics is not assessed here, despite its importance as discussed in many studies (CHANG, 2000; ORLANSKI; SHELDON, 1995). Therefore, it is reasonable to expect that the development of systems in geographically remote regions may impact on the local energetics of a COL.

In the study of Rivière et al. (2015), it was found that vertical ageostrophic fluxes are important for the redistribution of energy downwards, and the further intensification of extratropical winter storms in the NH. These vertical fluxes have been checked in this study and their contribution was found to be very small compared to the other terms considered in the discussion above. The fact that some COLs extend toward the surface it is not well understood, although contributions from the AFC in the development phase and the BRC conversion in the mature stages are possibly the most important factor determining the COL deepening.

There are some issues related to the approach used to compute the EKE budget. One is the unknown contribution from the friction that appears as a large residual in the decay of COLs. The frictional effect is difficult to assess because this is "not computed directly, but is obtained as the residual arising out of any imbalance among the other terms" (FRANK, 1970). An alternative approach to improve the EKE representation could be using numerical models where individual processes can be resolved more accurately. It is possible that other mechanisms that are not included in the formulation may be involved in the production of EKE, such as the diabatic heating, that could contribute to the cold-core dissipation, as suggested by Kousky and Gan (1981). The latent heat released by the convection on the east side of the COLs is an important source of EPE, which can be converted to EKE. Its effect on the COL evolution was found to be important in weakening the cold-core, contributing to the system decay (GARREAUD; FUENZALIDA, 2007; HOSKINS et al., 1985; SAKAMOTO; TAKAHASHI, 2005). However, the system at low levels is intensified as a consequence of the diabatic PV modification (DAVIES; EMANUEL, 1991; REED et al., 1993; STOELINGA, 1996) and the interaction between the upper-level COL and the lower level disturbance, as discussed in Chapters 6 and 7.

One of the key aspects of the EKE budget is that the generation of EKE by diabatic sources is not well reproduced by the models, mostly because of the latent heat release which generates EAPE. Hence, part of the residual is due to uncertainties in the estimates of diabatic heating profiles. In particular, the vertical distribution of diabatic heating within the systems is not fairly represented primarily by the models based on convective parameterization. Models with explicit cloud microphysics tend to simulate

more realistically. Alternatively, there are methods that can be employed to estimate the diabatic contribution, for example, by using the thermodynamic equation (CARON et al., 2007) or a PV framework (STOELINGA, 1996). Therefore, further studies are needed to determine how diabatic forcing modifies the dynamics of COLs and their energetics.

# 9 MAIN CONCLUSIONS AND FUTURE WORK

This thesis has investigated SH COLs and the aspects related to their identification, climatology, structure and energetics. Section 9.1 gives a summary of the main results and conclusions in relation to the scientific questions presented in Chapter 1. Finally, Section 9.2 outlines some suggestions for future studies based on questions or concerns that have been raised from this study.

## 9.1 Summary and conclusions

Over the thirty past years, there have been great efforts to have a better understanding of COLs. In the SH advances have occurred only recently (since 2000) by analysing individual cases, numerical experimentation, energetics, and climatologies with an emphasis on their seasonality, trends and interannual variability. While several climatological aspects of COLs are well known (e.g. location, intensity, lifetime, trajectories), other aspects are still to be understood, for example, why the seasonality and frequency of COLs differ widely between studies, and what implications the different type of identification methods and reanalyses have on the results. Moreover, the structure and development mechanisms of COLs and the regional dependence of these properties are poorly known and limited to few studies focusing on restricted areas. These key topics lead to the formulation of the science questions introduced in Section 1.1 and addressed in this thesis and answered as follows:

- **How sensitive are COLs to identification criteria?**

The idea of considering a unique method to identify COLs and providing consistent results is particularly important, but difficult to realise because of the different criteria often chosen to define the COL features motivated by different conceptual ideas of what a COL is. One of the more subtle points in COL identification is the method by which a COL is defined. Most COLs are analysed using geopotential or vorticity fields with additional criteria introduced to determine the cold core condition, though COLs can also be defined based on a conceptual model in terms of high cyclonic PV (stratospheric tracer) and baroclinic zones. Using methods based on multiple criteria generally implies smaller samples of identified COLs compared to simpler methods. In this study, different methodologies to identify COLs and estimate their vertical depth were

compared. The verification showed that the use of filtering is needed as a post-tracking step in order to separate COLs from other systems. The four-point filter was considered the best compromise for the COL identification since this minimizes issues associated with the increase (decrease) in number of identified troughs (COLs). These methods include four schemes to identify COLs and selected different types of systems, where multi-criteria methods including the use of $PV_{300}$ were found to be a good choice to identify the strongest COLs, whereas the simpler methods (e.g. without cold-core and $PV_{300}$) are less selective and appropriate to detect a large sample of systems.

- **How can COLs be objectively identified in gridded data sets such as reanalyses, and what is the uncertainty between reanalyses?**

A comparison between four modern reanalyses (ERAI, NCEP-CFSR, MERRA-2, and JRA-55) and the older JRA-25 was performed for a 30-year period (1980-2009). Overall, there are obvious improvements in the agreement between the newer reanalysis datasets compared to the older JRA-25. The differences found for the comparison between the newer reanalyses are likely associated with improvements in the forecast models and the use of improved data assimilation methods used in each reanalysis, with ERAI and JRA-55 using 4D-Var, whereas NCEP-CFSR and MERRA-2 use the 3D-Var GSI system. Improvements were observed in different aspects related to location and intensity of COLs. The deficiencies are particularly apparent in the vorticity distributions, because of the dependence on the reanalysis resolution, where NCEP-CFSR and MERRA-2 have the strongest COLs and JRA-25 has the weakest COLs.

- **What is the hemispheric distribution of COLs and what are the main properties, in particular those related to precipitation?**

A twofold perspective of COLs and their spatial distribution is achieved using both $\xi_{300}$ and $Z'_{300}$. The results show that the track density of $Z'_{300}$ is comparable with the track density of $\xi_{300}$ in terms of location and seasonality. However, the track density values for $\xi_{300}$ are substantially larger than for $Z'_{300}$ due to the differences in scale, as discussed in Hoskins and Hodges (2002). The results confirm that the peak activity occurs around the continents (Australia, South America, and Africa) and more minor activity over the oceans, as observed in previous studies (FAVRE et al., 2012;

FUENZALIDA et al., 2005; NDARANA; WAUGH, 2010; REBOITA et al., 2010). However, the maximum occurrences migrate to oceanic areas in summer, mostly due to small-scale $\xi_{300}$ systems. The reason for the maxima in the COL distribution observed over oceans may be associated with diabatic processes over warm continents, which are found to be an important mechanism for the COL decay (GARREAUD; FUENZALIDA, 2007; HOSKINS et al. 1985; KOUKSY; GAN, 1981; SAKAMOTO; TAKAHASHI, 2005).

- **What is the structure of COLs, how does this vary regionally and how is it related to precipitation?**

Different features of conceptual models of COL structure are identified such as baroclinic zones, cold and warm cores, and tropopause folding. The three-dimensional structure of COLs is examined for the 200 strongest systems observed in the SH. Results reveal a symmetrical circulation at upper levels with maximum intensity at 300 hPa. The sharpest horizontal and vertical temperature gradients are found across the edges of the cold core (400-500 hPa), where upper-level fronts propagate downstream throughout the COL life cycle, which agrees well with the conceptual model described by Keyser and Shapiro (1985). The warm core of stratospheric origin contributes to create frontal zones near the tropopause. As a result of the COL formation, large amounts of stratospheric air are transported into the troposphere, modifying the vertical distribution of PV and $O_3$ in the troposphere.

Results showed that precipitation in COLs varies widely throughout their life cycle, reaching a peak about 24 hours after the maximum intensity ($\xi_{300}$). There is a clear association between medium and high cloud cover and precipitation, where maximum values are found east of the COL centre due to the moist uplift at middle levels and the strong divergence at upper levels. The possible link between intensity/moisture and precipitation suggests that moisture is important for controlling the areal coverage of precipitation, whereas the intensity of the COLs, measured by the $\xi_{300}$, affects the magnitude of precipitation. This makes sense in terms of the quasi-geostrophic theory, and the Q-vector relation with the vertical motion. The largest precipitation zones were

found for the summer and autumn COLs, though winter and spring have the strongest COLs.

A new approach was introduced to estimate the vertical depth of COLs. Results indicate that COLs are relatively deep in the western Pacific, Australia and New Zealand, where more than 30% of the total number extend vertically toward the surface. These systems contrast with those observed in southern Africa where only about 15% of them reach the surface. Large differences in vertical structure were also found for COLs occurring in the vicinity of South America. The COLs on the upslope side of the Andes are normally deep in the mid-troposphere, but weaken toward the surface. In contrast, much deeper COLs are found on the lee side of the Andes, possibly as a result of the moisture and heat transport from the Amazon region onto the system. Hence, the upper troposphere disturbance weakens due to the increase in latent heating, but the disturbance at low levels is strengthened with enhanced vertical motion, leading eventually to surface cyclogenesis.

The large variation in the observed structure suggests two distinct types of COLs, which differ in their properties such as intensity, vertical depth of the cyclonic centre, and precipitation. Figure 9.1 shows the differences in characteristics between the two types of COLs. The shallow-COL type (left side) presents a well-defined structure at upper levels, but weakens toward the surface. In contrast, although the strongest COLs (right side) have a similar structure consisting of prevailing uplift motion and precipitation east of the vortex centre, a much deeper structure than the shallow type is seen at all levels, with a structure similar to midlatitude cyclones. As a consequence, the deep-COL type results in larger precipitation amounts compared to the shallow ones. The conceptual model presented here is an attempt to help meteorologists better understand the different structures and rain type associated with COLs, improving the forecast of such events.

Figure 9.1: A three-dimensional schematic view of Shallow and Deep Cut-off Lows.

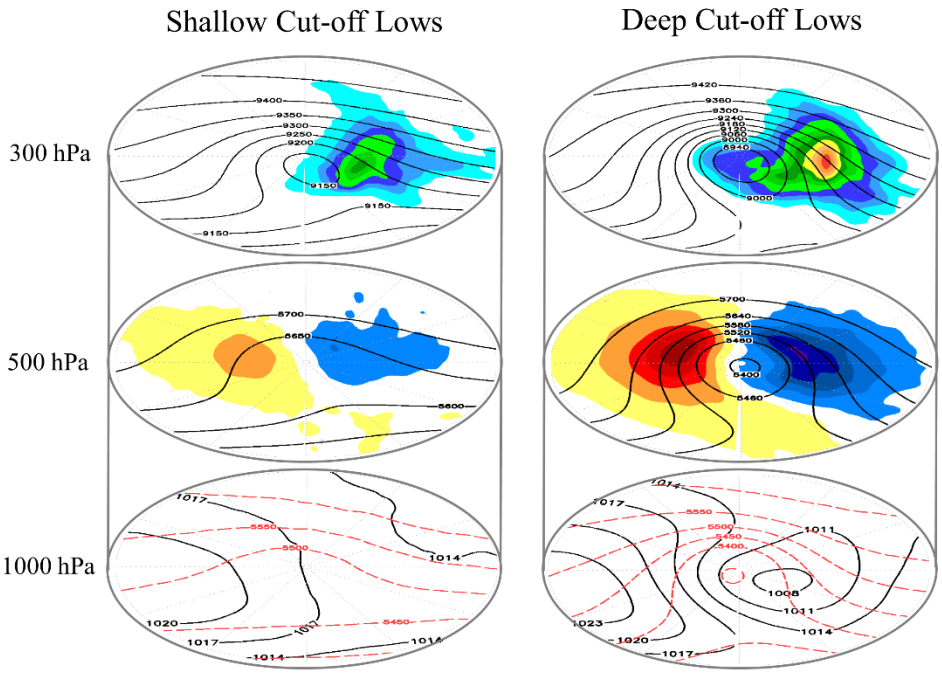


Unit is gpm for geopotential height in black line (top/middle), Pa $s^{-1}$ for 500-hPa vertical velocity in shaded (middle), mm/h for precipitation in shaded (top), mean sea level pressure in black line, and 1000-500 hPa thichness in red dashed line (bottom). Analysis using the ERAI reanalysis for a 36-year period (1979-2014).Source: Author's production.

- **What are the main development mechanisms of COLs and which mechanisms are more important in deepening the COLs?**

The relative contributions of the most important mechanisms for COL development was examined through the main terms of the Eddy Kinetic Energy (EKE) budget. The Ageostrophic Flux Convergence (AFC) was found to be the most important contributor to the COL intensification. This initially acts to import energy from an upstream upper-level system, while strong dispersive fluxes together with frictional effects lead to the COL decay. The EKE growth is enhanced by the baroclinic (BRC) conversion during two distinct phases, first through the descent of cold air on the western side of COLs during the development phase (positive conversion in this sector), and after through the ascent of warm air on the eastern side during the decay phase (positive conversion in this sector). The BRT conversion contributes negatively to the COL development by transferring EKE to the zonal flow kinetic energy. Overall, there are two types of

development which differ only by the decay phase: one type are COLs that have a horizontal tilt eastward and the energy is exported by the ageostrophic fluxes westward along their southern flank, until it disappears through friction and dispersive fluxes; the second type of COLs are those which have a horizontal westward tilt that dominates throughout their lifecycle, and the energy is exported downstream from the decaying COL, which may contribute to the development of another system downstream. Regional analyses indicated that the amplitude of the AFC and BRC terms are more pronounced in the deeper COLs. This is the case for the COLs originating on the lee side of the Andes (namely Atlantic COLs), where local effects seem to induce vertical motion and the system is intensified via BRC conversion.

## 9.2 Future work

The results related to the main scientific questions are documented in the previous section, which represent substantial improvements in the knowledge of the structure of the COLs and description of the main development mechanisms of these systems in the SH. However, several questions are still open to be answered, and some of these are briefly described.

- **What is the structure of NH COLs, and how does this vary regionally?**

In the literature, there are a number of studies of COLs looking at different aspects and using varying identification methodologies, whose criteria differ widely, introducing uncertainties between the studies and their conclusions. An intriguing aspect of the COL identification is the different levels used to detect cold-cores and how this affects the results. Probably the most widely used objective method for COL identification is that of Nieto et al. (2005), in which the cold core search is performed in the layer 200-300 hPa. However, the results of this thesis for the SH indicated that the cold core is better defined at middle levels. This raises the question of whether the different conceptual models are due to the differences in structure between the NH COLs and SH COLs. Thus, further study is needed to investigate the COL structure using a common set of analysis methods and applied to particular regions to see how this is related to precipitation and air pollutants such as ozone.

- **How does the vertical structure of COLs change through the lifecycle?**

Although the analysis of the EKE budget has contributed to understand the mechanisms that control the COL development, the way in which the COL vertical deepening occurs is still not well understood. Further research could investigate this process through the projection of the reanalysis gridded data on vertical modes, similarly to Silva Dias et al. (1985). The vertical mode energy exchange might be a key to understanding the vertical structure changes during the COL lifecycle through the vertical modal decomposition in terms of kinetic energy and available potential energy (KASAHARA; SILVA DIAS, 1986).

- **How well is precipitation associated with COLs represented in the datasets such as reanalyses?**

Perhaps the most important COL-related variable is precipitation, which is extensively studied in this thesis through frequency distributions and spatial and time evolution composites, indicating the magnitude and location of precipitation in COLs. One aspect that could be investigated in future studies is the magnitude and geographical distribution of COL associated precipitation and their percentage contribution to total precipitation, such as has been performed more generally for extratropical cyclones (HAWCROFT et al., 2012, 2017). This analysis could be extended to other recent reanalyses in addition to ERAI, particular those produced with increased resolution and more modern data assimilation methods and forecast models (e.g. ERA-5). The use of remote sensing data such as International Satellite Cloud Climatology Project (ISCCP) (ROSSOW; SCHIFFER, 1991) and CloudSat (STEPHENS et al., 2002) satellite simulators could be an alternative for further studies in order to examine the cloud features and precipitation in COLs.

- **How do large-scale and low-frequency atmospheric modes influence the COLs?**

The SH COLs have been found to be associated with large-scale circulation patterns such as Rossby wave breaking (NDARANA; WAUGH, 2010) and teleconnections patterns such as El Niño - Southern Oscillation (ENSO), Semi-annual Oscillation (SAO), and Southern Annular Mode (SAM) (FAVRE et al., 2012; RISBEY et al., 2009; SINGLETON; REASON, 2007). There are other atmospheric variability modes in the

SH that may affect COLs such as the Pacific South America (PSA), Pacific Decadal Oscillation (PDO), Quasi-Biennal Oscillation (QBO), and Trans-Polar Index (TPI). Understanding the influence of the large-scale environmental factors on COL related properties (e.g. location, intensity and precipitation) is a problem of great scientific importance and crucial for understanding the climate and its variation. Additionally, it is important to assess the ability of numerical weather prediction (NWP) models in representing the simulated response of COL activity to teleconnections as well as the stratosphere/troposphere interaction, which requires a higher vertical resolution in the stratosphere, primarily at the tropopause.

- **How much are COLs affected by moist processes such as latent heat release, and what are the implications for COLs in a warmer climate?**

The representation of diabatic processes is critical for the accuracy of weather and climate models. Since modelling studies have consistently shown that the latent heat release weakens the upper-level disturbances (DAVIS; EMANUEL, 1991; GARREAUD; FUENZALIDA, 2007; STOELINGA, 1996), it is reasonable to consider that a realistic representation of the development mechanisms of COLs will depend on how the diabatic heating and its effects are represented. Therefore, an additional attempt is needed to examine the potential effects of latent heat on the COLs in terms of structure and energetics. This could be done by using high-resolution numerical models with parameterised convection to isolate the diabatic effects on COLs or using even higher resolution models in which the moist-convective processes are treated explicitly, thereby avoiding the issues related to the cumulus parameterisation. One region of possible future investigation is the east side of the Andes, where diabatic processes are enhanced due to the moist warm air associated with the Amazon region.

Another scientific question to be answered is how COLs respond to climate warming, and what implications the latent heating has in particular scenarios. Future climate scenarios indicate that the increase in the temperature may cause a poleward shift of mid-latitude jet streams and a decrease in the cyclonic Rossby wave breaking (BARNES; HARTMANN, 2012; BENGTSSON et al., 2006), although there is no well-established consensus in the literature to explain the last result. At the same time, it is expected that the humidity will increase in a warmer climate (ALLEN; INGRAM, 2002;

HELD; SODEN, 2006), providing more latent energy to drive the storms. It is uncertain how these competing effects will affect COLs and their precipitation in a future climate. Therefore, there exists a considerable void in understanding how current climate models simulate aspects of COLs such as number, generation, intensity, and the way they may change in the future. This has been hampered in the past by the limited availability of high frequency data and sufficient levels in past climate change simulations (e.g. Coupled Model Intercomparison Project 5 - CMIP5), but this may change with CMIP6 (ERYING et al., 2016; KAGEYAMA et al., 2018) and other programs such as European H2020 project PRIMAVERA (HAARSMA et al., 2016).

## REFERENCES


AHMADI-GIVI, F.; GRAIG, G. C.; PLANT, R. S. The dynamics of a midlatitude cyclone with very strong latent-heat release. **Quarterly Journal of the Royal Meteorological Society**, v. 130, p. 295–323, 2004.

ALLEN, M. R.; INGRAM, W. J. Constraints on future changes in climate and the hydrologic cycle. **Nature**, v. 419, n. 6903, p. 224, 2002.

ANCELLET, G.; BEEKMANN, M.; PAPAYIANNIS, A. Impact of a cut-off development on downward transport of ozone in the stratosphere. **Journal of Geophysical Research**, v. 99, p. 3451-3463, 1994.

ANDERSON, D.; HODGES, K. I.; HOSKINS, B. J. Sensitivity of feature-based analysis methods of storm tracks to the form of background field removal. **Monthly Weather Review**, v. 131, n. 3, p. 565–573, 2003.

ANDERSSON, E.; JÄRVINEN, H. Variational quality control. **Quarterly Journal of the Royal Meteorological Society**, v. 125, p. 697–722, 1999.

ANDREWS, D. G.; HOLTON, J. R.; LEOVY, C. B. **Middle atmospheric dynamics**. New York: Academic Press, 1987. 489p.

APOSTOLOV, E. M. Quasi-biennial oscillation in sunspot activity. **Bulletin of the Astronomical Institutes of Czechoslovakia**, v. 36, p. 97-102, 1985.

AZAD, R.; SORTEBERG, A. The vorticity budgets of North Atlantic winter extratropical cyclone life cycles in MERRA reanalysis. Part I: development phase*. **Journal of the Atmospheric Sciences**, v. 71, n. 9, p. 3109–3128, 2014.

BALDWIN, M. P.; DUNKERTON, T. J. Stratospheric harbingers of anomalous weather regimes. **Science**, v. 294, n. 5542, p. 581–584, 2001.

BAMBER, D. J.; HEALEY, P. G.; JONES, B. M.; PENKET, S. A.; TUCK, A. F.; VAUGHAN, G. Vertical profiles of tropospheric gases – chemical consequences of stratospheric intrusions. **Atmospheric Environment**, v. 18, p. 1759-1766, 1984.

BARNES, E. A.; HARTMANN, D. L. Detection of Rossby wave breaking and its response to shifts of the midlatitude jet with climate change. **Journal of Geophysical Research: Atmospheres**, v. 117, n. D9, 2012.

BASSET, H. A.; GAHEIN, A. Diagnostic study on the relation between ozone and potential vorticity. **Revista Atmósfera**, v. 16, n. 2, p. 67-82, 2003.

BJERKNES, J. On the structure of moving cyclones. **Monthly Weather Review**, v. 47, p. 95–99, 1919.

BELL, G. D. E.; BOSART, L. F. A case study diagnosis of the formation of an upper-level cut off cyclonic circulation over the eastern United States. **Monthly Weather Review**, v. 121, n. 6, p. 1635-1655, 1993.

BELL, G. D.; KEYSER, D. Shear and curvature vorticity and potential vorticity interchanges: interpretation and application to a cut-off cyclone event. **Monthly Weather Review**, v. 121, n. 6, p. 76-102, 1993.

BENGTSSON, L.; KANAMITSU, M.; KALLBERG, P.; UPPALA, S. FGGE research activities at ECMWF. **Bulletin of the American Meteorological Society**, v. 63, n. 3, p. 277-303, 1982.

BENGTSSON, L.; HODGES, K. I.; HAGEMANN S. Sensitivity of the ERA40 reanalysis to the observing system: determination of the global atmospheric circulation from reduced observations. **Tellus**, v. 56, p. 456–471, 2004.

BENGTSSON, L.; HODGES, K. I.; ROECKNER, E. Storm tracks and climate change. **Journal of Climate**, v. 19, n. 15, p. 3518–3543, 2006.

BENGTSSON, L.; HODGES, K. I.; ESCH, M.; KEENLYSIDE, N.; KORNBLUEH, L.; LUO, J. J.; YAMAGATA, T. How may tropical cyclones change in a warmer climate? **Tellus, Series A: Dynamic Meteorology and Oceanography**, v. 59 A, n. 4, p. 539–561, 2007.

BENGTSSON, L; HODGES, K. I.; KEENLYSIDE, N. Will extratopical storms intensify in a warmer climate? **Journal of Climate**, v. 22, p. 2276-2301, 2009.

BERRISFORD, P; HOSKINS, B. J.; TYRLIS, E. Blocking and Rossby wave breaking on the dynamical tropopause in the Southern Hemisphere. **Journal of the Atmospheric Sciences**, v. 64, p. 2881–2898, 2007.

BONATTI, J. P. **Alguns aspectos observados e teóricos do aquecimento estratosférico brusco nos Hemisférios Sul e Norte**. 1979. 113 p. (INPE-1671-TDI/016) Dissertação (Mestrado em Meteorologia) - Instituto Nacional de Pesquisas Espaciais (INPE), São José dos Campos, 1979.

BUTLER, A. H.; SJOBERG, J. P.; SEIDEL, D. J.; ROSENLOF, K. H. A sudden stratospheric warming compendium. **Earth System Science Data**, v. 9, p. 63-76, 2017.

BUZZI, A.; TIBALDI, S. Cyclogenesis in the lee of the Alps: a case study. **Quarterly Journal of the Royal Meteorological Society**, v. 104, n. 440, p. 271-287, 1978.

BUZZI, G. D.; TIBALDI, S.; TOSI, E. A unified theory of orographic influences upon cyclogenesis. **Meteorology and Atmospheric Physics**, v. 36, p. 91-107, 1987.

CAMPETELLA, C.; VERA, C. The influence of the Andes Mountains on the South American low-level flow. **Geophysical Research Letters**, v. 29, n. 17, p. 1826, 2002.

CAMPETELLA, C.; POSSIA, N. Upper-level cut-off lows in southern South America. **Meteorology and Atmospheric Physics**, v. 96, n. 1-2, p. 181-191, 2007.

CARLSON, T. N. **Mid-latitude weather systems**. [S.l]: Harper Collins Academic, 1991. 507 p.

CASARIN, D. P.; KOUSKY, V.E. Rainfall anomalies in southern Brazil and related atmospheric circulation features. **Revista Brasileira de Meteorologia**, v. 1, p. 83-90, 1986.

CATTO, J. L.; SHAFFREY, L. C.; HODGES, K. I. Can climate models capture the structure of extratropical cyclones? **Journal of Climate**, v. 23, p. 1621–1635, 2010.

CATTO, J. L. Extratropical cyclone classification and its use. **Reviews of Geosphysics**, v. 54, p. 486–520, 2016.

CHANG, E. K. M. Downstream development of baroclinic waves as inferred from regression analysis. **Journal of the Atmospheric Sciences**, v. 50, n.13, p. 2038-2053, 1993.

CHANG, E. K. M.; ORLANSKI, I. On the dynamics of a storm track. **Journal of the Atmospheric Sciences**, v. 50, n. 7, p. 999-1015, 1993.

CHANG, E. K. M.; ORLANSKI, I. On energy flux and group velocity of waves in baroclinic flows. **Journal of the Atmospheric Sciences**, v. 51, n. 24, p 3823-3828, 1994.

CHANG E. K. M. Wave packets and life cycles of troughs in the upper troposphere: examples from the Southern hemisphere summer season of 1984/85. **Monthly Weather Review**, v. 128, p. 25–50, 2000.

CHARNEY, J. G. The dynamics of long waves in a baroclinic westerly current. **Journal of Meteorology**, v. 4, n. 5, p. 136–162, 1947.

CHARLTON, A. J.; O'NEILL, A.; LAHOZ, W. A.; MASSACAND, A. C.; BERRISFORD, P. The impact of the stratosphere on the troposphere during the southern hemisphere stratospheric sudden warming, September 2002. **Quarterly Journal of the Royal Meteorological Society**, v. 131, n. 609, p. 2171–2188, 2005.

CLARKE, L. C.; RENARD, R. J. The U.S. Navy numerical frontal analysis scheme: further development and a limited evaluation. **Journal of Applied Meteorology**, v. 5, p. 764–777, 1966.

COLTON, D. E. Barotropic scale interactions in the tropical upper troposphere during the northern summer. **Journal of the Atmospheric Sciences**, v. 30, p. 1287–1302, 1973.

COMPO, G. P. et al. The Twentieth Century reanalysis project. **Quarterly Journal of the Royal Meteorological Society**, v. 137, n. 654, p. 1-28, 2011.

COSTA, S. B. **Balanço de vorticidade e energia aplicados aos vórtices ciclônicos de altos níveis atuantes no Oceano Atlântico Tropical Sul e adjacências**. 2009. 85 p. Dissertação (Mestrado em Meteorologia) - Instituto Nacional de Astronomia, Geofísica

e Ciências Atmosféricas (IAG), Universidade de São Paulo, São Paulo, 2009.

COUTINHO, M. D. L. **Método objetivo de identificação dos vórtices ciclônicos de altos níveis na região Tropical Sul**: validação e climatologia. 2008. 119 p. (INPE-15460 - TDI/1422). Dissertação (Mestrado em Meteorologia) - Instituto Nacional de Pesquisas Espaciais (INPE), São José dos Campos, 2008.

COUTINHO, M. D. L.; GAN, M. A.; RAO, V. B. Método objetivo de identificação dos vórtices ciclônicos de altos níveis na região Tropical Sul: validação. **Revista Brasileira de Meteorologia**, v. 25, p. 311–323, 2010.

DACRE, H. F.; HAWCROFT, M. K.; STRINGER, M. A.; HODGES, K. I. An extratropical cyclone atlas: a tool for illustrating cyclone structure and evolution characteristics. **Bulletin of the American Meteorological Society**, v. 93, p. 1497–1502, 2012.

DANIELSON, R. E.; GYAKUM, J. R.; STRAUB, D. Examples of downstream baroclinic development among 41 cold-season eastern North Pacific cyclones. **Atmosphere-Ocean**, v. 42, n. 4, p. 235-250, 2004.

DANIELSON, R. E.; GYAKUM, J. R.; STRAUB, D. N. A case study of downstream baroclinic development over the North Pacific Ocean. Part II: diagnoses of eddy energy and wave activity. **Monthly Weather Review**, v. 134, n. 5, p. 1549–1567, 2006.

DAVIS, C. A.; EMANUEL, K. A. Potential vorticity diagnostics of cyclogenesis. **Monthly Weather Review**, v. 119, n. 8, p. 1929-1953, 1991.

DAVIES, C. A.; STOELINGA, M. T.; KUO, Y. The integrated effect of condensation in numerical simulations of extratropical dyclogenesis. **Monthly Weather Review**, v. 121, p. 2309–2330, 1993.

DECKER, S. G.; MARTIN, J. E. A local energetics analysis of the life cycle differences between consecutive, explosively deepening, continental cyclones. **Monthly Weather Review**, v. 133, n. 1, p. 295–316, 2005.

DEE, D. P. et al. The ERAI reanalysis: configuration and performance of the data assimilation system. **Quarterly Journal of the Royal Meteorological Society**, v. 137, n. 656, p. 553–597, 2011.

DELGADO, G.; REDAÑO, G.; LORENTE, J.; NIETO, R.; GIMENO, L.; RIBERA, P.; BARRIOPEDRO, D.; GARCÍA-HERRERAS, R.; SERRANO, A. Cloud cover analysis associated to cut-off low pressure systems over Europe using Meteosat imagery. **Meteorology and Atmospheric Physics**, v. 96, p. 141–157, 2007.

DEVESON, A. C. L.; BROWNING, K. A.; HEWSON, T. D. A classification of FASTEX cyclones using a height-attributable quasi-geostrophic vertical-motion diagnostic. **Quarterly Journal of the Royal Meteorological Society**, v. 128, n. 579, p. 93–117, 2002.

EADY, E. T. Long waves and cyclone waves. **Tellus**, v. 1, n. 3, p. 33–52, 1949.

EBEL, A.; HASS, H.; JAKOBS, H. J. et al. Simulation of ozone intrusion caused by tropopause fold and COL. **Atmospheric Environment Part A. General Topics**, v. 25, n. 10, p. 2131–2144, 1991.

EMANUEL, K. A. Genesis and maintenance of "Mediterranean hurricanes". **Advances in Geosciences**, v. 2, p. 217–220, 2005.

ERICKSON, C. O. Diagnostic study of a tropical disturbance. **Monthly Weather Review**, v. 99, n. 1, p. 67-79, 1971.

EVANS, M. S. et al. A satellite-derived classification scheme for rapid maritime cyclogenesis. **Monthly Weather Review**, v. 122, n. 7, p. 1381-1416, 1994.

EYRING, V. et al. Overview of the Coupled Model Intercomparison Project Phase 6 (CMIP6) experimental design and organization. **Geoscientific Model Development**, v. 9, p. 1937-1958, 2016.

FAVRE, A.; HEWITSON, B.; TADROSS, M.; LENNARD, C.; CEREZO-MOTA, R. Relationships between cut-off lows and the semiannual and southern oscillations. **Climate Dynamics**, v. 38, p. 1473–1487, 2011.

FAVRE, A.; HEWITSON, B.; LENNARD, C.; CEREZO-MOTA, R.; TADROSS, M. Cut-off lows in the South Africa region and their contribution to precipitation. **Climate dynamics**, v. 41 n. 9-10, p. 2331-2351, 2013.

FEDOROVA, N.; CARVALHO, M. H.; FEDOROV, D. Formação de vórtices observados no campo de nebulosidade sobre a América do Sul. **Revista Brasileira de Meteorologia**, v. 14, n. 2, p. 15-27, 1999.

FIELD, P. R.; WOOD, R. Precipitation and cloud structure in midlatitude cyclones. **Journal of Climate**, v. 20, n. 2, p. 233–254, 2007.

FIGUEROA, S. N. **Estudo dos sistemas de circulação de verão sobre a América do Sul e suas simulações com modelos numéricos**. 1997. 181 p. (INPE-7121-TDI/672). Tese (Doutorado em Meteorologia) - Instituto Nacional de Pesquisas Espaciais (INPE), São Jose dos Campos, 1997.

FRANK, N. L. **The weather distribution with upper tropospheric cold lows in the tropics**. United States: Weather Bureau, 1966.

FRANK, N. L. On the energetics of cold lows. In: SYMPOSIUM ON TROPICAL METEOROLOGY, 1970. **Proceedings…** American Meteorological Society, 1970. p.EIV 1 – EIV 6.

FUENZALIDA, H.; SÁNCHEZ, R.; GARREAUD, R. A climatology of cutoff lows in the Southern Hemisphere. **Journal of Geophysical Research**, v. 110, p. 1-10, 2005.

GAN, M. A. **Um estudo observacional sobre as baixas frias da alta troposfera, nas latitudes subtropicais do Atlântico sul e leste do Brasil**. 1982. 80p. (INPE-2685-

TDL/126). Dissertação (Mestrado em Meteorologia) - Instituto Nacional de Pesquisas Espaciais (INPE), São José dos Campos, 1982.

GAN, M. A.; RAO, V. B. Surface cyclogenesis over South America. **Monthly Weather Review**, v. 119, p. 1293–1302, 1991.

GAN, M. A. **Ciclogêneses e ciclones sobre a América do Sul**. 1992. (INPE-5400-TDI/479). Teste (Doutorado em Meteorologia) - Instituto Nacional de Pesquisas Espaciais (INPE), São José dos Campos, 1992.

GAN, M. A.; RAO, V. B. The influence of the Andes Cordillera on transient disturbances. **Monthly Weather Review**, v. 122, n.6, p. 1141-1157, 1994.

GAN, M. A.; DAL PIVA, E. Energetics of a Southeastern Pacific cut-off low. **Atmospheric Science Letters**, v. 14, p. 272–280, 2013.

GAN, M. A.; DAL PIVA, E. Energetics of southeastern Pacific cut-off lows. **Climate Dynamics**, v. 46, n. 11–12, p. 3453–3462, 2016.

GARCÍA, F.; FONT, R.; RIVERA, A. **Situación atmosférica causante de las lluvias torrenciales durante los días 19 al 21 de Octubre de 1982 en el Levante Español**. Madrid, Espanha: Instituto Nacional de Meteorologia, 1982.

GARCÍA-HERRERA, R.; PUYOL, D. G.; MARTÍN, E. H.; PRESA, L. G.; RODRÍGUEZ, P. R. Influence of the North Atlantic oscillation on the Canary Islands precipitation. **Journal of Climate**, v. 14, p. 889–3903, 2001.

GARREAUD, R. D.; FUENZALIDA, H. A. The influence of the Andes on cutoff lows: a modeling study. **Monthly Weather Review**, v. 135, p. 1596-1613, 2007.

GELEYN, J. F.; HOLLINGSWORTH, A. An economical analytical method for the computation of the interaction between scattering and line absorption of radiation. **Beitraege zur Physik der Atmosphaere**, v. 52, p. 1-16, 1979.

GODOY, A. A. et al. A cut-off low in southern South America: dynamic and thermodynamic processes. **Revista Brasileira de Meteorologia**, v. 26, n. 4, p. 503–514, 2011.

GRAF, M. A.; WERNLI, H.; SPRENGER, M. Objective classification of extratropical cyclogenesis. **Quarterly Journal of the Royal Meteorological Society**, v. 143, n. 703, p. 1047–1061, 2017.

GRIFFITHS, M.; REEDER, M. J.; LOW, D. J.; VINCENT, R. A. Observation of a cut-off Low over southern Australia. **Quaterly Journal of the Royal Meteorological Society**, v. 124, p. 1109-1132, 1998.

GRIFFIES, S. M.; HARRISON, M. J.; PACANOWSKI, R. C.; ROSATI, A. Technical guide to MOM4. **GFDL Ocean Group Technical Report**, n. 5, p. 337, 2004. Available from <https://www.gfdl.noaa.gov/~fms> Accessed on 02 August 2018.

HAARSMA, R. J. et al. High resolution model intercomparison project (HighResMIP v1. 0) for CMIP6. **Geoscientific Model Development**, v. 9, n. 1, p. 4185-4208, 2016.

HART, R. E. A Cyclone phase space derived from thermal wind and thermal asymmetry. **Monthly Weather Review**, v. 131, p. 585–616, 2003.

GUIA, C. V. F. **Análises das características sinóticas das trajetórias dos ciclones extratropicais que atuam na América do Sul e vizinhança**s. (INPE-11.26.17.17-TDI). 2010. p. 98. Dissertação (Mestrado em Meteorologia) - Instituto Nacional de Pesquisas Espaciais (INPE), São José dos Campos, 2010.

HAWCROFT, M. K.; SHAFFREY, L. C.; HODGES, K. I.; DACRE, H. F. How much Northern Hemisphere precipitation is associated with extratropical cyclones? **Geophysical Research Letters**, v. 39, n. 24, p. 1–7, 2012.

HAWCROFT, M.; DACRE, H.; FORBES, R.; HODGES, K.; SHAFFREY, L.; STEIN, T. Using satellite and reanalysis data to evaluate the representation of latent heating in extratropical cyclones in a climate model. **Climate Dynamics**, v. 48, n. 7–8, p. 2255–2278, 2017.

HAYASHI, Yoshikazu. A theory of large-scale equatorial waves generated by condensation heat and accelerating. **Journal of the Meteorological Society of Japan. Ser. II**, v. 48, n. 2, p. 140-160, 1970.

HAYES, J. L.; WILLIAMS, R. T.; RENNICK, M. A. Lee cyclogenesis. Part I. analytic studies. **Journal of the Atmospheric Sciences**, v. 44, n. 2, p. 432-442. 1987.

HAYES, J. L.; WILLIAMS, R. T.; RENNICK, M. A. Lee Cyclogenesis. Part II: numerical Studies. **Journal of the Atmospheric Sciences**, v. 50, p. 2354–2368, 1993.

HELD, I. M.; SODEN, B. J. Robust responses of the hydrological cycle to global warming. **Journal of Climate**, v. 19, n. 21, p. 5686-5699, 2006.

HIRSCHBERG, P. A.; FRITSCH, J. M. Tropopause undulations and the development of extratropical cyclones. Part I: overview and observations from a cyclone event. **Monthly Weather Review**, v. 119, n. 2, p. 496-517, 1991.

HODGES, K. I. A general Method for tracking analysis and its application to meteorological data. **American Meteorological Society**, v. 122, p. 2573-2585, 1994.

HODGES, K. I. Feature tracking on the unit sphere, **Monthly Weather Review**, v.123, p. 3458–3465, 1995.

HODGES, K. I. Spherical nonparametric estimators applied to the UGAMP model integration for AMIP. **Monthly Weather Review**, v. 124, p. 2914–2932, 1996.

HODGES, K. I. Adaptive constraints for feature tracking. **Monthly Weather Review**, v. 127, p. 1362-1373, 1999.

HODGES, K. I.; BOYLE, J.; HOSKINS, B. J.; THORNCROFT C. A comparison of recent reanalysis datasets using objective feature tracking: storm tracks and tropical easterly waves. **Monthly Weather Review**, v. 131, p. 2012-2037, 2003.

HODGES, K. I. Confidence intervals and significance tests for spherical data derived from feature tracking. **Monthly Weather Review**, v. 136, n. 5, p. 1758–1776, 2008.

HODGES, K. I.; LEE, R. W.; BENGTSSON, L. A comparison of extratropical cyclones in recent reanalyses ERAI, NASA MERRA, NCEP CFSR, and JRA-25. **Journal of Climate**, v. 24, n. 18, p. 4888–4906, 2011.

HODGES, K.; COBB, A.; VIDALE, P. L.; HODGES, K.; COBB, A.; VIDALE, P. L. How well are tropical cyclones represented in reanalysis datasets? **Journal of Climate**, v. 30, n. 14, p. 5243–5264, 2017.

HOLTON, J. R. **An introduction to dinamic meteorology**. 4.ed. Walthan: Academic Press, 1992.

HOSKINS, B. J. Atmospheric frontogenesis models: some solutions. **Quaterly Journal of the Royal Meteorological Society**, v. 97, p. 139-153, 1971.

HOSKINS, B. J.; SARDESHMUKH, P. D. Spectral smoothing on the sphere. **Monthly Weather Review**, v. 112, p. 2524–2529, 1984.

HOSKINS, B. J.; McINTYRE, M. E.; ROBERTSON, A. W. On the use and significance of isentropic potential vorticity maps. **Quaterly Journal of the Royal Meteorological Society**, v. 111, p. 877-946, 1985.

HOSKINS, J. B.; HODGES, K. I. New perspectives on the Northern Hemisphere winter storm tracks. **Journal of Atmospheric Science**, v. 59, p. 1041–1061, 2002.

HOSKINS, J. B.; HODGES, K. I. A new perspective on the Northern Hemisphere winter storms tracks. **Journal of Climate**, v. 18, p. 4108-4129, 2005.

HSIEH, Y. An investigation of a selected cold vortex over North America. **Journal of Meteorology**, v. 6, p. 401–410, 1949.

HUSAIN, L.; COFFEY, P.; MEYERS, R.; CEDERWALL, R. Ozone transport from stratosphere to troposphere. **Geophysical Research Letters**, v. 4, p. 363-365, 1977.

INNESS, A. et al. The MACC reanalysis: an 8 yr data set of atmospheric composition. **Atmospheric Chemistry and Physics**, v. 13, n. 8, p. 4073-4109, 2013.

INTERGOVERNMENTAL PANEL ON CLIMATE CHANGE - IPCC. **Climate change 2007**: the physical science basis. Cambridge: Cambridge University Press, 2007.

IWABE, C. N.; ROCHA, R. P. An event of stratospheric air intrusion and its associated secondary surface cyclogenesis over the South Atlantic Ocean. **Journal of Geophysical Research**, v. 114, p. D09101, 2009.

KAGEYAMA, M. et al. The PMIP4 contribution to CMIP6–Part 1: overview and over-arching analysis plan. **Geoscientific Model Development**, v. 11, n. 1, p. 1033-1057, 2018.

KALNAY, E. et al. The NCEP/NCAR 40-year reanalysis project. **Bulletin of the American Meteorological Society**, v. 77, n. 3, p. 437-471, 1996.

KANAMITSU, M. et al. NCEP-DOE AMIP-II reanalysis (R-2). **Bulletin of the American Meteorological Society**, v. 83, n. 11, p. 1631–1643, 2002.

KASAHARA, A.; DIAS, P. L. S. Response of planetary waves to stationary tropical heating in a global atmosphere with meridional and vertical shears. **Journal of the Atmospheric Sciences**, v. 43, p. 1893-1911, 1986.

KATZFEY, J. J.; MCINNES, K. L. GCM simulations of eastern Australian cutoff lows. **Journal of Climate**, v. 9, p. 2337–2355, 1996.

KÄLBERG, P. **Forecast drift in ERAI**. Reading: ECMWF, 2011.

KELLEY, W. E.; MOCK, D. R. A diagnostic study of upper tropospheric cold lows over the western North Pacific. **Monthly Weather Review**, v. 110, n. 6, p. 471-480, 1982.

KENTARCHOS, A. S.; DAVIS, T. D. A climatology of cut-off lows at 200 hPa in the Northern Hemisphere, 1990–1994. **International Journal of Climatology**. v. 18, p. 379–390, 1998.

KENTARCHOS, A. S.; ROELOFS, G. J.; LELIEVELD, J. Model study of a stratospheric intrusion event at lower midlatitudes associated with the development of a cutoff low. **Journal of Geophysical Research Atmospheres**, v. 104, n. D1, p. 1717–1727, 1999a.

KENTARCHOS, A. S.; ROELOFS, G. J.; LELIEVELD, J.; CUEVAS, E. On the origin of elevated surface ozone concentrations at Izana Observatory during the last days of March 1996: a model study. **Geophysical Research Letters**, v. 27, p. 3699-3702, 1999b.

KEYSER, D.; SHAPIRO, M. A. A review of the structure and dynamics of upper-level frontal zones. **Monthly Weather Review**, v. 114, p. 452-499, 1986.

KLEIST, D. T. et al. Introduction of the GSI into the NCEP global data assimilation system. **Weather and Forecasting**, v. 24, n. 6, p. 1691–1705, 2009.

KNIPPERTZ, P.; MARTIN, J. E. Tropical plumes and extreme precipitation in subtropical and tropical West Africa. **Quarterly Journal of the Royal Meteorological Society**, v. 131, p. 2337–2365, 2005.

KNIPPERTZ, P.; MARTIN, J. E. The role of dynamics and diabatic processes in the generation of cut-off lows over Northwest Africa. **Meteorology and Atmospheric Physics**, v. 96, p. 3-19, 2007.

KNOWLAND, K. E.; DOHERTY, R. M.; HODGES, K. I. The effects of springtime mid-latitude storms on trace gas composition determined from the MACC reanalysis. **Atmospheric Chemistry and Physics**, v. 15, p. 3605–3628, 2015.

KOBAYASHI, S. et al. The JRA-55 reanalysis: general specifications and basic characteristics. **Journal of the Meteorological Society of Japan Serie II**, v. 93, n. 1, p. 5–48, 2015.

KOUSKY, V. E.; GAN, M. L. Upper tropospheric cyclonic vortices in the subtropical South Atlantic. **Tellus**, v. 33, p. 538-551, 1981.

KRUGER, K., NAUJOKAT, B.; LABITZKE, K. The unusual midwinter warming in the Southern Hemisphere stratosphere 2002. **Journal of the Atmospheric Sciences**, v. 62, p. 603–613, 2005.

KUNZ, A.; KONOPKA, P.; MULLER, R.; PAN, L. L. Dynamical tropopause based on isentropic potential vorticity gradients. **Journal of Geophysical Research: Atmospheres**, v. 116, D01110, 2011.

KUO, H. L. Dynamic instability of two-dimensional non-divergent flow in a baroclinic atmosphere. **Journal of Meteorology**, v.6, p. 105-122, 1949.

KUO, Y.; LOW-NAM, S.; REED, R. J. Effects of surface energy fluxes during the early development and rapid intensification stages of seven explosive cyclones in the Western Atlantic. **Monthly Weather Review**, v. 119, p. 457–476, 1991.

LAMB, V. R. **The response of the tropical atmosphere to middle latitude forcing**. PhD thesis, University of California, Los Angeles, p. 155, 1973.

LANGFORD, A. O. et al. Stratospheric influence on surface ozone in the Los Angeles area during late spring and early summer of 2010. **Journal of Geophysical Research: Atmospheres**, v. 117, p. D00V06, 2012.

LAWRENCE, H.; DAINGERFIELD, H. Kona storms. **Monthly Weather Review**, v. 49, n. 6, 1921.

LEJEÑAS, H. Characteristics of Southern Hemisphere blocking as determined from a long time series of observational data. **Quarterly Journal of the Royal Meteorological Society**, v. 110, p. 967-979, 1984.

LEVY II, H. L.; MAHLMAN, J. D.; MOXIM, W. J. Tropospheric ozone: the role of transport. **Journal of Geophysical Research**, v. 90, n. D2, p. 3753–3772, 1985.

LIMPASUVAN, V.; THOMPSON, D. W. J.; HARTMANN, D. L. The life cycle of the Northern Hemisphere sudden stratospheric warmings. **Journal of Climate**, v. 17, n. 13, p. 2584–2596, 2004.

LIVEZEY, R. E.; CHEN, W. Y. Statistical field significance and its determination by Monte Carlo techniques. **Monthly Weather Review**, v. 111, p. 46-59, 1983.

LLASAT, M. C.; MARTÍN, F.; BARRERA, A. From the concept of "Kaltlufttropfen" (cold air pool) to the cut-off low. The case of September 1971 in Spain as an example of their role in heavy rainfalls. **Meteorology and Atmospheric Physics**, v. 96, p. 43-60, 2007.

LOURENÇO, M. C. M. **Vórtices ciclônicos em altos níveis que atuam no sul da América do Sul**. 1996. 77 p. (INPE-10462-TDI/929). Dissertação (Mestrado em Meteorologia) - Instituto Nacional de Pesquisas Espaciais (INPE), São José dos Campos, 1996.

MAGAÑA, V.; YANAI, M. Mixed Rossby-gravity waves triggered by lateral forcing. **Journal of the atmospheric sciences**, v. 52, n. 9, p. 1473-1486, 1995.

MAK, M. K. Laterally driven stochastic motions in the tropics. **Journal of the Atmospheric Sciences**, v. 26, n. 1, p. 41-64, 1969.

MARQUES, R. F. C. **Bloqueio atmosférico no Hemisfério Sul**. 1996. 158 p. (INPE-6742-TDI/632). Tese (Doutorado em Meteorologia) - Instituto Nacional de Pesquisas Espaciais (INPE), São José dos Campos, 1996.

MARQUES, R. F. C.; RAO, V. B. A Diagnosis of a long-lasting blocking event over the Southeast Pacific Ocean. **Monthly Weather Review**, v. 127, p. 1761–1776, 1999.

MARQUES, R. F. C.; RAO, V. B. Interannual variations of blockings in the Southern Hemisphere. **Journal of Computational Physics**, v. 105, n. D4, p. 4625–4636, 2000.

MARTÍN, F**. Las gotas frías/DANAs**: ideas y conceptos básicos. Madrid: INM, 2003. (Nota Técnica S.T.A.P, 38).

MARTÍNEZ-ALVARADO, O.; PLANT, R. S. Parametrized diabatic processes in numerical simulations of an extratropical cyclone. **Quarterly Journal of the Royal Meteorological Society**, v. 140, n. 682, p. 1742–1755, 2014.

MCTAGGART-COWAN, R.; BOSART, L. F. ; DAVIS, C. A.; ATALLAH, E. H.; GYAKUM, J R.; EMANUEL, K. A. Analysis of hurricane Catarina (2004). **Monthly Weather Review**, v. 134, p. 3029–3053, 2006.

MCINNES, K. L.; HUBBERT, G. D. The impact of eastern Australian cut-off lows on coastal sea levels. **Meteorological Applications**, v. 8, n. 2, p. 229-244, 2001.

MCINTYRE M. E.; PALMER, T. N. Breaking planetary waves in the stratosphere. **Nature**, v. 305, p. 593–600, 1983.

MCINTYRE M. E.; PALMER, T. N. A Note on the general concept of wave breaking for rossby and gravity waves. **Pure and Applied Geophysics**, v. 123, n. 6, p. 964-975, 1985.

MENDES, D. et al. Climatology of extratropical cyclones over the South American-southern oceans sector. **Theoretical and Applied Climatology**, v. 100, n. 3, p. 239–250, 2010.

MENDES, M. C. D.; CAVALCANTI, I. F. A.; HERDIES, D. L. Southern Hemisphere atmospheric blocking diagnostic by ECMWF and NCEP/NCAR data. **Revista Brasileira de Meteorologia**, v. 27, n. 3, p. 263–271, 2012.

MICHAELIDES, S. C. Limited area energetics of genoa cyclogenesis. **Monthly Weather Review**, v. 115, n. 1, p. 13-26, 1987.

MIKY FUNATSU, B.; GAN, M. A.; CAETANO, E. A case study of orographic cyclogenesis over South America. **Revista Atmosfera**, v. 17, n. 2, p. 91-113, 2004.

MIRÓ-GRANADA; GELABERT, J. Una implicación jurídica de una predicción meteorológica sobre lluvias catastróficas. **Revista del Aficionado a la Meteorología**, v. 8, 2003. Available from <http://www.meteored.com/ram/numero8/implicacionjuridica.asp>. Accesses in: 31 July 2018.

MISHRA, S. K.; RAO, V. B.; GAN, M. A. Structure and evolution of the large-scale flow and an embedded upper-tropospheric cyclonic vortex over northeast Brazil. **Monthly Weather Review**, v. 129, n. 7, p. 1673–1688, 2001.

MOLOD, A. Constraints on the profiles of total water PDF in AGCMs from AIRS and a high-resolution mode. **Journal of Climate**, v. 25, n. 23, p. 8341–8352, 2012.

MOLOD, A.; TAKACS, L.; SUAREZ, M.; BACMEISTER, J. Development of the GEOS-5 atmospheric general circulation model: evolution from MERRA to MERRA2. **Geoscientific Model Development**, v. 8, n. 5, p. 1339–1356, 2015.

MORAIS, M. D. C. **Vórtices ciclônicos de altos níveis que atuam no bordeste do Brasil:** estudo observacional e numérico. 2018. 231 p. (INPE-01.25.15.04-TDI). Tese (Doutorado em Meteorologia) - Instituto Nacional de Pesquisas Espaciais (INPE), São José dos Campos, 2016.

MUENCH, H. S. On the dynamics of the wintertime stratosphere circulation. **Journal of the Atmospheric Sciences**, v. 22, n. 4, p. 349-360, 1965.

NASCIMENTO, E. L.; AMBRIZZI, T. The influence of atmospheric blocking on the rossby wave propagation in Southern Hemisphere winter flows. **Journal of the Meteorological Society of Japan**, v. 80, n. 2, p. 139–159, 2002,

NDARANA, T.; WAUGH, D. W. The link between cut-off lows and Rossby wave breaking in the Southern Hemisphere. **Quarterly Journal of the Royal Meteorological Society**, v. 136, n. 649, p. 869–885, 2010.

NENG, S.; JUN-QIANG, G.; YAN-MING, Y.; ZHEN-MIN, L. An improved south Asian summer monsoon index with Monte Carlo test. **Chinese Physics**, v. 14, n. 4, p. 844–849, 2005.

NEWMAN, P. A.; NASH, E. R. The unusual Southern Hemisphere stratospheric winter of 2002. **Journal of the Atmospheric Science**, v. 62, p. 614–628, 2005.

NICHOLSON, S. E. Rainfall and atmospheric circulation during drought periods and wetter years in West Africa. **Monthly Weather Review**, v. 109, p. 2191–2208, 1981.

NICHOLSON, S. E. The nature of rainfall variability over Africa on time scales of decades to millenia. **Global and Planetary Change**, v. 26, n. 1–3, p. 137–158, 2000.

NIETO, R.; GIMENO. L.; TORRE, L. D. L.; RIBERA, P.; GALLEGO, D.; GARCIA-

HERRERA, R., GARCIA, J. A.; NUNEG, M.; REDAUO, A.; LORENTE, J. Climatological features of cutoff low systems in the Northern Hemisphere. **Journal of Climate**, v.18, n. 16, p. 3085–3103, 2005

NIETO, R.; GIMENO, L.; DE LA TORRE, L.; RIBERA, P.; BARRIOPEDRO, D.; HERRERA, R. G.; SERRANO, A.; GORDILHO, A.; REDANO, A.; LORENTE, J. Interanual variability of cut-off low systems over the European sector: the role of blocking and the Northern Hemisphere circulation modes. **Meteorology Atmospheric Physics**, v. 96, n. 1-2, p. 85-101, 2007a.

NIETO, R.; GIMENO, L.; AÑEL, J. A.; DE LA TORRE, L.; GALLEGO, D., BARRIOPEDRO, D.; GALLEGO, M.; GORDILLO, A.; REDAÑO, A.; DELGADO, G. Analysis of the precipitation and cloudiness associated with COLs occurrence in the Iberian Peninsula. **Meteorology and Atmospheric Physics**, v. 96, n. 1-2, p.103-119, 2007b.

NIETO, R.; SPRENGER, M.; WERNLI, H.; TRIGO, R. M.; GIMENO, L. Identification and climatology of cut-off low near the tropopause. **Annals of the New York Academy of Sciences**, v. 1146, n. 1, p. 256-290, 2008.

NOGUÉS-PAEGLE, J.; MO, K. C. Alternating wet and dry conditions over South America during summer. **Monthly Weather Review**, v. 125, p. 279–291, 1997.

ONOGI, K. et al. The JRA-25 reanalysis. **Journal of the Meteorological Society of Japan Serie II**, v. 85, n. 3, p. 369–432, 2007.

OORT, A. H.; PEIXOTO, J. P. Global angular momentum and energy balance requirements from observations. **Advances in Geophysics,** v. 25, p. 355–490, 1983.

ORLANSKI, I.; KATZFEY. J. The life cycle of a cyclone wave in the Southern Hemisphere: eddy energy budget. **Journal of the Atmospheric Sciences**, v. 48, p. 1972–1998, 1991.

ORLANSKI, I.; SHELDON, J. A. Case of downstream baroclinic development over Western North America. **Monthly Weather Review**, v. 121, p. 2929- 2950, 1993.

ORLANSKI, I.; SHELDON, J. P. Stages in the energetics of baroclinic systems. **Tellus**, v. 47a, p. 605–628, 1995.

ORSOLINI, Y.; RANDALL, C. An observational study of the final breakdown of the Southern Hemisphere stratospheric vortex in 2002. **Journal of the Atmospheric Sciences**, v. 62, p. 735–747, 2005.

PAIXÃO, E. B. **Caracterização do vórtice ciclônico de ar superior no Nordeste do Brasil**. 1999. 103p. Dissertação (Mestrado em Meteorologia) – Instituto Astronômico e Geofísico, Universidade de São Paulo, São Paulo, 1999.

PALMÉN, E. Origin and structure of high-level cyclones south of the maximum westerlies. **Tellus**, v. 1, p. 22-31, 1949.

PALMÉN, E.; NEWTON, C. W. **Atmospheric circulation systems**: their structure and physical interpretation. New York:Academic Press, 1969.

PALMER, C. E. On high-level cyclones originating in the tropics. **Transactions of American Geophysics Union**, v. 32, n. 5, p. 683-695, 1951.

PEDLOSKY, J. **Geophysical Fluid Dynamics**. 2.ed. Berlin: Springer-Verlag, 1987.

PINHEIRO, H. R. **Validação do método TRACK para identificação objetiva dos Vórtices Ciclônicos de Altos Níveis em regiões subtropicais**. 2010. 156 p. (INPE-16736-TDI/1672). Dissertação (Mestrado em Meteorologia) - Instituto Nacional de Pesquisas Espaciais (INPE), São José dos Campos, 2010.

PETTERSSEN, S. **Weather analysis and forecasting**. 2.ed. New York: Academic Press, 1956.

PETTERSSEN, S.; SMEBYE, S. J. On the development of extratropical cyclones. **Quarterly Journal of the Royal Meteorological Society**, v. 97, p. 457–482, 1971.

PEZZA, A. B.; AMBRIZZI, T. Variability of Southern Hemisphere cyclone and anticyclone behavior: further analysis. **Journal of Climate**, v. 16, n. 7, p. 1075–1083, 2003.

PEZZA, A. B.; SIMMONDS, I.; RENWICK, J. A. Southern Hemisphere cyclones and anticyclones: recent trends and links with decadal variability in the Pacific Ocean. **International Journal of Climatology**, v. 27, n. 11, p. 1403–1419, 2007.

PINHEIRO, H. R.; HODGES, K. I.; GAN, M. A.; FERREIRA, N. J. A new perspective of the climatological features of upper-level cut-off lows in the Southern Hemisphere. **Climate Dynamics**, v. 48, n. 1-2, p. 541–559, 2017.

PIVA, E. D.; GAN, M. A.; RAO, V. B. An objective study of 500-hPa moving troughs in the Southern Hemisphere. **Monthly Weather Review**, v. 136, n. 6, p. 2186–2200, 2008.

PIVA, E. D.; GAN, M. A.; RAO, V. B. Energetics of winter troughs entering South America. **Monthly Weather Review**, v. 138, n. 4, p. 1084–1103, 2010.

PIVA, E. D.; GAN, M. A. The role of latent and sensible heat fluxes in an explosive cyclogenesis over the South American East coast. **Journal of the Meteorological Society of Japan**, v. 86, n.6, p. 637-663, 2011.

PLANT, R. S.; CRAIG, G. C.; GRAY, S. L. On a threefold classification of extratropical cyclogenesis. **Quarterly Journal of the Royal Meteorological Society**, v. 129, n. 594, p. 2989–3012, 2003.

POOK, M. J.; MCINTOSH, P. C.; MEYERS, G. A. The synoptic decomposition of cool-season rainfall in the southeastern Australian cropping region. **Journal of Applied Meteorology and Climatology**, v. 45, n. 8, p. 1156–1170, 2006.

POOK, M. J.; RISBEY, J. S.; MCINTOSH, P. C. The synoptic climatology of cool-season rainfall in the central wheatbelt of Western Australia. **Monthly Weather Review**, v. 140, n. 1, p. 28–43, 2012.

PORCÙ, F. et al. A study on cut-off low vertical structure and precipitation in the Mediterranean region. **Meteorology and Atmospheric Physics**, v. 96, n. 1-2, p. 121-140, 2007.

PORCÙ, F.; CARRASSI, A. Toward an estimation of the relationship between cyclonic structures and damages at the ground in Europe. **Natural Hazards and Earth System Sciences**, v. 9, n. 3, p. 823-829, 2009.

PRICE, J. D.; VAUGHAN, G. Statistical studies of cut-off low systems. **Annales Geophysicae**, v. 10 p. 96-102, 1992.

PRICE, J. D.; VAUGHAN, G. The potential for stratosphere-troposphere exchange in cut-off low systems. **Quaterly Journal of the Royal Meteorological Society**, v. 119, p. 343-365, 1993.

QI, L.; LESLIE, L. M.; ZHAO, S. X. Cut-off low pressure systems over southern Australia: climatology and case study. **International Journal of Climatology**, v. 19, p. 1633-1649, 1999.

QUISPE, N.; AVALOS, G. Intense snowstorm in the southern mountains of Peru associated to the incursion to the incursion of cut-off low-pressure systems at upper level. In: INTERNATIONAL CONFERENCE ON SOUTHERN HEMISPHERE METEOROLOGY AND OCEANOGRAPHY (ICSHMO), 8., 2006, Foz do Iguaçu, PR. **Proceedings…** 2006. p. 1945-1958.

RAMAGE, C. S. The subtropical cyclone. **Journal of Geophysical Research**, v. 67, n. 4, p. 1401-1411, 1962.

RAMIREZ, M. C. V.; FERREIRA, N. J.; GAN, M. A. Vórtices ciclônicos desprendidos em altos níveis que originam-se no leste do Pacífico Tropical Sul—Parte I: aspectos sinóticos relacionados a sua formação. In: CONGRESSO BRASILEIRO DE METEOROLOGIA, 11, 2000. Rio de Janeiro, Brasil. **Anais…** 2000.

RAMASWAMY, V.; SCHWARZKOPF, M. D.; SHINE, K. P. Radiative forcing of climate from halocarbon induced global stratospheric ozone loss. **Nature**, v. 355, p. 810–812, 1992.

RANCIC, M.; DERBER, J. C.; PARRISH, D.; TREADON, R.; KLEIST, D. T. The

development of the first-order time extrapolation to the observation (FOTO) method and its application in the NCEP global data assimilation system. In: SYMPOSIUM ON INTEGRATED OBSERVING AND ASSIMILATION SYSTEMS FOR THE ATMOSPHERE, OCEANS, AND LAND SURFACE (IOAS-AOLS), 12., 2008. **Proceedings…** 2008. p. 1–4.

RANDEL, W. J.; STANFORD, J. L. The observed life cycle of a baroclinic instability. **Journal of the Atmospheric Sciences***,* v. 42, n. 13, p. 1364–1373, 1985.

RAO, V. B.; BONATTI, J. P. On the origin of upper tropospheric cyclonic vortices in the South Atlantic Ocean and adjoining Brazil during the summer. **Meteorology and Atmospheric Physics**, v. 37, n. 1, p. 11-16, 1987.

REBOITA, M. S.; NIETO, R.; GIMENO, L.; ROCHA, R. P.; AMBRIZZI, T.; GARREAUD, R; KRUGER, L. F. Climatological features of cutoff low systems in the Southern Hemisphere. **Journal of Geophysical Research: Atmospheres**, v. 115, D17104, 2010.

REBOITA, M. S.; VEIGA, J. A. P. Análise sinótica e energética de um VCAN que causou chuva no deserto do atacama em março de 2015. **Revista Brasileira de Meteorologia**, v. 32, n. 1, p. 123–139, 2017.

REED, R. J.; STOELINGA, M. T.; KUO, Y. H. A model-aided study of the origin and evolution of the anomalously high potential vorticity in the inner region of a rapidly deepening marine cyclone. **Monthly Weather Review**, v. 120, n. 6, p. 893-913, 1992.

REICHLE, R. H.; KOSTER, R. D.; DE LANNOY, G. J. M.; FORMAN, B. A.; LIU, Q.; MAHANAMA, S. P. P.; TOURE, A. Assessment and enhancement of MERRA land surface hydrology estimates. **Journal of Climate**, v. 24, n. 24, p. 6322–6338, 2011.

RENARD, R. J.; CLARKE, L. C. Experiments in numerical objective frontal analysis. **Monthly Weather Review**, v. 93, p. 547–556, 1965.

RICKS, E. L. **On the structure and maintenance of high tropospheric cold-core cyclones of the tropics**. Dissertation (Master's in Geophysics) - The University of Chicago, Chicago, 1959.

RIENECKER, M. M. et al. **The GEOS-5 data assimilation system**: documentation of versions 5.0.1, 5.1.0, and 5.2.0. Washington: NASA, 2008.

RIENECKER, M. M. et al. MERRA: NASA's modern-era retrospective analysis for research and applications. **Journal of Climate**, v. 24, p. 3624–3648, 2011.

RISBEY, J. S.; POOK, M. J.; MCINTOSH, P. C.; UMMENHOFER, C. C.; MEYERS, G. Characteristics and variability of synoptic features associated with cool season rainfall in southeastern Australia. **International Journal of Climatology**, v. 29, n. 11, p. 1595–1613, 2009.

RIVIÈRE, G.; ARBOGAST, P.; JOLY, A. Eddy kinetic energy redistribution within windstorms Klaus and Friedhelm. **Quarterly Journal of the Royal Meteorological**

**Society**, v. 141, n. 688, p. 925–938, 2015.

RONDANELLI, R.; GALLARDO, L.; GARREAUD, R. D. Rapid changes in ozone mixing ratios at Cerro Tololo (30°10_S, 70°48_W, 2200 m) in connection with cut-off lows and deep troughs. **Journal of Geophysical**, v. 107, p. 420, 2002.

ROMERO, R.; SUMNER, G.; RAMIS, C.; GENOVÉS, A. A classification of the atmospheric circulation patterns producing significant daily rainfall in the Spanish Mediterranean area. **International Journal of Climatology**, v. 19, p. 765-785, 1999.

ROSSBY, C. G. On the propagation of frequencies and energy in certain types of atmospheric and oceanic waves. **Journal of Meteorology**, v. 2, n. 4, p. 187-204, 1945.

ROSSOW, W. B; SCHIFFER, R. A. ISCCP cloud data products. **Bulletin of the American Meteorological Society**, v. 72, n. 1, p. 2–20, 1991.

SABO, P. Application of the thermal front parameter to baroclinic zones around cut-off lows. **Meteorology and Atmospheric Physics**, v. 47, n. 2–4, p. 107–115, 1992.

SAHA, S. et al. The NCEP climate forecast system reanalysis. **Bulletin of the American Meteorological Society**, v. 91, n. 8, p. 1015–1057, 2010.

SAKAMOTO K.; TAKAHASHI M. Cut off and weakening processes of an upper cold low. **Journal of the Meteorological Society of Japan**, v. 83, p. 817-834. 2005.

SALIO, P.; NICOLINI, M.; SAULO, A. C. Chaco low-level jet events characterization during the austral summer season. **Journal of Geophysical Research: Atmospheres**, v. 107, n. D24, p. ACL 32-1-ACL 32-17, 2002.

SATYAMURTY, P.; DOS SANTOS, R. P.; LEMS, M. A. M. On the stationary trough generated by the Andes. **Monthly Weather Review**, v. 108, n. 4, p. 510-520, 1980.

SATYAMURTY, P; GAN, M. A.; FERREIRA, C. C. Cyclonic vortices over South America. **Tellus**, v. 42a, p. 194-201, 1990.

SATYAMURTY, P; SELUCHI, M. E. Characteristics and structure of an upper air cold vortex in the subtropics of South America. **Meteorology and Atmospheric Physics**, v. 96, p. 203-220, 2007.

SCHERHAG, R. Ein grenzfall atmosphärischer steuerung: die bodenisobaren steuern ein Höhentief. **Annalen der Hydrographie und Maritimen Meteorologie**, v. 65, p. 27, 1937.

SCHERHAG, R. Der kälteeinbruch mitte Dezember 1938. **Annalen Der Hydrographie und Maritimen Meteorologie**, v. 67, p. 142, 1939.

SELUCHI, M. E.; SAULO, A. C. Possible mechanisms yielding an explosive coastal cyclogenesis over South America: experiments using a limited area model. **Australian Meteorological Magazine**, v. 47, p. 309-320, 1998.

SELUCHI, M. E.; GARREAUD, R.; NORTE, F. A.; SAULO, A. C. Influence of the Subtropical Andes on Baroclinic Disturbances: a cold front case study. **Monthly Weather Review**, v. 134, n. 11, p. 3317–3335, 2006.

SHAPIRO, M. A. On the applicability of the geostrophic approximation to upper-level frontal-scale motions. **Journal of the Atmospheric Sciences**, v. 27, p. 408-420, 1970.

SILVA DIAS, P. L.; SCHUBERT, W. H.; DEMARIA, M. Large-scale response of the tropical atmosphere to transient convection. **Journal of the Atmospheric Sciences**, v. 40, n. 11, p. 2689-2707, 1983.

SILVA DIAS, P. L.; BONATTI, J. P. A preliminary study of the observed vertical mode structure of the summer circulation over tropical South America. **Tellus A**, v. 37, n. 2, p. 185-195, 1985.

SIMMONDS I.; JONES, D. A. The mean structure and temporal variability of the semiannual oscillation in the southern extratropics. **International Journal of Climatology**, v. 18, p. 473–504, 1998.

SIMPSON, R. H. Evolution of the Kona Storm, a subtropical cyclone. **Journal of Meteorology**, v. 9, p. 24-35, 1952.

SIMMONDS, I.; KEAY, K. Variability of Southern Hemisphere extratropical cyclone behavior, 1958-97. **Journal of Climate**, v. 13, n. 3, p. 550–561, 2000.

SIMMONS, A.; UPPALA, S.; DEE, D.; KOBAYASHI, S. ERA Interim: New ECMWF reanalysis products from 1989 onwards. **ECMWF Newsletter**, n. 110, p. 25-35, 2007.

SIMMONS, A. et al. Low-frequency variations in surface atmospheric humidity, temperature, and precipitation: inferences from reanalyses and monthly gridded observational data sets. **Journal of Geophysical Research**, v. 115, D01110, 2010.

SINCLAIR, M. R. An objective cyclone climatology for the Southern Hemisphere. **Monthly Weather Review**, v. 122, n. 10, p. 2239–2256, 1994.

SINCLAIR, M. R.; REVELL, M. J. Classification and composite diagnosis of extratropical cyclogenesis events in the Southwest Pacific. **Monthly Weather Review**, v. 128, n. 4, p. 1089–1105, 2000.

SINGLETON, A. T.; REASON, C. J. C. A Numerical model study of an intense cutoff low pressure system over South Africa. **Monthly Weather Review**, v. 135, p. 1128–1150, 2006.

SINGLETON, A. T.; REASON, C. J. C. Variability in the characteristics of cut-off low-pressure systems over subtropical southern Africa. **International Journal of Climatology**, v. 27, p. 295-310, 2007.

SIQUEIRA, V.; REBOITA, M.; DUTRA, L. Processos físicos associados à gênese de um VCAN entre o Oceano Pacífico e a América do Sul em abril de 2013. **Ciência e Natura**, p. 391–395, 2013.

SMITH, R. B. Further development of a theory of lee cyclogenesis. **Journal of the atmospheric sciences**, v. 43, n. 15, p. 1582-1602, 1986.

STEPHENS, G. L. et al. The CloudSat mission and the A-Train: a new dimension of space-based observations of clouds and precipitation. **Bulletin of the American Meteorological Society**, v. 83, n. 12, p. 1771-1790, 2002.

STOELINGA, M. T. A potential vorticity-based study of the role of diabatic heating and friction in a numerically simulated baroclinic cyclone. **Monthly Weather Review**, v. 124, n. 5, p. 849-874, 1996.

SUTCLIFFE, R. C. A contribution to the problem of development. **Quarterly Journal of the Royal Meteorological Society**, v. 73, p. 370-383, 1947.

TALJAARD, J. J. Cut-off lows in the South African region. **South African Weather Bureau Technical Paper**, v. 14, p. 153, 1985.

TAYLOR, K. E. An analysis of biases in traditional cyclone frequency maps. **Monthly Weather Review**, v. 114, p. 1481-1490, 1986.

THOMPSON, D. W.; BALDWIN, M.; SOLOMON, S. Stratosphere – Troposphere coupling in the Southern Hemisphere. **Journal of Atmospheric Sciences**, v. 62, p. 708–715, 2005.

THORPE, A. J. Diagnosis of balanced vortex structure using potential vorticity. **Journal of the Atmospheric Sciences**, v. 42, p. 397–406, 1985.

TRENBERTH, K. E. On the interpretation of the diagnostic quasi-geostrophic omega equation. **Monthly Weather Review**, v. 106, p. 131-137, 1978.

TRENBERTH, K. E.; MO, K. C. Blocking in the Southern Hemisphere. **Monthly Weather Review**, v. 113, p. 3-21, 1985.

TRIPOLI, G. J.; MEDAGLIA, C. M.; DIETRICH, S. M.; MUGNAI, A.; PANEGROSSI, G.; PINORI, S.; SMITH, E. A. The 9–10 November 2001 Algerian flood: a numerical study. **Bulletin of the American Meteorological Society** v. 86, p. 1229–1235, 2005.

VAN LOON, H. Blocking action in the Southern Hemisphere, Part I. **Notos**, v. 5, p. 171-175, 1956.

VAN LOON, H. The half-yearly oscillations in middle and high southern latitudes and coreless winter. **Journal of the Atmospheric Sciences**, v. 24, p. 472–486, 1967.

VAN LOON, H.; JENNE, R. L.; LABITZKE, K. Zonal harmonic standing waves. **Journal of Geophysical Research**, v. 78, p. 4463–4471, 1973.

VAROTSOS, C. The extraordinary events of the major, sudden stratospheric warming, the diminutive antarctic ozone hole, and its split in 2002. **Environmental Science and Pollution Research**, v. 11, n. 6, p. 405–411, 2004.

VAUGHAN, G.; PRICE, J. D. Ozone transport into the troposphere in a cut-off low event. In: QUADRENNIAL OZONE SYMPOSIUM 1988; TROPOSPHERIC OZONE WORKSHOP, 1989. **Proceedings…** Deepak Publishing, 1989.

VEIGA, J. A. P. et al. An analysis of the environmental energetics associated with the transition of the first South Atlantic hurricane. **Geophysical Research Letters**, v. 35, n. 15, 2008.

VELDEN, C. S.; HAYDEN, C. M.; NIEMAN, S. J.; MENZEL, W. P.; WANZONG, S.; GOERSS, J. S. Upper-tropospheric winds derived from geostationary satellite water vapor observations. **Bulletin of the American Meteorological Society**, v. 78, p. 173-195, 1997.

VERA, C. S.; VIGLIAROLO, P. K. A diagnostic study of cold-air outbreaks over South America. **Monthly Weather Review**, v. 128, n. 1, p. 3-24, 2000.

WANG, X.; SWAIL, V. R.; ZWIERS, F. Climatology and changes of extratropical cyclone activity: comparison of ERA-40 with NCEP–NCAR reanalysis for 1958–2001. **Journal of Climate**, v.19, p. 3145–3166, 2006.

WERNLI, H.; SPRENGER, M. Identification and ERA-15 climatology of potential vorticity streamers and cutoffs near the extratropical tropopause. **Journal of the Atmospheric Sciences**, v. 64, p. 1569-1586, 2007.

WILLMOTT, A. J. A note on the steepening of long Rossby waves. **Deep Sea Research Part A. Oceanographic Research Papers**, v. 32, n. 5, p. 613-617, 1985.

WINKLER, R.; ZWATZ-MEISE, V. **Manual of synoptic satellite meteorology:** conceptual models. Version 6.0. Vienna, Austria: Central Institute for Meteorology and Geodynamics Hohe Warte, 2001.

WRIGHT, A. D. **Blocking action in the Australian region**. Canberra, Australia: Bureau of Meteorology, 1974.

YANAI, M.; MARUYAMA, T. Stratospheric wave disturbances propagating over the equatorial Pacific. **Journal of the Meteorological Society of Japan. Ser. II**, v. 44, n. 5, p. 291-294, 1966.

YEH, T. C. On energy dispersion in the atmosphere. **Journal of Meteorology**, v. 6, p. 1-16, 1949.

## APPENDIX A – THE COST FUNCTION

The original cost function developed by Salari and Sethi (1990) has been adapted to be used on a spherical domain (Hodges, 1995) subject to displacement distances and smoothness constraints (Hodges, 1999). This provides the maximum gain in smoothness by minimizing the cost function as given in the following equation:

$$\Xi \sum_{i=1}^{m} \sum_{k=2}^{n-1} D\left(P_i^{k-1}, P_i^k, P_i^{k+1}\right) \qquad (A.1)$$

where $D\left(P_i^{k-1}, P_i^k, P_i^{k+1}\right)$ is the local deviation at a time step $k$, with $m$ the total number of tracks and $n$ the total number of frames or time steps. $P_i^k$ denotes the position vector in a Cartesian space for a track $i$ in a time step $k$. The local deviation is defined as:

$$D\left(P_i^{k-1}, P_i^k, P_i^{k+1}\right) = \begin{cases} 0 & (i) \\ \psi\left(P_i^{k-1}, P_i^k, P_i^{k+1}\right) & (ii) \\ \Psi & (iii) \end{cases} \qquad (A.2)$$

$(i)$ if $P_i^{k-1}$ is a phantom feature point, and $P_i^k$ and $P_i^{k+1}$ are real or phantom;

$(ii)$ if $P_i^{k-1}, P_i^k$ and $P_i^{k+1}$ are feature points;

$(iii)$ otherwise,

The term $\psi\left(P_i^{k-1}, P_i^k, P_i^{k+1}\right)$ is the upper bound on the local smoothness measured as change of speed and direction over three time steps, and $\Psi$ is a global upper bound on $\psi$. The function $\psi\left(P_i^{k-1}, P_i^k, P_i^{k+1}\right)$ is given by:

$$= 0.5w_1\left(1 - \frac{P_i^{k-1}P_i^k . P_i^k P_i^{k+1}}{\left\|P_i^{k-1}P_i^k\right\|\left\|P_i^k P_i^{k+1}\right\|}\right) + w_2\left[1 - \frac{2\left(\left\|P_i^{k-1}P_i^k\right\|\left\|P_i^k P_i^{k+1}\right\|\right)^{1/2}}{\left\|P_i^{k-1}P_i^k\right\| + \left\|P_i^k P_i^{k+1}\right\|}\right] \qquad (A.3)$$

where $P_i^{k-1}P_i^k$ is the displacement distance on a spherical domain between $P_i^{k-1}$ and $P_i^k$, and $w_1$and $w_2$ are weights set as 0.2 and 0.8, respectively. In Eq. A.3 the first term represents the change in direction and the second terms represents the change in speed.

## APPENDIX B – THE THERMAL FRONTAL PARAMETER

The thermal frontal parameter ($TFP$) is computed as:

$$TFP = -\nabla\,|\nabla\tau|.\frac{\nabla\tau}{|\nabla\tau|} \qquad (B.1)$$

which $\tau$ is a horizontal two-dimensional thermal field (e.g. temperature, potential temperature). Assuming $\tau$ is temperature, the $TFP$ represents the change of the temperature gradient along its gradient.

The $TFP$ is a function developed by Renard and Clark (1965) as a methodology for identifying and locating fronts. The schematic representation of the operators used in the $TFP$ is demonstrated in Figure B.1. In a typical frontal system, the maximum temperature gradient (namely, $\nabla T$ which is the first term of the $TFP$) is located on the cold-side of a cold-front, while the temperature gradient in the direction of the temperature gradient (namely, $-\nabla\ |\nabla T|$ which is the second term of the $TFP$) coincides with the position of the cold-front. Hence, the maximum $TFP$ can be used to locate the fronts in a surface or in a deep layer in the atmosphere. Hewson (1998) summarizes the wide range of front-related variables derived from the $TFP$ (see his Table 1).

Figure B.1: Schematic representation of a front and the distribution for three operators used in the thermal frontal parameter function: $T$ (temperature, top), $\nabla T$ (temperature gradient, middle), and $-\nabla |\nabla T|$ (temperature gradient in the direction of the temperature gradient, bottom).

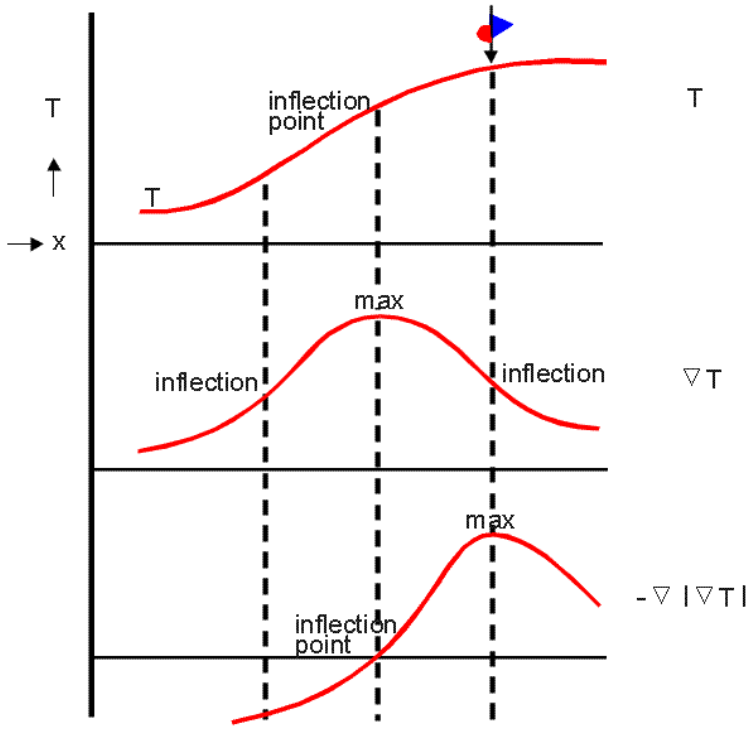


Source: EUMETSAT

## APPENDIX C – INDIVIDUAL COMPOSITES OF THE THERMAL FRONTAL PARAMETER

The identification of baroclinic zones in a COL is based on the TFP averaged in the layer 500-300 hPa. The analysis of individual cases indicates that the maximum TFP originates upstream of the upper-level trough axis and propagates cyclonic downstream along the northern boundary of the COL. This is clearly seen in cases 1, 2 and 3 (Figs. C.1, C.2, and C.3, respectively). For case 3, in particular, a new intensification phase occurs in the late stage, since the TFP increases in the western side of the COL.

Figure C.1: Lifecycle of a Cut-off Low (case 1) for $Z_{300}$ and themal frontal parameter at 500-300 hPa for 6 hourly interval.

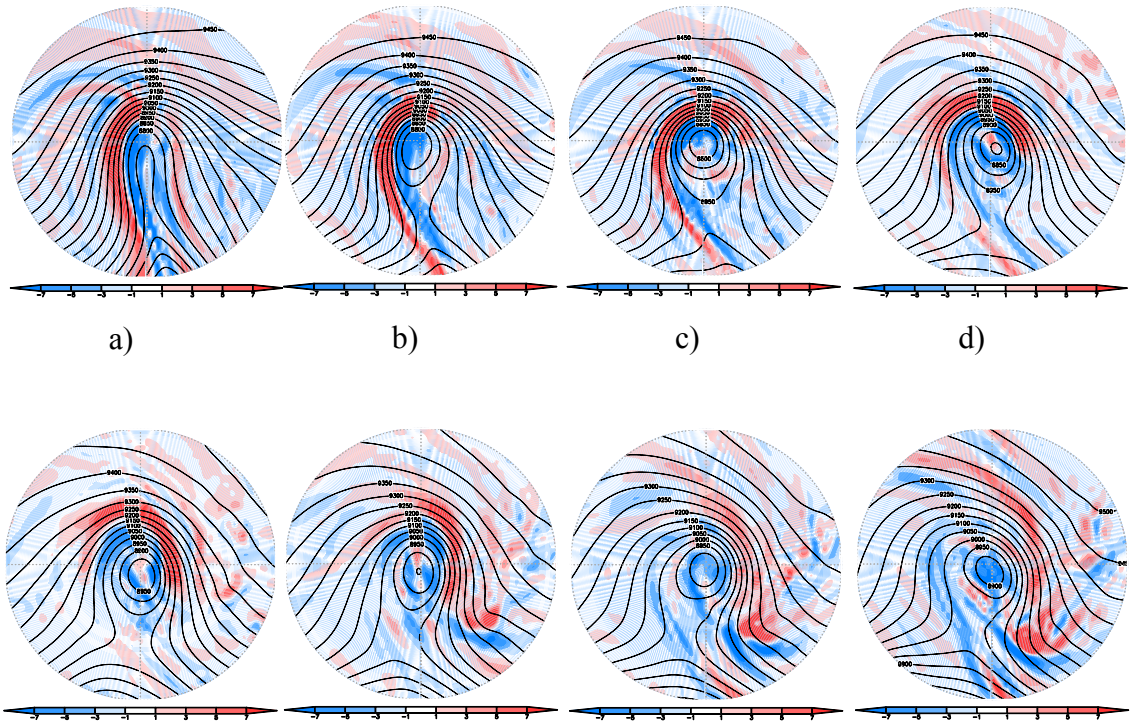


Unit is $10^{11}$ $^{o}$C/(100km)$^2$ for themal frontal parameter, gpm for geopotential height.

Source: Author's production.

Figure C.2: Lifecycle of a Cut-off Low (case 2) for $Z_{300}$ and themal frontal parameter at 500-300 hPa for 6 hourly interval.

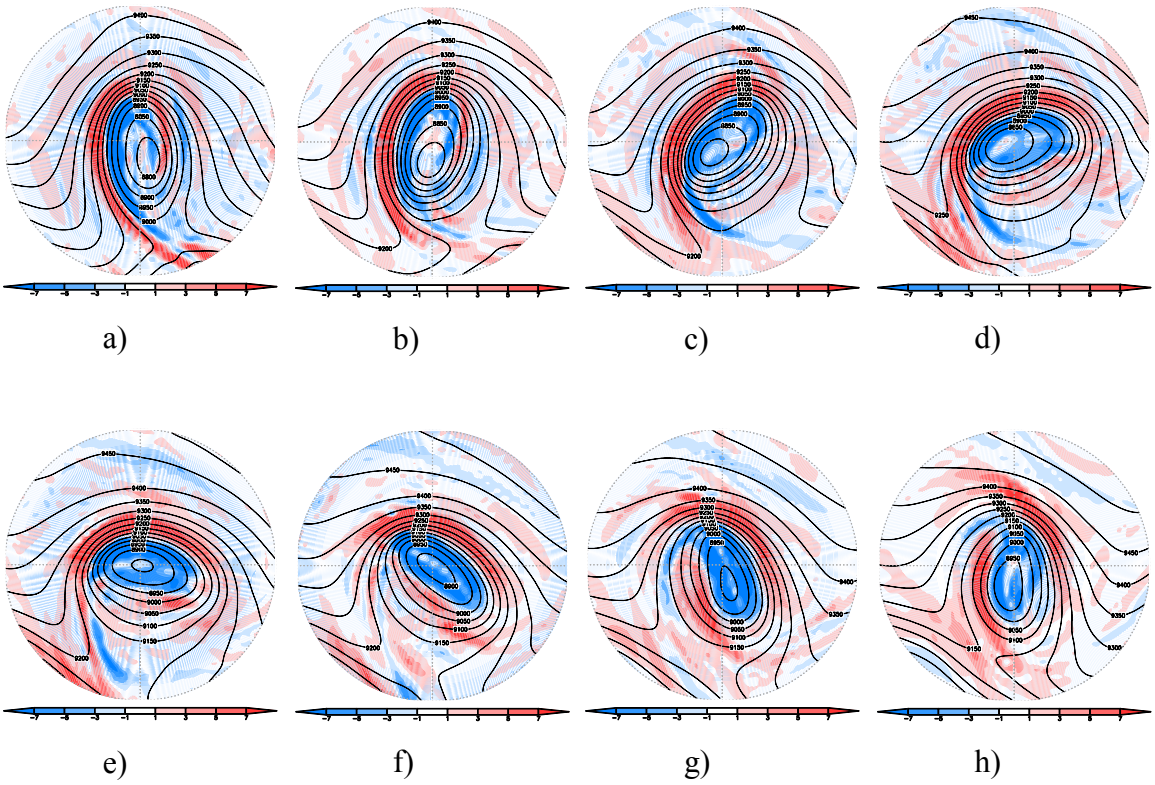


Unit is $10^{11}$ $^{o}$C/(100km)$^2$ for themal frontal parameter, gpm for geopotential height.

Source: Author's production.

Figure C.3: Lifecycle of a Cut-off Lows (case 3) for $Z_{300}$ and themal frontal parameter at 500-300 hPa for 6 hourly interval.

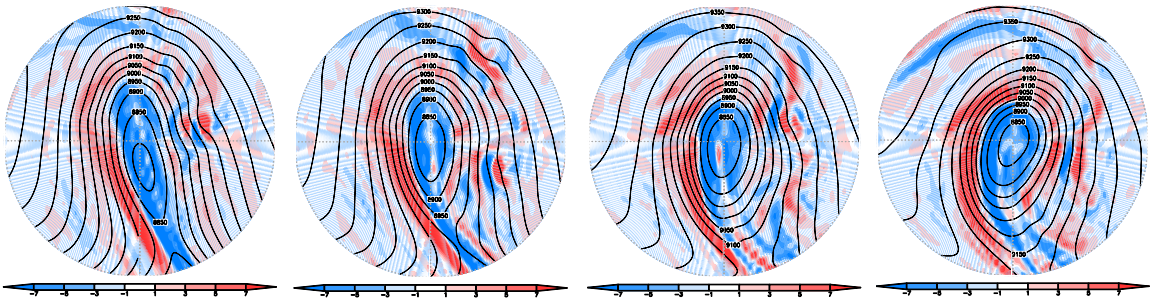

a) b) c) d)

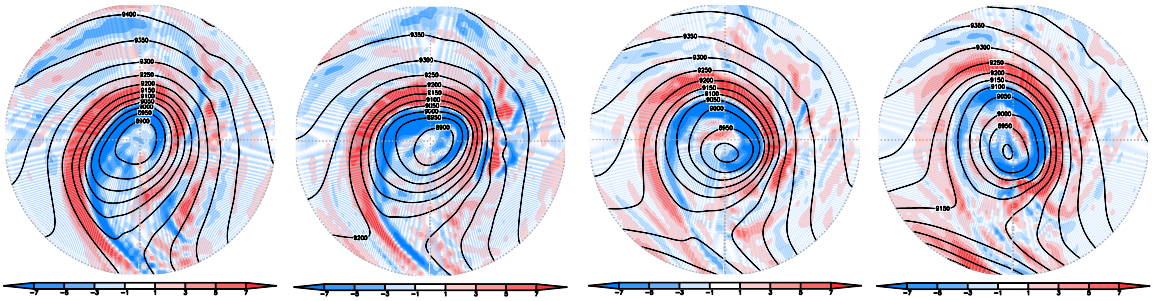

e) f) g) h)

Unit is $10^{11}$ ºC/(100km)$^2$ for themal frontal parameter, gpm for geopotential height.

Source: Author's production.

## APPENDIX D – INDIVIDUAL COMPOSITES OF THE VERTICAL STRUCTURE

The vertical cross-sections along the west-east line of five COL cases in the SH are shown in Figure D.1. Fields are winds, temperature anomaly, and potential vorticity, the same fields shown in Figure 6.10 in Chapter 6. This shows that there is a marked variation from case to case. A deep intrusion occurs in cases 1 associated with the anomalous tropopause which descends down to 700 hPa in the western side of the COL, as denoted by the 2 PVU. This is also the case for case 4. Some COLs show a strong asymmetry in the circulation such as in cases 4 and 5, despite the fact that the cross sections is determined for the maximum intensity time. For the thermal structure, there are also many differences between the selected COLs, the cold-core can extend toward the surface (as seen in case 1) or remain limited to the mid-upper troposphere (as seen in case 3). Similarly, the horizontal extent of the cold and warm cores is quite variable. Therefore, it should be kept in mind that there is a great diversity of structures when the COLs are examined individually which are smoothed out when the most intense systems are combined by the compositing.

Figure D.1: Vertical cross-section along the west-east line of five Cut-off Low cases in the Southern Hemisphere. Fields are zonal and meridional winds, temperature anomaly, and potential vorticity.

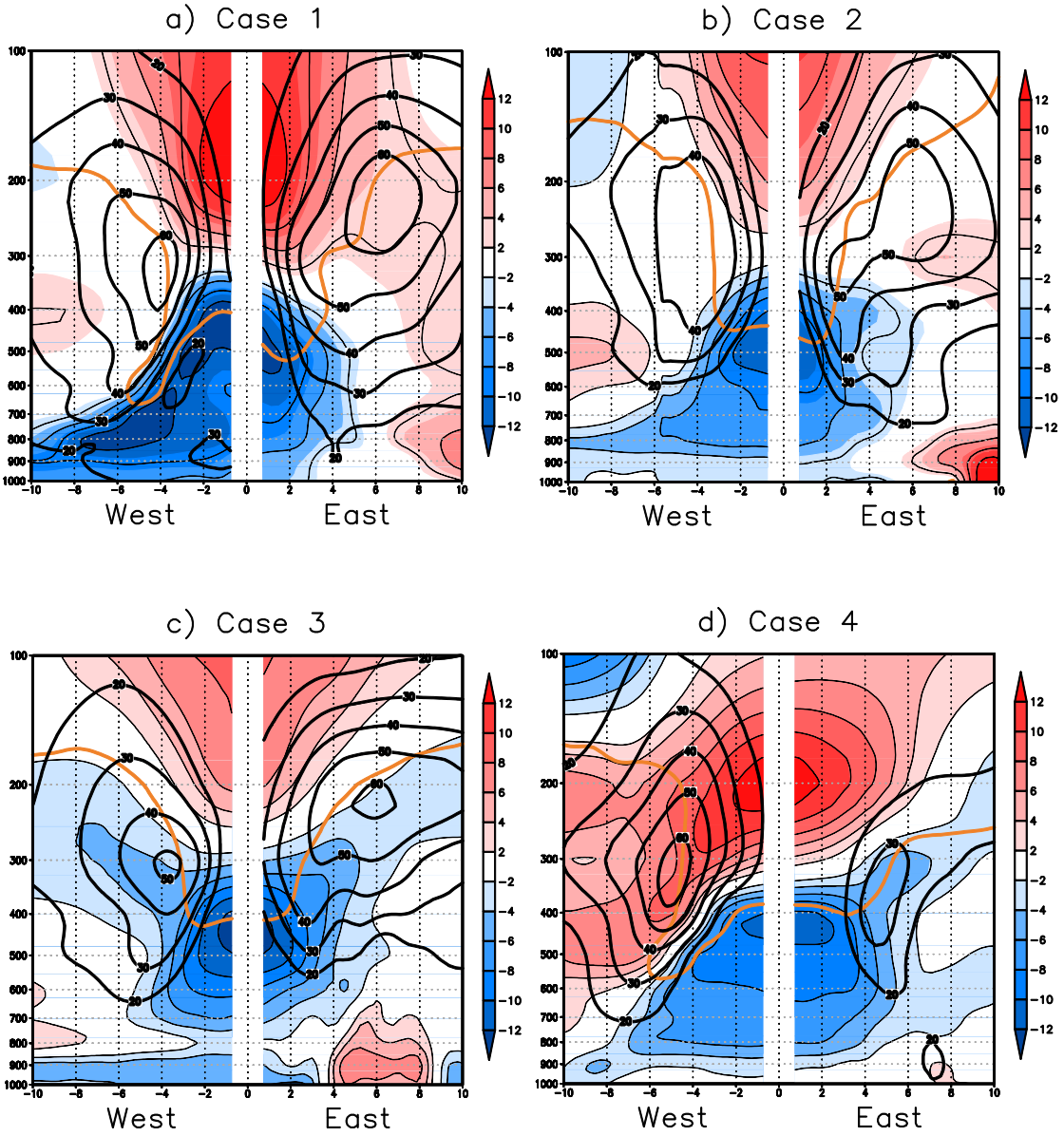


Vertical cross-sections are centered on the time and space relative to the $\xi_{300}$ minimum. The total distance in the $x$ axis is 20º geodesic. Magnitude of horizontal winds (thick solid line) from 20 m/s for the contour intervals 10 m/s. Temperature zonal anomaly in K (shaded). Potential vorticity for the 2 PVU (1 PVU = $10^{-6}$ m$^2$ s$^{-1}$ K kg$^{-1}$) (orange line). The gap in the centre of the composite is due to the missing data which it requires to be interpolated. The multiple step scheme is used to select the COLs.

Source: Author's production.

Figure D.1: Continuation.

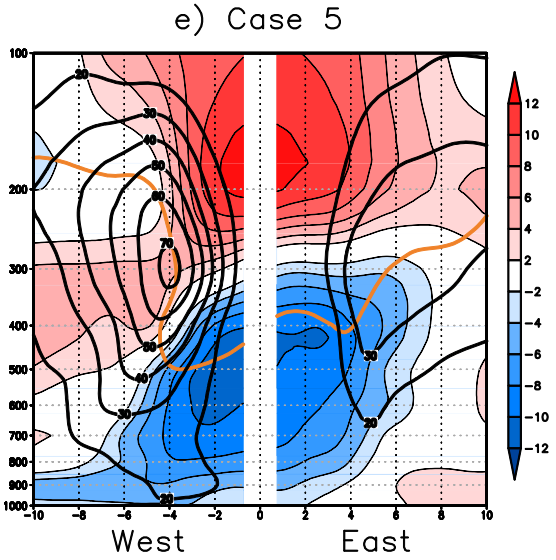


Source: Author's production.

# ANNEX A – MANUSCRIPT PUBLISHED IN *CLIMATE DYNAMICS* JOURNAL

Figure A.1: First page of the manuscript published in the *Climate Dynamics* Journal, Volume 48, Issue 1-2, p. 541-559.

Clim Dyn
DOI 10.1007/s00382-016-3093-8

CrossMark

## A new perspective of the climatological features of upper-level cut-off lows in the Southern Hemisphere

**Henri Rossi Pinheiro[1] · Kevin Ivan Hodges[2] · Manoel Alonso Gan[1] · Nelson Jesuz Ferreira[1]**

Received: 16 November 2015 / Accepted: 18 March 2016
© The Author(s) 2016. This article is published with open access at Springerlink.com

**Abstract** This study presents a detailed view of the seasonal variability of upper-level cut-off lows (COLs) in the Southern Hemisphere. The COLs are identified and tracked using data from a 36-year period of the European Centre for Medium Range Weather Forecast reanalysis (ERA-Interim). The objective identification of the COLs uses a new approach, which is based on 300 hPa relative vorticity minima, and three restrictive criteria of the presence of a cold-core, stratospheric potential vorticity intrusion, and cut-off cyclonic circulation. The highest COL activity is in agreement with previous studies, located near three main continental areas (Australia, South America, and Africa), with maximum frequencies usually observed in the austral autumn. The COL mean intensity values show a marked seasonal and spatial variation, with maximum (minimum) values during the austral winter (summer), a unique feature that has not been observed previously in studies based on the geopotential. The link between intensity and lysis is examined, and finds that weaker systems are more susceptible to lysis in the vicinity of the Andes Cordillera, associated with the topographic Rossby wave. Lysis and genesis regions are close to each other, confirming that COLs are quasi-stationary systems. Also, COLs tend to move eastward and are faster over the higher latitudes. The mean growth/decay rates coincide with the major genesis and lysis density regions, such as the significant decay values across the Andes all year. As a consequence of using vorticity for the tracking method a longer lifetime of COLs is detected than in other studies, but this does not affect the total frequency of occurrence. Comparisons with other studies suggest that the differences in seasonality are due to uncertainties in the reanalyses and the methods used to identify COLs.

**Keywords** Cut-off lows · Climatology · Southern hemisphere · Variability

### 1 Introduction

Cut-off Low pressure systems (COLs) are defined as cold-core lows in the middle and upper troposphere that form after their detachment from the mid-latitude westerlies (Palmén and Newton 1969). COLs develop from a pre-existing cold trough in the upper air flow and move toward the equatorward side of the jet stream, leaving an isolated cold cyclonic vortex. The intensity of COLs associated with their cyclonic circulation is usually highest at upper levels but decreases toward the Earth's surface. They may remain confined at upper levels or deepen downward resulting in surface cyclogenesis (Miky Funatsu et al. 2004). COLs usually move slowly and preferably eastward, but may remain stationary or move westward, i.e., retrogressive motion. A common COL feature is their relatively short lifetime with the majority of events lasting no more than 3 days (Price and Vaughan 1992).

COLs often affect surface weather conditions via their associated rainfall, for example, they have caused heavy rainfall and floods in South Africa (Taljaard 1985; Singleton and Reason 2006) and snowfall in the Andean highland region (Vuille and Ammann 1997). COLs also play an

✉ Henri Rossi Pinheiro
henri.pinheiro@cptec.inpe.br

[1] Center for Weather Forecast and Climate Studies, National Institute for Space Research, Sao Jose dos Campos, SP, Brazil

[2] Department of Meteorology, The University of Reading, Reading, UK

Published online: 28 April 2016



Source: Pinheiro et al. (2017)

## PUBLICAÇÕES TÉCNICO-CIENTÍFICAS EDITADAS PELO INPE

### Teses e Dissertações (TDI)

Teses e Dissertações apresentadas nos Cursos de Pós-Graduação do INPE.

### Manuais Técnicos (MAN)

São publicações de caráter técnico que incluem normas, procedimentos, instruções e orientações.

### Notas Técnico-Científicas (NTC)

Incluem resultados preliminares de pesquisa, descrição de equipamentos, descrição e ou documentação de programa de computador, descrição de sistemas e experimentos, apresenta- ção de testes, dados, atlas, e docu- mentação de projetos de engenharia.

### Relatórios de Pesquisa (RPQ)

Reportam resultados ou progressos de pesquisas tanto de natureza técnica quanto científica, cujo nível seja compatível com o de uma publicação em periódico nacional ou internacional.

### Propostas e Relatórios de Projetos (PRP)

São propostas de projetos técnico-científicos e relatórios de acompanha- mento de projetos, atividades e convê- nios.

### Publicações Didáticas (PUD)

Incluem apostilas, notas de aula e manuais didáticos.

### Publicações Seriadas

São os seriados técnico-científicos: boletins, periódicos, anuários e anais de eventos (simpósios e congressos). Constam destas publicações o Internacional Standard Serial Number (ISSN), que é um código único e definitivo para identificação de títulos de seriados.

### Programas de Computador (PDC)

São as sequências de instruções ou códigos, expressos em uma linguagem de programação compilada ou inter- pretada, a ser executada por um computador para alcançar um determi- nado objetivo. São aceitos tanto programas fonte quanto executáveis.

### Pré-publicações (PRE)

Todos os artigos publicados em periódicos, anais e como capítulos de livros.